MICRO AIR VEHICLE MOTION TRACKING AND AERODYNAMIC MODELING

BY

DANIEL V. UHLIG

DISSERTATION

Submitted in partial fulfillment of the requirements
for the degree of Doctor of Philosophy in Aerospace Engineering
in the Graduate College of the
University of Illinois at Urbana-Champaign, 2014

Urbana, Illinois

Doctoral Committee:

   Associate Professor Michael S. Selig, Director of Research and Chair
   Professor Emeritus Michael B. Bragg
   Professor Kenneth T. Christensen
   Assistant Professor Soon-Jo Chung

Abstract

Aerodynamic performance of small-scale fixed-wing flight is not well understood, and flight data are needed to gain a better understanding of the aerodynamics of micro air vehicles (MAVs) flying at Reynolds numbers between 10,000 and 30,000. Experimental studies have shown the aerodynamic effects of low Reynolds number flow on wings and airfoils, but the amount of work that has been conducted is not extensive and mostly limited to tests in wind and water tunnels.

In addition to wind and water tunnel testing, flight characteristics of aircraft can be gathered through flight testing. The small size and low weight of MAVs prevent the use of conventional on-board instrumentation systems, but motion tracking systems that use off-board triangulation can capture flight trajectories (position and attitude) of MAVs with minimal onboard instrumentation. Because captured motion trajectories include minute noise that depends on the aircraft size, the trajectory results were verified in this work using repeatability tests. From the captured glide trajectories, the aerodynamic characteristics of five unpowered aircraft were determined.

Test results for the five MAVs showed the forces and moments acting on the aircraft throughout the test flights. In addition, the airspeed, angle of attack, and sideslip angle were also determined from the trajectories. Results for low angles of attack (less than approximately 20 deg) showed the lift, drag, and moment coefficients during nominal gliding flight. For the lift curve, the results showed a linear curve until stall that was generally less than finite wing predictions. The drag curve was well described by a polar. The moment coefficients during the gliding flights were used to determine longitudinal and lateral stability derivatives. The neutral point, weather-vane stability and the dihedral effect showed some variation with different trim speeds (different angles of attack). In the gliding flights, the aerodynamic characteristics exhibited quasi-steady effects caused by small variations in the angle of attack. The quasi-steady effects, or small unsteady effects, caused variations in the aerodynamic characteristics (particularly incrementing the lift curve), and the magnitude of the influence depended on the angle-of-attack rate.

In addition to nominal gliding flight, MAVs in general are capable of flying over a wide flight envelope including agile maneuvers such as perching, hovering, deep stall and maneuvering in confined spaces. From

the captured motion trajectories, the aerodynamic characteristics during the numerous unsteady flights were gathered without the complexity required for unsteady wind tunnel tests. Experimental results for the MAVs show large flight envelopes that included high angles of attack (on the order of 90 deg) and high angular rates, and the aerodynamic coefficients had dynamic stall hysteresis loops and large values.

From the large number of unsteady high angle-of-attack flights, an aerodynamic modeling method was developed and refined for unsteady MAV flight at high angles of attack. The method was based on a separation parameter that depended on the time history of the angle of attack and angle-of-attack rate. The separation parameter accounted for the time lag inherit in the longitudinal characteristics during dynamic maneuvers. The method was applied to three MAVs and showed general agreement with unsteady experimental results and with nominal gliding flight results.

The flight tests with the MAVs indicate that modern motion tracking systems are capable of capturing the flight trajectories, and the captured trajectories can be used to determine the aerodynamic characteristics. From the captured trajectories, low Reynolds number MAV flight is explored in both nominal gliding flight and unsteady high angle-of-attack flight. Building on the experimental results, a modeling method for the longitudinal characteristics is developed that is applicable to the full flight envelope.

To Virginia, Henry, and Peter

Acknowledgments

I would like to thank Professor Michael S. Selig for exciting me about post-stall aerodynamics. His ideas, expertise, and probing questions have helped me refine the results presented here. My journey to a doctoral degree would not have been possible without the support of many people. Professor Natasha Neogi pushed me to do research and begin my PhD. She encouraged me to do research in graduate school. My initial researched involved building and flight testing UAVs along side two excellent fellow students—Keerti Bhamidipati and Andres Ortiz. Throughout school, the support and ideas from Heather Arneson, Aaron Becker, Scot Campbell, Miles Johnson, and Andres Ortiz helped me in countless ways. I enjoyed the many useful research discussions with my labmates: Gavin Ananda, Rob Deters, Brent Pomeroy, and especially, Arjun Rao for his help fully verifying my methods. I am thankful for Professor Soon-Jo Chung for sharing the testing equipment and for the conversations with his students—particularly Dan Morgan and Aditya Paranjape. Testing required coordinating schedules with the aerospace machine shop (Greg Milner) and Professor James Phillips, and I am grateful that they were helpful and kept the process simple. Finally, I am thankful for the opportunity to learn from and teach with Dr. Cinda Heeren while working along side and learning from the extremely dedicated CS 225 staff.

Table of Contents

List of Tables

List of Figures

Nomenclature

a	=	semichord
$\mathbf{a}$	=	translational acceleration vector
$\mathcal{R}$	=	aspect ratio
b	=	wingspan
c	=	wing root chord
$\bar{c}$	=	wing mean aerodynamic chord
C_D	=	drag coefficient $[D/(qS_{ref})]$
C_{D_o}	=	parasite drag coefficient
C_L	=	lift coefficient $[L/(qS_{ref})]$
C_{L_α}	=	airplane lift curve slope
C_{l_α}	=	airfoil lift curve slope
C_l, C_m, C_n	=	aerodynamic moment coefficients (roll, pitch, and yaw)
C_N	=	normal force coefficient ($\sqrt{C_L^2 + C_D^2}$)
D	=	drag force
e_o	=	Oswald efficiency factor
$\mathbf{F}$	=	force vector
g	=	gravitational acceleration
$\mathbf{I}$	=	inertia matrix
K	=	constant for induced drag coefficient
k	=	reduced frequency of the angle-of-attack rate $[\dot{\alpha}c/(2V)]$
L	=	lift force
L, M, N	=	roll, pitch, and yaw moments
m	=	airplane mass
p, q, r	=	roll, pitch, and yaw rates
q	=	dynamic pressure ($\frac{1}{2}\rho V^2$)

Re	=	Reynolds number based on mean aerodynamic chord ($V\bar{c}/\nu$)
$\mathbf{R}$	=	transformation or rotation matrix
$\mathbf{r}$	=	offset vector between tracked point and center of gravity
S_{ref}	=	wing reference area
$u,\ v,\ w$	=	body-fixed translational velocity
V	=	inertial speed
x	=	separation parameter
$x,\ y,\ z$	=	position of the airplane track
α	=	angle of attack (referenced to fuselage)
$\dot{\alpha}$	=	angle-of-attack rate
β	=	sideslip angle
$\tau_1,\ \tau_2$	=	time constants
$\phi,\ \theta,\ \psi$	=	roll, pitch, and heading angles
ρ	=	density of air
ν	=	kinematic viscosity
$\boldsymbol{\omega}$	=	angular rates $[p\,q\,r]^T$

Subscripts

b	=	body-fixed axes system
e	=	Earth-fixed axes system
ac	=	aerodynamic center
cg	=	center of gravity
h	=	property of the horizontal stabilator
$trim$	=	property at trim flight conditions
w	=	property of the wing

Chapter 1

Introduction and Literature Review

1.1 Introduction

The use of MAVs and the research interest in MAVs has grown significantly in recent years [1, 2], but accurate and detailed experimental aerodynamic data in the Reynolds number range of 10,000 to 30,000 is limited. Further testing at low Reynolds numbers is needed to refine models and predictions of MAV aerodynamic characteristics. The complexity of low Reynolds number flow can be observed from the test results of airfoils and wings at Reynolds number less than 500,000 [3–11]. Limited results are available at Reynolds numbers below 100,000 where the effects associated with low Reynolds numbers become more pronounced [3, 12, 13].

In addition to the aerodynamic changes due to low Reynolds numbers, MAVs typically have high structural strength-to-weight ratios and high thrust-to-weight ratios which enable them to readily operate over a larger flight envelope than most full-sized airplanes. MAVs operate over a large range of angles of attack during agile maneuvers such as perching [14–16], hovering [17, 18], deep stall [19, 20], and dynamic maneuvering in confined spaces [21]. Consequently, experimental data for the aerodynamic characteristics are needed at large angles of attack (on the order of 90 deg) and over a range of angular rates.

Low Reynolds number experimental flight data for small MAVs have been previously gathered using off-board motion tracking systems to capture flight trajectories. Modern motion tracking systems measure the position and orientation of small objects, and the accurate, high-speed measurements of flight trajectories can be used to determine aerodynamic characteristics of MAVs [14, 22]. In addition, motion tracking can be used to determine the effect of unsteady aerodynamics without a complex and costly apparatus that is normally required in wind tunnel tests [23, 24]. This research uses off-board flight measurements to understand the aerodynamics of free-flight MAVs for both nominal low angle-of-attack flight and unsteady high angle of attack flight. Flight tests at low angles of attack (on the order of the stall angle of attack) and with low angular rates had only small unsteady effects and thus, are referred to as quasi-steady flights. Second, dynamic high angle-of-attack flight where the maximum angle of attack was large (on the order of 90 deg) and the angular rates were large was explored. Together, the experimental data show low

Reynolds number flight characteristics of MAVs in quasi-steady nominal gliding flight and unsteady high angle-of-attack flight.

Beyond additional experimental data for MAVs, better modeling approaches are needed for the aerodynamic characteristics over the large flight envelope—particularly unsteady and high angle-of-attack flight. Previous work has used motion tracking data to gather aerodynamic coefficients and model flight dynamics of MAVs over limited flight envelopes. One approach used trajectories to estimate the aerodynamic coefficients for MAVs at angles of attack up to 30 deg but neglected the dynamic effects [25]. A work that showed aerodynamic coefficients during unsteady high angle-of-attack flight did not attempt to model the aerodynamic coefficients of the MAV [23, 24]. In Refs. [14] and [22], high angle-of-attack flight was modeled using flat plate theory while neglecting the complexities of unsteady effects. Modeling unsteady flight is challenging because the aerodynamic coefficients depend on the time history of the angle of attack and the angle-of-attack rate. One approach to modeling unsteady high angle-of-attack flight involves using indicial functions [26, 27]. Another approach involves an additional state variable that includes a time dependent lag [28, 29]. The additional state variable is referred to as the separation parameter [29, 30], and the method has generally been applied to airfoils or large aircraft with peak angles of attack in between 30 and 60 deg [31–33]. As previously mention MAVs often operate at angles of attack up to and exceeding 90 deg, and recently, the expanded state-space method was adapted to model the lift coefficient for a four-element cascade wing at angles of attack up to 90 deg [34, 35]. Using the experimental high angle of attack data in this work, a model was developed based on the expanded state-space method for longitudinal flight of three MAVs, and the methodology is applicable to the full flight envelope of the MAVs which includes flight at angles of attack exceeding 90 deg.

This research measured the aerodynamic characteristics of five MAVs using flight testing and expanded on the existing results by testing a variety of airframes. The analysis included results in both quasi-steady nominal gliding flight and unsteady high angle-of-attack flight. The objective was to use numerous flights to gather results in different flight conditions and use multiple flights at each of the conditions to reduce the uncertainty in the results. Results for five tested MAVs are presented and analyzed in this dissertation to demonstrate how flight trajectories were used to gather aerodynamic characteristics for both quasi-steady and high angular rate flight. For the unsteady high angle-of-attack flight, modeling methods are developed and applied to the longitudinal flight dynamics. The data that were collected for MAV flight at low Reynolds numbers increases the understanding of the aerodynamic characteristics and flight characteristics of MAVs for both quasi-steady and unsteady high angle of attack flight.
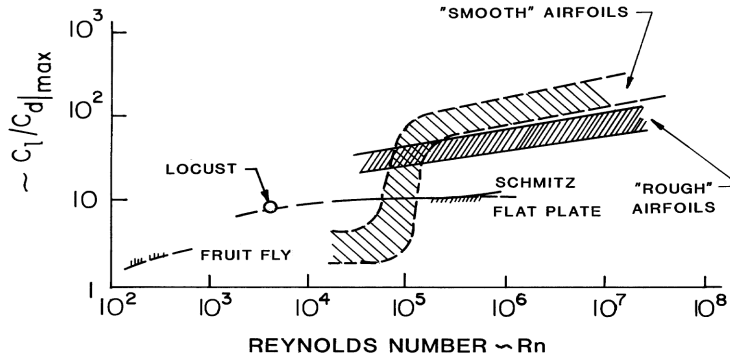
Figure 1.1: Maximum lift-to-drag ratio as a function of Reynolds number (reproduced from Ref. 36).

1.2   Literature Review

MAVs fly at low Reynolds numbers which is a term that usually refers to Reynolds numbers below 1×10^6. In low Reynolds numbers flow, viscous forces have a larger influence, and aerodynamic efficiency of airplanes generally decreases [3]. There is a broad set of literature for airfoils below a Reynolds number of 1×10^6 that includes experimental results, computational results, and design methodologies for Reynolds number range of 1×10^5 to 1×10^6 [5–11]. Some of the work includes results at lower Reynolds numbers where MAVs typically operate, but only limited experimental data for aerodynamic characteristics exist at that scale.

At low Reynolds numbers, scaling effects decrease the lift and increase the drag as illustrated in Fig. 1.1 (reproduced from McMaster and Henderson [36]). The decrease in L/D becomes more pronounced as the Reynolds number decreases to 10,000–30,000. Spedding and McArthur [13] investigated a wing with an aspect ratio of 6 and the Eppler 387 airfoil at low Reynolds numbers, and they found that the lift curve slope decreased as a function of the Reynolds number in the range of 10,000–60,000. The research presented here shows low Reynolds number (below 30,000) aerodynamics—particularly the performance of the entire airplane instead of only airfoils and wings alone.

In addition to operating at lower Reynolds numbers, MAVs operate over a larger flight regime and experience high angles of attack and larger unsteady flight conditions than larger full-scale airplanes. MAVs are capable of executing maneuvers such as perching, deep stall descent, and highly dynamic flight in confined spaces which all include flight at high angles of attack that often include unsteady flight conditions. Perching begins with a rapid increase in the angle of attack past stall to slow the airplane to a stop at a specific landing point [16, 22, 37]. Deep stall descent requires transitioning from low angles of attack to a stable high angle-of-attack flight condition. Maneuvering MAVs in confined spaces involves maneuvering at slow speeds and flight into the post-stall high angle-of-attack regime. Executing such dynamic maneuvers can cause a

3

MAV to experience an angle of attack range of almost ±180 deg and a wide range of angle-of-attack rates. Unsteady effects of changing angle of attack are normally quantified as a function of the reduced frequency, and thin airfoil theory has been extended to include the changing flow of oscillating airfoils [38–40]. Some of these methods can be used to model small unsteady effects (referred to as quasi-steady effects) [41, 42], and ongoing research [32, 43–50] continues to investigate the unsteady aerodynamics of airplanes during dynamic stall.

Flight testing allows the aerodynamic characteristics of an entire vehicle to be measured and studied. Traditionally, on-board sensors, such as inertial measurement units, are used to gather flight data [18, 51, 52]. However, the size and weight restrictions of MAVs require off-board measurement approaches that use multiple cameras to track objects based on triangulation. Many researchers have used Vicon [53] motion capture systems to provide accurate MAV positioning data to pursue controls problems such as implementing new controllers or researching multi-agent control [14–18, 21–24, 54–57]. For this research, a Vicon motion capture system with 8 to 16 T20 cameras was used to track infrared reflections from small retro-reflective markers.

Motion tracking has also been used to analyze the aerodynamics of aircraft but has only been used in a few investigations. Before modern motion tracking, simple trajectory analysis (with a tape measure and stopwatch) completed by Bauer [58] in 1975 showed the time averaged aerodynamic characteristics of a number of small MAVs in free flight. He concluded that the flow was mostly laminar and further work in laminar airfoil design was needed to increase the performance of small gliders. More recently, Vicon motion tracking technology has been applied to track and determine aerodynamic characteristics of MAVs in gliding flight. Cory and Tedrake [14, 22] used motion tracking data to model glider aerodynamics over a large range of angles of attack to aid in the development of a controller for automated perching. Figures 1.2 and 1.3 show their results for lift and drag over a large range of angles of attack. The data only shows pitch-up maneuvers because the researchers were only interested in the pitch-up maneuver and truncated the flight trajectories. The simple model shown in Fig. 1.2 and 1.3 (the red lines) was based on a flat plate model and achieved the required accuracy during the perching maneuver. No attempt was made to model nonlinear effects such as stall or the effects of angular rates. Cory and Tedrake's work showed the importance of collecting data from numerous flights in order to achieve reliable results. While their work showed that aerodynamic forces could be measured using a motion tracking system, the results lacked detailed analysis of the aerodynamics and did not attempt to model dynamic stall.

In a separate investigation, Mettler and Rhinehart [23, 24], tested a glider in free flight and presented nominal gliding flight results along with the results for a single post-stall high angle-of-attack flight. First,
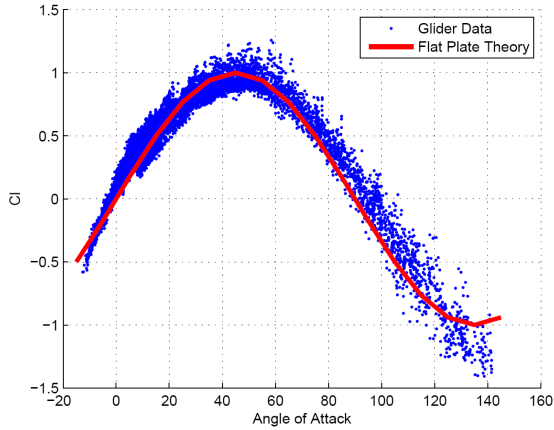
Figure 1.2: The lift coefficient as a function of angle of attack for a glider (taken from Ref. 14).
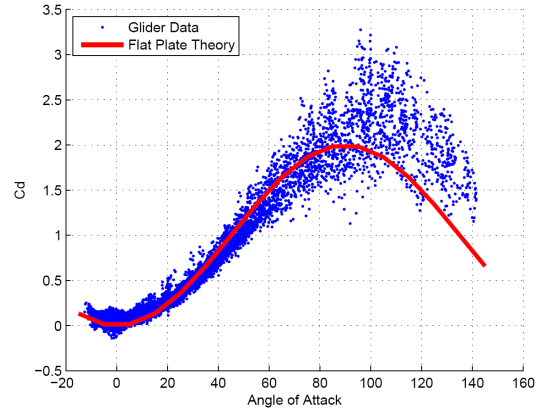
Figure 1.3: The drag coefficient as a function of angle of attack for a glider (taken from Ref. 14).
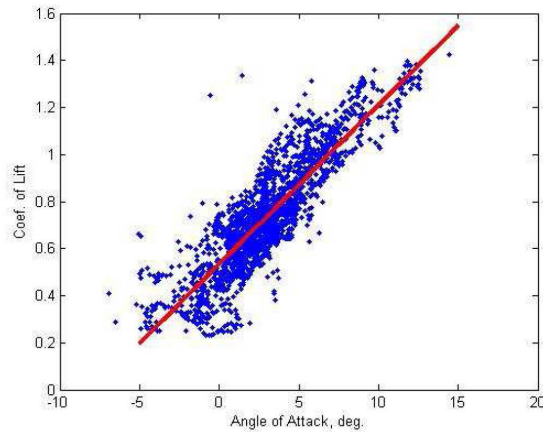
Figure 1.4: The lift coefficient as a function of angle of attack for a small glider (taken from Ref. 23).

the aerodynamic characteristics in quasi-steady nominal gliding flight were determined from the data, and the results for lift are shown in Fig. 1.4. In addition to nominal gliding flight, flight at high angles of attack was analyzed in detail to show the dynamic effects of the glider entering stall, pitching up rapidly, flying at high angles of attack and finally recovering. As shown in Fig. 1.5, the lift curve followed a dynamic stall hysteresis loop caused by the unsteady effects. Drag, shown in Fig. 1.6, also showed hysteresis due to the persistent separation at low Reynolds number. The data showed the large effect that unsteady flow has on the aerodynamic characteristics of MAV flight, and additional flight tests across a range of flight conditions need to be analyzed to better model the unsteady effects.

Flight trajectory data from MAV flight tests were used by Meckstroth and Reich [25] to generate aerodynamic coefficients for a small aircraft flying at angles of attack of up to 30 deg (above stall). The model was based on a linear lift curve, parabolic drag polar, and a linear moment coefficient and did not
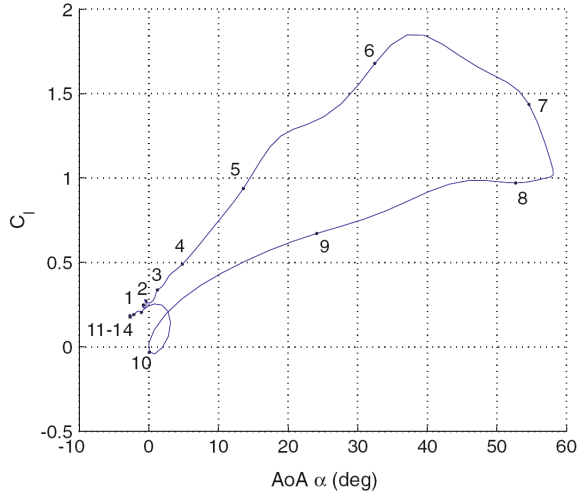
Figure 1.5: The lift coefficient as a function of angle of attack for a small glider showing the dynamic effect of changing flight conditions (taken from Ref. 24).
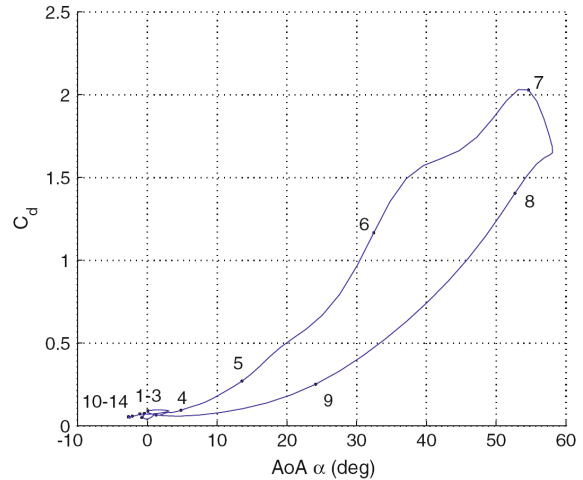
Figure 1.6: The lift coefficient as a function of angle of attack for a small glider showing the dynamic effect of changing flight conditions. (taken from Ref. 24).

account for any unsteady aerodynamics. The model was applied to guide the MAV to a state with specific velocity and orientation located 1 m from the perching location. The location was selected based on previous open-loop tests to result in a successful perch, and so the challenges of modeling unsteady aerodynamics were avoided.

Modeling unsteady high angle-of-attack flight is challenging because the aerodynamic characteristics are no longer just a function of the instantaneous angle of attack [59, 60] but depend on the time history of the angle of attack and the angle-of-attack rate. For example, a rapid increase in the angle of attack causes a dynamic stall condition which increases the stall angle of attack beyond the static stall angle [46, 47]. Models for aerodynamic characteristics during aggressive stall maneuvers need to account for unsteady behavior at angles of attack as high as 90 deg [61].

Existing methods can model lift, drag, and moment over a full range of angles of attack (± 180 deg) under steady-state conditions based on experimental results, [62–64] but modeling unsteady high angle-of-attack flight is more challenging because of the effects of angle-of-attack rate and time lag. Rapid increases in the angle of attack causes a leading edge vortex to form, and the vortex moves downstream with the flow. The vortex influences the aerodynamic characteristics, and the influence on the aerodynamic characteristics decreases as the vortex moves downstream resulting in a time dependency. An approach based on work by Goman and Khrabrov [29, 30] accounts for the unsteady effects by expanding the state-space representation of the airfoil or the aircraft to include first-order time lag with a flow separation parameter [29–34, 65–67]. During unsteady flight, the separation parameter is changed through a first-order lag differential equation

6

that is driven by a forcing function. The forcing function depends on the angle of attack, the angle-of-attack rate and a time constant. The lag in the changing separation parameter is used to model the lag associated with unsteady aerodynamic characteristics.

The state-space representation with the separation parameter as developed by Goman and Khrabrov in Refs. [29] and [30] did not rely on experimentally determined lift curve slopes and only modeled lift and moment coefficients but not drag. Later developments in the literature included higher-order polynomial models for lift and drag [33] as well as applying the method to airplanes [31, 65]. Recently, the method was adapted to model the lift coefficient of a four-element cascade wing at angles of attack up to 90 deg [34, 35]. The method was also applied to MAVs with flapping wings by including additional terms such as apparent mass and circulation effects based on Theodorsen's method [38]. The additional terms were included in the approach to account for the rapid up-and-down motion of flapping wings [32, 68]. Additionally, the state-space model was applied to unsteady delta wing lift, drag, and moment measurements [69–71]. This work expanded on the existing state-space method and applied it to fixed-wing MAVs using the data captured via motion tracking for flights with dynamic stall .

The research that was discussed shows the need to gather and model aerodynamic characteristics of MAVs from flight tests and the potential of using the Vicon system for aerodynamic analysis. The works by Cory and Tedrake [14, 22], as well as Rhinehart and Mettler [23, 24], showed how motion tracking can be used to analyze the aerodynamic performance of maneuvering MAVs. This research builds on the existing knowledge of low Reynolds number aerodynamics to further the understanding of the aerodynamic characteristics of MAVs. Furthermore, the MAV flight test data was used to develop aerodynamic models, particularly for unsteady high angle-of-attack flight based on methodology proposed by Goman and Khrabrov [29, 30]. The modeling methodology captured the lag associated with large dynamic-stall hysteresis loops and was applied to MAV flight at angles of attack exceeding 90 deg.

The goal of this dissertation is to gather experimental data for a number of MAVs from flight tests captured using a motion tracking system and to use that data to better understand and model low Reynolds number aerodynamics. The flights include quasi-steady nominal glides as well as unsteady high angle-of-attack flights with aggressive stalls. Low angle-of-attack test results show the aerodynamic characteristics in quasi-steady flight. From the data, the lift curve, drag polar, neutral point, weather vane stability, and roll due to yaw are determined. A trim point analysis is developed and used to determine the trim lift, drag, and angle of attack for numerous flights which decreases the variation caused by the quasi-steady nature of the nominal gliding flights. In addition to low angle-of-attack results, flight tests in deep stall show the lift and drag at post-stall angles of attack (up to 100 deg). Unsteady high angle-of-attack

7

results reveal the influence of the angle-of-attack rate during mild to aggressive stalls. As a result, all of the longitudinal characteristics include significant hysteresis loops due to dynamic stall effects. From the extensive unsteady high angle-of-attack flight data, a reduced-order modeling approach is first developed for the MAVs, and then the coefficients are found based on experimental flights. Results from applying the model demonstrated that the model is applicable to a wide range of flight conditions as was observed experimentally. This dissertation studies MAV aerodynamics based on flight test results and reveals the large flight envelope of MAVs. Additionally, this dissertation develops a model applicable throughout the large flight envelopes typical of MAVs.

Chapter 2

Experimental Methodology

The MAVs were tested by gathering flight trajectories of gliding uncontrolled flight in a capture volume. In order to track each airplane, reflective markers were affixed to the MAVs, and the instrumented MAVs were launched and tracked during flight tests to gather experimental data. The position and attitude time history of each flight test was captured using a Vicon motion capture system, and from the time history, aerodynamic forces and moments were determined throughout flight. Unpowered flights were used to eliminate the complexity of propeller effects. Results for five gliders are included in this work.

2.1   Test Environment

Experimental data from MAV flights were gathered using a Vicon motion capture system capable of tracking small retro-reflective markers using infrared cameras. In this research, a system with 8 to 16 Vicon T20 cameras was used, and the software provided by Vicon triangulated the location of the individual markers within the capture volume (space visible to the cameras). Three to six reflective markers were placed on each MAV in an asymmetric pattern on the wing and fuselage. The tracking system required an asymmetric arrangement of markers to ensure proper triangulation. marker selection varied between each airplane and was a combination of spherical markers [approximately 2-mm (0.08-in) to 5-mm (0.2-in) diameter] and circular stickers [approximately 7-mm (0.3-in) to 10-mm (0.4-in) diameter]. From the reflections, skeletal graphical models were constructed in the software to form objects defined as rigid sets of multiple markers. From the skeleton model, the motion capture system recorded the position and attitude time history of the test aircraft during each flight.

To gather test data, the instrumented MAVs were tracked during flights through the capture volume which varied from approximately 3.6×6.1 m (12×20 ft) with a height of approximately 3 m (10 ft) to 7.6×10 m (25×35 ft) with a height of approximately 5 m (17 ft). In the smaller capture volume 8 cameras were used. While in the larger capture volume 14 to 16 cameras were used. As the MAVs flew through the capture volume, the corresponding set of markers or object was tracked, and the Earth-referenced position

along with the Euler angles was recorded by the motion capture system at a rate of 200 Hz. The length of the trajectory time histories was limited by the size of the capture volume, and the time histories usually yielded 1–2 s of useful data for a given flight. When the system could not triangulate the object (because enough markers were not visible to enough cameras), there was a measurement void in the trajectory time history. Typically there were no voids, but sometimes measurements at one to five time steps were missing from a flight. Flights with numerous missing measurements were not included in the results.

The aerodynamic characteristics of each aircraft were observed for numerous flights that covered a variety of flight conditions. All of the tests were unpowered gliding flights that began with a hand launch, and each MAV was tested over a range of aircraft configurations including different centers of gravity, elevator deflections and launch conditions. Additionally, multiple flights for each configuration were performed to increase the number of data points. By combining multiple tests over a variety of configurations, a broader picture of the aerodynamic characteristics was observed.

From the experiments, the time histories of Earth-referenced position and Euler angles were measured by the motion capture system for each MAV flight test. In order to determine the aerodynamic characteristics of the MAVs, the velocity, forces, angular rates, and moments acting on the airplane were needed and determined from the trajectory time history as explain in the next section.

2.2   Data Processing

Multiple steps were used to determine the aerodynamic characteristics of the MAV from the raw measurements of the flight trajectory (position and attitude) which were recorded in the Earth-referenced coordinate system. First, the raw measurements were smoothed and differentiated twice with respect to time to determine the velocities and accelerations in the Earth-referenced axes system. Next, the determined velocities and accelerations needed to be transformed to the body-fixed axes system. Then, the forces and moments were determined using the aircraft mass and mass moments of inertia. Finally, the forces and moments in the body-fixed axes system were used to calculate the aerodynamic characteristics of the MAV in flight.

2.2.1   Approaches to Filtering and Differentiation

The raw measurements from the motion tracking system included uncertainty, noise, and scatter, so the raw measurements of position and attitude need to be filtered to reduce the effect of noise. The velocity and

acceleration for both the position and the Euler angles were required to determine the aerodynamic forces and moments and were found using numerical differentiation.

Numerical differentiation increases the effect of any measurement noise because the difference between two noisy measurements is taken and scaled by the time difference (sampling rate). For example, a first-order finite difference method

$$\dot{x} = \frac{x(t+1) - x(t)}{\Delta t} \tag{2.1}$$

increases the noise when applied to a time dependent variable with uncertainty. In this example, x represents the time dependent variable, and it could be any of the Euler angles or components of the position vector. The standard deviation $\sigma_{x(t)}$ is used to represent the measurement uncertainty as a function of time. Noise increases [24] due to the finite difference method as in

$$\sigma_{\dot{x}} = \frac{\sigma_{x(t+1)} + \sigma_{x(t)}}{\Delta t} \tag{2.2}$$

Assuming the standard deviation $\sigma_{x(t)}$ is independent of time $(\sigma_{x(t+1)} = \sigma_{x(t)})$ results in

$$\sigma_{\dot{x}} = \frac{2\sigma_x}{\Delta t} \tag{2.3}$$

which shows the uncertainty in x doubles due to subtraction and scales with the time between measurements Δt (the inverse of the sampling frequency). When taking the second derivative, the increase in uncertainty is larger because four measurements are used and Δt is squared. In order to reduce the noise in the final results, filtering techniques are needed for the raw measurements, and the derivatives must be found using methods to reduce the effect of numerical differentiation. Post-processing occurs after the flight is complete so non-causal filters (often referred to as smoothing) can be used to take advantage of the complete time history.

A number of filtering and smoothing methods were explored to determine accurate measurements for the position and attitude time history as well as the velocities and accelerations for both the position and attitude. Prior to smoothing, any time steps in the trajectory (the position and attitude) where the system was unable to triangulate the aircraft were estimated using a linear regression on the neighboring points. After filling in these few points (less than 1%), the raw measurements were smoothed and differentiated. A variety of methods such as Kalman smoothing, low pass filtering, and higher-order finite difference methods were explored. In the following paragraphs, results for the polynomial regression method, the robust smoothing method and low pass filtering method are shown in more detail.
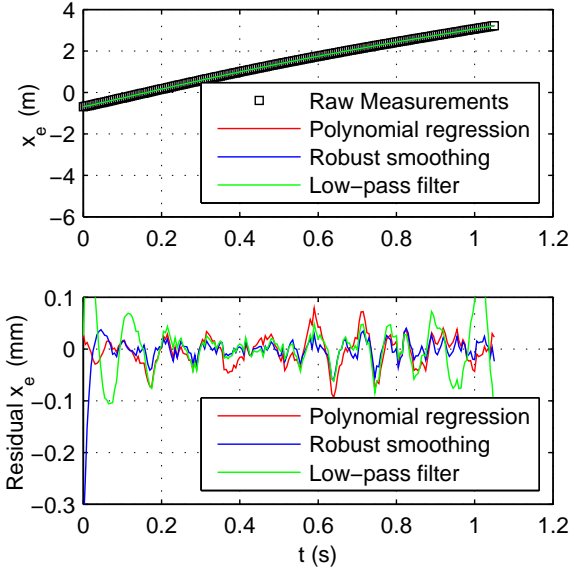
Figure 2.1: An example using one axis of the measured Earth-referenced position (x_e) from a single airplane flight to illustrate the three filtering techniques that where explored in detail and the residuals of each of the techniques.
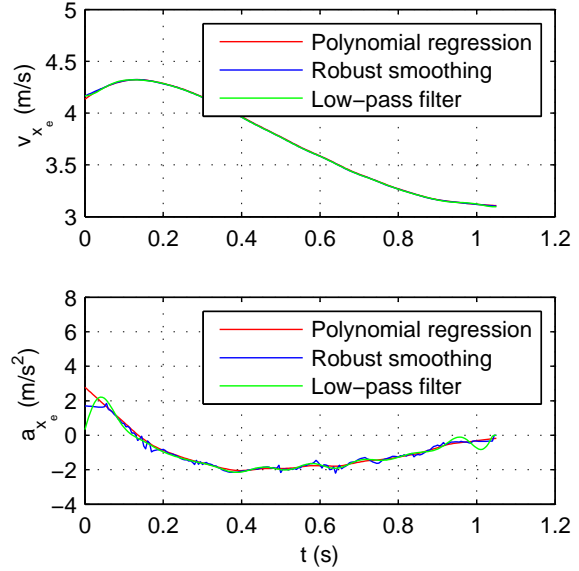
Figure 2.2: An example using one axis of the measured Earth-referenced position (x_e) from a single airplane flight to illustrate the three differentiation methods that were used to find the Earth-referenced velocity v_{x_e} and acceleration a_{x_e}.

Figure 2.1 shows a comparison of the selected smoothing and filtering techniques as applied to the Earth-referenced x direction for a single flight recorded at 200 Hz. The polynomial regression results used the Savitzky-Golay algorithm with a third-order polynomial and a moving time window of 33 raw measurements [51, 72, 73]. Next, the robust smoothing method used a robust locally weighted scatter plot smoothing which iteratively calculated a second-order polynomial over a moving time window while minimizing the weight of outlying points [74]. The final method shown is an eighth-order low pass Butterworth filter that was applied both backward and forward to eliminate time lag.

At both the beginning and end of the time history, the three methods often diverged from the raw measurements and each other. This behavior is not unexpected, because at both ends of the data, the smoothing and filtering methods have to use asymmetric windows of data. Through trial-and-error, it was found that small adjustments to the beginning and end point of the window to be post-processed often eliminated this behavior. Additionally, in some cases, the first or last few data points were trimmed from the processed results to remove the divergent points. The results in Fig. 2.1 show that the three methods exhibit few variations in the middle region of the test data (approximately 0.2–0.9 s) and the robust smoothing and low-pass filter diverge at the end of the flight.

In addition to filtering (or smoothing) the raw measurements, the velocity and acceleration need to be determined for both the position and attitude. Figure 2.2 shows the derivatives found using the three different methods for one Earth-referenced axis (x_e) of an single airplane flight. Within the Savitzky-Golay algorithm, the velocity and acceleration for the polynomial regression method was determined by differentiating the polynomial for each time step. For the robust smoothing and the low-pass filter, a first-order finite difference method was used on smoothed or filtered measurements to determine the velocity. The finite difference of the velocity was used to determine the acceleration. As shown in Fig. 2.2, the results for the three methods are almost the same for the velocity, and the three methods follow the same trends for acceleration but have slight variations. Even though it is barely noticeable on the graph, the robust smoothing result has sharp changes in acceleration, and the low-pass filter had some divergence at both ends. The polynomial regression result for acceleration is continuous throughout the time history with minimal divergence at the ends.

The three methods provided a smoothed estimate of the Earth-referenced aircraft trajectory (x_e, y_e, z_e, ϕ, θ, and ψ) as well as the Earth-referenced velocity ($\dot{x}_e$, $\dot{y}_e$, $\dot{z}_e$), acceleration ($\ddot{x}_e$, $\ddot{y}_e$, $\ddot{z}_e$), angular velocity ($\dot{\phi}$, $\dot{\theta}$, and $\dot{\psi}$), and angular acceleration ($\ddot{\phi}$, $\ddot{\theta}$, and $\ddot{\psi}$) throughout the MAV flight tests. Fully processed results were investigated with a variety of filtering techniques. However, polynomial regression smoothing was selected for the results presented because the smoothed position and acceleration had less divergence at the end points, and the smoothed acceleration data results were nearly continuous with little variation.

2.2.2 Calculating Aerodynamic Forces and Moments in the Body-Axes System

The motion tracking data in the Earth-fixed frame was transformed to the airplane body-fixed frame (defined by an axes system with x out the nose and y out the right wing) for aerodynamic analysis. In order to rotate between the two axes systems, a standard rotation matrix through the three Euler angles (ϕ, θ, and ψ) was used, that is

$$\mathbf{R} = \begin{bmatrix} \cos\theta\cos\psi & \cos\theta\sin\psi & -\sin\theta \\ \sin\phi\sin\theta\cos\psi - \cos\phi\sin\psi & \sin\phi\sin\theta\sin\psi - \cos\phi\cos\psi & \sin\phi\cos\theta \\ \cos\phi\sin\theta\cos\psi - \sin\phi\sin\psi & \cos\phi\sin\theta\sin\psi - \sin\phi\cos\psi & \cos\phi\cos\theta \end{bmatrix} \tag{2.4}$$

Position, velocity, and acceleration vectors can be translated between the Earth-fixed and body-fixed frame using the matrix in Eq. 2.4. The location on the airplane tracked by cameras did not correspond exactly to the airplane center of gravity. A small rotational offset (three Euler angles) between the tracked orientation and the body-fixed axes system generated an offset rotation matrix $\mathbf{R}_{TB}$ using Eq. 2.4. The attitude of the

airplane was found from

$$\mathbf{R}_{EB} = \mathbf{R}_{ET}\mathbf{R}_{TB} \tag{2.5}$$

where $\mathbf{R}_{ET}$ is the attitude recorded at each time step. From the matrix $\mathbf{R}_{EB}$, the Euler angles of the airplane were calculated, and the angular velocity and acceleration in the Earth-fixed frame were found using smoothing and numerical difference methods discussed in Section 2.2.1. Similar to the angular offset, an offset vector $\mathbf{r}$ represented the measured distance from the tracked point to the center of gravity of the airplane, and $\mathbf{r}$ was used when determining the velocity and acceleration.

The accelerations and velocity in the airplane body frame were determined using a set of transformations. First, the body-fixed angular velocity $\boldsymbol{\omega}$ was determined from the Euler angle rates given by

$$
\begin{bmatrix} p \\ q \\ r \end{bmatrix} = \begin{bmatrix} 1 & 0 & -\sin\theta \\ 0 & \cos\phi & \sin\phi\cos\theta \\ 0 & -\sin\phi & \cos\phi\cos\theta \end{bmatrix} \begin{bmatrix} \dot{\phi} \\ \dot{\theta} \\ \dot{\psi} \end{bmatrix} \tag{2.6}
$$

and next, the body-fixed angular acceleration $\dot{\boldsymbol{\omega}}$ was determined using

$$
\begin{bmatrix} \dot{p} \\ \dot{q} \\ \dot{r} \end{bmatrix} = \begin{bmatrix} 1 & 0 & -\sin\theta \\ 0 & \cos\phi & \sin\phi\cos\theta \\ 0 & -\sin\phi & \cos\phi\cos\theta \end{bmatrix} \begin{bmatrix} \ddot{\phi} \\ \ddot{\theta} \\ \ddot{\psi} \end{bmatrix}
$$
$$
+ \begin{bmatrix} 0 & 0 & -\dot{\theta}\cos\theta \\ 0 & -\dot{\phi}\sin\phi & -\dot{\theta}\sin\phi\sin\theta + \dot{\phi}\cos\phi\cos\theta \\ 0 & -\dot{\phi}\cos\phi & -\dot{\theta}\cos\phi\sin\theta - \dot{\phi}\sin\phi\cos\theta \end{bmatrix} \begin{bmatrix} \dot{\phi} \\ \dot{\theta} \\ \dot{\psi} \end{bmatrix} \tag{2.7}
$$

from the Euler angle rates and accelerations.

Third, the Earth-referenced accelerations $[\ddot{x}_e \ \ddot{y}_e \ \ddot{z}_e]^T$ were used to determine the acceleration in the body-fixed frame at each time step, that is

$$\mathbf{a}_b = \mathbf{R}_{EB}[\ddot{x}_e \ \ddot{y}_e \ \ddot{z}_e]^T + \dot{\boldsymbol{\omega}} \times \boldsymbol{r} + \boldsymbol{\omega} \times (\boldsymbol{\omega} \times \mathbf{r}) \tag{2.8}$$

where $\boldsymbol{\omega}$ represents the angular velocity (from Eq 2.6) and $\mathbf{a}_b$ is the acceleration in the body-fixed frame $[a_{b,x} \ a_{b,y} \ a_{b,z}]^T$. Finally, the velocity in the airplane body-fixed frame (u, v, and w) was determined using

$$[u \ v \ w]^T = \mathbf{R}_{EB}[\dot{x}_e \ \dot{y}_e \ \dot{z}_e]^T + (\boldsymbol{\omega} \times \mathbf{r}) \tag{2.9}$$

14

where $[\dot{x}_e \ \dot{y}_e \ \dot{z}_e]^T$ are the Earth-fixed velocities. The total inertial speed

$$V = \sqrt{u^2 + v^2 + w^2} \tag{2.10}$$

was found from the three components of velocity, and V was used as the total airspeed because the air in the test volume was assumed to be quiescent. With the angular velocity, angular acceleration, translational velocity, and translational acceleration known in the body-fixed frame, the aerodynamic characteristics of the MAV were determined as discussed next.

The angle of attack and sideslip angle were calculated from the inertial velocity components using

$$\alpha = \tan^{-1}(w/u) \tag{2.11a}$$

$$\beta = \sin^{-1}(v/V) \tag{2.11b}$$

because two assumptions were made. First, the air in the test volume was assumed to be quiescent (as was already assumed with V in Eq. 2.10), and second, the induced flow effects are negligible. Time derivatives of the angles were taken to yield $\dot{\alpha}$ and $\dot{\beta}$.

Body-axes accelerations $\mathbf{a}_b$ obtained from the motion track in Eq. 2.8 were used in

$$\mathbf{F}_{ext} = m\mathbf{a}_b \tag{2.12}$$

to determined the external force acting on the aircraft. By subtracting other forces such as gravity

$$\mathbf{F}_G = mg \left[-\sin\theta \quad \sin\phi\cos\theta \quad \cos\phi\cos\theta \right]^T \tag{2.13}$$

the aerodynamic force $\mathbf{F}_{aero}$ acting on the aircraft was found using

$$\mathbf{F}_{aero} = \mathbf{F}_{ext} - \mathbf{F}_G \tag{2.14}$$

The resulting force vector

$$\mathbf{F}_{aero} = \left[F_{aero,x} \quad F_{aero,y} \quad F_{aero,z} \right]^T \tag{2.15}$$

contained the components of the aerodynamic force in the body-fixed frame (as previously defined with x out the nose and y out the right wing) which were used to determine the aerodynamic loading on the airplane. To calculate lift and drag, the forces in the body-fixed frame were transformed [42, 51, 75] to the

wind referenced frame using

$$L = -F_{aero,z} \cos \alpha + F_{aero,x} \sin \alpha \tag{2.16a}$$

$$D = -F_{aero,z} \sin \alpha \cos \beta - F_{aero,x} \cos \beta \cos \alpha - F_{aero,y} \sin \beta \tag{2.16b}$$

The resulting lift and drag force in the wind axes were nondimensionalized to analyze the aircraft performance throughout flight using

$$C_L = \frac{L}{qS_{ref}} \tag{2.17a}$$

$$C_D = \frac{D}{qS_{ref}} \tag{2.17b}$$

where S_{ref} is the wing reference area for the airplane, and q is the dynamic pressure based on V.

The moments on the airplane were calculated from the changing attitude of the airplane using

$$\frac{d(\mathbf{I}\,\boldsymbol{\omega})}{dt} = \mathbf{M}_{ext} \tag{2.18}$$

Starting with the body-fixed angular velocity $\boldsymbol{\omega}$ from Eq. 2.6, angular acceleration $\dot{\boldsymbol{\omega}}$ from Eq.2.7 and the inertia matrix $\mathbf{I}$, the moments acting on the airplane were found using the rotational equations of motion [24, 51],

$$\mathbf{M}_{ext} = \mathbf{I}\dot{\boldsymbol{\omega}} + \boldsymbol{\omega} \times \mathbf{I}\boldsymbol{\omega} \tag{2.19}$$

where $\mathbf{M}_{ext}$ included all of the moments acting on the airplane. The roll, pitch, and yaw moment (L, M, and N, respectively) were the three components of the moment vector and were nondimensionalized

$$C_l = \frac{L}{qS_{ref}b} \tag{2.20a}$$

$$C_m = \frac{M}{qS_{ref}\bar{c}} \tag{2.20b}$$

$$C_n = \frac{N}{qS_{ref}b} \tag{2.20c}$$

using the wingspan b, the mean aerodynamic chord $\bar{c}$, and the dynamic pressure q.

The resulting time histories of lift, drag, and moment coefficients were used to determine the aerodynamic characteristics of the aircraft throughout flight. Multiple flights were used to ascertain general trends in the aerodynamic characteristics across a variety of flight conditions and to reduce the effects of measurement uncertainty from any one flight.

Table 2.1: Physical Properties of the Five MAVs Tested

	Vapor		SU-26xp		Model glider	
Mass	14.44 g	(0.5094 oz)	36.93 g	(1.303 oz)	8.738 g	(0.3082 oz)
Wing properties						
Span	37.47 cm	(14.75 in)	40.05 cm	(15.76 in)	24.41 cm	(9.61 in)
Area (S_{ref})	546.3 cm^2	(84.67 in^2)	312.5 cm^2	(48.42 in^2)	144.00 cm^2	(22.32 in^2)
Chord (at root)	15.00 cm	(5.90 in)	10.20 cm	(4.00 in)	6.58 cm	(2.59 in)
Aspect ratio ($\mathcal{R}$)	2.56		5.12		4.13	
Incidence angle	3.0 deg		2.0 deg		3.5 deg	
Dihedral	9.5 deg		0		8.0 deg	
Airfoil camber	6.7%		0%		0%	
Length	38.74 cm	(15.25 in)	34.93 cm	(13.75 in)	31.32 cm	(12.33 in)
Stabilator area (S_h)	175.9 cm^2	(27.27 in^2)			19.4 cm^2	(3.01 in^2)
Horizontal tail area (S_h)			79.87 cm^2	(12.38 in^2)		
Elevator area			51.48 cm^2	(7.979 in^2)		
Vertical fin area	99.87 cm^2	(15.48 in^2)	45.24 cm^2	(7.012 in^2)	11.1 cm^2	(1.72 in^2)
I_{xx}	369.9 g cm^2	(2.022 oz in^2)	1255. g cm^2	(6.861 oz in^2)	113.8 g cm^2	(0.622 oz in^2)
I_{yy}	1129. g cm^2	(6.173 oz in^2)	2461. g cm^2	(13.45 oz in^2)	658.4 g cm^2	(3.600 oz in^2)
I_{zz}	1242. g cm^2	(6.792 oz in^2)	3569. g cm^2	(19.51 oz in^2)	761.2 g cm^2	(4.161 oz in^2)
I_{xz}	87.57 g cm^2	(0.479 oz in^2)	42.07 g cm^2	(0.230 oz in^2)	31.86 g cm^2	(0.174 oz in^2)

	Balsa Glider (High $\mathcal{R}$)		Balsa Glider (Low $\mathcal{R}$)	
Mass	7.42 g	(0.263 oz)	5.91 g	(0.209 oz)
Wing properties				
Span	35.56 cm	(14.00 in)	25.02 cm	(9.85 in)
Area (S_{ref})	107.8 cm^2	(16.71 in^2)	103.1 cm^2	(15.98 in^2)
Chord (at root)	3.18 cm	(1.25 in)	4.32 cm	(1.70 in)
Aspect ratio ($\mathcal{R}$)	11.7		6.07	
Incidence angle	0 deg		0 deg	
Polyhedral	15 deg		15 deg	
Airfoil camber	3.1%		2.6 %	
Length	23.01 cm	(9.06 in)	22.90 cm	(9.02 in)
Stabilator area (S_h)	19.4 cm^2	(3.01 in^2)	18.7 cm^2	(2.91 in^2)
Vertical fin area	3.98 cm^2	(0.618 in^2)	6.11 cm^2	(0.947 in^2)
I_{xx}	290.8 g cm^2	(1.590 oz in^2)	126.2 g cm^2	(0.690 oz in^2)
I_{yy}	275.7 g cm^2	(1.507 oz in^2)	280.7 g cm^2	(1.535 oz in^2)
I_{zz}	561.4 g cm^2	(3.069 oz in^2)	402.0 g cm^2	(2.198 oz in^2)
I_{xz}	7.34 g cm^2	(0.040 oz in^2)	7.42 g cm^2	(0.041 oz in^2)

2.3 Test Aircraft

In the work presented in this dissertation, five different airplanes were tested to determine their aerodynamic characteristics at low Reynolds number. Table 2.1 lists the physical properties of all five airplanes. The geometric characteristics (wingspan, chord, etc,) of each airplane were measured using either a ruler or a caliper, and each airplane was weighed. The mass moments of inertia were calculated by subdividing the airplane into small parts and using the weight and location of each piece to determine the moments of inertia. A brief description of each airplane follows:
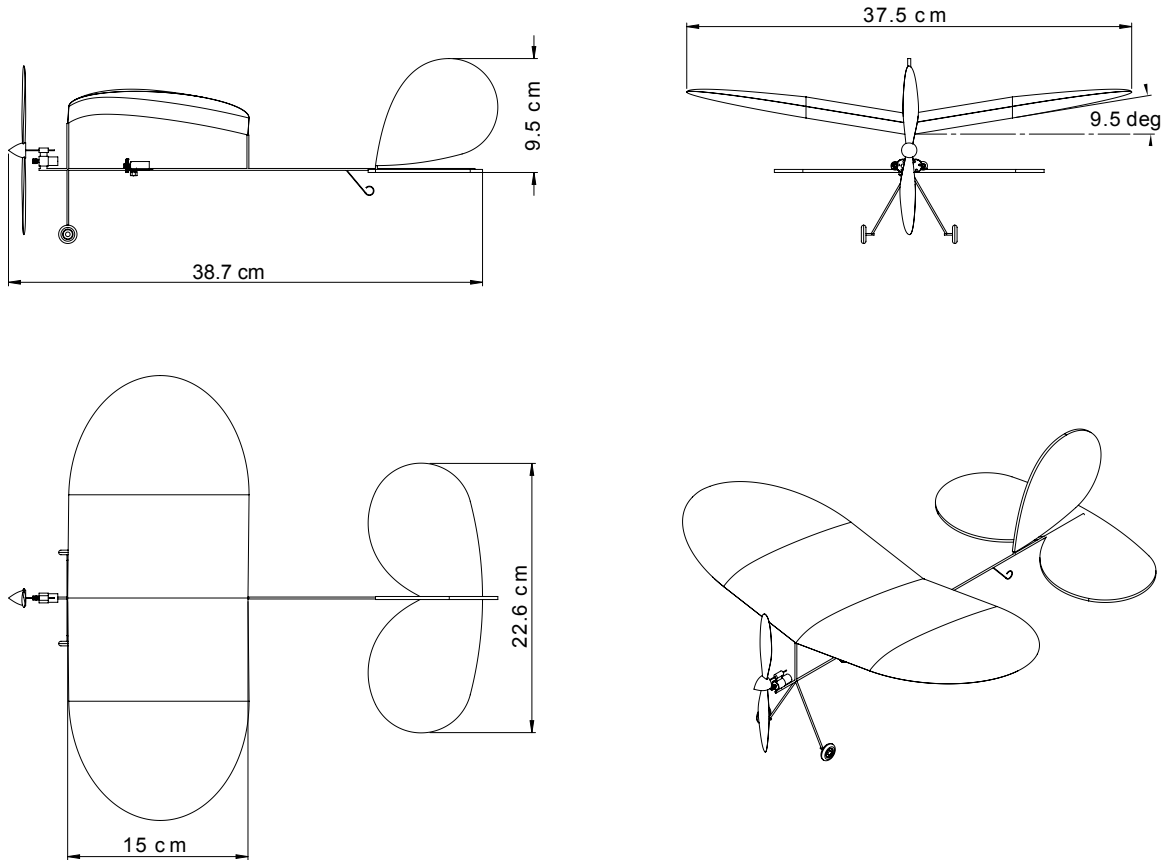
Figure 2.3: A three-view drawing showing the geometry of the Vapor aircraft.

Vapor: The Vapor is a commercially manufactured airplane [76] which has a 37.47-cm (14.75-in) wingspan and weighs 14.44 g (0.5094 oz). A three-view drawing of the Vapor is shown in Fig. 2.3, and the airplane has a nominal cruise Reynolds number based on the mean aerodynamic chord of approximately 22,000 [77]. The airframe was constructed with carbon fiber supports and cambered ribs for the main wing. A thin plastic film was stretched over the wing and tail structures to form membrane aerodynamic surfaces.

SU-26xp: The SU-26xp is another commercially manufactured RC airplane [78] and is shown in Fig. 2.4 with reflective markers attached. It weighed 36.93 g (1.303 oz), had a wingspan of 40.05 cm (15.76 in) and flew at a Reynolds number of approximately 26,000 [79]. It was constructed from expanded polystyrene foam and had linearly tapered wing with an aspect ratio of 5.12 and an 11% thick symmetric airfoil. The tail surfaces were thin flat plates and included an elevator and rudder that were actuated using servos. In addition, the wing had actuated ailerons. A small battery-powered RC receiver controlled servos for the four control surfaces and a speed controller for the miniature electric motor. Only glide

tests were performed, so the propeller was removed while the motor remained in place so the center of gravity would be close to the desired value.

Model Glider: Figure 2.5 shows the free-flight model glider with the reflective markers attached. The model glider was constructed from 1 mm Depron foam and a balsa wood fuselage [79]. The incidence angle of the horizontal tail could be adjusted, and the nominal flight Reynolds number was 15,000.

Balsa Gliders: Two balsa gliders were designed and constructed based on concepts for low Reynolds number glider plans published by Frank Zaic [80, 81]. Both gliders had similar fuselage and tail configurations with the vertical tail extending down below the horizontal tail as shown in Figs. 2.7 and 2.6. The downward extension of the vertical tail matched the plans, and the design decision is not uncommon for MAVs. As a result of the downward direction of the vertical tail, the horizontal tail could be positioned on top of the fuselage without physically interfering with the vertical tail. Both wings had similar wing areas, but different aspect ratios—6.07 and 11.7. The wings had polyhedral with the center portion being flat and the outboard section having dihedral. For the balsa gliders, the nominal Reynolds numbers were 12,000 and 10,000 for an aspect ratio of 6.07 and 11,7, respectively.
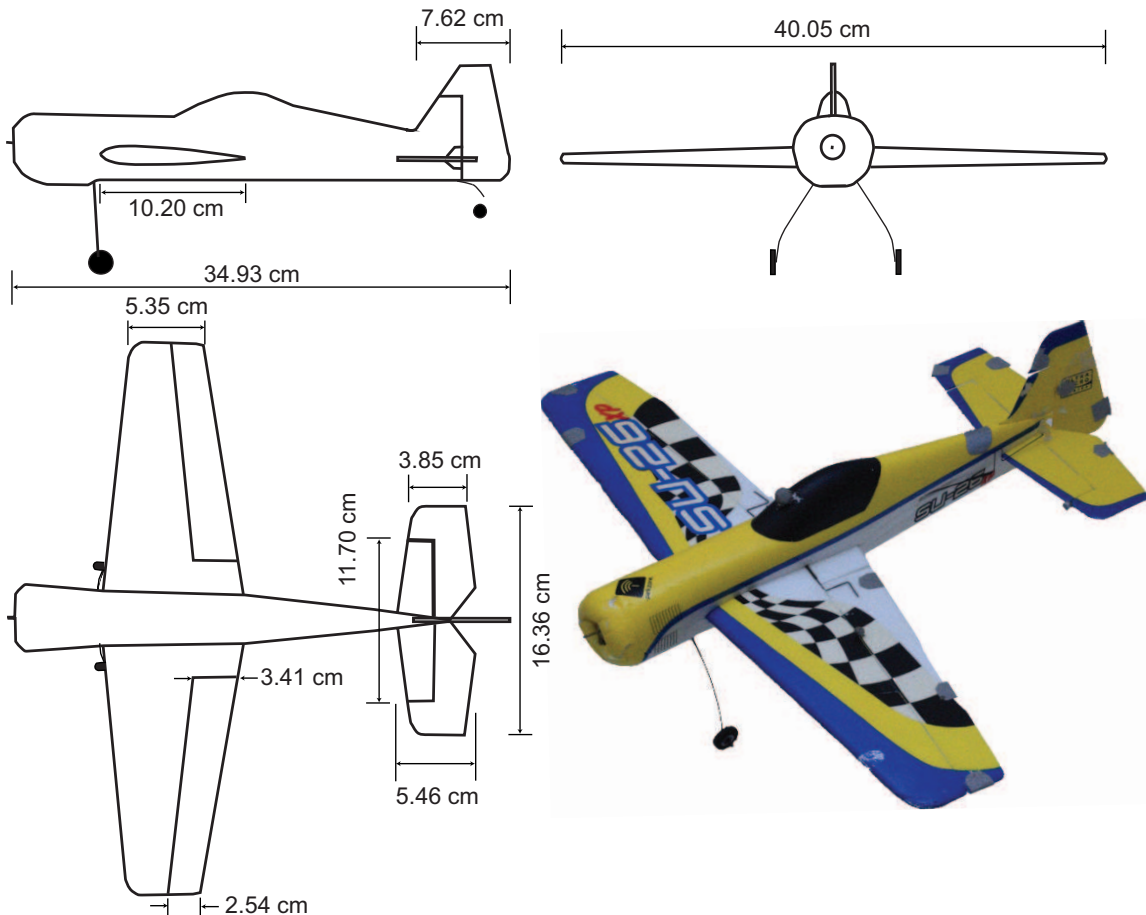
Figure 2.4: A three-view drawing of the SU-26xp with an isometric photograph showing the attached reflective markers.
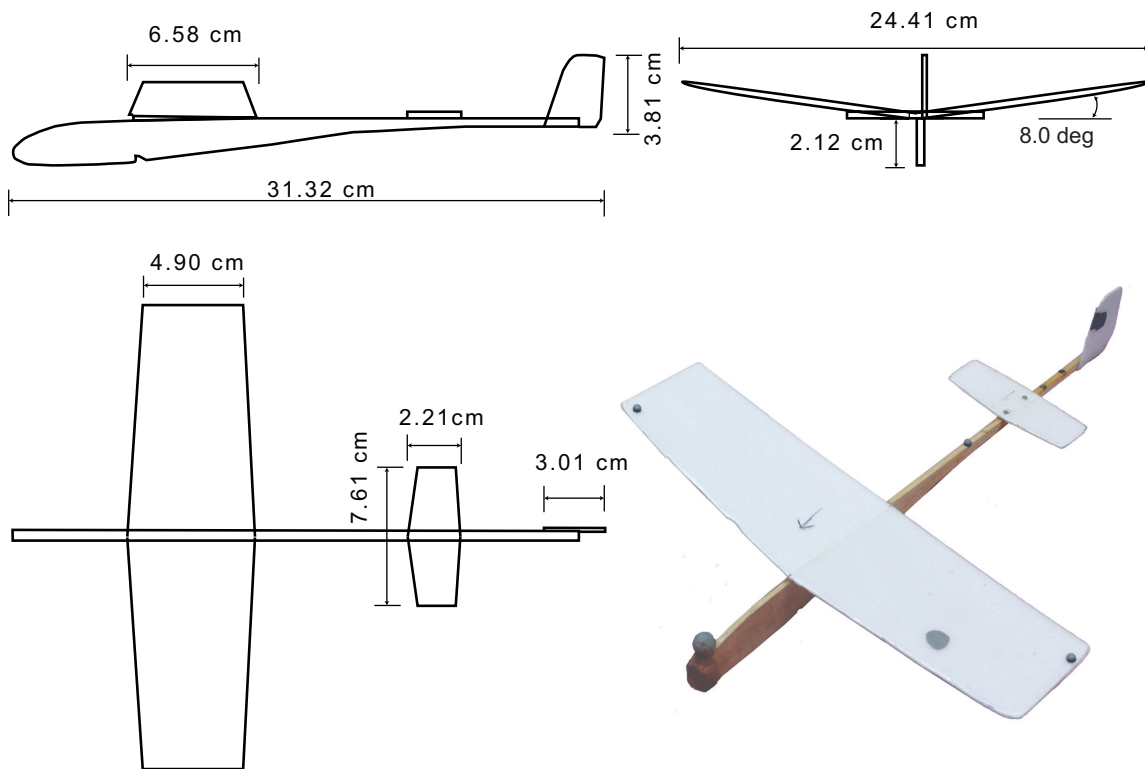
Figure 2.5: A three-view drawing of the model glider with an isometric photograph showing the attached reflective markers.
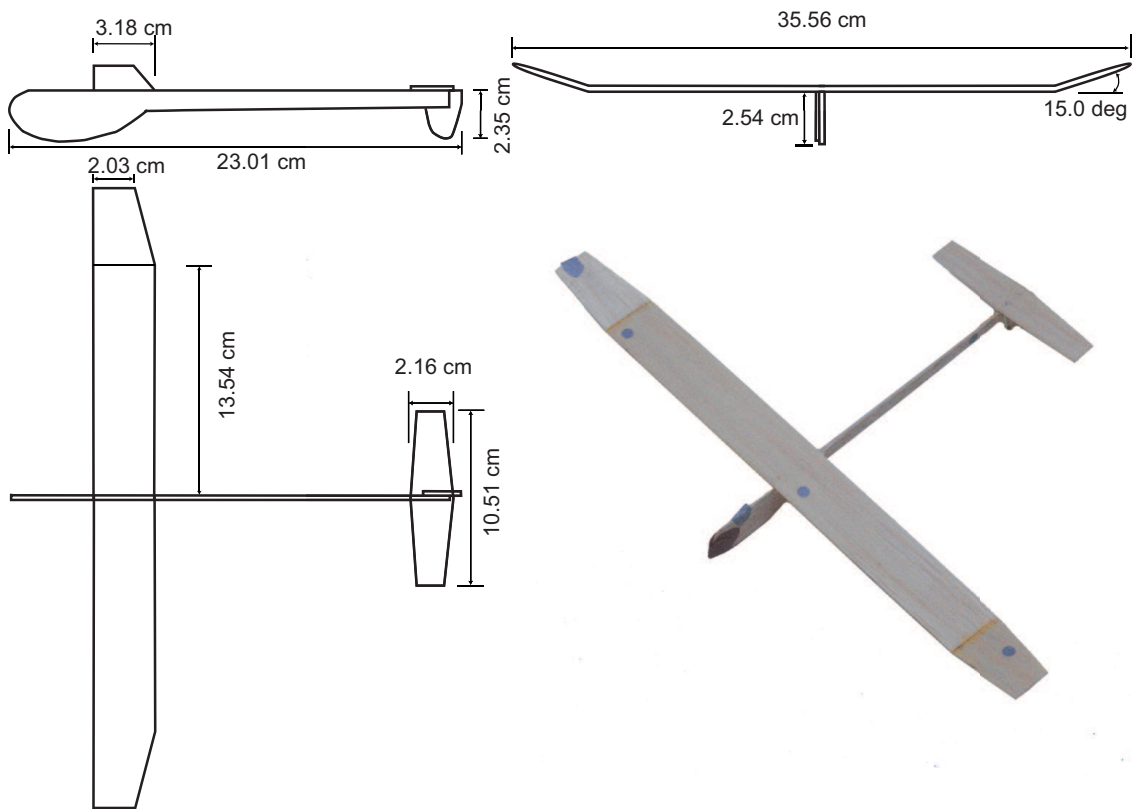
Figure 2.6: A three-view drawing of the 11.7 aspect ratio balsa glider with an isometric photograph showing the attached reflective markers.
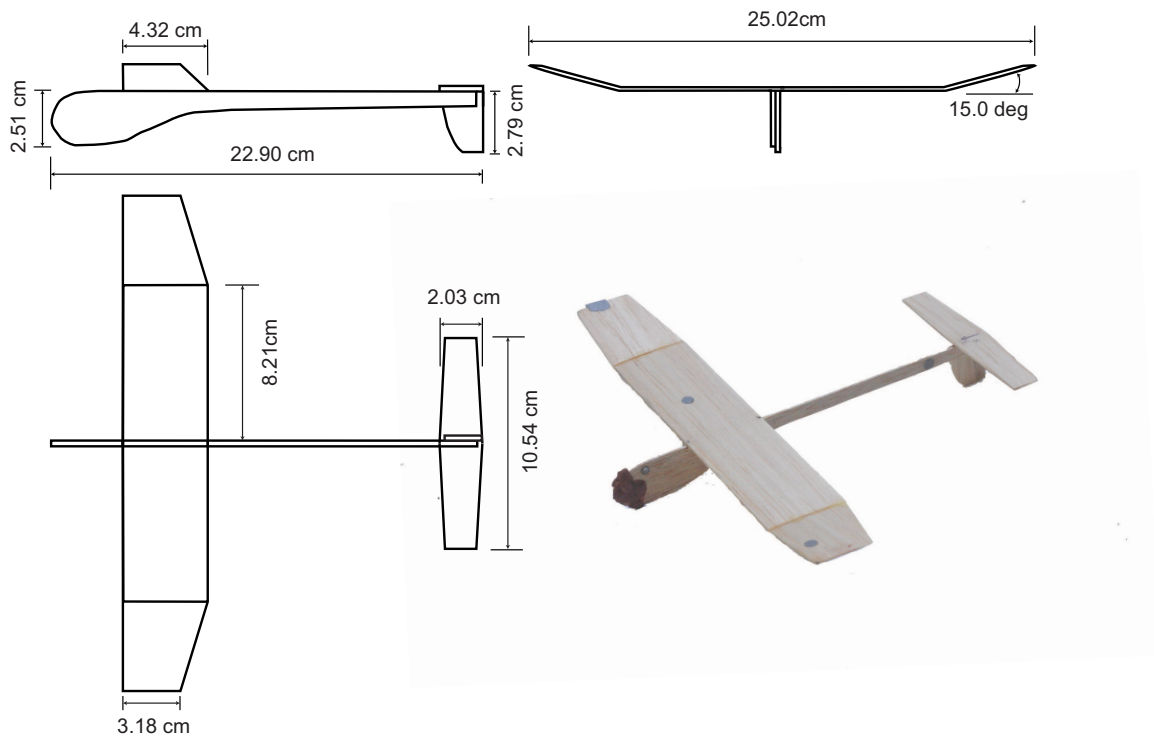
Figure 2.7: A three-view drawing of the 6.07 aspect ratio balsa glider with an isometric photograph showing the attached reflective markers.

Chapter 3

Verification of the Motion Tracking System

In order to understand the uncertainty in the aerodynamic characteristics determined from the captured motion trajectories, the accuracy of the tracking system measurements was quantified experimentally through a variety of tests. First, stationary tests were used to analyze the noise within the measurements of each MAV. Second, a rotating rod attached to an optical encoder was used to verify angular measurements during motion. Next, a sphere accelerating due to gravity was used to verify the acceleration measurements. Finally, repeatability tests showed that the aerodynamic characteristics from a free-flight model glider were consistent across repeated launches. The uncertainties in the final derived quantities (such as C_L, α or C_D) varied between the different aircraft and were determined based on the uncertainty in the stationary noise measurements of each MAV tested. While uncertainty exists within the final results, the tests showed the system can accurately measure aerodynamic characteristics.

3.1 Analysis of Uncertainty in the Motion Capture Trajectories

A MAV with markers attached was positioned at rest in the motion capture volume in order to gather stationary test results to analyze the variations in the measurement from the Vicon system. Figure 3.1 shows a time history of the position and attitude during a 2.5 s stationary test recorded at 200 Hz for the Vapor aircraft. From the results, the standard deviation for the distance measurement was 0.079 mm (0.0031 in), and the standard deviation for the norm of the Euler angle vector was 0.034 deg. The standard deviation for all components of the position and attitude for the Vapor are listed in Table 3.1 along with the results from a comparable noise analysis by Mettler [24] that showed similar uncertainties in the position and slightly larger uncertainties in the attitude. The slight difference in the uncertainties was mostly due to differences in marker separation because Mettler's airplane was half the size of the Vapor MAV used in this test. Additional causes for the difference include the setup of camera coverage, marker size, marker visibility, and the distance between the cameras and the aircraft.
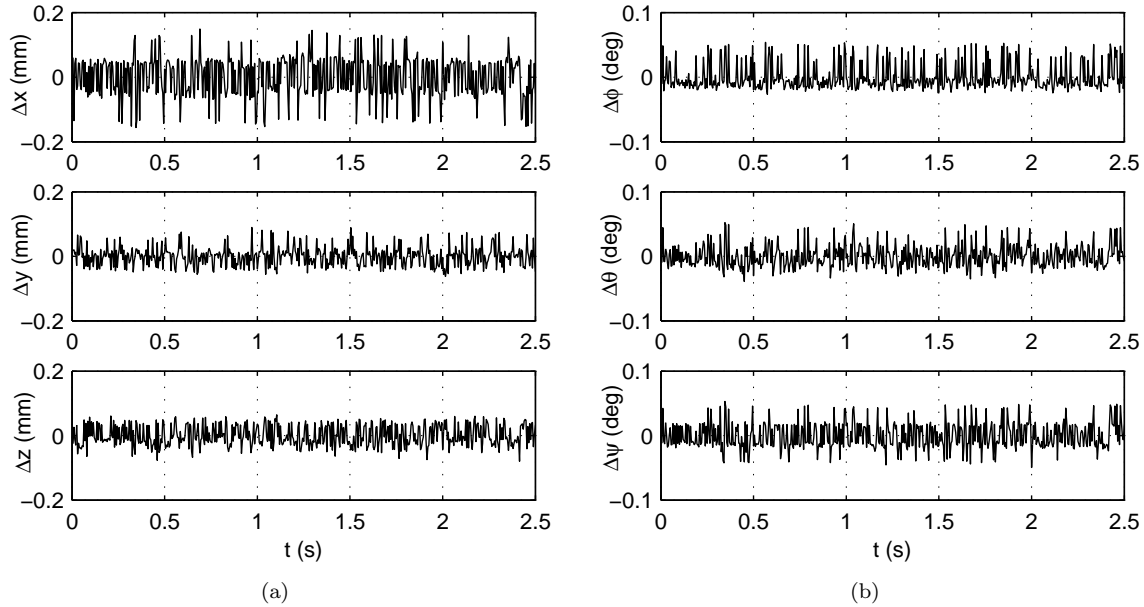
Figure 3.1: The 2.5 s time history of the (a) position and (b) attitude of the stationary Vapor aircraft showing minute measurement noise.

Similar stationary tests were completed for all of the aircraft listed in Section 2.3, and the results are tabulated in Table 3.2. In all of the cases the noise was minute, and as shown in Fig. 3.2, there was a trend with aircraft size—the larger aircraft had smaller uncertainties due to the greater marker separation and the smaller aircraft had larger uncertainties. The two exceptions to the general trend in Fig. 3.2 were the Vapor and SU-26xp. Both MAVs were tested with only eight cameras as opposed to 14–16 cameras for the other MAVs. The uncertainty in the derived aerodynamic properties for each aircraft (see Section 3.3) will be discussed after explaining the additional system verification tests.

In addition to the stationary test, a rotating rod was tracked to quantify the uncertainty of the motion tracking system during simple motion. The rod rotated about an end that was attached an optical rotary encoder which provided data for comparison to the captured motion trajectory. The data from the optical encoder was recorded at 512 Hz using an US Digital H6-1800-I-S optical encoder that was accurate to

Table 3.1: Standard Deviation for the Position and Attitude Components for a Stationary 2.5 s Motion Track Recorded at 200 Hz

Position (mm)	x	y	z
Vapor Data	0.0650	0.0303	0.0329
Mettler Glider [24]	0.077	0.083	0.044
Attitude (deg)	ϕ	θ	ψ
Vapor Data	0.0207	0.0175	0.0208
Mettler Glider [24]	0.051	0.022	0.038

Table 3.2: Standard Deviation for the Position and Attitude Components for Six MAVs.

Aircraft	Position (mm)			Attitude (deg)			wingspan (cm)
	σ_x	σ_y	σ_z	σ_ϕ	σ_θ	σ_ψ	b
Vapor	0.0650	0.0303	0.0329	0.0207	0.0175	0.0208	37.47
SU-26xp	0.0587	0.0382	0.0554	0.0314	0.0323	0.0231	40.05
Model Glider	0.0242	0.0463	0.0258	0.0207	0.0252	0.0172	24.41
Balsa Glider (AR=11.7)	0.0250	0.0179	0.0251	0.0137	0.0172	0.0094	35.56
Balsa Glider (AR=6.07)	0.0424	0.0261	0.0252	0.0221	0.0637	0.0237	25.02
Mettler Glider [24]	0.077	0.083	0.044	0.051	0.022	0.038	18
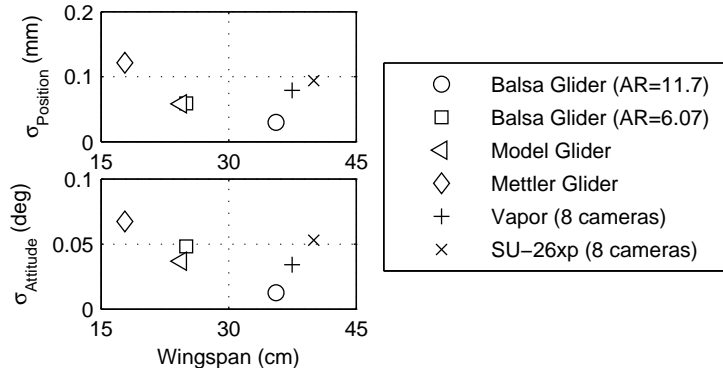
Figure 3.2: The standard deviation for the position and attitude decreases with wingspan.

0.05 deg [82]. Reflective markers were attached to the center of rotation and the tip of the rod. The two markers were measured to be 25.73 cm (10.13 in) apart. The motion track of the tip of the rod formed an arc, and the relative angle was calculated from the captured trajectory.

Figure 3.3 shows a comparison of the angle measured by the optical encoder to the results from the captured motion trajectory. During the stationary portion (the first 0.5 s), the residual is within ±0.04 deg. The uncertainty range is similar to that for the attitude of the stationary aircraft which is shown in Fig. 3.1(b). When the rod started to rotate, the residual peaked to 0.2 deg and was almost an order of magnitude larger than the stationary tests. Once motion was established (after $t \approx 1$ s), the residual decreased to ±0.06 deg which is small but larger than what it was during the stationary portion of the test.

Next, the acceleration of a 5.4-kg (12-lb) cast iron sphere (shot put) in free fall was used to verify the accelerations determined from the captured motion tracking trajectories. Two forces were acting on the 11-cm (4.4-in) diameter sphere as it fell from approximately 1.6 m (5.3 ft)—the gravitation force of approximately 53 N (12 lb) and aerodynamic drag. From theoretical steady-state spherical drag [83] calculations, the drag force estimated was 0.01–0.07 N (0.003–0.02 lb) depending on the velocity of the sphere which corresponded to a deceleration of 0.002–0.01 m/s^2 (0.007–0.04 ft/s^2) for the sphere.
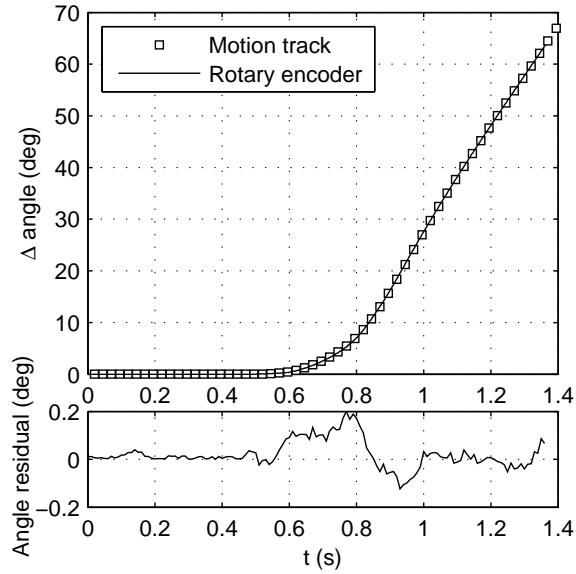
Figure 3.3: Angular measurements from the motion tracking system compare with measurements from an optical rotary encoder.

Six circular sticker-type markers were placed on the sphere to allow the motion tracking system to capture the free-fall trajectory. All of the visible markers at each time instance were used in a least squares regression to locate the center of the sphere formed by the markers, and the time history of the center of the sphere formed the trajectory. A second-order polynomial regression of each trajectory (height versus time) was used to calculate the acceleration during five free fall tests. The trajectories were trimmed at the beginning and the end to remove the effects of release and the impact with a deceleration system on the floor. Figure 3.4 shows the raw trajectories normalized to match the initial time and height and the residuals of the second-order polynomial regression for each test.

Figure 3.5 shows the constant acceleration determined from the second-order polynomial regression, the mean of experiments, and the theoretical acceleration due to gravity. The error bars are used to illustrate the sensitivity of each test to changing the start and end time for the second-order regression. The start and endpoint were varied by 11 points (for up to 121 combinations) to show how changing the range would modify the test results, and the error bars for each test show one standard deviation of the 121 different accelerations. The mean of tests results is 9.800 m/sec^2 (32.152 ft/sec^2) which is slightly less than the local gravity taken from geodetic surveys of localized gravity [84, 85]. Local gravity was found to be 9.8012 m/sec^2 (32.1562 ft/sec^2) using Talbot Laboratory* as the location (the tests were conducted in the basement) [86]. The mean of the five tests is slightly less than the local value of gravity, which is expected

*located at 104 South Wright Street Urbana, IL 61801, N 40.111 deg, W -88.228 deg
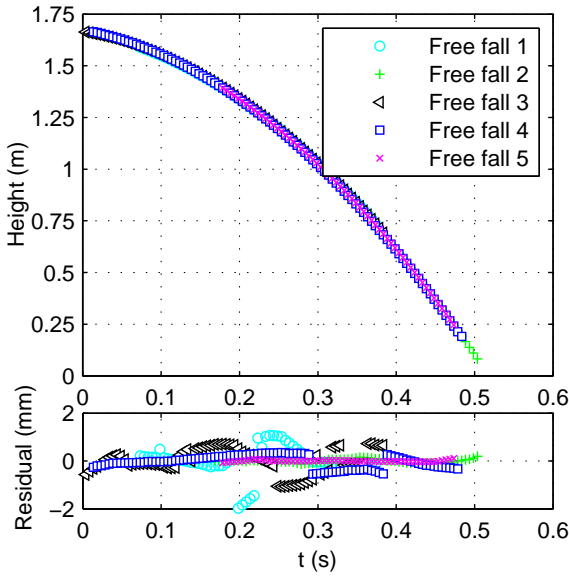
Figure 3.4: The trajectory as a function of time during five free falls with the start time and start height normalized, and the residuals of the second-order regression.
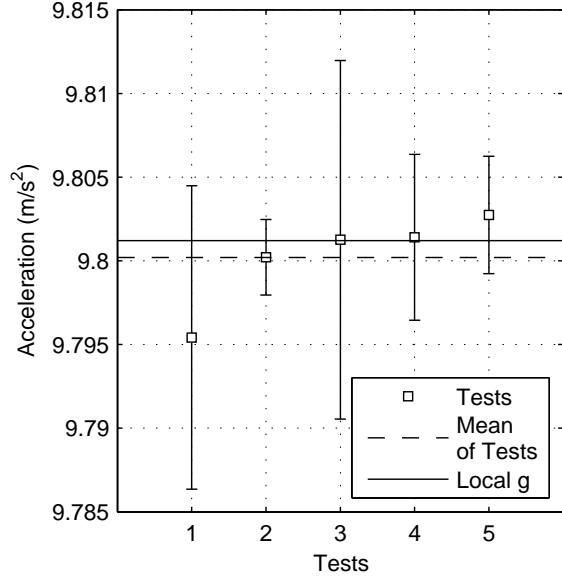
Figure 3.5: The acceleration determined from a second-order polynomial regression for the free-fall tests with the bars showing the sensitivity to the start and end point selection.

because of aerodynamic drag. The measured gravity is within 0.01% of local gravity [within 0.0012 m/sec^2 (0.0042 ft/sec^2)] which shows that the captured motion trajectories are accurate enough to determine the acceleration of an object and hence the forces acting on the object.

3.2 Repeatability of Flight Test Results

The final system verification method involved repeatability tests with a small model glider. The tests were conducted using a rail launching system to achieve consistent initial flight conditions with the free-flight model glider. The model glider weighed approximately 8.738 g (0.3082 oz) and operated at a cruise Reynolds number of approximately 16,000 [79]. The launch rail was placed at an inclined angle, and a cart carrying the airplane was accelerated down the track by a falling weight. At the end of the track the cart fell down and separated from the airplane as the airplane started to glide. The launch conditions could be adjusted by changing the acceleration of the cart and the angle of the track incline. By repeating launches with the same conditions, a set of initial conditions could be repeated across multiple flights, and the repeatability of measurements from the system could be gauged by examining the flight conditions and the determined aerodynamic characteristics of the airplane.
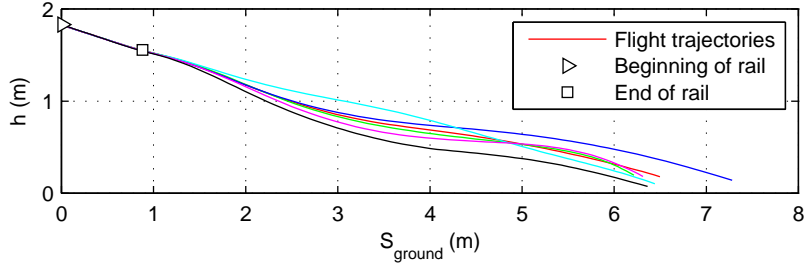
Figure 3.6: Distance traveled during six different repeatability tests with the triangle and square markers respectively indicating the location of the start and end of the launching rail.
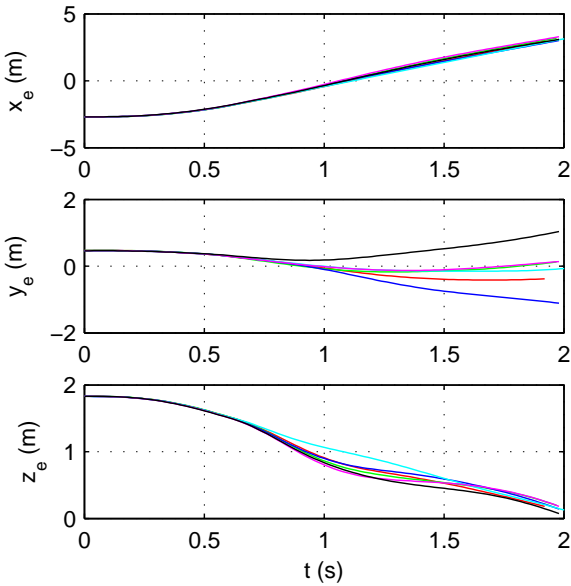
Figure 3.7: The position track of six flights with repeatable initial conditions.
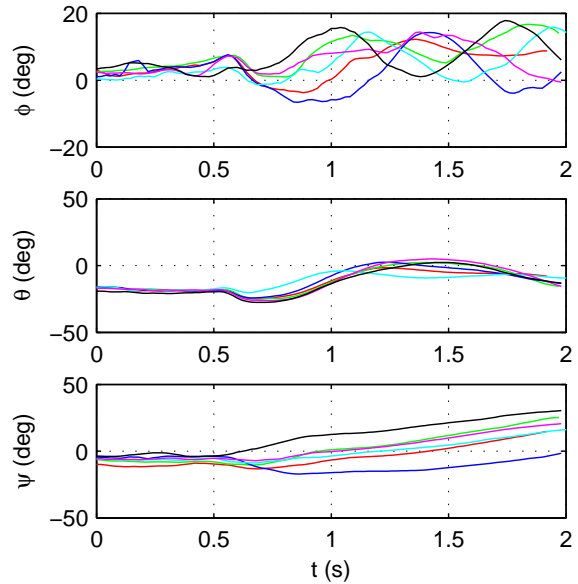
Figure 3.8: The attitude track of six flights with repeatable initial conditions.

Figure 3.6 shows the height of the airplane as a function of the distance traveled during six rail-launched flights. The small triangle approximates the beginning of the rail, and the small square approximates the point where the airplane separated from the cart and started to glide. The color coding is consistent across Figs. 3.6–3.10 for each flight. Each flight had the same launch conditions starting at a height of approximately 1.8 m (6 ft) and ending on or close to the floor. While all the flights showed a similar trend, there are some differences in the flight paths. Figures 3.7 and 3.8 show the similarity of airplane trajectory in each axis and direction across the six flights. The heading angle ψ had the most variation which was caused by the initial yaw angle varying between -3 and -10 deg. Inconsistencies in the initial yaw angle caused the variation in the flight path (illustrated by y_e in Fig. 3.7) and in the yaw angle time history (illustrated by ψ in Fig. 3.8). Figure 3.9 shows the velocity history of the airplane was consistent across the flights.

29
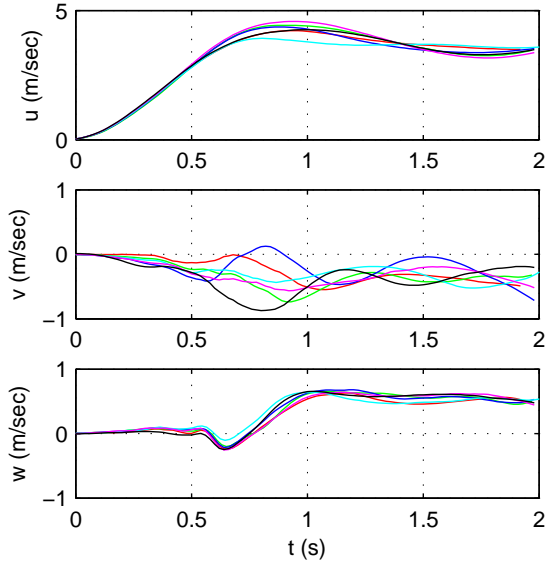
Figure 3.9: The time history of the velocity from six flights with repeatable initial conditions.
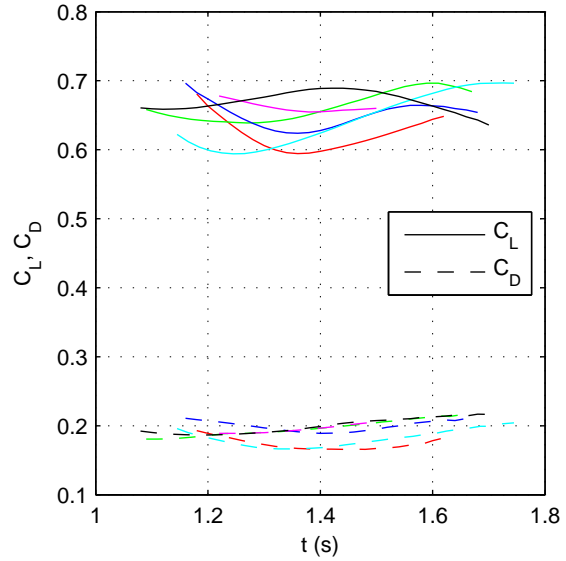
Figure 3.10: The time history of the lift and drag coefficients from six flights with repeatable initial conditions.
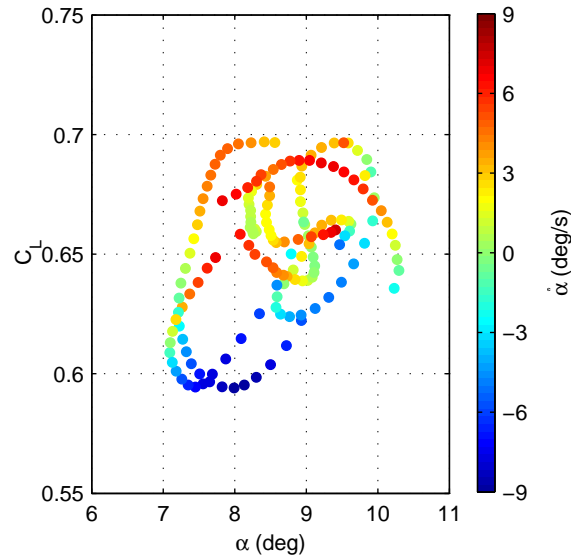
Figure 3.11: Lift coefficient as a function of angle of attack and rate of change of angle of attack for six repeatability flights.

The lift and drag coefficients were found by processing the six flights and are shown in Fig. 3.10. A limited time history was used for C_L and C_D to ignore the changing conditions immediately after launch and at the end of each flight. Across the set of tests, C_L varies between 0.6 and 0.7 while C_D fluctuates close to 0.2. Figure 3.11 shows the lift coefficient as a function of angle of attack which accounts for some of the variation.
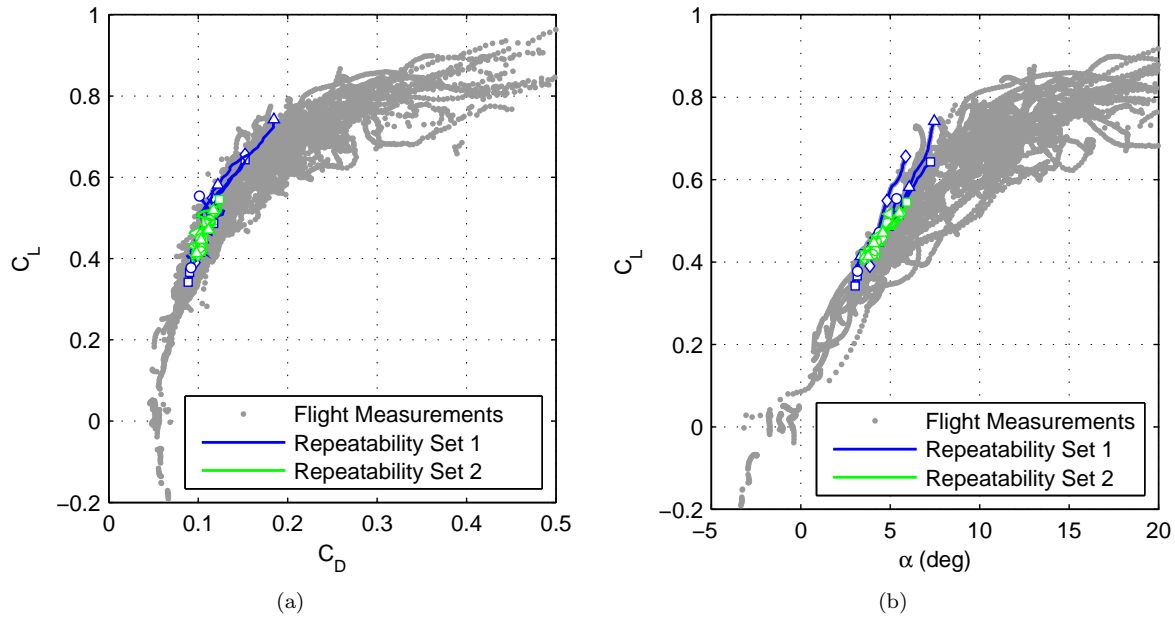
Figure 3.12: Experimental (a) drag polar and (b) lift curve for two sets of five flights with each set having different initial conditions co-plotted with data from over 50 flight tests.

Variation due to unsteady effects of angle-of-attack rate $\dot{\alpha}$ is shown by the color of the markers in Fig. 3.11. The points with increasing angle of attack ($\dot{\alpha} > 0$) had a larger value of C_L while points with decreasing angle of attack ($\dot{\alpha} < 0$) had lower values for C_L. Unsteady effects of the angle-of-attack rate are expected to cause variation in the lift. This set of repeatability flights presented a number of complete trajectories as well as demonstrated the repeatability of the aerodynamic forces being measured by the system.

Another series of repeatability tests used 10 flights with two different launch conditions. After launch, each flight had an angle of attack that was above trim, and the angle of attack decreased to the trim value of approximately 4.5 deg. In Fig. 3.12, the first five flights are shown in blue with each flight designated by a different marker. After the first five flights, the launch speed was increased for the second set of five flights which are shown in Fig. 3.12 with green lines and different markers for each flight. The second five flights covered a smaller angle of attack range than the first five flights because the initial angle of attack for the second five flights was lower due to the increased forward velocity at launch.

In the background of Fig. 3.12, the lift and drag data from over 50 hand launched flights (over 10,000 data points) are co-plotted with the repeatability results. While there is a greater spread in the hand-launched results, the two sets of repeatability results are in agreement with the general trend of the 50 flights.

Figure 3.13, shows a 2D histogram from over 50 launches of the model glider. Each small colored square shows how many data points are within each small bin of α and C_L or C_D and C_L. Even though the flight
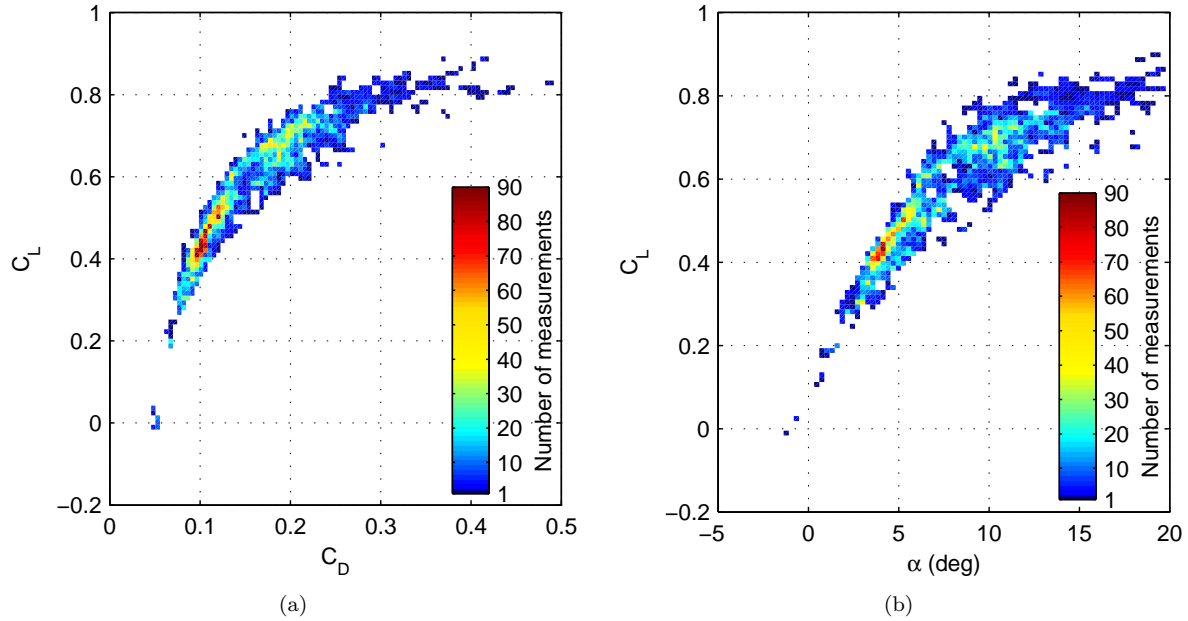
Figure 3.13: A 2D histogram for the (a) drag polar and (b) lift curve where the color of each small square represents the number of measurements recorded during 50 flight tests.

measurements are spread out and have outliers, the histograms in Fig. 3.13 show that the majority of data points are clustered along the expected trend lines and some of the scatter in Fig. 3.12 is due to outliers.

3.3 Uncertainty Propagation

The uncertainties in the determined aerodynamic characteristics depend on the uncertainties of the measured aircraft position and attitude. The standard deviation from the stationary tests (listed in Table 3.2), along with measurement uncertainties for the physical properties of each MAV and for the density of the air, were used to determine the uncertainty in each of the aerodynamic characteristics. The standard deviation for each of the determined aerodynamic characteristics was found using the root-sum-square (RSS) method [87]. Each determined quantity (such as α or C_L) was a function (generically designated as R here) of the measurements as outlined in Section 2.2.2 and the RSS method used the function for the determined quantity

$$R = f(x, y, z, \phi, \theta, \psi, b, \bar{c}, S_{ref}, \rho) \tag{3.1}$$

32

As outlined for the RSS method, the uncertainties were combined using partial derivatives of function R as in

$$\sigma^2_{combined} = \left(\frac{\partial R}{\partial x}\sigma_x\right)^2 + \left(\frac{\partial R}{\partial y}\sigma_y\right)^2 + \left(\frac{\partial R}{\partial z}\sigma_z\right)^2 + \left(\frac{\partial R}{\partial \phi}\sigma_\phi\right)^2 + \left(\frac{\partial R}{\partial \theta}\sigma_\theta\right)^2 + \left(\frac{\partial R}{\partial \psi}\sigma_\psi\right)^2 + \left(\frac{\partial R}{\partial b}\sigma_b\right)^2$$
$$+ \left(\frac{\partial R}{\partial S_{ref}}\sigma_{S_{ref}}\right)^2 + \left(\frac{\partial R}{\partial \bar{c}}\sigma_{\bar{c}}\right)^2 + \left(\frac{\partial R}{\partial \rho}\sigma_\rho\right)^2 + \left(\frac{\partial R}{\partial m}\sigma_m\right)^2$$

$$(3.2)$$

By finding the partial derivatives in Eq. 3.2 based on the different equations in Section 2.2.2, the uncertainties in all of the derived terms were found. For the flow angles (α and β), the partial derivatives from Eq. 2.11 were used to find the flow angle uncertainties. Similarly, the partial derivatives of Eq. 2.10 were use to find σ_V. The uncertainties for the nondimensional aerodynamic coefficients were found based on partial derivatives of Eqs. 2.17 and 2.20, and the standard deviation for the determined quantities are tabulated in Table 3.3 for the five aircraft. No clear trend exists with aircraft scale as previously shown for the uncertainties of the position and attitude measurements because the determined aerodynamic characteristics and flow conditions include additional variables such as aircraft weight, moments of inertia, and reference dimensions (S_{ref}, $\bar{c}$, and b) as well as the nominal flight speed and attitude. The resulting values in Table 3.3 show the standard deviation in the determined aerodynamic coefficients caused by the uncertainty in the measured position, attitude, physical properties, and the density of the air.

Aeroelastic deflections of the MAVs would increase the noise because the markers would move relative to each other. If the markers were far enough out of place, the tracking system would be unable to triangulate the object. Most of the aircraft were stiff so only minor deflections were observed, but the wing of the Vapor are flexible and deflect under loads. Statically loading a wing with weights determined the deflections of the wing for 2-g and 4-g loads to be 2 and 6 deg, respectively. Deflections on the order of 2 to 6 deg increased the standard deviation of C_L and the roll rate between 20% and 40%. The other coefficients were impacted much less by wing deflections (5–10%). After analyzing the data, large g loads were not found even in the aggressive dynamic stall results. Those flights had large values for C_L and C_D, but the g load was small because the large values of the coefficients corresponded with small values for the velocity (and dynamic pressure). Hence, the g loads remained small typically less than 1.5 or 2. As a result the effect of large deflections on the uncertainty were not included in the analysis.

Table 3.3: The Standard Deviation in the Determined Flow Conditions and Aerodynamic Characteristics for each MAV.

Aircraft	V (m/s)	α (deg)	β (deg)	C_L	C_D	C_Y	C_m	C_l	C_n
Vapor	0.015	0.0087	0.023	0.011	0.022	0.010	0.0060	0.00086	0.0028
SU-26xp	0.0036	0.0082	0.0014	0.028	0.029	0.020	0.030	0.0023	0.0049
Model Glider	0.0022	0.0065	0.0013	0.011	0.0097	0.017	0.023	0.00077	0.0041
Balsa Glider ($\mathcal{R}$=11.7)	0.0017	0.0035	0.00062	0.010	0.0082	0.0058	0.013	0.00081	0.0012
Balsa Glider ($\mathcal{R}$=6.07)	0.0050	0.021	0.0018	0.013	0.018	0.011	0.050	0.0012	0.0045
mean of all aircraft	0.0028	0.0096	0.0015	0.015	0.017	0.013	0.024	0.0012	0.0035

3.4   Discussion of System Verification

The analysis of the motion tracking system showed that the flight trajectories could be used to determine the aerodynamic characteristics of MAVs. Testing stationary MAVs showed that the accuracy of the motion tracking system for both the position and attitude measurements depended on the aircraft size and camera coverage. Using comparison data from a rotational encoder, the changing angle between two tracked markers was captured and showed the minute uncertainties for moving objects. Repeatedly dropping a dense sphere showed that the motion tracking system accurately measured the acceleration of the sphere which had an almost negligible drag force and a significant known gravitational force acting on it.

Testing an MAV under the same initial conditions showed the repeatability of the captured trajectories. The determined aerodynamic characteristics were consistent across different repeatability flights and showed some unsteady effects that can be attributed to the angle-of-attack rate. Additionally, two sets of five repeatability flight tests showed that changing the initial conditions varied the initial flight angle of attack as expected. From the uncertainty results, the accuracy of the trajectories captured by the motion tracking system were quantified and the analysis showed that a motion tracking system can be used to accurately determine the aerodynamic characteristics of small MAVs in free flight.

Propagating the standard deviation from the raw trajectory measurements to the determined aerodynamic characteristics provided insight on the uncertainty within the reported results. The uncertainties in the determined quantities varied between the airplanes because the uncertainties depended on physical properties and flight characteristics, but they are generally small.

Chapter 4

Quasi-Steady Flight Test Results

Flight tests in the nominal gliding regime were completed for the five airplanes discussed in Section 2.3 to determine aerodynamic characteristics of each plane in quasi-steady flight. The lift and drag characteristics for the Vapor, SU-26xp, and the two balsa gliders are shown in the nominal gliding regime, and the longitudinal and some of the lateral stability terms are shown for the SU-26xp, the free-flight glider, and the two balsa gliders.

4.1 Experimental Lift and Drag

The Vapor, SU-26xp, and the two balsa gliders (with different aspect ratios) were used to investigate the lift and drag performance in quasi-steady nominal gliding flight. Complete time histories of 14 flight tests were used to determine the flight characteristics of the Vapor aircraft. Results in these flights include an angle of attack range between -5 and 20 deg.

For the Vapor, complete time histories of 14 flight tests were used where the angle of attack was below stall for the airplane. For the SU-26xp, over 150 flight tests were used to analyze the lift and drag at different trim conditions from an angle of attack of 0 to 20 deg with most flight tests close to stall. A large number of flights (75 to 100) yielded aerodynamic data for the two balsa gliders for an angle of attack range of -2 and 16 deg. Additionally, the two balsa gliders were trimmed for quasi-stable deep stall flight to gather data at angles of attack between 20 and 105 deg.

4.1.1 Vapor in Nominal Gliding Flight

Data from 14 quasi-steady flights covered a range of initial conditions were collected, and Fig. 4.1 shows the trajectories of the hand-launched flights at the recording rate of 200 Hz. The trajectories were truncated when the airplane either approached landing or flew out of the capture volume. During each quasi-steady flight, the angle of attack and hence the lift and drag, varied as illustrated in Fig. 4.2. Unsteady aerodynamic effects are present in the data and will be discussed later in this section.
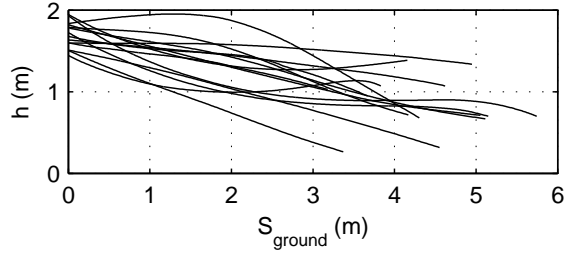
Figure 4.1: The quasi-steady flight trajectories of the MAV.

(a)

(b)
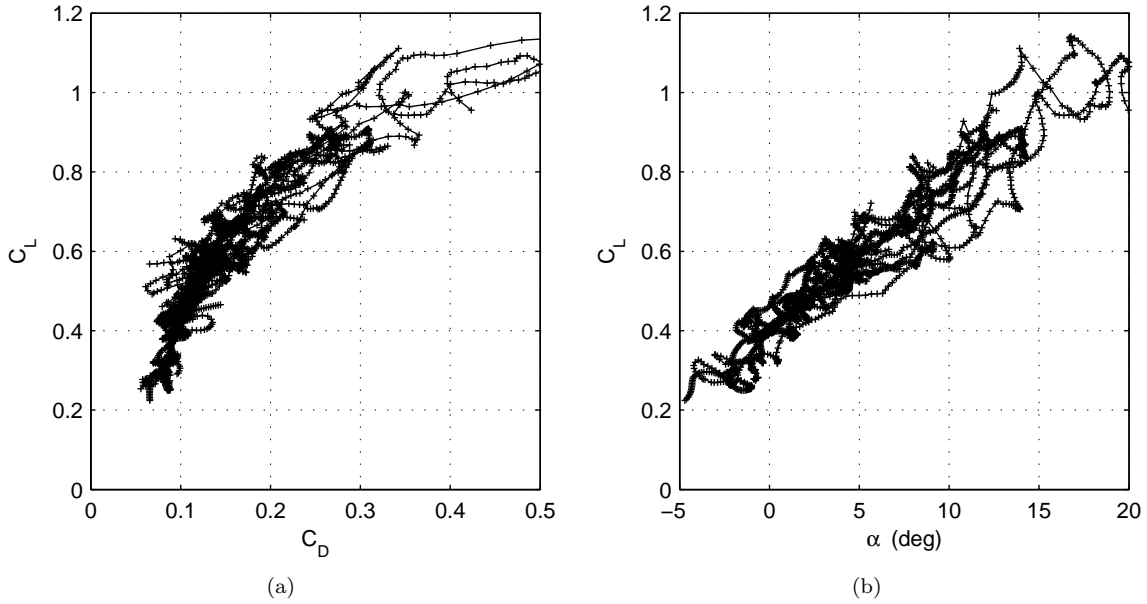
Figure 4.2: Experimental (a) drag polar and (b) lift curve for the quasi-steady flights of the Vapor.

The trajectories were conditionally sampled so that only time history segments with lower angular rates (< 30 deg/s) were used for a regression on the lift curve and drag polar. Quasi-steady data points with relatively larger angular rates were removed to reduce the effect of angular rates on the lift curve and drag polar. Figure 4.3 shows the conditionally-sampled low angular rate data with a least squares parabolic regression for the drag polar and a linear regression for the lift curve. Figure 4.3(a) shows the drag polar for the conditionally-sampled experimental data along with a parabolic drag polar regression in the form

$$C_D = C_{D_o} + KC_L^2 \tag{4.1}$$

where KC_L^2 is the induced drag of the airplane, that is

$$C_{D_i} = KC_L^2 \tag{4.2}$$

36
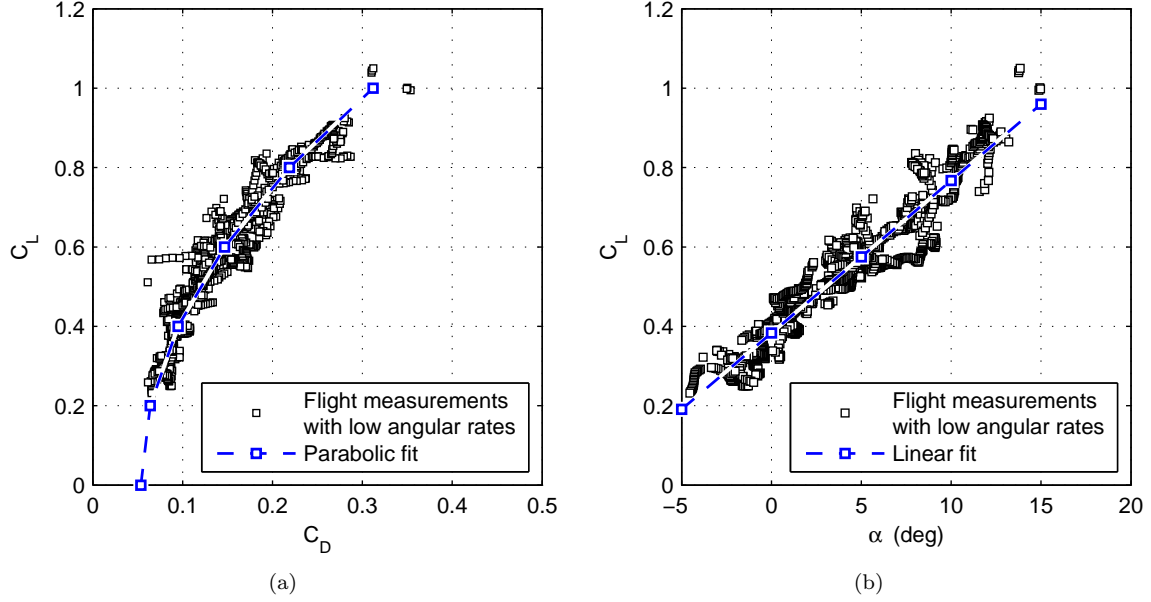
Figure 4.3: Conditionally-sampled (low angular rate) quasi-steady data for the Vapor including (a) drag polar with a quadratic regression and (b) lift curve with a linear regression.

where

$$K = \frac{1}{\pi e_o \mathcal{R}} \tag{4.3}$$

which depends on the aspect ratio $\mathcal{R}$ and Oswald efficiency factor e_o. The parabolic regression over the C_L range of 0 to 1.1 is $C_D = 0.054 + 0.26 C_L^2$. With K known, Eq. 4.3 can be used to calculate the Oswald efficiency factor using

$$e_o = \frac{1}{\pi K \mathcal{R}} \tag{4.4}$$

For the Vapor MAV tested, e_o was determined to be 0.48 for the entire aircraft having an wing aspect ratio of 2.56. The value is low and similar to other measurements at low Reynolds numbers. Specifically, Ref [13] determined e_o to be 0.53 from wind tunnel results for an aspect ratio 6 wing at Reynolds number of 20,000.

Wing Lift Calculations

All of the lift coefficient data shown previously were for the entire MAV and thereby included the aerodynamic force of the stabilator. By calculating the lift coefficient for just the wing, the experimental lift curve slope can be compared with results from theoretical calculations for the wing. The lift of the entire MAV depends on both the wing and the stabilator [88], viz

$$C_L = C_{L_w} + C_{L_h} \eta_h \frac{S_h}{S_{ref}} \tag{4.5}$$

37

where η_h is the dynamic pressure ratio at the tail and was taken to be 0.9, while the reference areas S_{ref} and S_h are given in Table 2.1. The pitching moment $C_{m_{cg}}$ is given by

$$C_{m_{cg}} = C_{m_{ac,w}} + C_{L_w}(\overline{x}_{cg} - \overline{x}_{ac,w}) - C_{L_h}\eta_h\frac{S_h}{S_{ref}}(\overline{x}_{ac,h} - \overline{x}_{cg}) \tag{4.6}$$

where the center of gravity $\overline{x}_{cg}$ was measured to be 36% of the wing root chord, and the aerodynamic center of the wing $\overline{x}_{ac,w}$ and the tail $\overline{x}_{ac,h}$ were approximated to be located at 25% of the mean aerodynamic chord for each respective surface. The pitching moment of the wing $C_{m_{ac,w}}$ was estimated to be -0.12 based XFOIL[†] results for a generic thin 6.7% cambered airfoil and experimental results [11] for a thin cambered airfoil (such as the GOE 417A). The values for $C_{m_{ac,w}}$ were found to vary from -0.09 to -0.15 depending on the angle of attack and Reynolds number. The lift curve slope did not vary with different values of the wing pitching moment. However, the wing lift coefficient at zero angle of attack depended on the value of $C_{m_{ac,w}}$.

During flight, $C_{m_{cg}}$ and C_L for the airplane were determined from the flight trajectory using Eqs 2.17a and 2.20b. In Eqs. 4.5 and 4.6, the only remaining unknowns are the wing C_{L_w} and the tail C_{L_h}. Solving the two equations simultaneously results in

$$C_{L_h} = \frac{C_{m_{ac,w}} - C_{m_{cg}} + C_L(\overline{x}_{cg} - \overline{x}_{ac,w})}{\frac{S_h}{S_{ref}}\eta_h(\overline{x}_{ac,h} - \overline{x}_{ac,w})} \tag{4.7a}$$

$$C_{L_w} = \frac{C_{m_{cg}} - C_{m_{ac,w}} + C_L(\overline{x}_{ac,h} - \overline{x}_{cg})}{(\overline{x}_{ac,h} - \overline{x}_{ac,w})} \tag{4.7b}$$

which can be used to find the lift coefficient of the wing and tail during flight tests.

Figure 4.4 shows C_L for the entire aircraft and C_{L_w} from Eq. 4.7(b) for the conditionally-sampled quasi-steady flight data [previously shown in Fig. 4.3(b)]. A linear regression was used to determine the lift curve slope for both cases. The lift curve slope for the entire aircraft is 2.21/rad [the line shown in Fig. 4.3(b)], and the lift curve slope for the wing alone is 2.06/rad (the line shown in Fig. 4.4). The calculated lift of the wing was less than the lift of the entire aircraft which indicates a lifting stabilator.

The measured wing lift curve slope of 2.06/rad can be compared with predictions using the wing aspect ratio of 2.56. An ideal lift curve slope of 3.52/rad is obtained using finite wing approximations based on lifting line theory for an elliptically loaded wing, that is

$$C_{L_\alpha} = 2\pi\left(\frac{\mathit{Æ}}{\mathit{Æ}+2}\right) \tag{4.8}$$

[†]Drela, M., 2008, available at http://web.mit.edu/drela/Public/web/xfoil/, 22 November, 2013
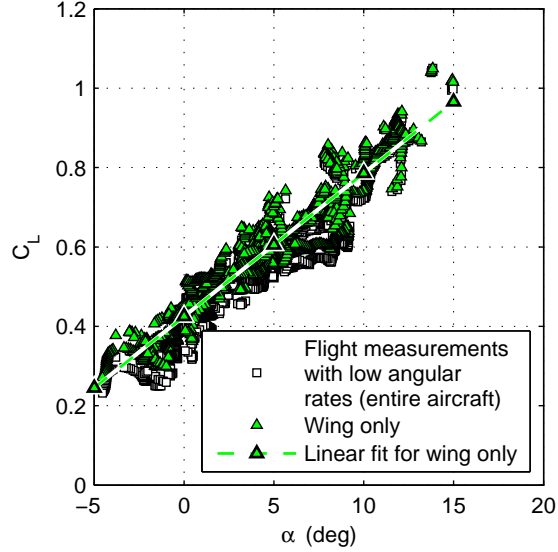
Figure 4.4: The lift coefficient of the wing compared with the lift coefficient for the entire airplane (Vapor) during the conditionally-sampled quasi-steady flights.

However, a lower lift curve slope of 3.06/rad is found using the more applicable low-aspect ratio Helmbold equation given by [60]

$$C_{L_\alpha} = 2\pi \left(\frac{\mathcal{R}}{2 + \sqrt{4 + \mathcal{R}^2}} \right) \tag{4.9}$$

As expected, both of these results from theory (with Eq. 4.9 being more appropriate for the aspect ratio) overpredict the lift curve slope primarily as a result of low Reynolds number viscous effects, and this result is consistent with past measurements [13].

Effect of Quasi-Steady Lift

A component of the unsteady aerodynamics can be characterized by the reduced frequency given by

$$k = \frac{\dot{\alpha} c}{2V} \tag{4.10}$$

As described in Refs. [38] and [40], the varying angle of attack during the unsteady motion produces an effective camber that results in an incremental change in the lift coefficient expressed as

$$\Delta C_{l,k} = 2\pi k \left(\frac{1}{2} - a \right) \tag{4.11}$$

where $a = -1$ at the leading edge, 1 at the trailing edge, and thus $a = -0.5$ at the wing quarter chord, the latter of which was used for the following calculations. The change in lift due to unsteady effects $\Delta C_{l,k}$ is
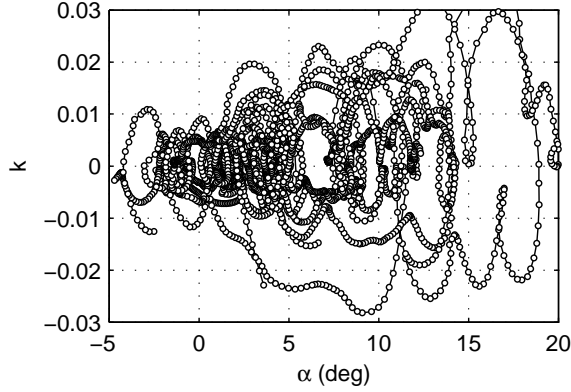
Figure 4.5: The reduced frequency during the quasi-steady flights.

additive to the steady-state lift curve. Once the 2D unsteady lift is known, the 3D unsteady lift is found using

$$\Delta C_{L,k} = \frac{C_{L_\alpha}}{C_{l_\alpha}} \Delta C_{l,k} \tag{4.12}$$

where C_{l_α} is 2π and C_{L_α} is the lift curve slope for the entire aircraft. When combined with Eq. 4.11, Eq. 4.12 becomes

$$\Delta C_{L,k} = C_{L_\alpha} k \left(\frac{1}{2} - a \right) \tag{4.13}$$

which uses the experimentally determined lift curve slope for the entire aircraft. While the result is based on thin airfoil theory which overpredicts the lift curve slope at low Reynolds number, the method provides an estimate of the incremental lift due to quasi-steady effects. In addition, the final result in Eq. 4.13 uses the experimentally determined lift curve slope (of the entire aircraft) to avoid problems of overprediction. In the following paragraph, an estimate of the change in lift $\Delta C_{L,k}$ is found using Eq. 4.13, and the results based on theory are compared with the experimental results.

Figure 4.5 shows the reduced frequency k as a function of the angle of attack during the quasi-steady flights. A general observation is that while the excursions are within the range of $k \approx \pm 0.03$, the range of the reduced frequency increases with angle of attack, and this increase is primarily due to the flight dynamics—smaller trajectory excursions at higher speeds (low α) and vice versa. The predicted $\Delta C_{L,k}$ was calculated using Eq. 4.12 along with the time histories of the reduced frequency.

Figure 4.6 shows the linear lift curve augmented with the unsteady effects (due to k) calculated from the flight conditions for the complete time histories of the quasi-steady flights. The variation in the lift coefficient in Fig. 4.6 can be compared with the previously shown quasi-steady experimental data [Fig. 4.2(b)]. While both results have similar trends in the variation, the variation in the experimental results is larger than in
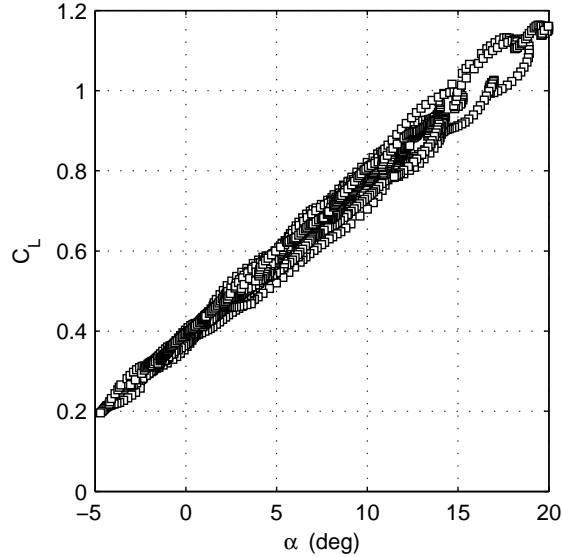
Figure 4.6: The linear lift curve model augmented with $\Delta C_{L,k}$ for the quasi-steady flights.

the predicted results. The standard deviation from the linear lift curve slope for the experimental results is 0.057 while for the theoretical results it is only 0.018. The results show how the effective camber model can be used to estimate a component of the quasi-steady influence on MAV lift, but the model underpredicts the influence because it does not include all of the effects of quasi-steady flow. Specifically, the effective camber model used only included effects due to k and neglected additional unsteady effects such as time lag, quasi-steady lift from the horizontal tail, and additional effects that might be attributed to low Reynolds number separation bubble dynamics. The results show the influence $\dot{\alpha}$ has on the lift coefficient of MAVs even in the quasi-steady regime and that the quasi-steady effective camber model does not predict all of the quasi-steady influences on lift for MAVs.

4.1.2 SU-26xp in Nominal Gliding Flight

The time histories of the SU-26xp were analyzed to find the trim lift and drag for each flight instead of using the complete time histories of C_L and C_D. By finding trim conditions for each flight, near-steady state results were observed at angles of attack below stall as well as above stall for the SU-26xp. In order to vary the trim speed during the more than 150 flights, the SU-26xp was flown with two different center of gravity locations and nine elevator deflections. Each combination of center of gravity location and elevator deflection was flown between 5 and 15 times.

For any flight, the trim point could be found by analyzing the pitching moment as a function of angle of attack, and the lift and drag corresponding to that angle of attack could be subsequently found. Details of
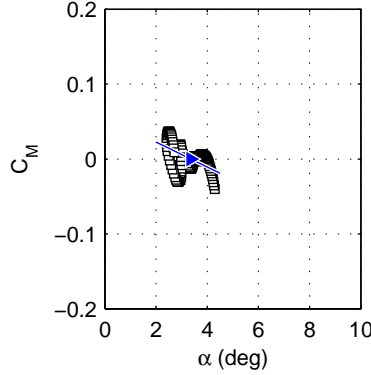
Figure 4.7: The trim point for a single flight.

the method are first outlined using an representative example, and then the lift and drag results are analyzed for the SU-26xp. The representative example illustrates how the method is applied to a set of 11 flights.

The trim angle of attack for each individual flight was determined first using a least squares regression for the moment coefficient as a function of angle of attack. The functional form of the regression was assumed to be linear in angle of attack,

$$C_m = C_{m_o} + C_{m_\alpha}\alpha \tag{4.14}$$

Figure 4.7 shows an example of the C_m versus α for a single short quasi-steady flight with the linear regression line. Evaluating the regression at $C_{m_{cg}} = 0$ yielded the trim angle of attack α_{trim} for the flight and α_{trim} is marked on Fig. 4.7 with the blue triangle. Repeating the analysis for many flights resulted in a large set of trim points and similar trim angles of attack could be combined.

Second, flights with the same center of gravity and a similar trim angle of attack (within 0.75 deg) were combined so variations between individual flights were removed. Figure 4.8(a) shows the pitching moment for the illustrative example set of 11 flights. From a linear regression on moment coefficient for these combined flights, the trim point for each flight was found and is indicated with the blue triangle (at $\alpha = 4.6$ deg). Next, a local lift curve was found using a linear regression on the lift coefficient versus angle of attack. Based on the low angle of attack assumptions (linear lift curve), the functional form was assumed to be linear, viz

$$C_L = C_{L_o} + C_{L_\alpha}\alpha \tag{4.15}$$

Continuing with the example, Fig. 4.8(b) shows the lift curve and the linear regression. Evaluating the regression at the trim angle of attack resulted in the trim lift coefficient which is again indicated with the blue triangle in Fig. 4.8(b). The determined result ($C_L = 0.46$ at $\alpha = 4.6$ deg) was used as an experimental trim point.
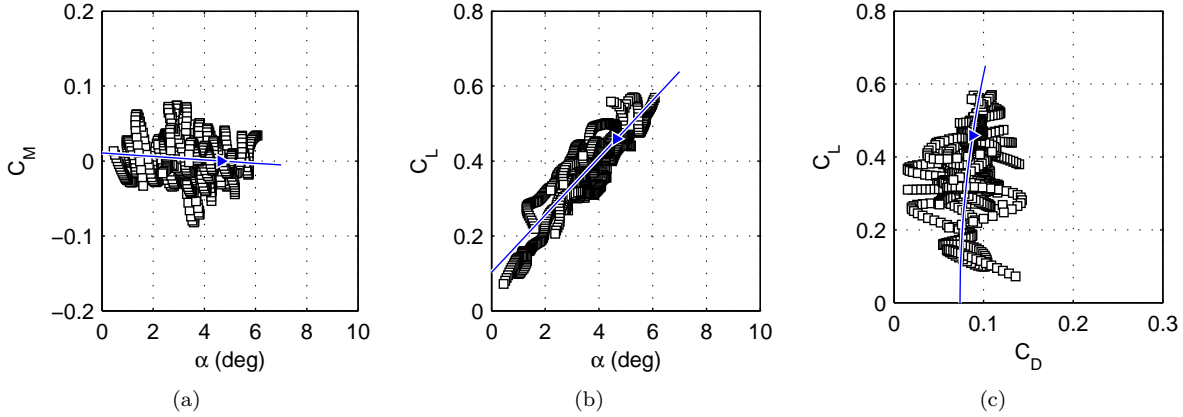
Figure 4.8: The trim point analysis for an example set of flights for the SU-26xp.

Finally, a regression on the drag polar in the form of

$$C_D = C_{D_o} + K C_L^2 \tag{4.16}$$

was used to find the trim drag conditions. Figure 4.8(c) shows the drag polar for the example set of 11 flights. Evaluating the drag polar at the trim conditions resulted in the trim drag coefficient for the specific flight condition ($C_D = 0.088$ at $C_L = 0.46$ deg). The example set of 11 flights illustrated the trim method that used functional forms based on linearized equations of motion to determine the trim point. The assumed functional forms (linear moment and lift curves and a drag polar) will continue to hold at higher angles of attack for small ranges of angle of attack. Applying the method to numerous flights with varying trim conditions can be used to determine the aircraft characteristics over a range of flight conditions.

Applying the trim method to 150 flights of the SU-26xp results in 23 trim points where the example illustrated through Fig. 4.8 is just one of the points. The lift and drag results from the trim method are shown in Fig. 4.9. The drag results in Fig 4.9(a) are characterized by a parabolic polar at angles of attack below stall. At approximately $C_D = 0.15$, separation is indicated by the drag rise and the departure of the trim points from the parabolic polar. After separation, the drag increases without a corresponding increase in the lift coefficient.

Trim lift coefficients for the entire aircraft C_L and just the wing $C_{L,w}$ are shown in Fig. 4.9(b). The lift coefficient is not precisely zero at zero angle of attack because the wing incidence angle was 2 deg and both ailerons drooped a couple of degrees. The wing lift coefficient is lower than the lift for the entire aircraft which indicates a lifting tail. The difference between C_L and $C_{L,w}$ increases with the angle of attack as the tail generates a larger stabilizing force and contributes more to the aircraft lift. Both C_L and $C_{L,w}$ follow
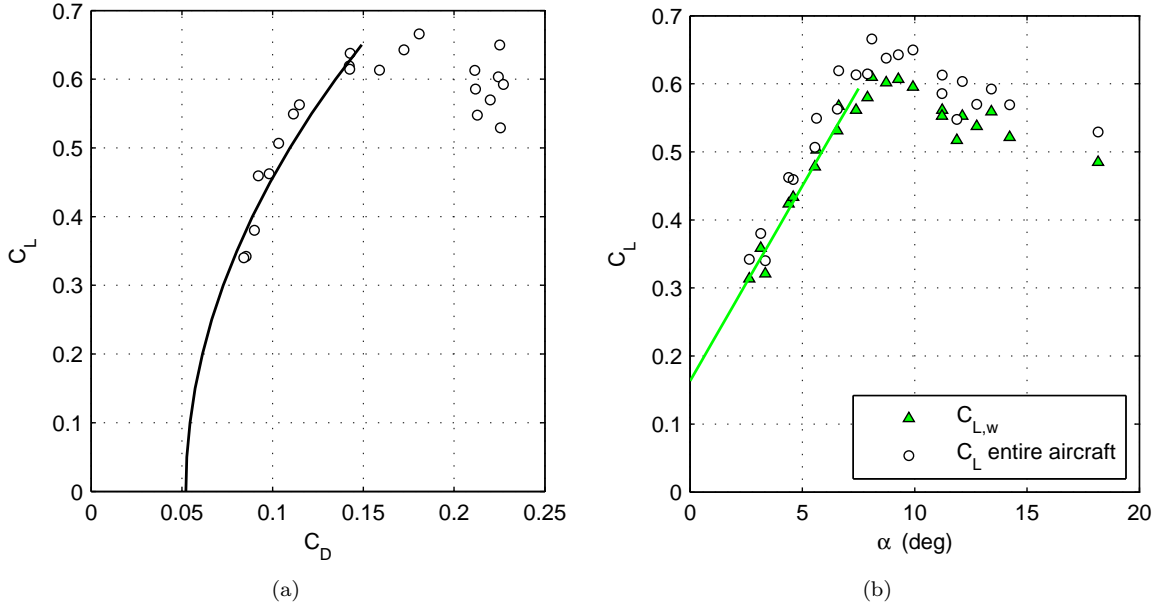
Figure 4.9: Experimental (a) drag polar and (b) lift curve for the SU-26xp.

an almost-linear trend until an angle of attack of 8 deg which indicates stall. After stall, the lift decreases, and the individual trim points have more variation as shown in Fig. 4.9(b).

To calculate the lift curve slope of the wing, a stall angle of 7.5 deg was assumed. Points above the stall angle of attack were ignored because the lift curve is no longer linear, and a least squares regression determined the wing lift curve slope to be 3.28/rad. The slope is less than the 4.51/rad predicted for an ideal finite wing (via Eq. 4.8) for $\mathcal{R} = 5.12$. As previously mentioned, the decrease is expected at low Reynolds numbers.

By analyzing the aerodynamic characteristics at a variety of trim speeds, the lift and drag coefficients of the SU-26xp were determined based on the quasi-steady flight trajectories. Across multiple flights, the trim angle of attack was varied from below stall, to near stall and finally just above stall. From the trim conditions of the flights, the steady lift and drag coefficients were determined as a function of trim angle of attack. Instead of analyzing the complete flight trajectories (which were used to show the quasi-steady nature of MAV flights in Section 4.1.1 and has been previously used by other researchers [14, 22–24]), the analysis of the numerous trim points of the SU-26xp was used to determine the steady state characteristics over a range of trim speeds—including post stall. Both methods can be used to assess the flight characteristics of MAVs from flight trajectories.

Table 4.1: Aerodynamic Characteristics of the Balsa Gliders

Parameter	$\mathcal{R}= 6.07$	$\mathcal{R}= 11.7$
C_{D_o}	0.048	0.046
K	0.178	0.159
C_{L_α}	4.65	5.13
C_{L_o}	0.103	0.153
Wing Only		
$\quad C_{L_\alpha}$	4.23	4.79
$\quad C_{L_o}$	0.097	0.160

4.1.3 Balsa Gliders in Nominal Gliding Flight

The two balsa gliders with similar wing areas but different aspect ratios (11.7 and 6.07), as noted in Table 2.1 were constructed to investigate the aerodynamic characteristics of higher aspect ratio gliders. The lift and drag results for the two gliders were found by locating the trim conditions from between 75 and 100 flights. Figure 4.10 shows the lift and drag of the trim points for each aircraft and each wing alone with a least squares regression for the lift curve and drag polar. The least squares regression was done for an angle of attack range of 0 to 8 deg and 0 to 6.5 deg for the lower and higher aspect ratio gliders, respectively. The upper bound was selected to approximately correspond to the stall angle as was observed in the experimental results. Table 4.1 lists the values for the different constants for the linear lift curve slope and drag polar.

The drag polars appear close to parallel in Fig. 4.10, but the higher aspect ratio wing has a lower value for the induced drag coefficient K (from Eq. 4.1) in Table 4.1. Above a C_L of approximately 0.7, the drag increases faster than the parabolic fit due to separation. The offset in minimum drag C_{D_o} between the two aircraft was due to minor differences in the two aircraft configurations and differences in Reynolds number. For each aircraft, the fuselage, wing, tail, and marker placement were similar, but not identical, and each of these components contributed to the drag of the airplane. Additionally, the two gliders operate at different Reynolds numbers with the lower aspect ratio glider operating at approximately 12,000 and the larger aspect ratio glider operating at approximately 8,900. The difference in Reynolds number was due to the wing of each glider having a different mean aerodynamic chord while both gliders had similar weight and wing area (see Table 2.1).

For the lift shown in Fig. 4.10(b), stall is indicated by the change in the lift curve slope at an angle of attack of 8 and 6.5 deg for the lower and higher aspect ratio gliders, respectively. In each case, the lift curve slope decreases after stall. By using the fact that at trim conditions the pitching moment is zero, the lift curve slope of the wing for each airplane was found using Eq. 4.7. For both balsa gliders, the wing lift curve is lower than the aircraft lift curve indicating lifting tails. The experimental results showed the lower
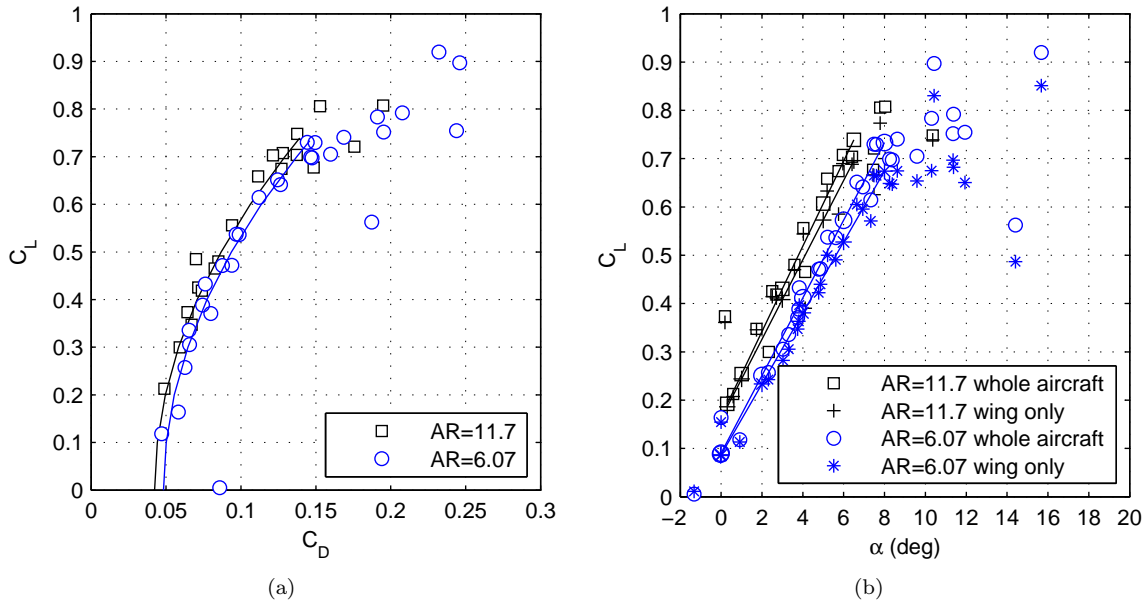
Figure 4.10: Experimental (a) drag polar and (b) lift curve for the two balsa gliders.

Figure 4.11: A sketch representative of the thin airfoil used on the two balsa gliders.

aspect ratio wing had a lift curve slope of 4.73 while the higher aspect ratio wing had a lift curve slope of 5.36. These results can be compared with theoretical values based on the aspect ratio for each wing and assuming an elliptically loaded wing. The experimental results are 90% and 89% of finite wing results for the lower and higher aspect ratio wing, respectively. These percentages are significantly higher than observed for the SU-26xp, model glider, or Vapor, and the difference may be due to the surface roughness of the different wings and the airfoil shapes. Surface roughness can cause transition between laminar and turbulent flow which has a significant effect on lift curve slopes of low Reynolds number airfoils [3]. The balsa wings were unpainted and finished with 220-grit sandpaper. The wings for both balsa gliders were sanded using methods and shapes discussed in Ref. [89]. The general airfoil shape for both of the balsa wings is sketched in Fig. 4.11. The lower surface of the airfoil is flat and the upper surfaces is curved from a round leading edge to the thickest point (approximately 7% thick at approximately 40% chord). Beyond the thickest point of the airfoil, the upper surface had a linear incline to the blunt trailing edge.

Figure 4.12 shows the lift-to-drag ratio of the two gliders as a function of the angle of attack. For both aircraft, the maximum lift-to-drag ratios are between 5 and 6 at an angle of attack a few degrees below stall. The higher aspect ratio wing has a slightly higher peak L/D as is expected, but the difference was
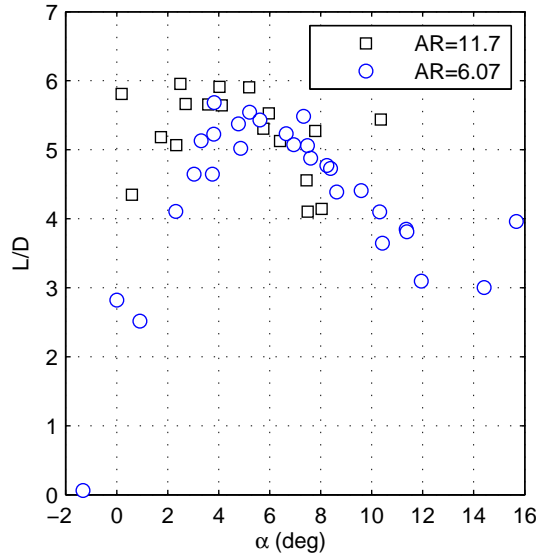
Figure 4.12: The lift-to-drag ratio of the two balsa gliders.

not significant because the higher aspect ratio glider flew at a lower Reynolds number than the lower aspect ratio glider (12,000 vs. 10,000).

4.1.4   Balsa Gliders at Large Angles of Attack

Beyond stable low angle-of-attack flight, airplanes can descend nearly vertically at high angles of attack in a deep stall descent. Deep stall descent is a stable flight condition at angles of attack higher than stall (typically $\alpha > 30$ deg). For full-sized aircraft, stable deep stall is considered dangerous and is generally avoided [90, 91]. However, some MAVs and smaller UAVs use stable deep stall descent as a method to land aircraft in confined areas [19, 20].

Flight tests were conducted with both balsa gliders in deep stall. To achieve quasi-steady deep stall flight, the standard stabilator that could deflect only a few degrees was replaced with a similarly sized stabilator shown in Fig. 4.13. The new high-deflection stabilator could deflect to incidence angles between 0 and more than 90 deg, and numerous flight tests were conducted with different stabilator incidence angles between 8 and 60 deg. In the flights, the balsa gliders descended with a steep glide slope and a slow speed. During the flights, the angle of attack varied around each trim point, and the magnitude of the reduced frequency remained less than 0.03 as shown in Figs. 4.14 and 4.15. The values of k are compared to quasi-steady flight values where $|k|$ was less than 0.2.

To find the trim lift and drag for the aircraft in deep stall, the trim point analysis used previously was applied to the quasi-steady deep stall trim points. The trim angles of attack for the different stabilator

47

(a)   (b)   (c)
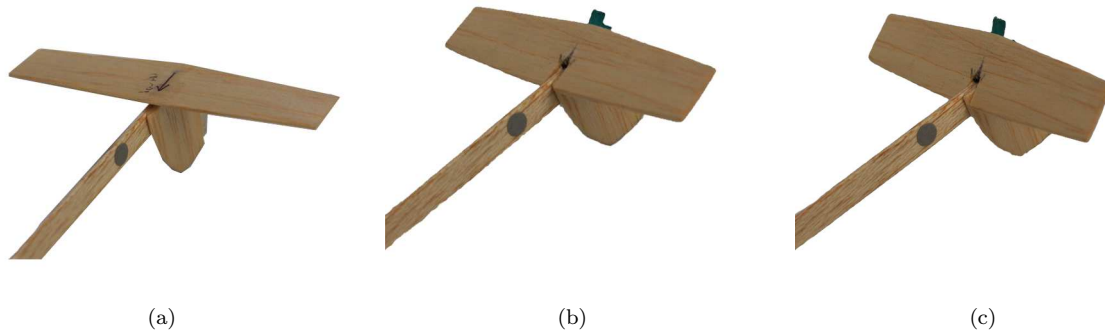
Figure 4.13: The (a) nominal stabilator, and the high-deflection stabilator at a (b) moderate and (c) high deflection angle.
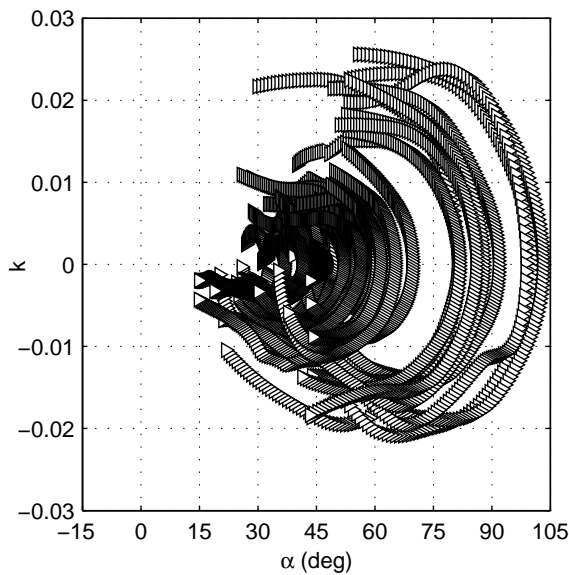
Figure 4.14: The reduced frequency during the quasi-steady deep-stall flights with the 11.07 aspect ratio balsa glider.
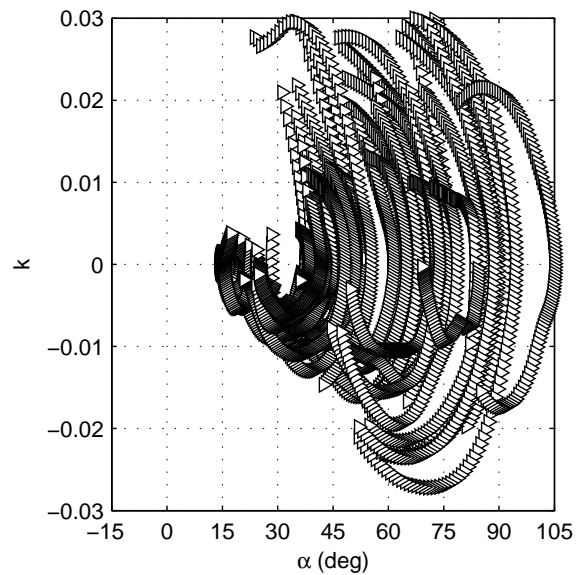
Figure 4.15: The reduced frequency during the quasi-steady deep-stall flights with the 6.70 aspect ratio balsa glider.

deflections are shown in Figs. 4.16 and 4.17 for the two balsa gliders. For the balsa glider with an aspect ratio of 11.7 (in Figs. 4.16) the trim points extend to 73 deg with a stabilator deflection of approximately 45 deg. The balsa glider with an aspect ratio of 6.07 (in Figs. 4.17) included higher deflection angles (up to 63 deg) and, thus, higher trim angles of attack (almost 90 deg) than for the other balsa glider.

Figure 4.18 shows the lift and drag at deep stall trim points for the balsa glider with an aspect ratio of 11.7. The drag coefficient [Fig. 4.18(a)] increases significantly from the pre-stall range, and the drag polar shows the circular nature at extreme angles of attack. The drag coefficient peaks at 1.43 at an angle of
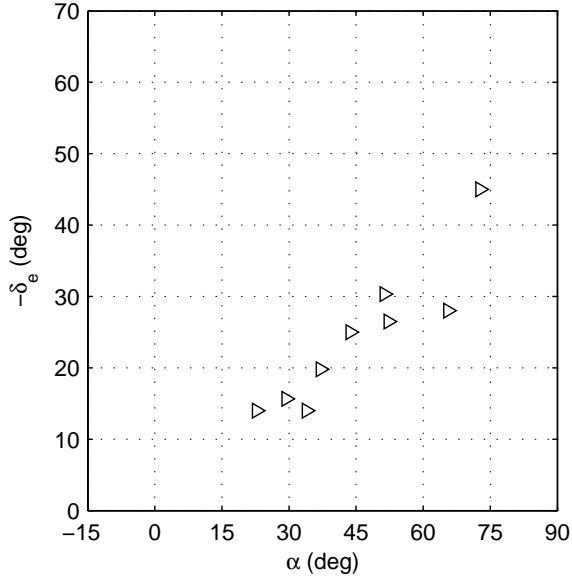
Figure 4.16: The stabilator deflection angles for the high angle-of-attack deep-stall trim points of the balsa glider with an aspect ratio of 11.7.
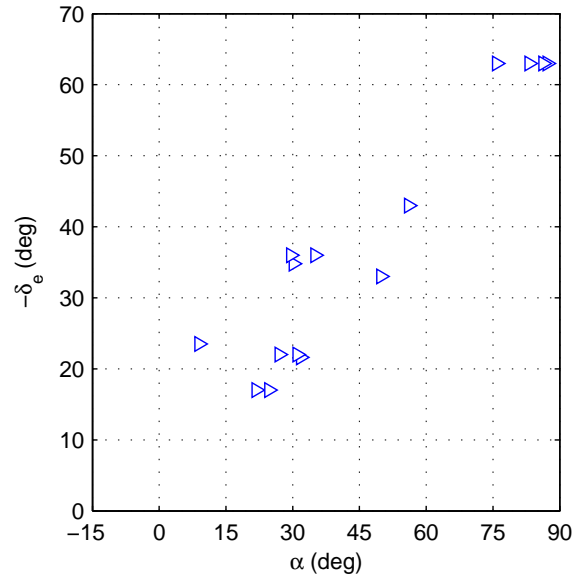
Figure 4.17: The stabilator deflection angles for the high angle-of-attack deep-stall trim points of the balsa glider with an aspect ratio of 6.07.

attack of 73 deg. Based on a finite flat plate at an angle of attack of 90 deg [64, 83], the drag of the wing at $\alpha = 90$ deg was estimated for comparison purposes using,

$$C_{D,90} = 1.11 + 0.018\mathcal{R} \tag{4.17}$$

The local angle of attack for the horizontal tail was much lower than 90 deg because of the high deflection angle of the tail. Hence, the component of drag due to the tail could not be estimated using the method for a finite flat plate at $\alpha = 90$ deg. For the balsa glider with an aspect ratio of 11.7, the theoretical drag coefficient at $\alpha = 90$ deg was found to be 1.32. While the experimental results are only up to an angle of attack of 73 deg, the observed trend in the experimental data can be extended to $\alpha = 90$, and the extension would be close to 1.5 which is just above the theoretical value of 1.32. The difference could be due to not including the drag of the horizontal tail and fuselage. The lift coefficient shown in Fig. 4.18(b) plateaus at approximately 0.9 between 30 and 50 deg before descending to 0.43 at 73 deg. Continuing the trend for C_L, lift would be zero at approximately $\alpha = 90$ deg as would be expected.

Similar results for the lower aspect ratio glider ($\mathcal{R} = 6.07$) are shown in Fig. 4.19. As shown in Fig. 4.17, the stabilator was tested at higher deflection angles than with the other balsa glider which resulted in experimental results at angles of attack close to 90 deg. Immediately after stall, the drag, and lift have more variation with peak C_L just above 1. As with the other balsa glider, the drag polar shown in Fig. 4.19(a)
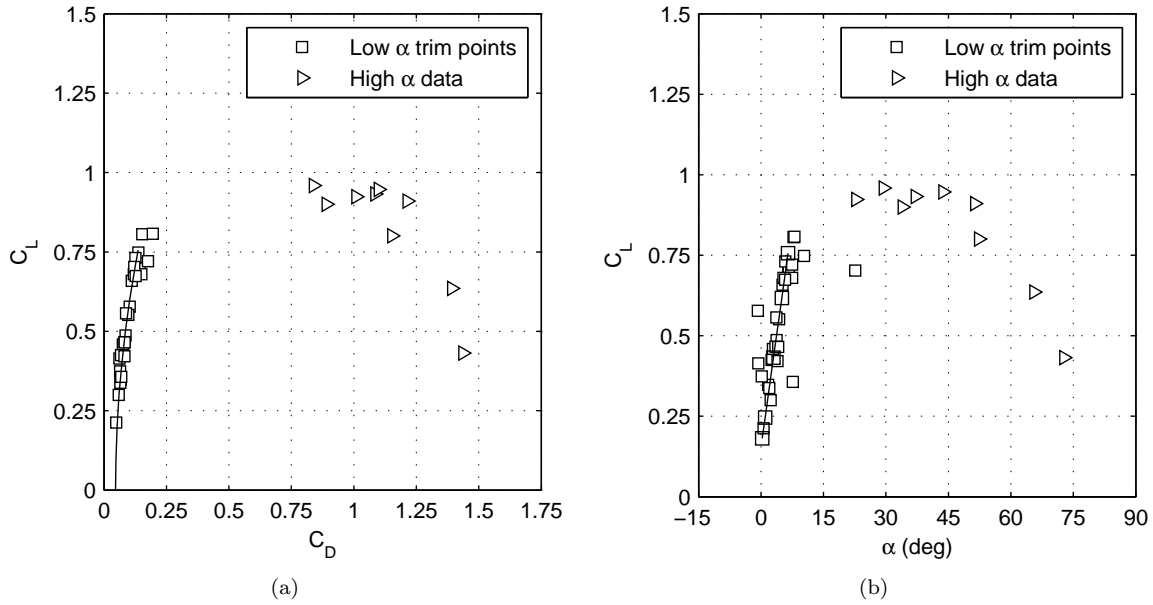
Figure 4.18: Experimental quasi-steady high angle-of-attack (a) drag polar and (b) lift curve results for the 11.7 aspect ratio glider with the results from the low angle-of-attack trim point analysis (circles) from Fig. 4.10.
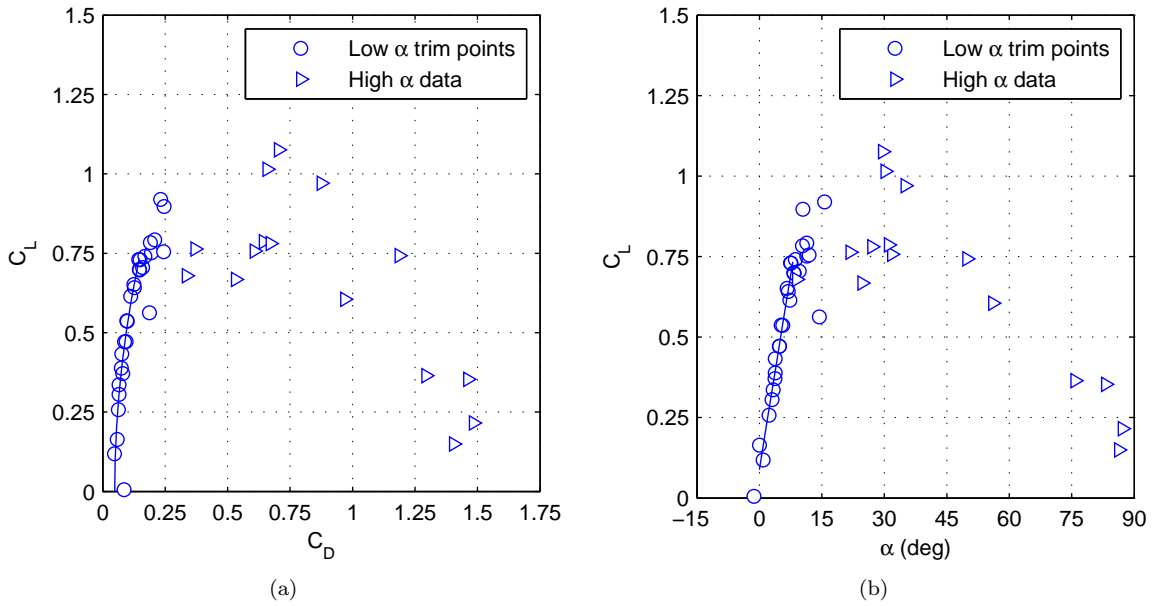
Figure 4.19: Experimental quasi-steady high angle-of-attack (a) drag polar and (b) lift curve results for the 6.07 aspect ratio glider with the results from the low angle-of-attack trim point analysis (circles) from Fig. 4.10.

looks circular over the large angle of attack range. Between an angle of attack of 80 and 90 deg, C_D varies between 1.4–1.5 with the largest value of 1.49 at an angle of attack of 87 deg. Theoretical drag for a wing with an aspect ratio of 6.07 at an angle of attack of 90 deg is 1.22 based on Eq. 4.17. As before, the calculated

value is less than that observed experimentally, and, again, the difference is due to not including the drag of the horizontal tail and fuselage in the model.

Figure 4.19(b) shows the lift coefficient has variation just after stall and follows a fairly linear trend above 45 deg angle of attack with zero lift occurring at an angle of attack of approximately 97 deg. Positive lift at an angle of attack of 90 deg is expected from the wing due to the curved leading edge and sharp trailing edge. In addition, the stabilator was set at a high incidence angle which resulted in the local angle of attack being significantly smaller than the angle of attack of the aircraft so the stabilator generated a force perpendicular (lift) to the flow. The deep stall experimental results show the aerodynamic characteristics of the balsa gliders during quasi-steady post stall flight at angles of attack between 15 and 100 deg.

4.2 Static Stability Derivatives

Aerodynamic moments acting on an airplane govern the stability and are used to control the airplane. Understanding the stability and control of MAVs is important to dynamics modeling, designing controllers, and trajectory planning for MAVs. The model glider (previously discussed in the repeatability tests), the SU-26xp (previously shown with the trim lift and drag analysis), and the two balsa gliders were analyzed to show stability and control characteristics of MAVs determined from the flight trajectories [79]. Both the static longitudinal and lateral stability were explored for the aircraft, and the phugoid mode is shown for the two balsa gliders.

4.2.1 Longitudinal Stability

Longitudinal stability ensures the airplane returns to a trim angle of attack when it is perturbed. The experimental pitching moment coefficient C_m about the center of gravity versus angle of attack for the SU-26xp is shown in Fig. 4.20 for four different elevator deflections (but the same center of gravity), and the slope C_{m_α} is changing with the trim angle of attack. The variation of slope could be caused by changing aerodynamic characteristics of the wing and horizontal tail, and a number of aerodynamic causes will be discussed in detail after outlining the factors that contribute to longitudinal stability and analyzing the neutral point location.

The change in C_{m_α} at different trim conditions, seen in Fig. 4.20, can be further explained when analyzing the neutral point location. The neutral point is the aerodynamic center of the airplane and is found from C_{m_α}, C_{L_α}, and the measured location of the center of gravity. Using the experimental lift curve slope for
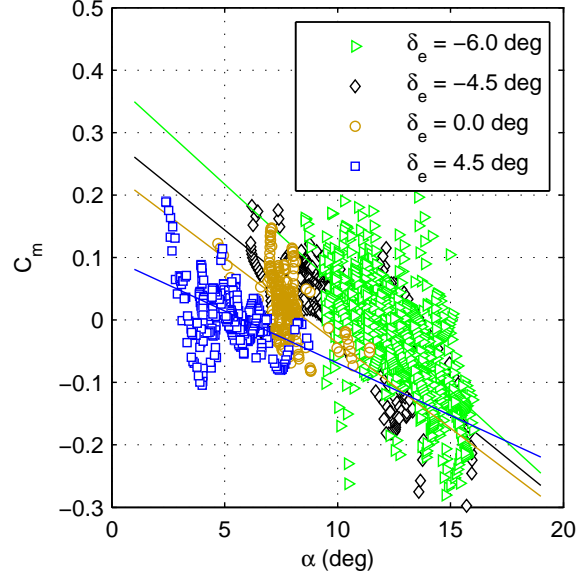
Figure 4.20: Experimental pitching moment versus angle of attack for the SU-26xp with the center of gravity at 42% of the root chord.

the wing (3.28/rad) and the static margin SM, the experimental neutral point can be found from

$$C_{m_\alpha} = C_{L_\alpha}(SM) \tag{4.18}$$

where the static margin is the nondimensionalized distance between the neutral point $\bar{x}_{np}$ and the known center of gravity $\bar{x}_{cg}$. The neutral point was measured from the wing root leading edge and normalized by the wing root chord.

Figure 4.21 shows the experimentally-determined neutral point as a function of angle of attack for two different center of gravity locations. Trim speed and α_{trim} were changed by varying the elevator deflection. The range of elevator deflections was limited to 5 to -6 deg to avoid extreme flight attitudes. At an elevator deflection of -6 deg, the aircraft was just past stall at an angle of attack of 12 deg.

The theoretical neutral point is found using [59, 60]

$$\bar{x}_{np} = \frac{C_{L_{\alpha,w}}\bar{x}_{ac,w} + \bar{x}_{ac,h}C_{L_{\alpha,h}}\eta_h\frac{S_h}{S_{ref}}(1 - \frac{\partial\epsilon}{\partial\alpha})}{C_{L_{\alpha,w}} + C_{L_{\alpha,h}}\eta_t\frac{S_h}{S_{ref}}(1 - \frac{\partial\epsilon}{\partial\alpha})} \tag{4.19}$$

where the subscripts of w and h represent the values of different variables for wing and horizontal tail respectively. The distance normalized by the wing root chord from the aerodynamic center of each surface to a reference point is $\bar{x}_{ac}$, and S_{ref} and S_h are the surface areas of the wing and tail, respectively. Downwash from the main wing at the tail and the velocity deficit ratio caused by the wake of the main wing at the tail
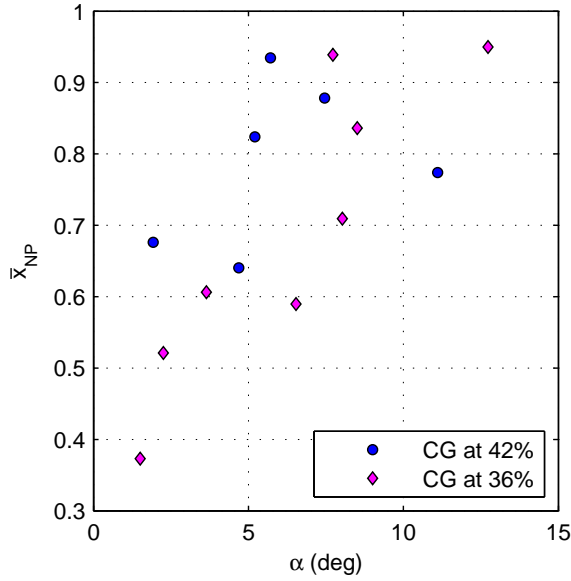
Figure 4.21: Experimentally-determined neutral point (percentage root chord from the wing leading edge) versus trim angle of attack for the SU-26xp.
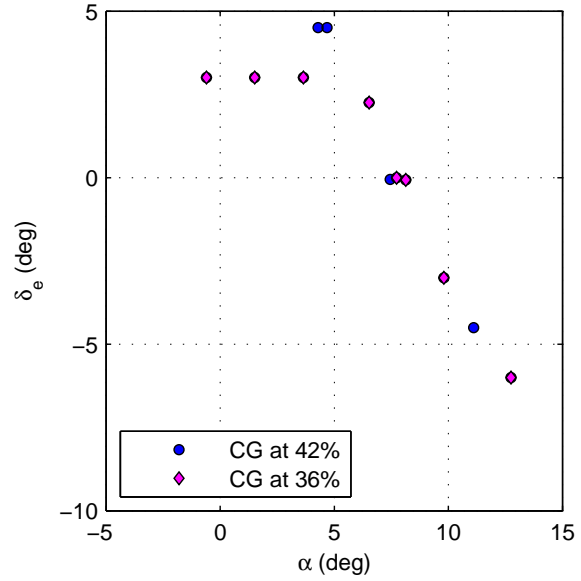
Figure 4.22: Effect of the elevator deflection on the trim angle of attack for the SU-26xp.

are the $\partial\epsilon/\partial\alpha$ and η_h terms, respectively. The neutral point $\bar{x}_{np}$ is measured from the wing root leading edge and is in percentage of wing root chord.

As outlined in Eq. 4.19, the neutral point depends on both the lift curve slope of the wing and tail as well as the aerodynamic center of each. Additionally, the wake from the wing affects the lift of the horizontal tail. In the angle of attack range where both lift curve slopes are linear, the neutral point theoretically remains constant. From Eq. 4.19, the theoretical value was calculated to be $\approx$35–45% which corresponds to the experimental neutral point (Fig. 4.21) only at low angles of attack. At higher angles of attack, the neutral point moves aft which implies that the tail becomes more effective with respect to the wing. The shift aft could be caused by a number of different effects changing the aerodynamic characteristics, particularly the lift curve slope of the wing and/or horizontal tail.

First, Eq. 4.19 assumes that the wing and tail lift curve slopes are linear, and any nonlinearity would cause the neutral point to change. A decrease in the wing lift curve slope would shift the neutral point aft while a decrease in the tail lift curve slope would shift the neutral point forward. Second, the induced flow effects from the wake of the main wing on the horizontal tail affects the neutral point. The downwash $\partial\epsilon/\partial\alpha$ and the velocity deficit η_h are caused by the wake of the main wing changing the flow at the horizontal tail. In the theoretical calculations $\partial\epsilon/\partial\alpha$ was set to $\approx$0.45 and η_h was set to $\approx$0.8. The theoretical formulation

53
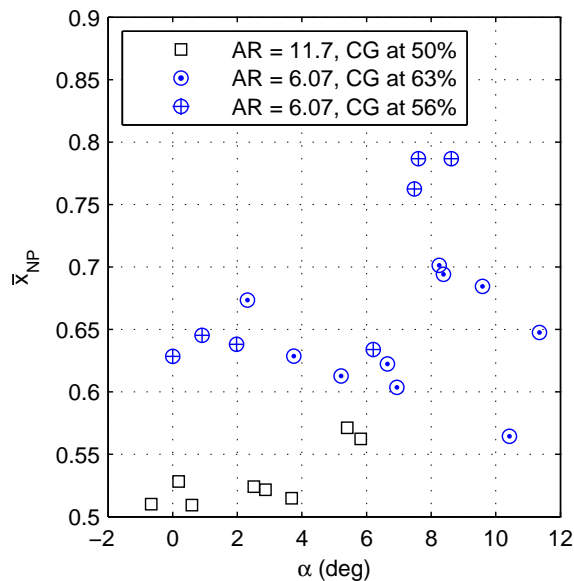
Figure 4.23: Experimentally-determined neutral point (percentage root chord from the wing leading edge) versus trim angle of attack for the two balsa gliders.

includes a $\partial\epsilon/\partial\alpha$ term that assumes the downwash effect is linear with the angle of attack. As the flight conditions (particularly α) change, the vertical location of the wake of the main wing at the tail can move up or down and the effect on the horizontal tail can change. The observed shift aft of the neutral point location could be caused by changes in the downwash and velocity deficit due to angle of attack changes. Thus, $\partial\epsilon/\partial\alpha$ and η_t need to depend on the angle of attack in the theoretical results. Finally, the aerodynamic center of the wing ($\bar{x}_{ac,w}$) and tail ($\bar{x}_{ac,h}$) move aft as the angle of attack increases because the quarter-chord assumption rarely holds for low Reynolds number airfoils [7, 8, 92]. In the theoretical models used, the aerodynamic center of each surface is assumed to stay at the quarter chord. However, if the wing and tail aerodynamic centers move aft with increased angle of attack, the shift needs to be included for each surface in the theoretical calculations. While none of these effects can fully explain the neutral point shift, the combination of all the effects can explain the shift.

Figure 4.22 shows the effect of the elevator deflection on the trim angle of attack for the SU-26xp. The SU-26xp elevator was 65% of the horizontal tail area with a deflection range of ±20 deg, but only a range of 5 to -10 deg was tested to limit the flight regime of the airplane. Increasing positive elevator (trailing edge down) caused the airplane to fly at lower angles of attack.

For the two balsa gliders, the neutral point did not move significantly until after the stall angle of attack as shown in Fig. 4.23. The balsa glider with an aspect ratio of 11.7 has a calculated neutral point of approximately 55% which is close to the experimental values of between 50% and 57% based on Eq. 4.19.

The variation of the neutral point increases just before an angle of attack of 6 deg which is just before the stall angle of approximately 6.5 deg. For the balsa glider with an aspect ratio of 6.07, two different center of gravity positions were tested, and Fig. 4.23 shows the experimental neutral point in the range of 60–67% which is comparable to the theoretical result of 61%. Again at angles of attack just before stall, which occurred at an angle of attack of approximately 8.5 deg, the neutral point shifts aft. For the balsa gliders, the neutral point is practically stationary until just before the stall angle of attack at which stage the neutral point starts to shift aft. This contrasts with the SU-26xp, where the neutral point shifted aft gradually beginning before stall (see Fig. 4.21).

4.2.2   Lateral Stability

For lateral stability, results from the model glider, the SU-26xp, and the two balsa gliders are presented. The model glider has 4.5 deg dihedral and a high wing configuration which contrasts with the 0 deg dihedral, mid-body wing of the SU-26xp, and the two balsa gliders had polyhedral, high wing and their vertical stabilizer extended down from the fuselage below the horizontal tail. Least squares regression was used to calculate the lateral stability terms using β, p, r, δ_a, δ_r, and ϕ as the independent variables.

Static yaw stability of an airplane is ensured by the vertical tail and measured by the yawing moment generated by the sideslip angle C_{n_β}. A positive C_{n_β} ensures the aircraft is stable and any sideslip will damp out. First, all of the flights for each airplane were combined and analyzed using the least squares regression. The results for the model glider, the SU-26xp, and the two balsa gliders are in Table 4.2 along with the 95% confidence intervals for the C_{n_β} regression. The model glider had a C_{n_β} of 0.0843 which was greater than the SU-26xp value of 0.0400. The difference between the two geometrically similar balsa gliders resulted from different vertical tail areas and hence different vertical tail volume coefficients. The balsa glider with an aspect ratio of 6.07 had a vertical tail volume coefficient of 0.036 while the higher aspect ratio glider had a vertical tail volume coefficient of 0.017. Second, the flights were separated into groups by the flight settings (center of gravity and elevator/stabilator angle) to show weather vane stability as a function of the angle of attack. Figure 4.24 shows that the weather vane stability does not have a clear trend with the angle of attack for either the Vapor or the model glider. For the separated groups, the 95% confidence bounds were larger and had an average value of ±0.0470 and ±0.0512 for the SU-26xp and the model glider, respectively. The wider confidence bounds for the separated groups of flights was due to the significantly fewer data points for each group. From the results in Fig. 4.25, C_{n_β} for the balsa gliders increases with the angle of attack, and the averaged 95% confidence bounds for the regression were ±0.00879 and ±0.00269 for the aspect ratio 6.07 and 11.7, respectively. The increasing stability with the angle of attack is caused by the vertical tail

Table 4.2: Lateral Stability Characteristics of the SU-26xp, the Model Glider, and the Balsa Gliders

	C_{n_β}	95% Confidence	C_{l_β}	95% Confidence
SU-26xp	0.0400	± 0.00494	-0.00176	± 0.00187
Model Glider	0.0843	± 0.00785	-0.0136	± 0.00234
Balsa Glider $\mathcal{R}$=6.07	0.0472	± 0.00157	-0.0109	± 0.00075
Balsa Glider $\mathcal{R}$=11.7	0.0285	± 0.00058	-0.00325	± 0.00043
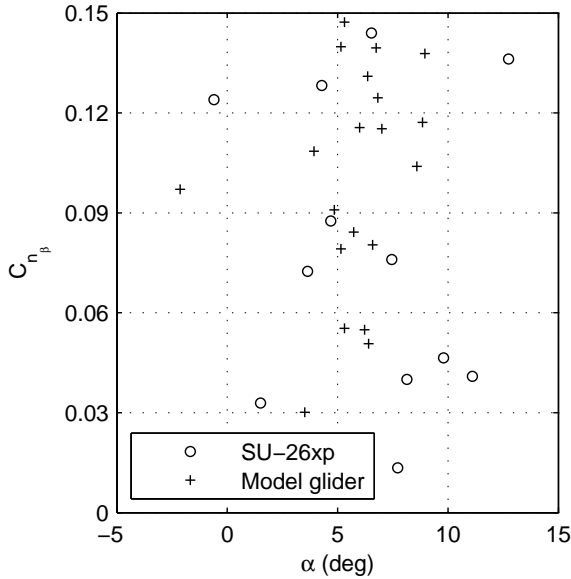
Figure 4.24: Experimental weather vane stability C_{n_β} for the SU-26xp and the model glider as a function of trim angle of attack.
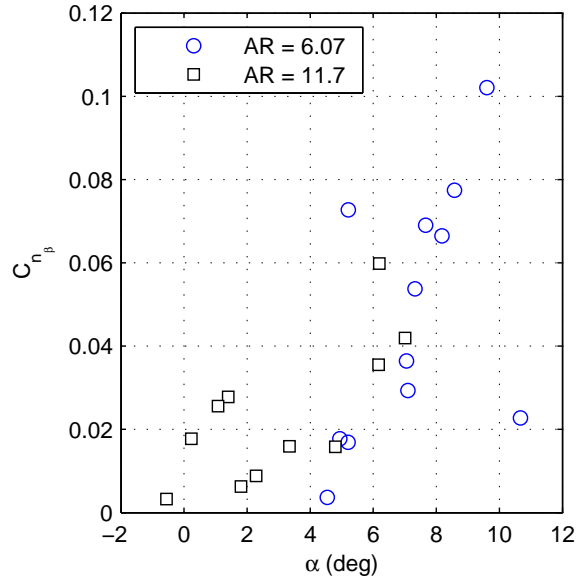
Figure 4.25: Experimental weather vane stability C_{n_β} for the balsa gliders as a function of trim angle of attack.

extending downward below the horizontal tail. In this position, the flow on the vertical tail is less influenced by the main wing and fuselage as the angle of attack increases.

Roll due to yaw C_{l_β} is the other major lateral stability derivative for an airplane and is often referred to as the dihedral effect. Negative values of C_{l_β} along with other stability terms, ensure stability so that when the airplane is perturbed it returns to zero sideslip. Table 4.2 lists the dihedral effect for the four airplanes based on the complete set of tests for both airplanes. The value of C_{l_β} for the SU-26xp is almost zero which is expected from the mid-body wing with no dihedral. For the model glider C_{l_β} is negative (stable) which is expected because of the high wing with 4.5 deg of dihedral. The balsa glider with an aspect ratio of 6.07 has a C_{l_β} that is more negative than the higher aspect ratio glider. Variations between the two planforms cause the observed differences in roll due to yaw. Some key variations include the polyhedral, the vertical position of the center of gravity, the vertical tail size and the fuselage cross-section distribution.
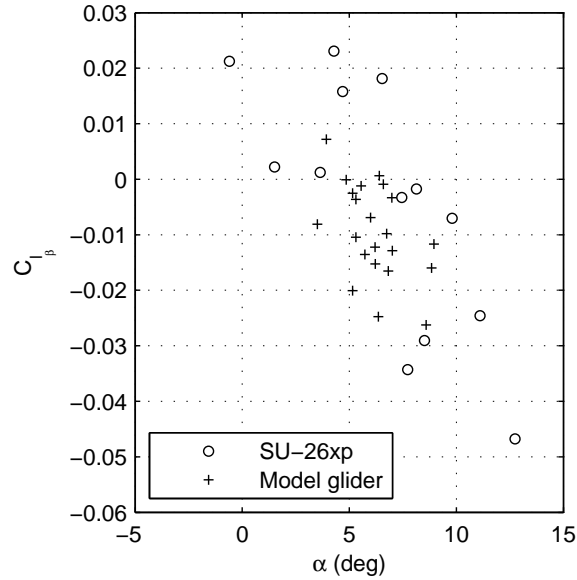
Figure 4.26: Experimental roll stability C_{l_β} for the SU-26xp and model glider as a function of the trim angle of attack.

Separating the flights by trim settings shows that C_{l_β} has a trend with the angle of attack for the SU-26xp and the model glider but not for the two balsa gliders which will not be shown. Figure 4.26 shows that C_{l_β} for the model glider and the SU-26xp becomes more negative (increasing dihedral effect) with increased angle of attack. For the SU-26xp, at low angles of attack C_{l_β} is slightly positive (marginally unstable). The averaged 95% confidence bounds for the separated groups was ± 0.0197 and ± 0.0151 for the SU-26xp and the model glider, respectively.

The results show how motion trajectories can be used to determined stability characteristics of different MAVs at low Reynolds numbers. Flight trajectories of four airplanes were used to determined the moment coefficients throughout flight, and subsequently, the stability characteristics. The longitudinal stability was analyzed for three airplanes, and one showed that the neutral point shifted gradually as a function of angle of attack while the other two only shifted with the onset of stall. The shifting neutral point indicated that at least some of the linear assumptions in the neutral point calculations (Eq. 4.19) are not holding for the SU-26xp. Lateral stability characteristics were also determined and indicated that the model glider had higher lateral stability than the aerobatic SU-26xp as expected from their respective wing configurations. The SU-26xp and model glider showed that C_{l_β} increased with the angle of attack, while their C_{n_β} did not change with the angle of attack. However, the opposite trend was observed for the two balsa gliders. For each balsa glider, C_{n_β} increased with the angle of attack, and C_{l_β} did not change with the angle of attack. The differences for the lateral stability terms can be traced to the different aircraft planforms. Overall, the

57

results showed how motion trajectories could be used to determine low Reynolds number stability coefficients which are crucial to designing controllers and path planning for MAVs.

4.3 Dynamic Stability

The dynamic stability of an aircraft governs the transient response of the aircraft to small perturbations [59, 88]. In the longitudinal direction, a key component of dynamic stability is the phugoid motion which involves the airplane exchanging altitude for airspeed as the flight path stabilizes. The aircraft climbs and loses airspeed, and then it descends and gains airspeed. The pitch of the airplane changes so the motion occurs at approximately a constant angle of attack. From the linearized longitudinal equations of motion, the frequency of the phugoid period is estimated using

$$\omega_{n,ph} = \frac{g}{V}\sqrt{2} \tag{4.20}$$

which depends on the gravitational constant g and velocity V [88]. From this relationship, the slower velocities of MAVs shortens the phugoid period as compared to faster full-sized aircraft. Determining the dynamic stability of the MAV from a flight trajectory was difficult because of the short length of the test. However, the dynamic response for the balsa gliders showed that the phugoid could be observed in the flight trajectories. Fig. 4.27 shows a typical time history for the balsa glider with an aspect ratio of 11.7 as it exchanges altitude for airspeed. The squares with cross-hatches indicate local extrema in the deviation of the altitude from a linear glide slope and the deviation of the velocity from a linear trend line. Just before 0.6 s, velocity reaches a minimum, and, just after 0.6 s, the altitude deviation reaches a maximum. Toward the end of the flight (1.3 s), velocity is at a maximum, but the flight track ends before the altitude can reach a minimum. As in this example, most flights were too short to have multiple extrema that could be used to find the period of the phugoid motion.

However in some cases, it was possible to observe a half period of the oscillation. Figure 4.28 shows a flight time history for the higher aspect ratio balsa glider with the extrema marked by the squares. The time between the extrema corresponds to the half period, and it is approximately 0.6 s which results in a full period of approximately 1.2 s. Based on the linearized longitudinal equations of motion (see Eq. 4.20), the undamped natural frequency was found to be approximately 1.9 s which is longer than the 1.2 s observed experimentally. Similarly, for the lower aspect ratio glider shown in Fig. 4.29, the time between the peaks is approximately 0.7 s so the full period is approximately 1.4 s. From the linearized equations of motion, the undamped natural frequency had a period of 1.55 s which is again longer than observed experimentally.
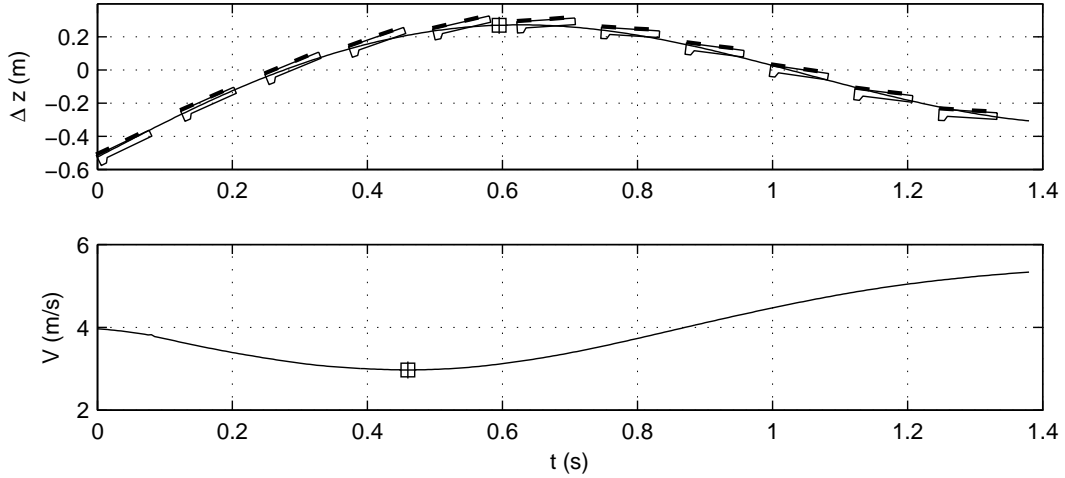
Figure 4.27: An example time history for the aspect ratio 11.7 balsa glider with the mark indicating extrema in the deviation of altitude from a linear glide slope and airspeed from a linear trend line.
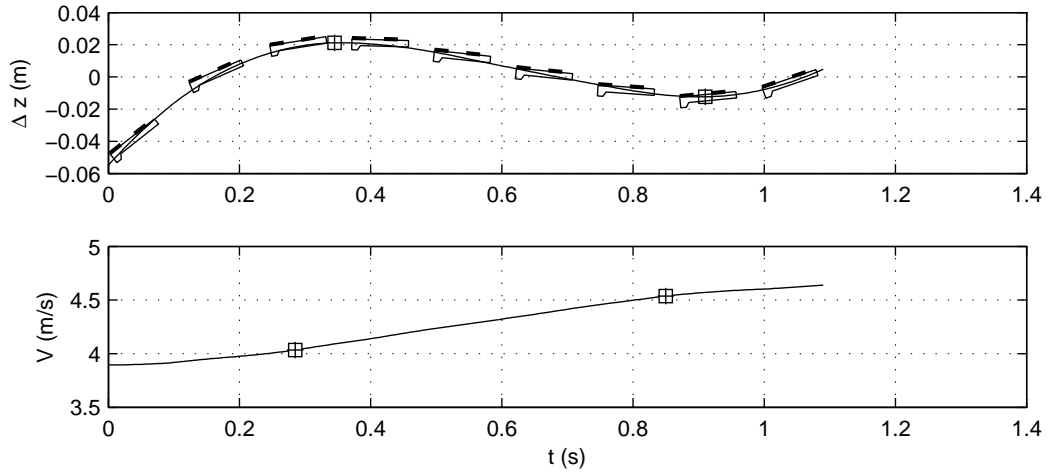
Figure 4.28: A time history for the aspect ratio 11.7 balsa glider with the marks indicating extrema in the deviation of altitude from a linear glide slope and airspeed from a linear trend line.

For both balsa gliders, the experimental results show the phugoid period to be less than predicted based on the linearized longitudinal equations of motion (from Eq. 4.20), but some variation from predicted results is expected [93]. Additional modes, such as the short period, were not definitively observed in the data. Typically, the short period is shorter than the phugoid and highly damped which makes the short period difficult to observe.
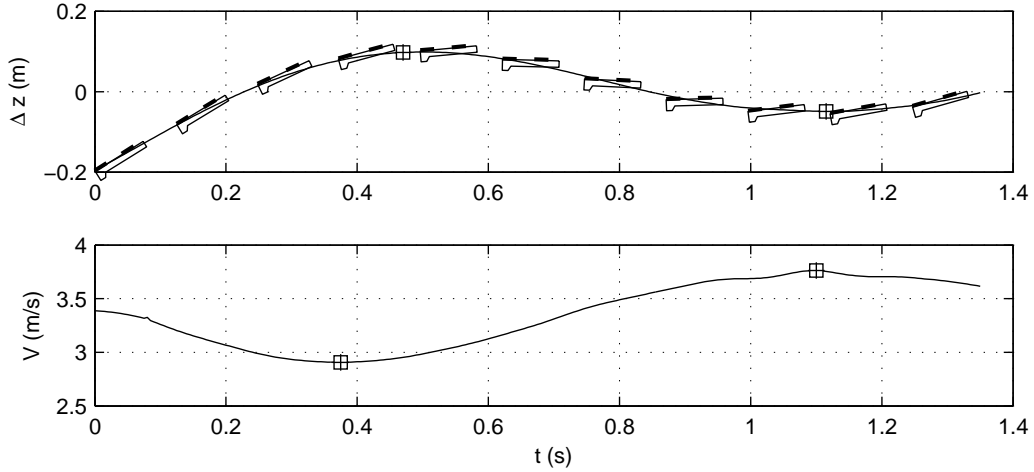
Figure 4.29: A time history for the aspect ratio 6.07 balsa glider with the marks indicating extrema in the deviation of altitude from a linear glide slope and airspeed from a linear trend line.

4.4 Discussion of Quasi-Steady Results

MAV flight in the quasi-steady flight regime was explored and studied using off-board motion tracking. Analyzing the full time histories of 14 Vapor flights showed the effect of unsteady aerodynamics on the measured lift and drag during quasi-steady flight. By analyzing the trim points from numerous flights for the SU-26xp and two balsa gliders, a lift curve and drag polar closer to steady state results were found from the quasi-steady results. In addition, the lift coefficient for the whole aircraft was separated out into the wing and tail lift using the moment coefficient as in Eq. 4.7(b). Results indicated that the MAVs had lifting tails and the wing lift curve slopes were generally less than theoretical values for an ideal wing as would be expected at such low Reynolds numbers. The two balsa gliders which were based on low Reynolds number designs, had lift curve slopes close to that of an ideal wing (elliptically loaded).

At angles of attack well past stall, results for the two balsa gliders in deep stall descent showed the lift and drag over an angle of attack range of 15–90 deg. Both lift and drag showed variation toward the lower portion of angles of attack (15–40 deg). Lift peaked between an angle of attack of 30 and 45 deg before decreasing to 0 just above an angle of attack of 90 deg. The drag polar began to take the shape of a circle with maximum drag occurring at zero lift and perpendicular flow.

Analyzing the moment coefficient time histories yielded the longitudinal stability and lateral stability for the different MAVs. For longitudinal stability, the neutral point shifted aft with increased angle of attack for the Vapor, which illustrated some of the shortcomings of using a linear dynamics model for low Reynolds number aircraft. On the other hand, the two balsa gliders had only small shifts in their neutral points until stall which indicates that the aerodynamics of the balsa gliders is closer to the assumptions behind the linear

60

dynamics models. It is also noted that the lift curve slopes of the two balsa gliders are also closer to the ideal wing results than the Vapor. These two observations indicate that the linear dynamics model assumptions are more applicable to the two balsa gliders as opposed to the Vapor. For the lateral stability, the weather vane stability and roll stability was shown for four aircraft. Some of the aircraft exhibited stability trends with angle of attack such as the weather vane stability increasing with angle of attack for the two balsa gliders, and the trend can be ascribe to the downward direction of their vertical tail.

Finally, the dynamic stability was investigated using the flight trajectories and it proved difficult due to the current capture volume and the limited duration of the flight trajectories. In a few of the flights for the two balsa gliders, a half period of the phugoid mode was observed and could be used to approximate the full phugoid period. The experimental phugoid period results were shorter than the approximations based on the linearized longitudinal equations of motion.

Chapter 5

Unsteady High Angle-of-Attack Flight Test Results

In addition to the quasi-steady flight tests, unsteady flights were recorded for the Vapor and two balsa gliders (see Figs. 2.3, 2.7, and 2.7). The recorded flights covered a wide flight regime to determine the lift, drag, and moment characteristics at angles of attack up to 90 deg. Both mild and aggressive stalls were observed. The flights included brief excursions to high angles of attack and unsteady conditions (due to changing angle of attack, translational acceleration, and rotational acceleration). MAVs operate in unsteady high angle-of-attack conditions as observed for these tests when undergoing rapid maneuvers such as perching, deep stall descent, and highly dynamic maneuvers in confined spaces.

5.1   Unsteady Aerodynamic Characteristics for the Vapor

The unsteady flight results depended on the angle-of-attack rate $\dot{\alpha}$, and, from Fig. 5.1, it is clear that the reduced frequency k (nondimensional $\dot{\alpha}$—see Eq. 4.10) covers a much larger range (-0.2 to 0.4) than for the quasi-steady flights (-0.03 to 0.03 in Fig. 4.5). In Fig. 5.1, the arrows indicate the direction the flight progresses beginning at low angles of attack (5 to 20 deg). As expected from the unsteady nature of the flights and the large range of k, Fig. 5.2(b) shows that C_L varies for a given angle of attack. Each flight began with increasing angle of attack (positive k) that led to stall, and the C_L values were larger with positive k than during the subsequent stall recovery with negative k. The unsteady nature of the flights resulted in a dynamic stall hysteresis loop illustrated by the flights in Fig. 5.2(b)—particularly the single selected flight which will be explained in detail below. In Fig. 5.3, the large positive values of k (pitch up) increased C_L, while the negative values of k during stall recoveries (pitch down) decreased C_L as expected from theoretical solutions to highly unsteady flow[40].

Figure 5.2(a) shows C_D varying from less than 0.1 during nominal gliding flight to above 2.0 during a number flights that included aggressive high angle-of-attack stall maneuvers. While nominal steady state drag for a finite flat plate perpendicular to the flow is approximately 1.5 [64, 83], unsteady effects have been shown to increase the drag coefficient [94]. For the moment coefficient shown in Fig. 5.2(c), the unsteady
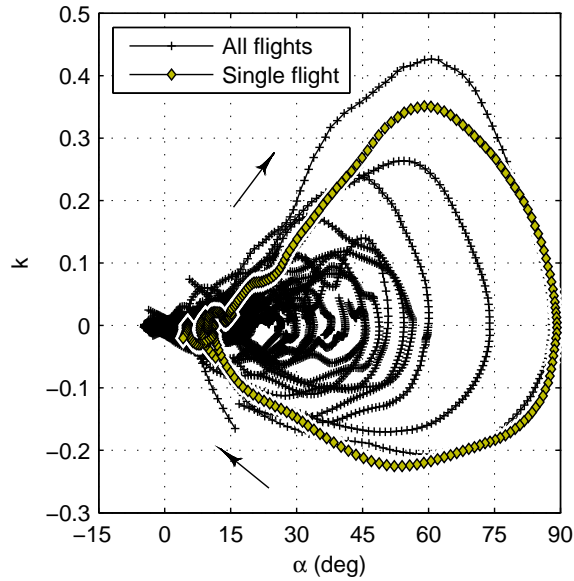
Figure 5.1: Reduced frequency as a function of angle of attack for unsteady flights that include mild to aggressive stalls of the Vapor.

effects cause a hysteresis loop in the counter clockwise direction. During the portions of flight with increasing angle of attack, the moment was more negative than during stall recovery.

One flight was selected to show the progression of an unsteady Vapor flight with an aggressive stall, and, in Figs 5.1 and 5.2, the flight is indicated by yellow diamonds. The single flight begins at an angle of attack of approximately 10 deg and progresses in the clockwise direction on the plot through a dynamic stall hysteresis loop. Figure 5.4 shows the trajectory and time history of selected flight parameters. As seen in the trajectory, the airplane entered an aggressive stall with the angle of attack increasing rapidly while the airspeed decreased. At 0.6 s, C_L peaked at a value of just less than 2, and at 0.66 s, k peaked at 0.35. The angle of attack continued to increase, but C_L decreased because the wing began to enter deep stall. From 0.75 to 1 s, the angle of attack was near 90 deg, which caused C_L to approach zero. After reaching the peak angle of attack (near 0.8 s), C_L began to increase during the stall recovery dive. The flight had large variation in C_L in the aggressive stall portion of flight illustrating the influence that large unsteady effects can have on the lift coefficient for high angular rate, high angle-of-attack flight.

For the selected flight, the progression of C_D during the initial rapid increase in angle of attack follows a parabolic trend [Fig. 5.2(a)] as a function of lift. After the peak C_L at 0.6 s (Fig. 5.4), the drag remains high as the lift decreases as the angle of attack continues to increase. The trend observed is most likely due to highly separated flow. Figure 5.4 shows that the C_D peak lags behind the reduced frequency, and that, during the stall recovery, the drag coefficient remains high. The drag remains high as the flow transitions
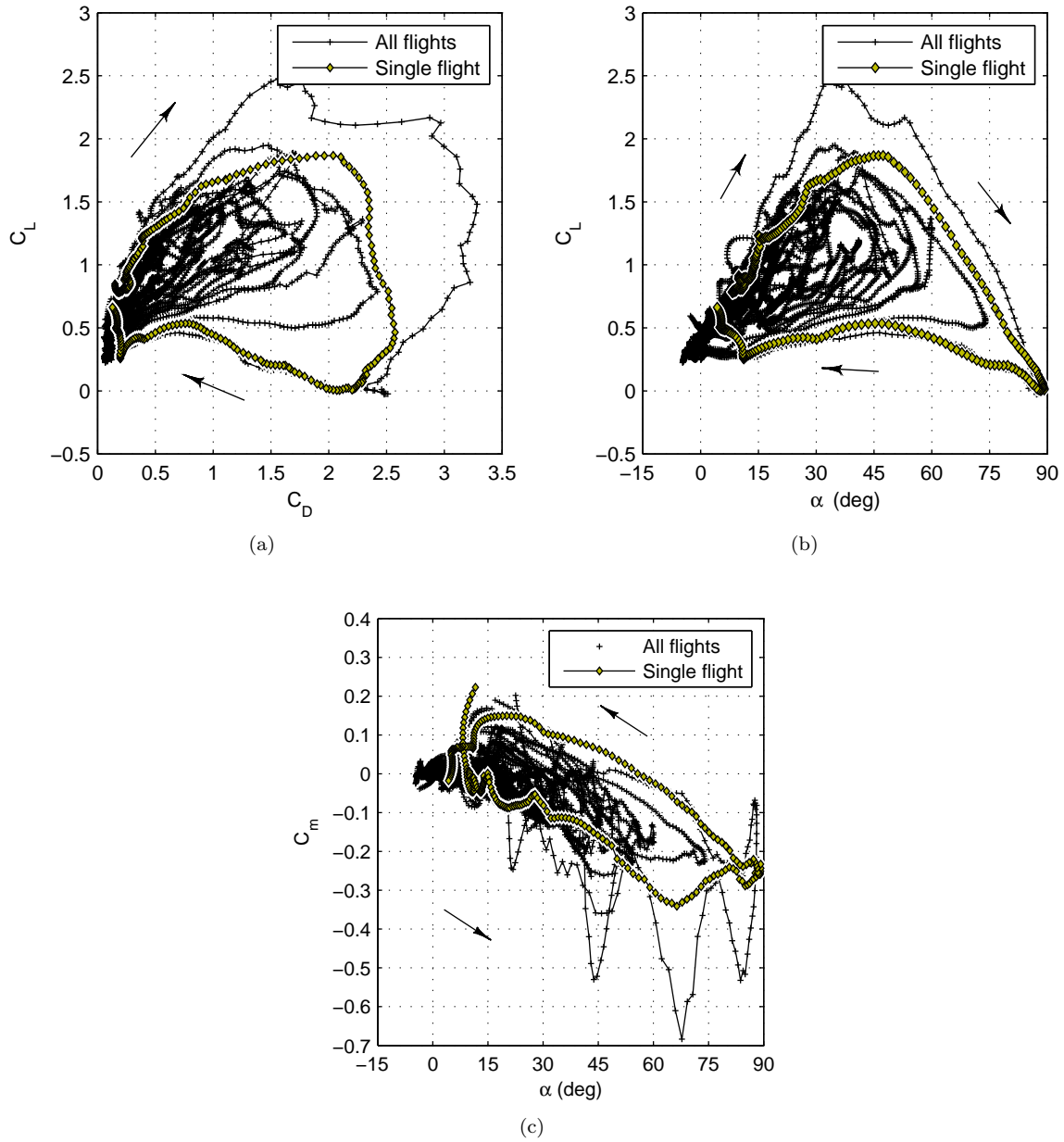
Figure 5.2: Experimental (a) drag, (b) lift, and (c) moment coefficient for unsteady flights of the Vapor.

from completely separated at high angles of attack to reattached at low angles of attack. Once the unsteady effects become small as both the reduced frequency and the angle of attack neared zero (≈ 1.25 s), the drag returns to steady-state C_D.

The moment coefficient decreases as the angle of attack begins to increase rapidly at approximately 0.4 s (see Fig. 5.4) in the selected flight, and C_m reaches at minimum of -0.33. The moment coefficient becomes positive at 0.9 s, which is during the recovery, and finally settles close to zero after the stall recovery.
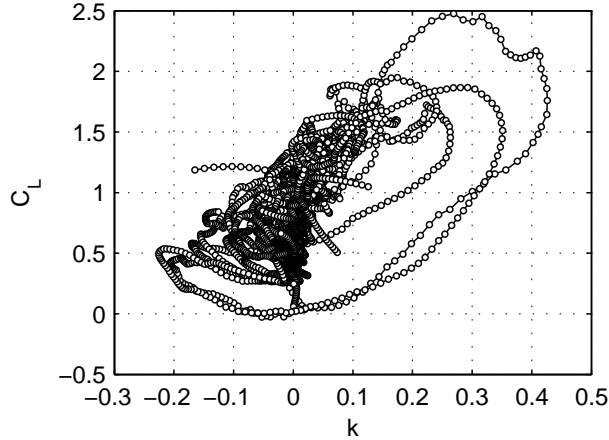
Figure 5.3: Lift coefficient increases with k for the unsteady flights of the Vapor.

Mettler [24] used a small glider with an aspect ratio of approximately 3 to explore unsteady high angle-of-attack flight and showed results for C_D, C_L, and C_m for one flight. The flight included rapid stall and a stall recovery similar to the unsteady Vapor flights. The small glider used by Mettler operated around a Reynolds number of 10,000 which is smaller than the Reynolds number range of 12,000-26,000 observed for the Vapor (see Fig. 5.4). In Fig. 5.5(a), the drag, lift, and moment results from Mettler include dynamic stall hysteresis loops and are compared with the results from the Vapor flights. The data set for the Vapor is larger than the data set in Mettler's work which allows the unsteady effects to be better analyzed.

In order to better understand the unsteady effects on lift, the lift coefficient data in Fig. 5.2(b) can alternatively be plotted as a smoothed contour as a function of angle of attack and reduced frequency, as in Fig. 5.6. For $k = 0$ in Fig. 5.6 ($\dot{\alpha} = 0$ as $\dot{\alpha}$ transitions from positive to negative), C_L increases with the angle of attack until approximately 45 deg where C_L is 1.2, after which C_L decreases to almost zero at an angle of attack of 90 deg. The lift behavior described follows the expected C_L versus α curve for steady-state conditions, but, as previously mentioned, when including the large unsteady effects, the range of C_L values becomes much larger and depends on k. For example, at an angle of attack of approximately 35 deg, Fig. 5.2(b) shows that C_L varies from approximately 0.3 to 2.5, and Fig. 5.6 shows that the C_L variation for the same angle of attack depends on the reduced frequency k which varies from approximately -0.22 to 0.30. Figure 5.6 also shows that the range of reduced frequency, and the influence of k, changes with the angle of attack during the maneuver. Even at lower angles of attack, the increased range of k in the unsteady flight data over the previously shown quasi-steady flight data is seen when comparing the variation of C_L. For example during the unsteady flights at an angle of attack of 10 deg, the range of k is
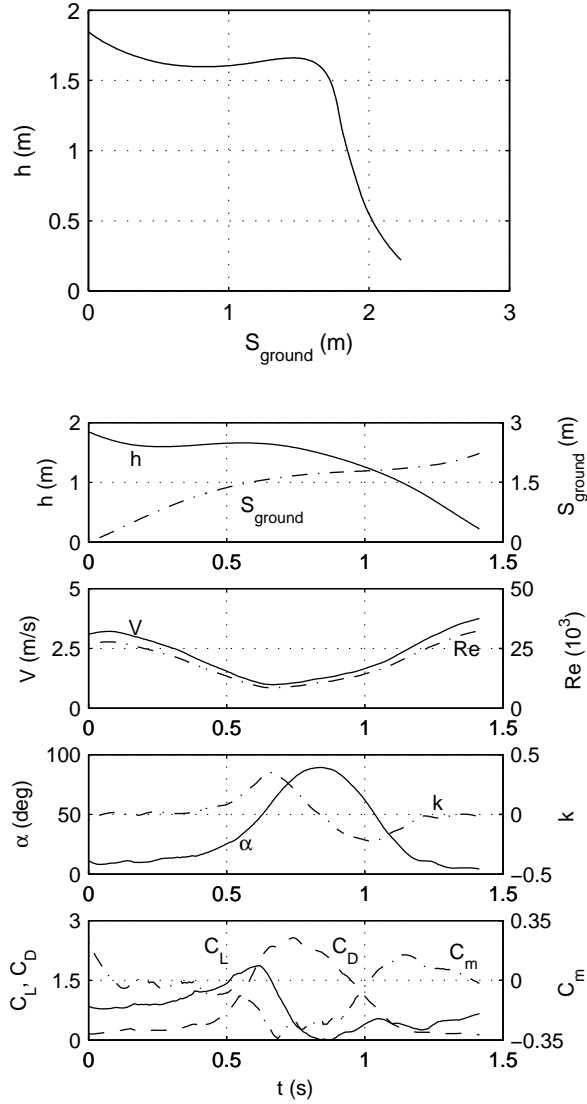
Figure 5.4: The flight trajectory of the single flight of the Vapor along with the time history of various parameters.

larger (-0.15 to 0.15) than was seen in the quasi-steady flights (-0.03 to 0.03), and subsequently C_L varies from zero to almost 1.6, which is quite large when compared with the quasi-steady results.

MAV flight can cover a larger flight envelope than full-sized airplanes and can include high angle-of-attack flight similar to the unsteady results shown here during agile maneuvers. The unsteady results in Fig. 5.2 highlights the significant influence that unsteady aerodynamics can have on both airplane lift and drag during rapid maneuvers. Figure 5.6 shows that, during stall maneuvers, the unsteady effects of reduced frequency are largest close to the stall angle of attack and $C_{L_{max}}$. In the range from $\alpha = 20$ to 50 deg, unsteady effects can have a large influence on lift as illustrated by the maximum C_L which was ≈ 1.2 in the

66
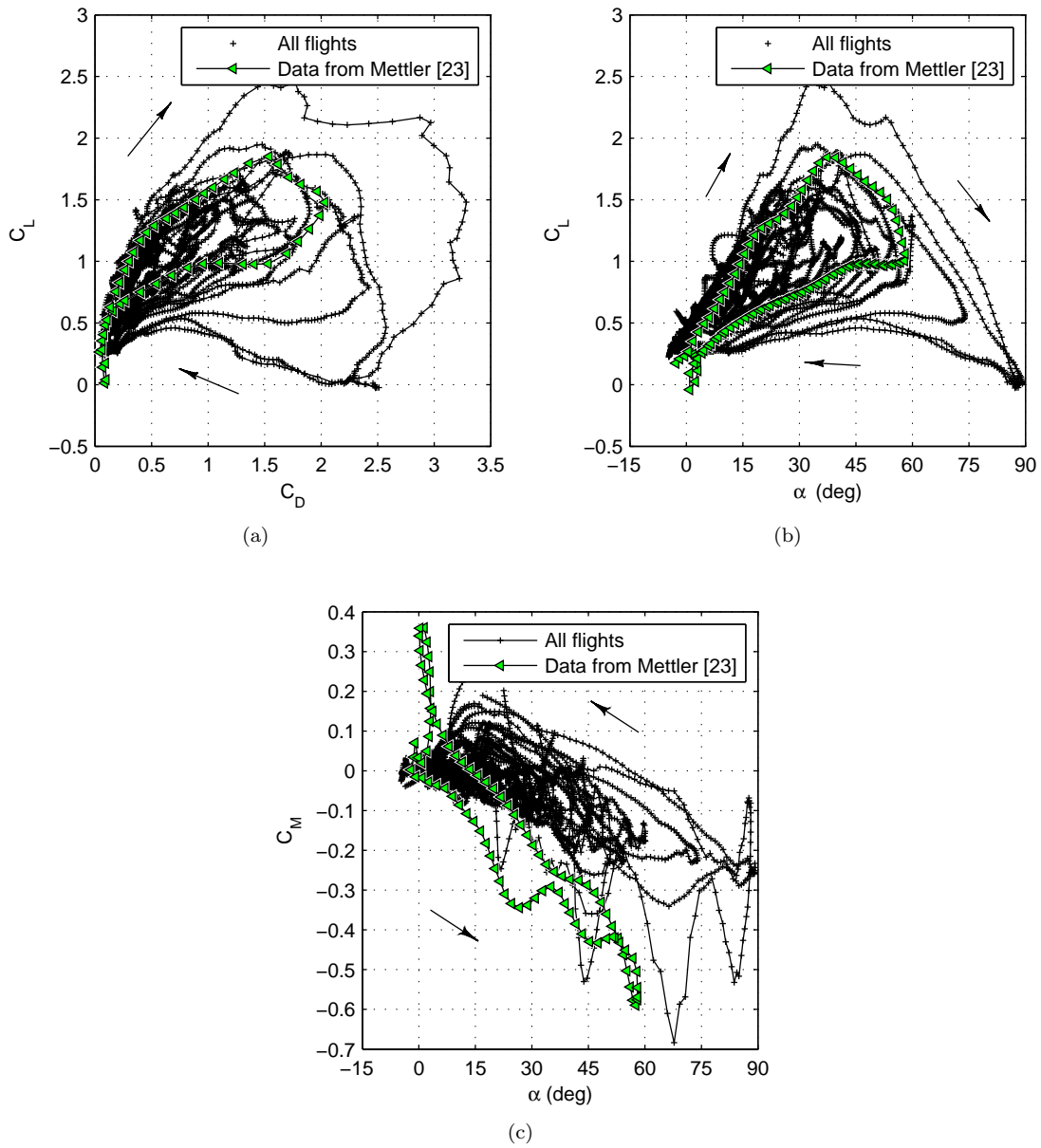
Figure 5.5: Comparison between the current results for the (a) drag, (b) lift, and (c) moment coefficient for the unsteady flights of the Vapor and Mettler's small glider.

steady state condition and increased to well above 2.0 in the unsteady case. However, the influence of k diminished during high angle-of-attack flight in deep stall ($\alpha > 70$ deg). Figure 5.6 shows that the range of C_L becomes smaller at high angles of attack and that the C_L variation as a function of k reduces as the angle of attack approaches 90 deg.
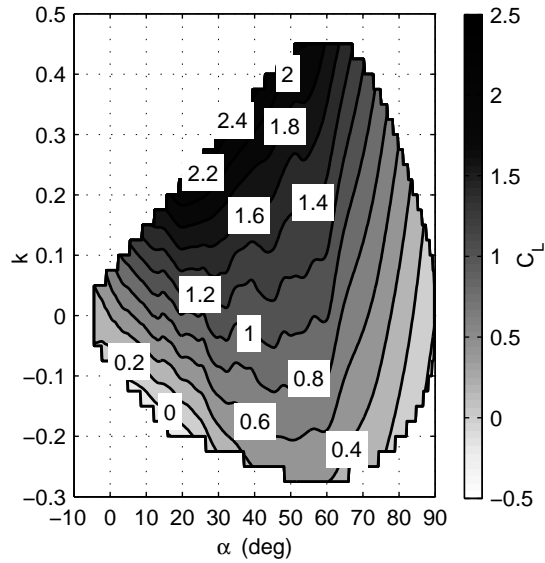
Figure 5.6: C_L as a function of α and k for the unsteady flights of the Vapor.
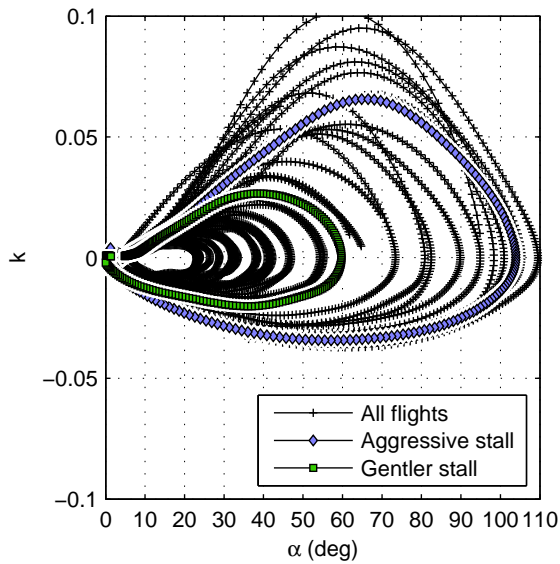
Figure 5.7: Reduced frequency as a function of angle of attack for the unsteady flights of the balsa glider with an aspect ratio of 11.7.
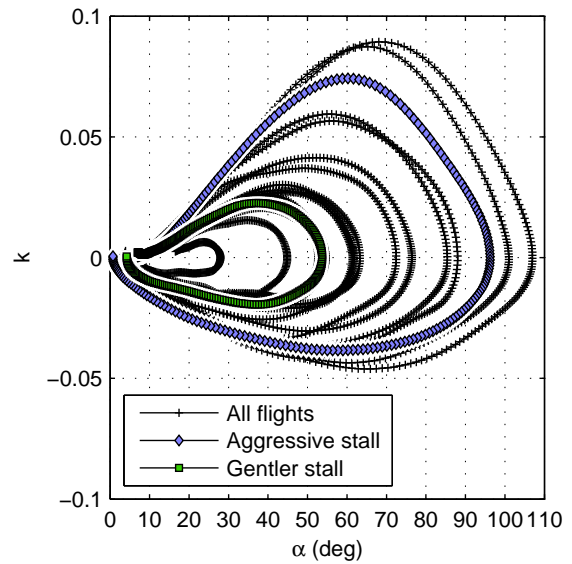
Figure 5.8: Reduced frequency as a function of angle of attack for the unsteady flights of the balsa glider with an aspect ratio of 6.07.

5.2 Unsteady Aerodynamic Characteristics for the Balsa Gliders

For the two balsa gliders, tests were conducted and data were collected for unsteady high angle-of-attack flight. The flights included aggressive stalls with the angle of attack exceeding 90 deg and large values of the reduced frequency as shown in Figs 5.7 and 5.8 for the 11.7 and 6.07 aspect ratio balsa glider, respectively. The balsa gliders have a smaller range for reduced frequency (maximum k of $\approx$0.1) than was observed for
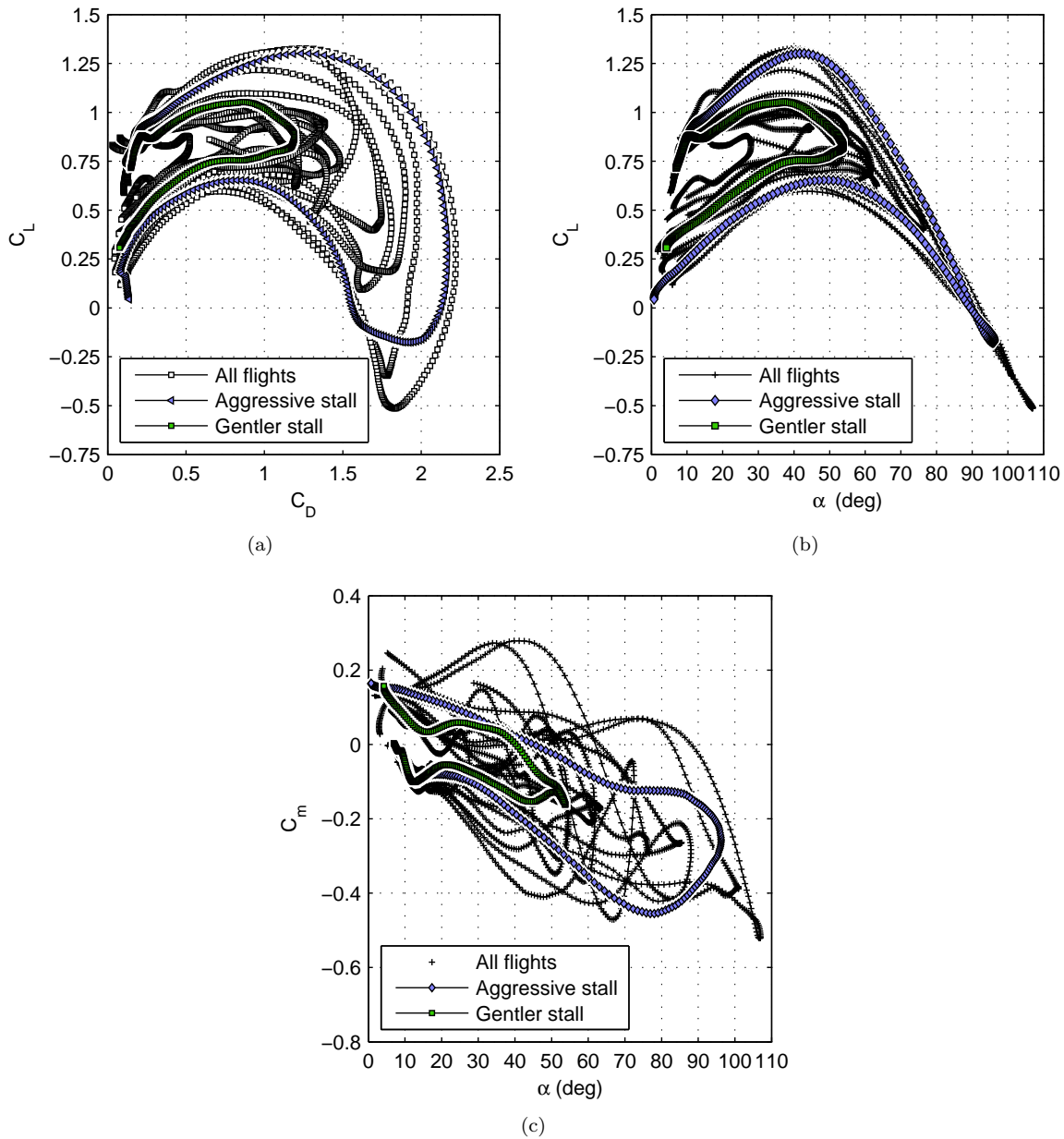
Figure 5.9: Experimental (a) drag, (b) lift, and (c) moment coefficient for the unsteady flights for the balsa glider with an aspect ratio of 6.07 (the trajectories for the highlighted flights are shown in Fig. 5.11).

the Vapor (maximum k of approximately 0.4). Even with the smaller values of reduced frequency, both of the gliders exhibit dynamic stall characteristics similar to the Vapor.

Figure 5.9 shows the drag, lift, and moment coefficient for the 6.07 aspect ratio glider in unsteady flight. The angle of attack exceeded 100 deg during two flights with aggressive stalls while other flights had lower values for angle of attack. The experimental results show a range of stalls from mild to aggressive. The two highlighted flights in Fig. 5.9 illustrate a more aggressive stall as well as a gentler stall (as compared

to the more aggressive example). The two flights were selected to compare the aerodynamic time histories of the flights. For all of the aerodynamic coefficients, hysteresis loops existed with differences between the portions of flight with increasing and decreasing angle of attack. As with the Vapor, drag in Fig. 5.9(a) follows a parabolic curve. For the lift coefficient data shown in Fig. 5.9(b), the degree of unsteadiness of the stalls (reduced frequency) had a large effect from stall until an angle of attack of 60–70 deg after which there is only a small difference in C_L between the portions of flight with increasing and decreasing angle of attack. Figure 5.9(c) shows a negative pitching-moment during the high angle-of-attack flight with some of the flights having a periodic variation and the two highlighted flights being relatively smooth.

In Fig. 5.9, the two highlighted flights were arbitrarily selected as representative flights with one being a more aggressive stall and the other being a gentler stall. The aggressive flight has a peak angle of attack of 96 deg while for the gentler flight the peak angle of attack is 54 deg. The reduced frequency range for the aggressive flight is −0.038 to 0.075 while the gentler flight has a reduced frequency range of −0.025 to 0.025 (shown in Fig. 5.8). The difference in degree of unsteadiness causes the hysteresis loops in the gentler case to have less separation between the portions of the flight with increasing and decreasing angle of attack (Fig. 5.9).

Figure 5.10 shows the trajectories and time histories of various parameters for the two highlighted flights from Fig. 5.9. The two plots have different axes limits and, thus, the two flights are co-plotted in Fig. 5.11 to allow comparison between the results. In Fig. 5.11, the flight with the more aggressive stall (dashed lines) has a larger increase in height, a slower minimum velocity and a steeper stall recovery dive than the gentler flight (solid lines). Both flights begin at a similar angle of attack below stall before the angle of attack rapidly increases to above 90 and 50 deg for the more aggressive and gentler stall, respectively. For the more aggressive flight, the angle of attack increases faster, which causes the difference in peak angle of attack (96 deg versus 54 deg) and the more dramatic variations in the time history of the aerodynamic characteristics. Hence, the lift coefficient in the more aggressive flight increases to a larger value and then decreases to a negative value. On the contrary, the lift coefficient changes more gradually, covers a smaller range and never becomes negative. Similarly, the drag coefficient is larger during the more aggressive stall—almost double at the peak. The moment coefficient becomes more negative during the more aggressive stall. For both flights the angle of attack is large, but the reduced frequency is much larger for the more aggressive flight which results in significantly different aerodynamic characteristics during the dynamic stall and stall recovery phases of flight. It is noted that the time between the initial increase in angle of attack and the return to low angle-of-attack flight is approximately the the same for both flights.
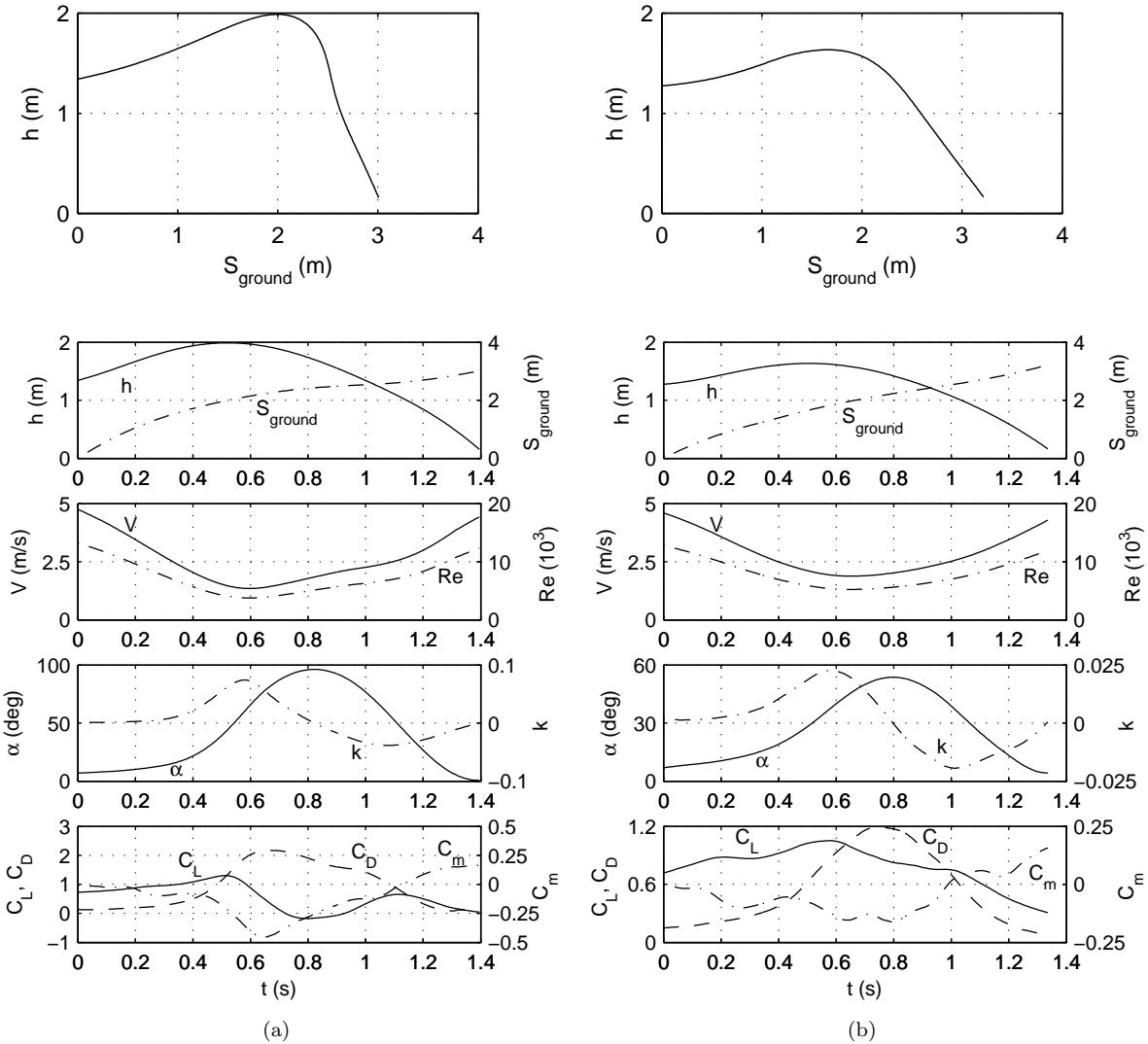
Figure 5.10: A flight trajectory along with the time history of various parameters for the highlighted flights for (a) the 'aggressive' stall and (b) for the 'gentler' stall of the balsa glider with an aspect ratio of 6.07.

Results for the 11.7 aspect ratio balsa glider are similar to the results shown for the 6.07 aspect ratio balsa glider. Figure 5.12 shows the lift, drag, and moment for the higher aspect ratio glider. Again, two flights are shown: one with an aggressive stall and one with a gentler stall are highlighted. Figure 5.12(a) shows a hysteresis loop for drag even at high angles of attack. For lift, the differences between the portions of flight with increasing and decreasing angle of attack is mostly before an angle of attack of 80 deg as shown in Fig. 5.12(b). After an angle of attack of 80 deg, the hysteresis effect is diminished and above an angle of attack of 90 deg there is little discernible difference between the portion of flight with increasing and decreasing angle of attack. The moment coefficient in Fig. 5.12(c) has differences between portions of

71
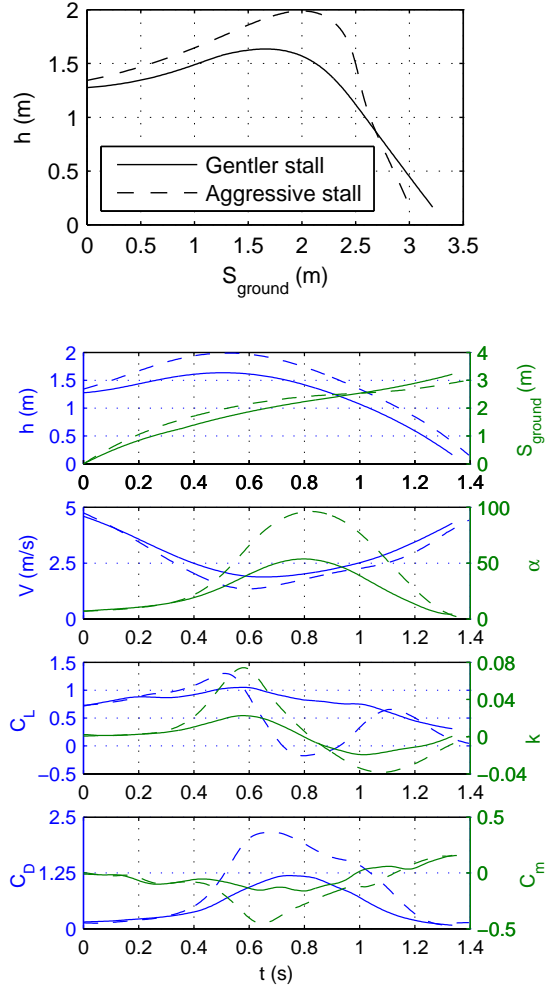
Figure 5.11: A comparison between the time history of various parameters for an aggressive stall (dashed line) and a gentler stall (solid line) for the balsa glider with an aspect ratio of 6.07.

flight with increasing and decreasing angle of attack throughout the angle of attack range just as with the drag.

Flight trajectories for the two flights that were highlighted in Fig. 5.12 are shown in Fig. 5.13, and the steepness of the stall recovery dives can be seen for the two flights of the balsa glider with an aspect ratio 11.7. The more aggressive stall [Fig. 5.13(a)] has a higher peak angle of attack, a larger $|k|$, and, as a result, a larger range for the aerodynamic coefficients than the gentler stall [Fig. 5.13(b)]. The two flights show some of the variation within the unsteady flights.
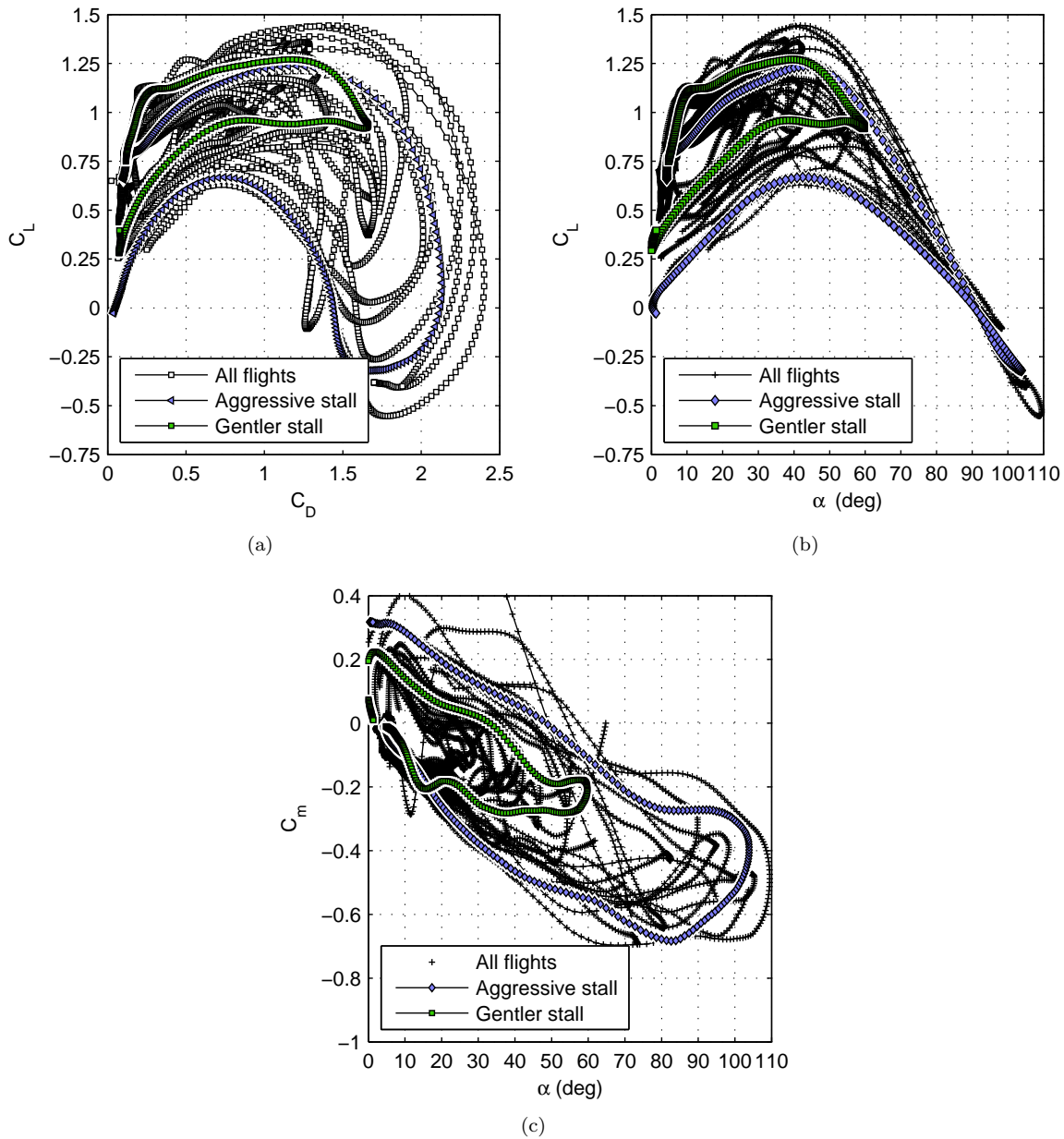
Figure 5.12: Experimental (a) drag, (b) lift, and (c) moment coefficient for the unsteady flights for the balsa glider with an aspect ratio of 11.7.

5.3 Discussion of Unsteady High Angle-of-Attack Results

The unsteady tests demonstrated the ability of the motion capture system to determine aircraft aerodynamic characteristics in unsteady flight without additional instrumentation or equipment. Specifically, the aerodynamic characteristics of the Vapor were shown for mild to aggressive stalls where the peak angle of attack was almost 90 deg, and the results included hysteresis loops for the lift, drag, and moment coefficient
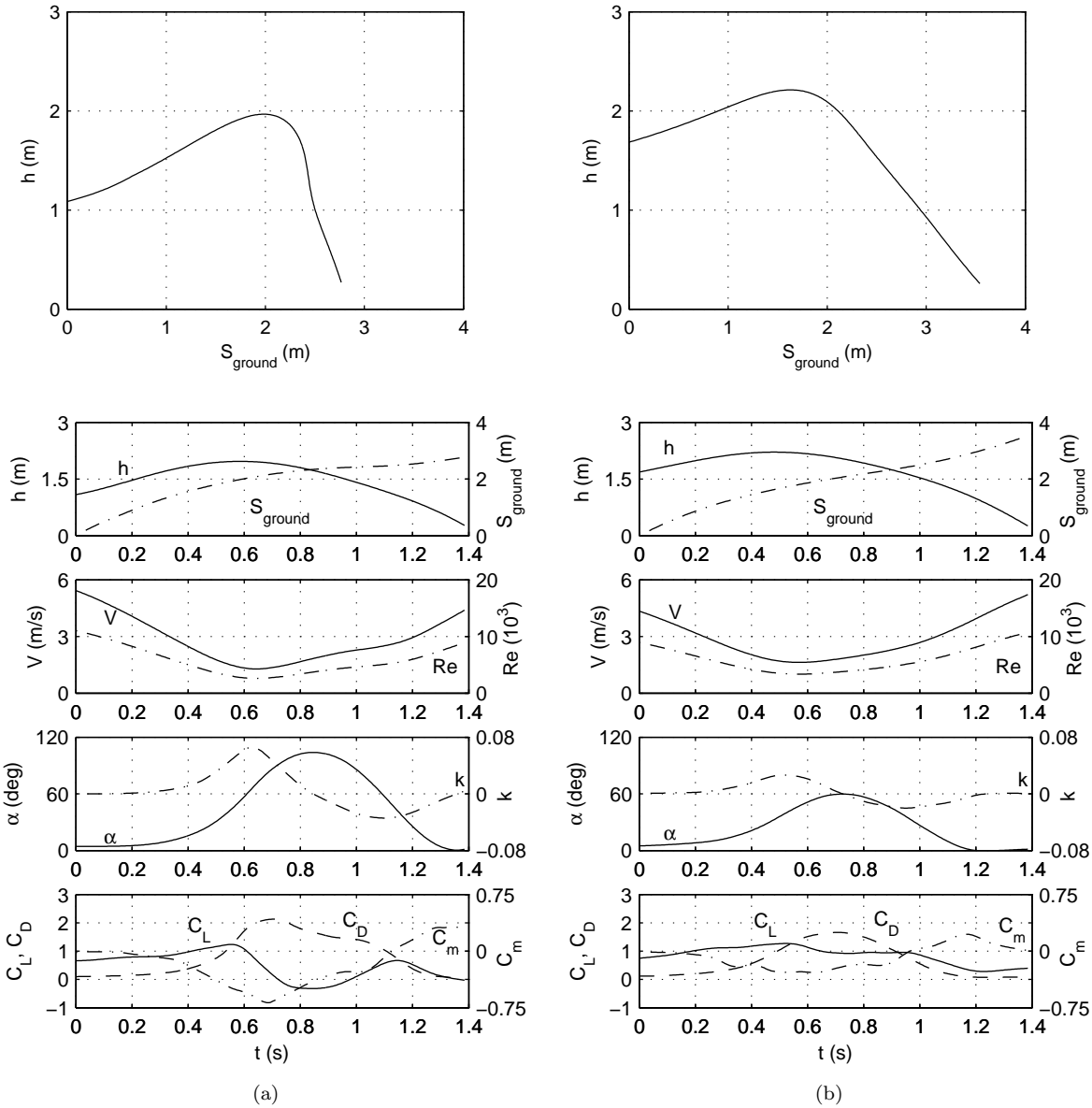
Figure 5.13: A flight trajectory along with the time history of various parameters for the highlighted flights for (a) the 'aggressive' stall and (b) for the 'gentler' stall of the balsa glider with an aspect ratio of 11.7.

as well as large drag coefficients due to unsteady flow. The two balsa gliders demonstrated aggressive stalls with angles of attack exceeding 90 deg as well as less aggressive stalls that also exhibited dynamic stall effects. With the balsa gliders, the differences in the lift coefficient between the portions of flight increasing and decreasing angle of attack were largest at angles of attack below 75 deg. Above an angle of attack of 90 deg, the lift coefficient barely changed between the portions of flight with increasing and decreasing angle of attack. On the other hand, the drag, and moment coefficients had differences between the portions of flight with increasing and decreasing angle of attack that remained over the full range of angles of attack.

74

The experimental results exhibited the influence and complexity of the unsteady flow on the aerodynamic characteristics of MAVs.

Chapter 6

Modeling Unsteady High Angle-of-Attack Flight

The approach used for modeling the unsteady aerodynamics is based on the expanded state-space method of Goman and Khrabrov [29, 30]. In this work, the method was applied to model the unsteady fixed-wing MAV flight data shown in Chapter 5. Modeling the Vapor and the two balsa gliders required extending the method to unsteady low Reynolds number MAV flight that included angles of attack on the order of 90 deg and dynamic stall hysteresis loops.

6.1 Approach to Unsteady Modeling

In order to model unsteady aerodynamics, Goman and Khrabrov [29, 30] used an additional state variable to track the degree of flow separation during unsteady motion. In their model, the additional variable is referred to as the separation parameter x, and the equations for the aerodynamic characteristics (C_L, C_D, and C_m), that normally depend only on the angle of attack, are expanded to include a dependence on the separation parameter. The separation parameter ranges from 0 to 1 with the two extremes representing fully separated and fully attached flow, respectively. As part of the model, a curve for the separation parameter as a function of the angle of attack is required, and it represents the steady-state location of the separation parameter as a function of angle of attack $x_o = f(\alpha)$. At angles of attack below stall, the separation point is 1 indicating fully attached until the trailing edge, and, above stall, x moves forward and eventually reaching 0 when the flow is fully separated (up to the leading edge). Even though the separation parameter is based on the idea of the separation point which could be measured experimentally or computationally, the x_o curve is not the separation point but is generally determined to match experimental coefficient data e.g., tune x_o using the C_L vs. α curve.

In unsteady flight, the separation parameter lags the x_o result for the instantaneous α, and the lag accounts for the hysteresis in the aerodynamic coefficients. Figure 6.1 is used by Goman and Khrabrov [29, 30] to illustrate results for the lift curve with the state-space method as well as the separation parameter for a representative airfoil. The steady-state separation x_o in Fig. 6.1 is a function of the angle of attack with stall
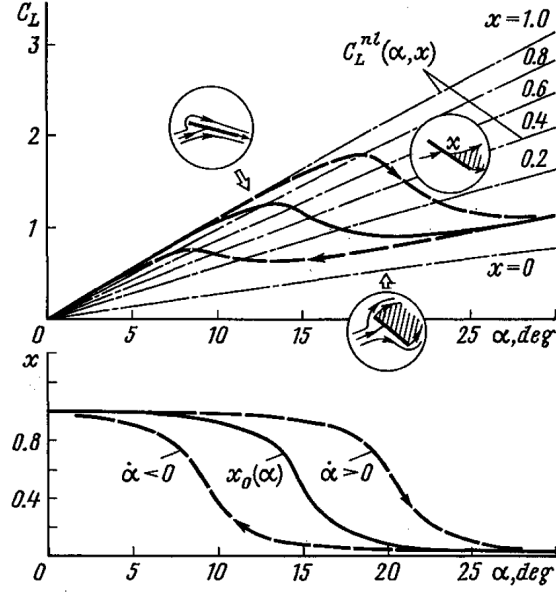
Figure 6.1: The steady and unsteady lift coefficient depending different values for the separation parameter (taken from [29]).

occurring at approximately 14 deg. In unsteady motion ($\dot{\alpha} > 0$ and $\dot{\alpha} < 0$), x lags behind the steady values so with increasing angle of attack x is larger than steady-state while x is smaller with decreasing angle of attack. To model C_L, the lift curve is a function of α and x, which means that the steady-state lift curve is C_L with x_o, and Fig. 6.1 shows a steady-state lift curve through stall and post stall to an angle of attack of 30 deg. In unsteady motion with increasing angle of attack, x is greater than x_o, so the lift coefficient is greater than the steady-state lift coefficient. During the subsequent decrease in angle of attack, x is smaller than x_o which decreases the lift coefficient.

In the state-space model, the lag of the separation parameter, which accounts for the overall effects of the unsteady flow on the entire aircraft, depends on the angle of attack and angle-of-attack rate. The value of the separation parameter is governed by a first-order lag equation,

$$\tau_1 \frac{dx}{dt} + x = x_f \tag{6.1}$$

where x_f is a forcing function

$$x_f = f(\alpha_{delayed}) \tag{6.2}$$

and

$$\alpha_{delayed} = \alpha - \tau_2 \dot{\alpha} \tag{6.3}$$

77

The first-order lag time constant τ_1 and the second time constant τ_2 scale with the characteristic time $\bar{c}/V$. The time constants have some association with physical phenomenal of unsteady flow but are not directly related to flow properties. The forcing function x_f evaluates the steady-state x_o at $\alpha_{delayed}$ that depends on the instantaneous angle of attack as well as $\dot{\alpha}$ and adds some delay in the response. The first-order lag time constant τ_1 can be loosely interpreted as representing the lag associated with the vortex shedding process. However, neither time constant is based on empirical measurements or first principles, and both parameters are tunable within the model, i.e. varied to best match unsteady experimental data.

Applying Eq. 6.1 to an case with increasing angle of attack results in the separation parameter lagging behind (and being larger than) the steady-state x_o curve. When the separation parameter is larger than the steady-state value for a given angle of attack, it indicates that the flow is more attached than x_o resulting in a larger value of C_L. The example in Fig. 6.1 has C_L reaching almost 2.0 when $\dot{\alpha}$ is positive before settling at the steady-state value with $\alpha = 30$. As the angle of attack decreases, the separation parameter lags and is smaller than x_o; consequently, C_L remains below the steady-state curve until the flow becomes fully attached at an angle of attack and approximately 6 deg.

For the lift, drag, and moment coefficients, semi-empirical formulations were developed in this work based on the unsteady flight test data for the Vapor and the two balsa gliders. The semi-empirical formulations were based on the low angle-of-attack assumptions and included terms for the linear lift curve, the drag polar, and the linear pitching moment. In addition to the low angle-of-attack assumptions, the formulations also depended on the separation parameter x and additional terms to capture the unsteady high angle-of-attack behavior. Specifically, functional forms for C_L, C_D, and C_m are given by

$$C_L(\alpha, x, k) = C_{L_\alpha} \left[(1 + \sqrt{x})/2\right]^2 \cos\alpha \cdot \sin\alpha + C_{L_o}\, x^2 + C_{L_k}\, k \tag{6.4a}$$

$$C_D(\alpha, x, C_L) = C_{D_o} + b_1\, C_L^2 + b_2 \sin^2\alpha + b_3\, x \cos\alpha \cdot (1 - \cos\alpha) + b_4\, x \sin\alpha \cdot (1 - \cos\alpha) \tag{6.4b}$$

$$C_m(\alpha, x, C_L, C_D) = C_{m_o} + C_{m_\alpha}\, \alpha + c_1 \sqrt{C_L^2 + C_D^2} + c_2 \left[(1 + \sqrt{x})/2\right]^2 + c_3\, k \tag{6.4c}$$

In Eq. 6.4(a), the first term accounts for the linear portion of the lift curve having a slope of C_{L_α} for the aircraft. In this work, an experimentally-determined lift curve slope for each MAV is used, but more generally, the lift curve slope can be adjusted to match computational or experimental results for a specific aircraft. To account for lift at high angles of attack, the trigonometric term $\cos\alpha \cdot \sin\alpha$ is used so that C_L peaks at an angle of attack of approximately 45 deg and decreases to zero at an angle of attack of approximately 90 deg which is consistent with flat plate theory. At small angles of attack, $\cos\alpha \approx 1$ and

78

$\sin\alpha \approx \alpha$, so the linear lift curve can be used with this specific trigonometric term as originally proposed in Ref. [62]. Previously, the functional form of the lift coefficient model in the state-space approach [29] used the $\sin\alpha$ term that is only accurate to an angle of attack of approximately 40 deg, while, in the current work, the $\cos\alpha \cdot \sin\alpha$ term is used for angles of attack up to 90 deg [34, 62]. The second term, $C_{L_o}x^2$, accounts for the lift at zero angle of attack due to the wing camber, and the effect of camber decreases at post-stall angles of attack as separation approaches the leading edge ($x = 0$). Finally, the stability derivative term C_{L_k} accounts for lift due to the instantaneous reduced frequency k.

Within the lift formulation [Eq. 6.4(a)], an apparent mass term is not explicitly included because during the flights, the apparent mass force was not significant, and, hence, was not needed in the formulation. It was observed to be generally on the order of 1–2% of the aircraft weight. There were short periods of time where the apparent mass was up to 5–10% of the aircraft weight. These small values are expected for fixed wing aircraft which, unlike flapping wing aircraft, have almost no acceleration perpendicular to the wings. As a result, including apparent mass effects did not influence the resulting fit lines for C_L, and, as such, Eq. 6.4(a) does not include an apparent mass term.

For the drag and pitching moment [Eqs. 6.4(b,c)], the first two terms are based on the low angle-of-attack assumptions—a parabolic drag polar and a linear moment curve. The drag equation includes the drag polar fit (C_{D_o} and b_1) that was determined from low angle-of-attack flight data in Section 4.1.1, while, for the pitching moment, the assumption is a linear pitching moment behavior described by the slope C_{m_α} and intercept C_{m_o}. At a steady-state angle of attack of 90 deg, the drag coefficient for the wing and horizontal tail was estimated using Eq. 4.17 as in Section 4.1.4, viz

$$C_{D,90} = 1.11 + 0.018 \mathit{R}$$
(6.5)

using the aspect ratio of the main wing and horizontal tail [64]. The total drag for the aircraft at $\alpha = 90$ deg was

$$C_{D,aircraft,90} = C_{D,w,90} + C_{D,tail,90}\frac{S_t}{S_{ref}}$$
(6.6)

where $C_{D,w}$ was the drag due to the wing at $\alpha = 90$ deg. The drag of the tail $C_{D,tail}$ was changed from being nondimensionalized by the tail reference area S_t to being nondimensionalized by the wing reference area S_{ref}. The drag of the tail was included in this case because the horizontal tail deflection angle was low which meant the local angle of attack for the tail was close to the aircraft angle of attack (90 deg). The total aircraft drag at $\alpha = 90$ deg from Eq. 6.6 was used in the b_2 term to represent the steady-state drag at an angle of attack of 90 deg. The next two terms, b_3 and b_4, were based on existing works [69–71] that were

found to be applicable to the MAV test data, particularly the high angle of attack flights. The coefficients c_1 and c_2 in Eq. 6.4(c) account for the moment at high angles of attack and c_3 captures the instantaneous unsteady effects.

Based on the unsteady flight data, the values of the semi-empirical coefficients in Eqs. 6.4(a–c), together with the curve for the separation parameter (x_o) and model time constants τ_1 and τ_2, were determined for each MAV. First, the terms characterizing flight at angles of attack below stall were determined experimentally by analyzing the quasi-steady flight results as shown in Chapter 4. These terms included the linear portion of the lift curve (C_{L_o} and C_{L_α}) and the drag polar (C_{D_o} and the induced drag term). Over the range of α below the experimentally-deduced stall angle, the separation parameter was set to be $x = 1$ which corresponded to attached flow. The development of the separation parameter curve continued with the separation parameter beginning to move toward the leading edge just before stall, thereby following the reduction in the measured lift curve slope. After stall, steady-state C_L should peak at $\alpha \approx 45$ deg before decreasing to zero at $\alpha \approx 90$ deg ($x = 0$). Using these key points, x as a function of the angle of attack was generally defined, but some final adjustments were later made to provide the best agreement with flight test results. For the two balsa gliders, the steady-state results from the model for high angle-of-attack flight were verified with the deep stall results from Section 4.1.4.

For the three MAVs (Vapor and two balsa gliders), the same formulation is used with different time constants and coefficients. In order to determined the time constants and coefficients, a subset of selected flights was used where the selected flights covered both the quasi-steady and unsteady flight regimes. To find the two time constants (τ_1 and τ_2) and C_{L_k}, all three were concurrently varied, and the resulting C_L from the model was compared with the experimental C_L for the selected flights. The best value of the time constants and C_{L_k} was used in the model. Once the time constants were determined, the unsteady separation parameter x was calculated throughout the selected flights and the coefficients in Eqs. 6.4(b–c) were determined by linear least squares regression using the same set of selected flights. After applying the regression, all of the terms in Eqs. 6.4(a–c) were known. For each MAV, the development of the model is shown starting with x_o, then the regression results, and finally the results of applying the model to a number of flights—both quasi-steady and unsteady.

6.2   Application of Modeling to the Vapor

For the Vapor, flight test results were presented in two groups. The low angle-of-attack quasi-steady results were presented in Section 4.1.1 and unsteady results high angle-of-attack results were presented in Section 5.1.
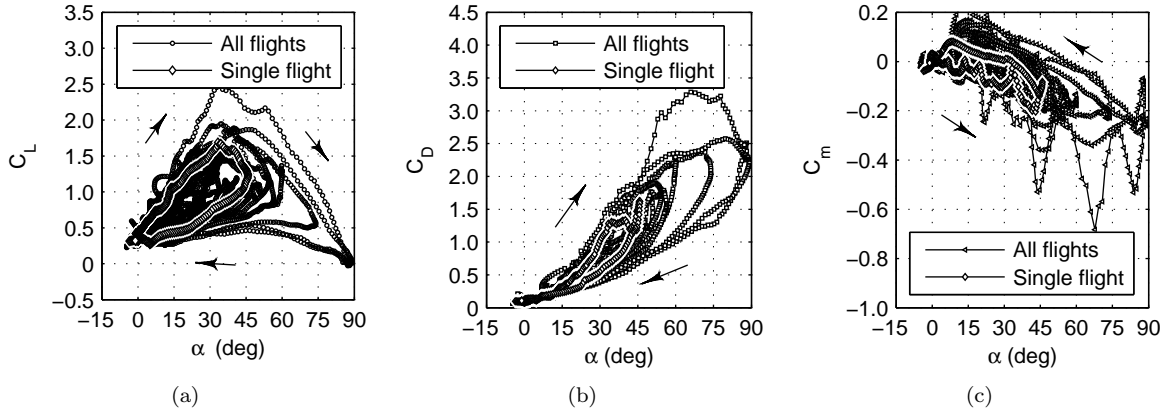
Figure 6.2: Experimental (a) lift, (b) drag, and (c) moment coefficient for the unsteady Vapor flights.

The flights classified as quasi-steady had $|k| < 0.05$ and were generally had angles of attack at or below stall. For the flights referred to as unsteady, the maximum angle of attack was well above stall and $|k|$ was larger than with the quasi-steady results. During each quasi-steady flight, the angle of attack had small variations on the order of 5 to 10 deg, while the unsteady flights included angle of attack excursions in the range of 20 to 90 deg.

The modeling method was developed to be applicable to the full range of lift, drag, and moment coefficient data shown in Fig. 6.2 (previously shown in Chapter 5 in Fig. 5.2). In the flights, the aerodynamic characteristics followed hysteresis loops that are easiest to observed in the single highlighted flight (see Fig. 6.2). The hysteresis loops illustrate the difference between the portions of flight with increasing and decreasing angle of attack, and the magnitude of the difference depends on the reduced frequency. For the lift and drag, the hysteresis loops proceed in the clockwise direction, and the larger values of lift and drag occur when k is positive (increasing α). For the moment coefficient data, the hysteresis loop goes in the counterclockwise direction, and the smaller values of moment occur when k is positive (increasing α).

In Fig. 6.2, the single highlighted flight (different from the single flight in Chapter 5) presents a fairly typical unsteady flight where the initial angle of attack was low and increased to a peak value before decreasing. Figure 6.3 shows the trajectory and time history data for the single highlighted flight with dynamic stall. The flight begins with decreasing height [see Figs. 6.3(a,b)], followed by an increase in height as the angle of attack increases and the velocity decreases [see Fig. 6.3(c)]. During the dynamic stall (shown in Fig. 6.2), the lift, drag, and moment coefficient data covered a large range of values and depended on the time history of the angle of attack as well as the angle-of-attack rate. Other flights with more aggressive stalls followed similar trends except with higher k values and a larger range for α, C_L, and C_D, while the gentler stalls had smaller ranges for k, α, C_L, and C_D.
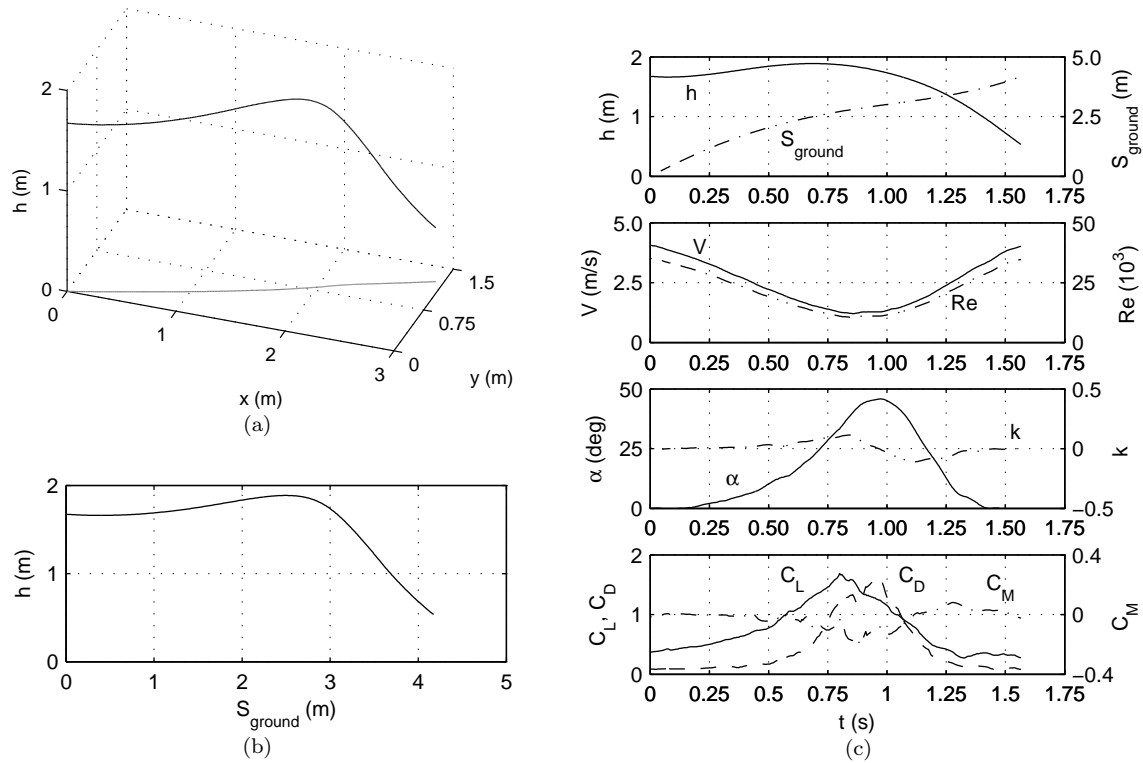
Figure 6.3: A single Vapor flight demonstrating an aggressive stall: (a) 3-D trajectory, (b) 2-D trajectory, and (c) time history data.

6.2.1   Development of the Vapor Model

From the data, it is clear that the model for the Vapor MAV must be applicable to a wide range of flight conditions from quasi-steady flight to unsteady high angle-of-attack flight. Figure 6.4 shows the maximum angle of attack and the maximum reduced frequency observed in each of the Vapor flights. The aggressive stalls have higher values for α and k, while the milder stalls have lower values of each. The flights that remain below the static stall angle of attack (experimentally-observed at ≈ 18 deg) with values for $|k| < 0.05$ are referred to as quasi-steady flights, as previously mentioned. The ten flights marked with pluses in Fig. 6.4 were used to determine the coefficients and time constants within the model, and the ten flights covered both the quasi-steady and unsteady flight regimes. Later, the results of the model will be shown for the flights with letter labels (A, B, C, and D). Flight A corresponds to the single flight highlighted in Fig. 6.3, and flight B corresponds to the single flight in Fig. 5.2 (from Chapter 5).

The first step in finding the model was to set the values in Eqs. 6.4(a–c) that were based on the low angle-of-attack flight regime. As such, the linear lift curve slope and the drag polar as found in Section 4.1.1 was used. Next, the semi-empirical $x_o = f(\alpha)$ curve as shown in Fig 6.5 was developed for the Vapor
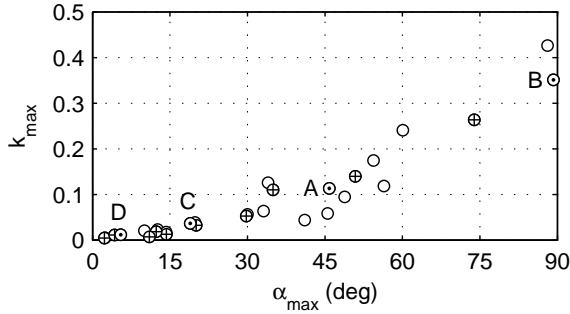
Figure 6.4: The degree of unsteadiness in the Vapor flights with the ten flights used for regression (circle-plus symbols) and the four example flights of the Vapor MAV labeled A, B, C, and D.
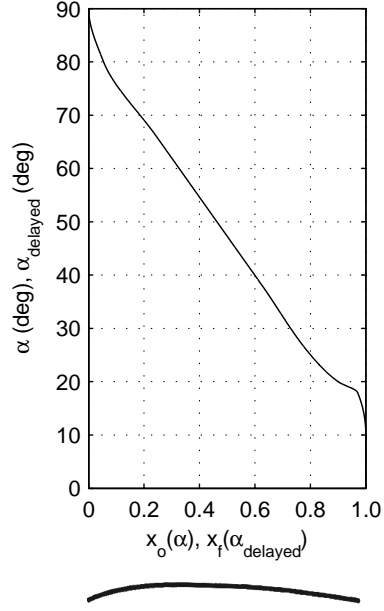
Figure 6.5: The curve showing the change in the separation parameter x with angle of attack together with a representative thin airfoil as used on the Vapor MAV.

MAV. For low angles of attack, the separation parameter was set to be $x_o = 1$ corresponding to flow fully "attached" until the trailing edge. Just before stall near $\alpha \approx$ 15 deg, the separation parameter begins to move forward (x_o decreases from 1). The decrease in x_o corresponds to the decrease in the lift curve slope associated with stall. After stall, the steady-state lift curve is known to peak at $\alpha \approx 45$ deg before decreasing to zero at $\alpha \approx 90$ deg ($x = 0$). Based on these key values, x_o as a function of the angle of attack curve was formed, but later, some adjustments were made between 60 and 90 deg to improve the agreement with flight test results.

The next step was to find the best values for the time constants and C_{L_k} coefficient for the lift coefficient in Eq. 6.4(a). Together, the three terms were varied while minimizing the difference between the predicted and experimental C_L, and the best result for the ten selected flights was achieved using $\tau_1 = 2.46\,\bar{c}/V$, $\tau_2 = 0.384\,\bar{c}/V$, and $C_{L_k} = 1.60$. With the time constants known, the separation parameter was calculated throughout the ten flights, and then the remaining coefficients in Eqs. 6.4(b–c) were found with a linear

least squares regression. After applying the regression, Eqs. 6.4(a–c) for lift, drag, and moment become

$$C_L(\alpha, x, k) = 2.21\,[(1 + \sqrt{x})/2]^2 \cos\alpha \cdot \sin\alpha + 0.38\,x^2 + 1.6\,k \tag{6.7a}$$

$$C_D(\alpha, x, C_L) = 0.054 + 0.26\,C_L^2 + 1.5\,\sin^2\alpha - 1.11\,x\cos\alpha \cdot (1 - \cos\alpha) + 1.59\,x\sin\alpha \cdot (1 - \cos\alpha) \tag{6.7b}$$

$$C_m(\alpha, x, C_L, C_D) = 0.464 - 0.571\,\alpha + 0.212\,\sqrt{C_L^2 + C_D^2} - 0.541\,[(1 + \sqrt{x})/2]^2 - 0.871\,k \tag{6.7c}$$

In order to better illustrate the model, details of the model will be shown, including the aerodynamic coefficients for angles of attack of 0–90 deg and the effects of varying lag. First, the sensitivity of the aerodynamic coefficients to the separation parameter is shown in Fig. 6.6 for C_L, C_D, and C_m. The coefficients are plotted for values of the separation parameter corresponding to fully "attached" ($x = 1$), steady-state ($x = x_o$), and fully "separated" ($x = 0$). For the lift shown in Fig. 6.6(a), the curve for the steady-state and the curve for the case $x = 1$ match for angles of attack below static stall. The steady-state lift curve decreases for the case of $x = 1$ at an angle of attack of approximately 18 deg which corresponds to wing stall deduced from flight test measurements. All three cases peak near an angle of attack of 45 deg and approach zero at an angle of attack of 90 deg. Figure 6.6(b) shows the drag curves, and the $x = 1$ curve matches the steady-state curve until separation. After static stall, the drag for the $x = 1$ case grows the fastest of the three cases because $x = 1$ has the largest lift coefficient, and consequently the highest induced drag. At high angles of attack, the steady-state drag coefficient approaches 1.5, which corresponds to the drag of the wing and tail in perpendicular ($\alpha = 90$ deg) flow. The steady-state moment coefficient curve is shown in Fig. 6.6(c), and at low angles of attack, the moment curve is linear; and static stability is indicted by the negative C_{m_α}.

Second, the effects of the time constants are illustrated using the time history data from Flight A. The velocity and angle of attack time history are in Fig 6.3(c). From Eq. 6.1, the separation parameter time history was calculated for three values of τ_1, while τ_2 remained constant at the baseline value, and then τ_2 varied while τ_1 remained constant. The baseline values for the time constants were the best values determined from the ten selected flights, and as previously stated they were $\tau_1 = 2.46\,\bar{c}/V$ or $\tau_2 = 0.384\,\bar{c}/V$. Figure 6.7 shows the progression of x during the flight for the different values of the time constants along with the steady-state curve (x_o). The lag associated with Eq. 6.1 depends on the time constants, and, as expected, the larger time constants, particularly τ_1, result in a slower response, while smaller time constants result in x more closely tracking the steady-state curve. While the second time constant τ_2 (from the forcing function Eq. 6.2) does not effect the lag of x as much as τ_1, it influences the time where x starts to decrease. For
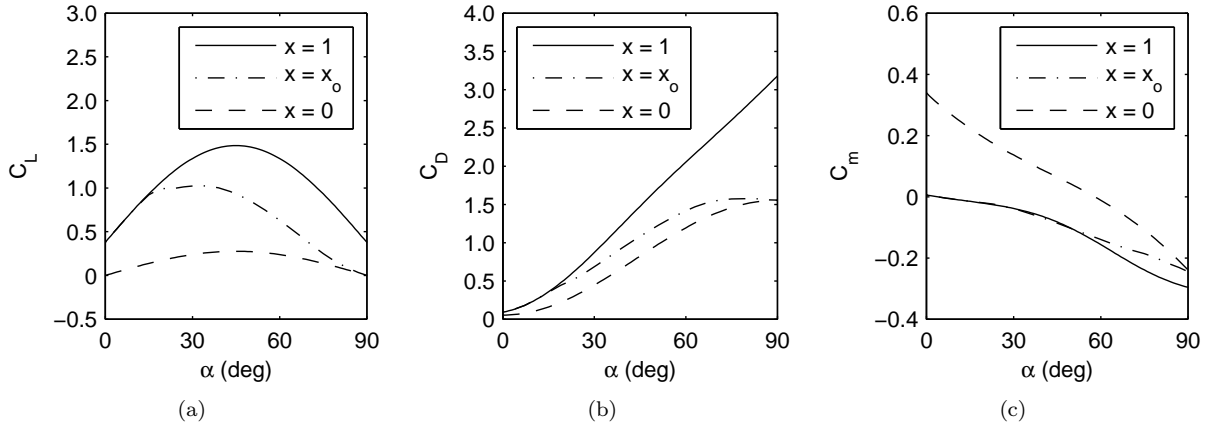
Figure 6.6: The (a) lift, (b) drag, and (c) moment coefficient curves for the Vapor MAV for the separation parameter values: fully "attached" $(x = 1)$, steady state $(x = x_o)$, and fully "separated" $(x = 0)$.
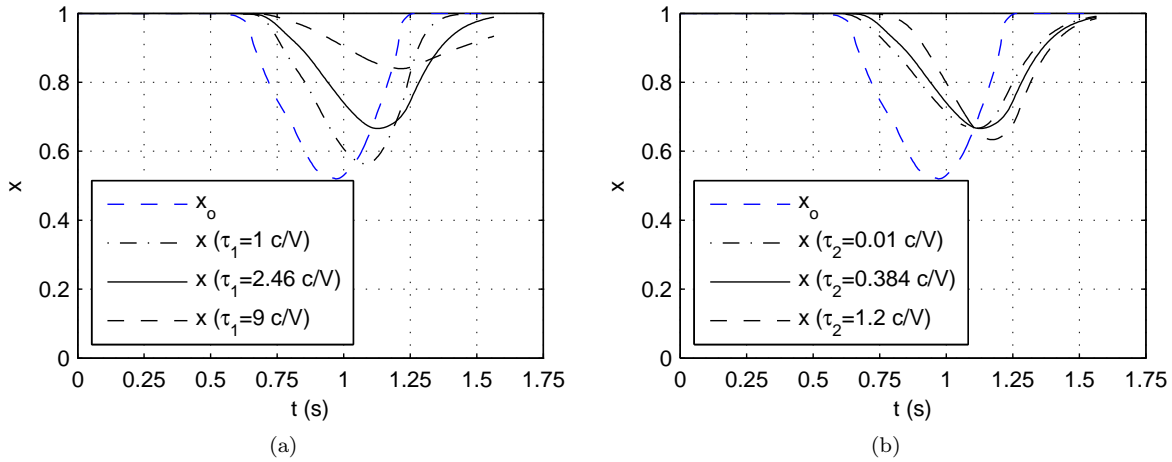
Figure 6.7: The separation parameter time history for flight A of the Vapor for (a) $\tau_1 = 1\,\bar{c}/V$, $2.46\,\bar{c}/V$ (baseline), and $9\,\bar{c}/V$ with $\tau_2 = 0.384\,\bar{c}/V$ (baseline) and for (b) $\tau_2 = 0.01\,\bar{c}/V$, $0.384\,\bar{c}/V$ (baseline), and $1.2\,\bar{c}/V$ with $\tau_1 = 2.46\,\bar{c}/V$ (baseline).

the three values of τ_2 in Fig. 6.7(b), the time instance (and hence angle of attack) at which x first starts to decrease depends on τ_2 while barely changing with the different values of τ_1.

Changes in the progression of x impact the aerodynamic coefficients as shown in Figs. 6.8 and 6.9 which plots C_L, C_D, and C_m for different values of τ_1 and τ_2. The hysteresis loops observed in Figs. 6.8 and 6.9 depend on the lag in x which depends on the time constants. Increased values of τ_1 create larger hysteresis loops with greater values of C_L and C_D, while smaller values of τ_1 create smaller hysteresis loops as illustrated in Fig. 6.8. In Fig. 6.9(a), the effect of τ_2 is illustrated by the different angles of attack (between 20 and 30 deg) where the lift curve slope begins to decrease. Similarly, in Fig. 6.9(b-c), the drag and moment curves change at different values of angle of attack depending on τ_2.

85
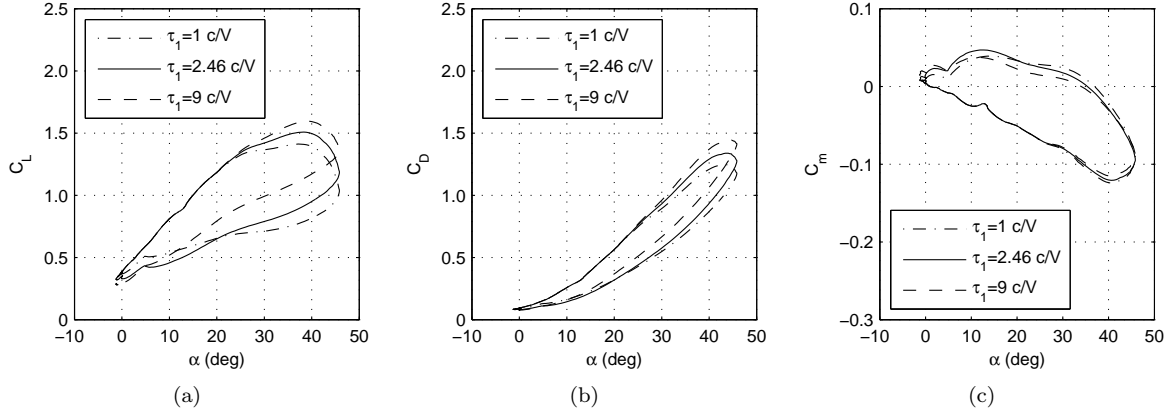
Figure 6.8: The modeling results for flight A of the Vapor for the (a) lift, (b) drag, and (c) moment coefficient for $\tau_1 = 1\,\bar{c}/V$, $2.46\,\bar{c}/V$, and $9\,\bar{c}/V$ with $\tau_2 = 0.384\,\bar{c}/V$.
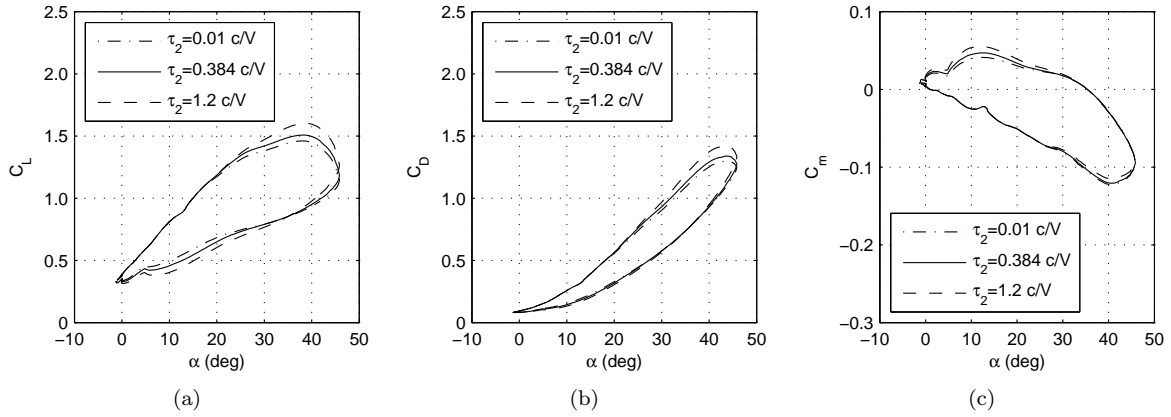
Figure 6.9: The modeling results for flight A of the Vapor for the (a) lift, (b) drag, and (c) moment coefficient for $\tau_2 = 0.01\,\bar{c}/V$, $0.384\,\bar{c}/V$, and $1.2\,\bar{c}/V$ with $\tau_1 = 2.46\,\bar{c}/V$.

Additionally, the amount of overshoot in the aerodynamic characteristics depend their sensitivity to x, e.g., $\partial C_L / \partial x$. As a result, any changes in the terms in formula for C_L as in Eq. 6.4(a) will impact the selected values for the time constants. While some correlation with fluid dynamics has been ascribed to the time constants, they are only semi-empirically based on physical flow properties and the lag observed in experimental data. As a result, the time constants vary within the literature [29, 33, 65] for different sets of unsteady test data.

6.2.2 Modeling Results for the Vapor

Using the model for the Vapor MAV developed and explained in the preceding section, it is possible to compare simulated results from the model with experimental results. The comparison was completed for four flights identified as A, B, C, and D that were first shown in Figure 6.4. Table 2 lists the angle of attack

Table 6.1: Characteristics of the Four Representative Flights of the Vapor

Flight	α range lower, upper (deg)	k range lower, upper
A	−1, 46	−0.10, 0.10
B	4, 90	−0.20, 0.40
C	−2, 19	−0.03, 0.04
D	−1, 6	−0.01, 0.01

and reduced frequency range for each flight. The flights included both unsteady (A and B) and quasi-steady (C and D) flights.

The flight 2-D trajectory of flight A in Fig. 6.10(a) shows a highly dynamic flight where the speed increases up to stall followed by steep descent. Figure 6.10(b) shows the time history of the various experimental parameters (black lines with markers) and the model predictions (green lines) for C_L, C_D, and C_m. The symbols (experimental results) are plotted at a rate of 20 Hz, while the actual experimental data was taken at a rate of 200 Hz. Overall, there is good agreement between the predictions and experiment for this highly dynamic flight with peak angle of attack of 46 deg. As previously shown in Fig. 6.8, the separation parameter corresponds to "fully" attached flow ($x = 1$) until the angle of attack increases to approximately 25 deg (which is above the static stall of $\approx$ 18 deg). Above 25 deg, the separation parameter decreases and C_L continues to increase until just above an angle of attack of 35 deg. Figure 6.11 presents the aerodynamic coefficient data as a function of angle of attack, and, in this format, the dynamic stall hysteresis loops are evident in both the experiment and model predictions. For lift, the model tracks the C_L dynamic stall loop well during the rapid increase of α to $\approx$ 45 deg (positive k). The drag model slightly overpredicts C_D during the initial increase in the angle of attack, and the predictions improve during the recovery. Figure 6.10 shows the moment time history, and the modeling results track the general trend but underpredict the peak magnitude at approximately 0.8 s and do not capture most of the detailed variations. Flight A illustrates the applicability of the model to flights with dynamic stall.

Flight B for the Vapor follows a similar trajectory to that of flight A. Figure 6.12(a) shows the trajectory including a climb, decrease in airspeed, and stall followed by a steep recovered dive. Flight B had larger values of the reduced frequency and the angle of attack than that of flight A. Even with the larger range of angle of attack, Fig. 6.12(b) shows that the model track the experimental coefficients fairly well. Just past stall (0.6 s), the predicted C_L lags behind the experimental lift coefficient. Similarly, the predicted C_D lags behind the experimental C_D starting at 0.7 s and the maximum value of C_D is underpredicted. The model for C_m matches the magnitude during the maneuver but overpredicts the maximum excursion (negative C_m) during the peak in angle of attack at approximately 0.75 s. In Fig. 6.13, the predictions follow the overall
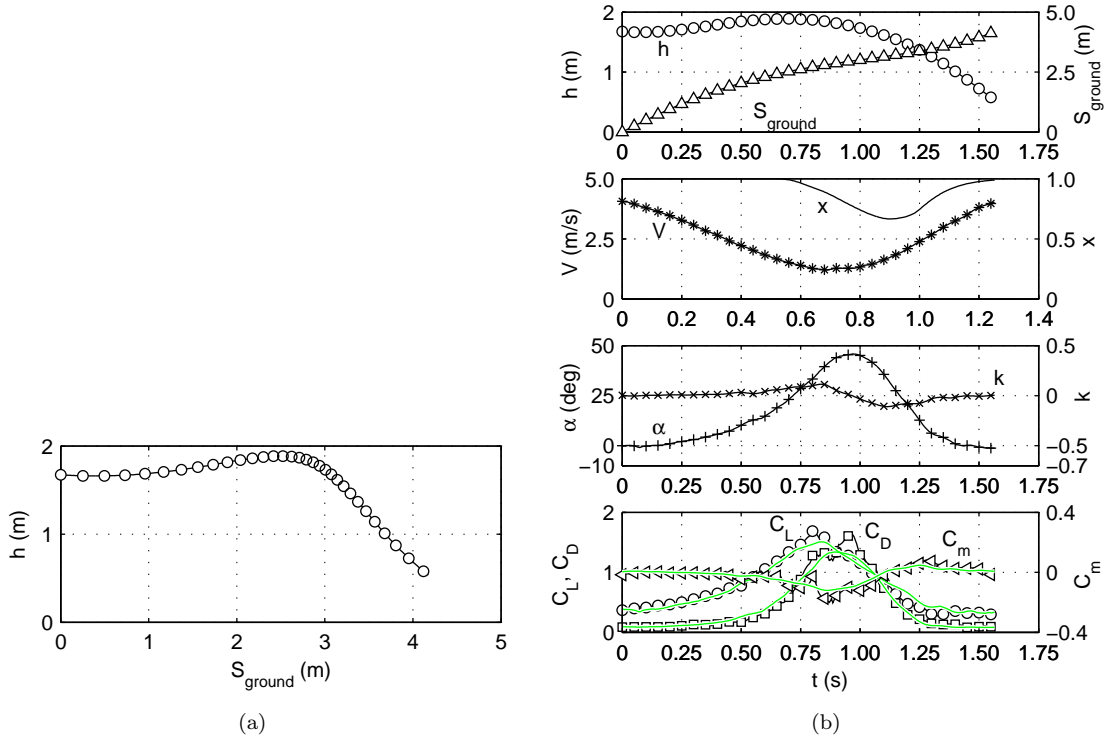
Figure 6.10: The (a) ground track and (b) time history of the modeling results (green lines) for flight A of the Vapor (corresponds to the flight seen in Fig. 6.3) compared with experiment (black markers).
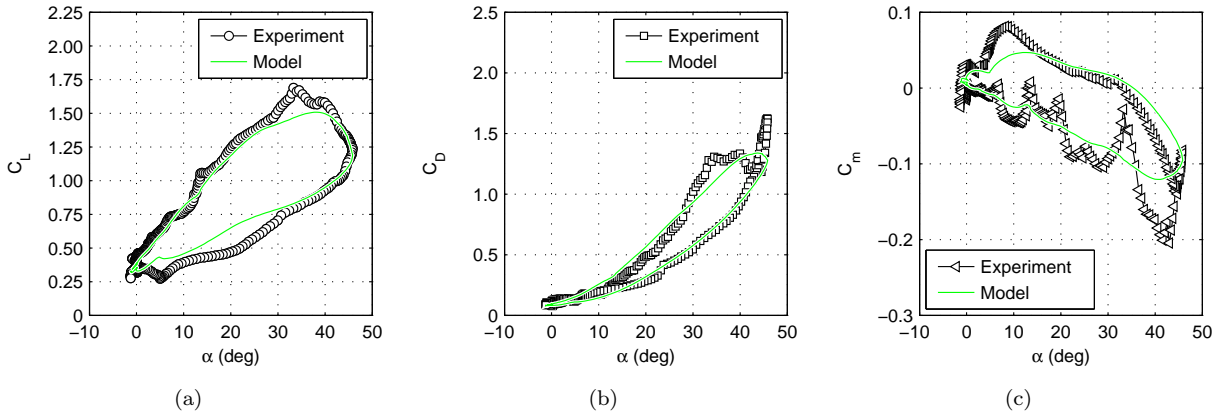
Figure 6.11: The modeling results (green lines) for flight A of the Vapor (corresponds to the flight seen in Fig. 6.3) for the (a) lift, (b) drag, and (c) moment coefficient compared with experiment (black markers).

trends of the measurements with both having large dynamic stall hysteresis loops, but some of the variations are not captured. Overall, it is shown that the model adequately captures the hysteresis loops observed in two highly dynamic and agile flights (A and B). The state-space model captures the differences between the two flights even though it is a reduced-order modeling method. Most of the existing variation between
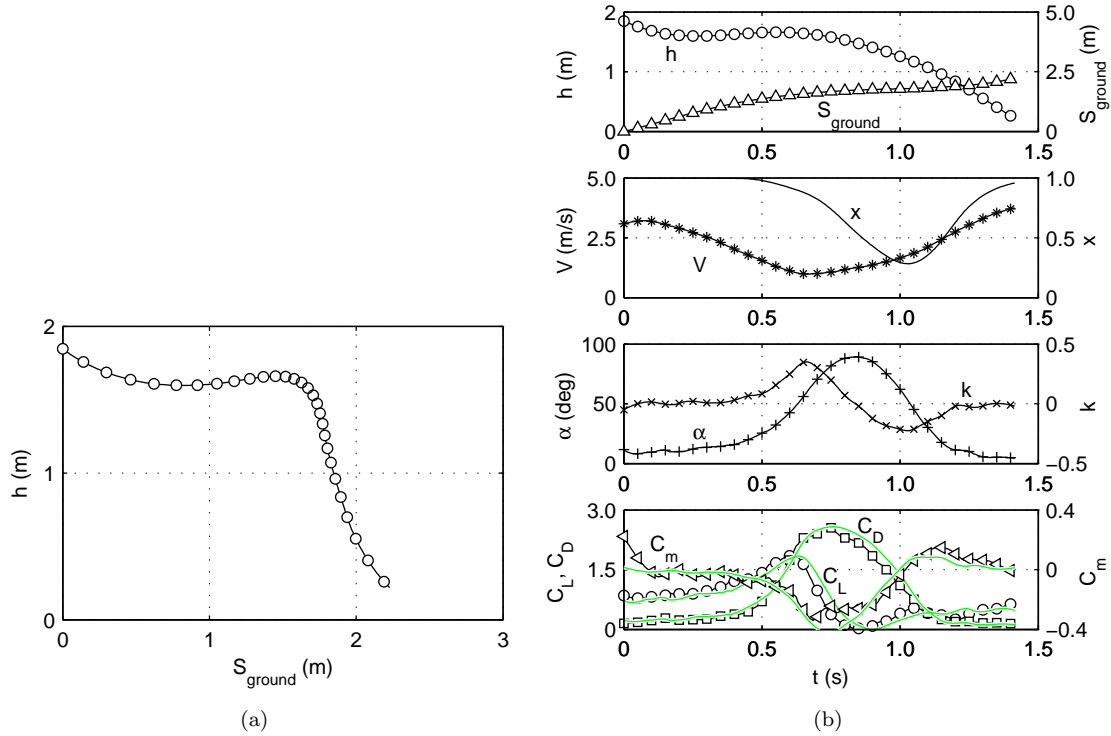
Figure 6.12: The (a) ground track and (b) time history of the modeling results (green lines) for flight B of the Vapor (corresponds to the flight seen in Fig. 5.4) compared with experiment (black markers).
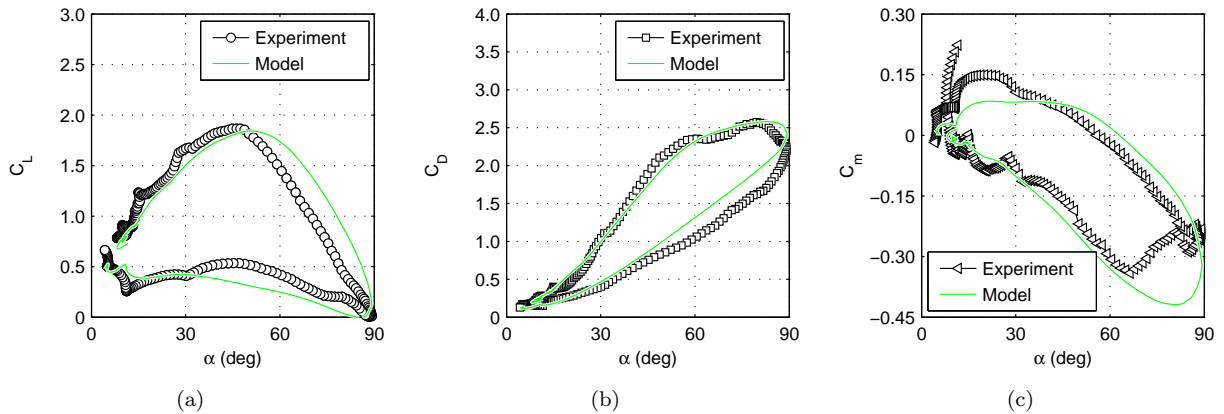
Figure 6.13: The modeling results (green lines) for flight B of the Vapor (corresponds to the flight seen in Fig. 5.4) for the (a) lift, (b) drag, and (c) moment coefficient compared with experiment (black markers).

measurements and predictions can be ascribed to higher-order dynamics and, as a result, some variations are expected given the limitations of the state-space method.

Initially, the influence of the trigonometric terms (b_3 and b_4) on Eq. 6.4(b) is not clear, but their effect on the drag prediction can be illustrated using the results from Flight B. Eliminating the terms from the model degrades the modeling results for C_D particularly at angles of attack above 45 deg. Figure 6.14 shows
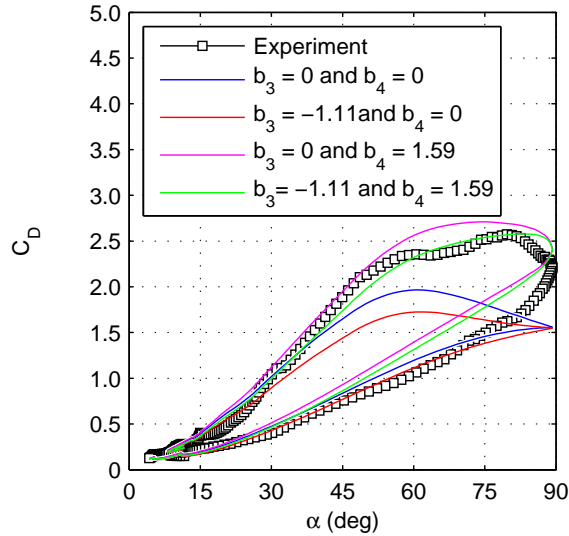
Figure 6.14: The effect of setting coefficients b_3 and b_4 in the drag model to zero as compared to nominal values of -1.11 and 1.59, respectively, for flight B of the Vapor.

the modeling results for C_D with b_3 and b_4 set to zero together and individually. The modeling results for flight B of the Vapor with both b_3 and b_4 set to zero is the blue line in Fig. 6.14, and, with the two terms set to zero, the hysteresis loop in the drag polar is not as large as in the experimental data. With just b_4 set to the nominal value, the hysteresis loop of the model starts to resemble the experimental results. With the addition of b_3, the modeling results more closely match the experimental results. The results of Fig. 6.14 show how the two trigonometric terms which were based on ideas from Refs. 69–71 influence results for C_D from the model particularly at high angles of attack.

In flight C, the angle of attack slightly exceeds static stall with the peak angle of attack of 19 deg. The time history in Fig. 6.15 shows the separation parameter decreasing only slightly from 1. After the initial increase in height [Fig 6.15(a)], the flight trajectory transitions to a near-steady glide path with increasing speed without any large values of k. Throughout the time history of the flight, the model is in close agreement with the experiment. Figure 6.16(a) shows the experimental lift curve with only a small difference between the portions of flight with increasing and decreasing angle of attack, and most of the differences are captured in the C_L model. The smaller hysteresis loop is due to the gentler stall and is in contrast to the large hysteresis loops seen previously in flights A and B. For drag [see Fig. 6.16(b)], the model follows the experimental results during the portion of the flight with increasing angle of attack but lacks the variations that occur with stall (between an angle of attack of 15 and 20 deg). Figure 6.16(c) confirms that the moment model captures the general trend and some of the variations in C_m. Flight C covers an angle of attack range where the linear steady-state flight model would hold, but with high quasi-steady values for
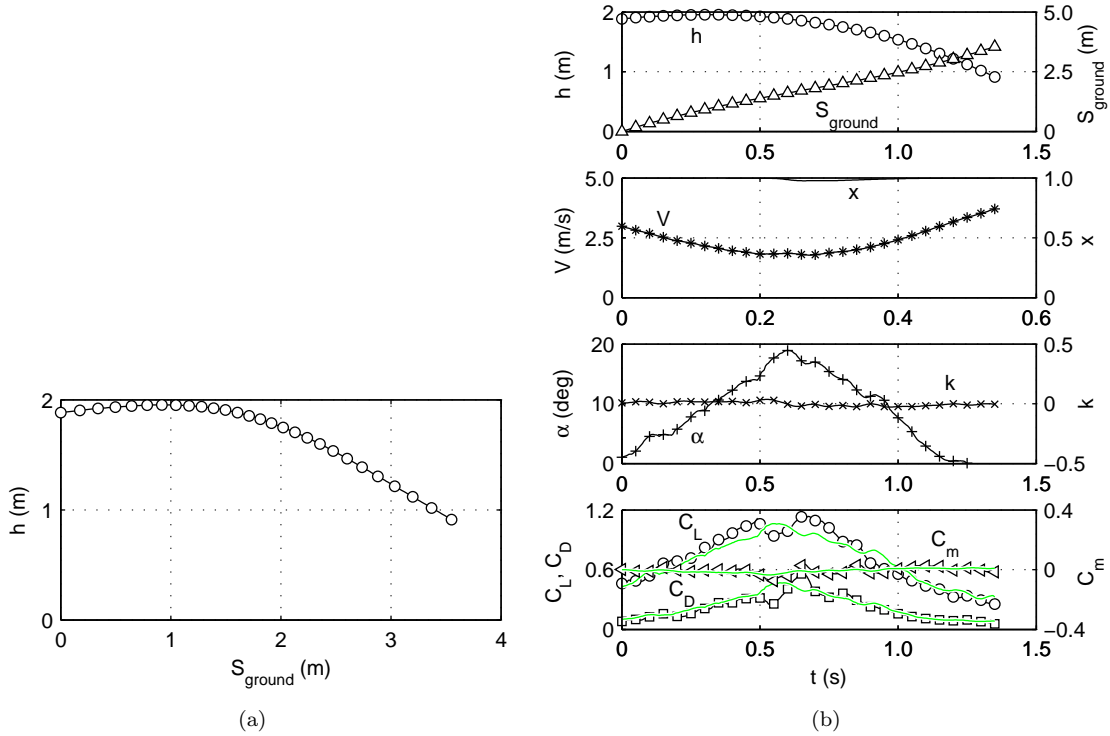
Figure 6.15: The (a) ground track and (b) time history of the modeling results (green lines) for flight C of the Vapor compared with experiment (black markers).
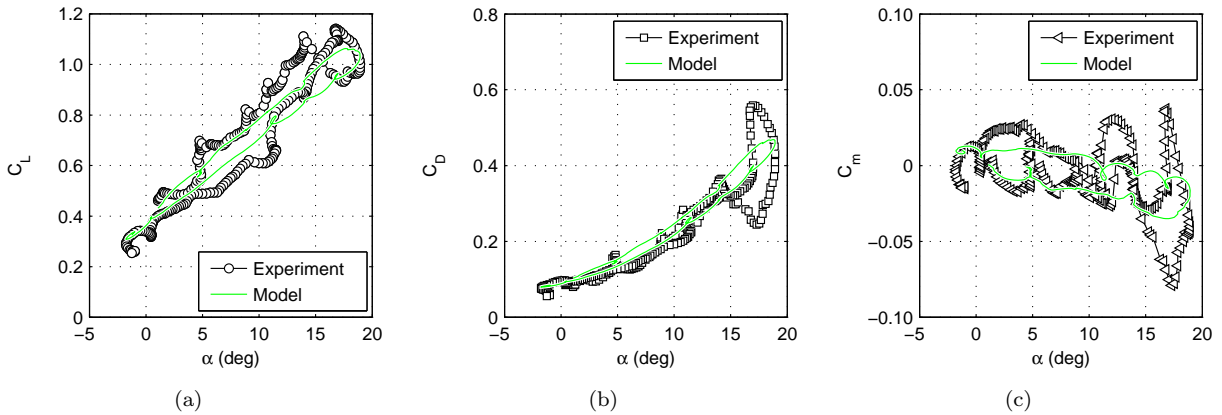
Figure 6.16: The modeling results (green lines) for flight C of the Vapor for the (a) lift, (b) drag, and (c) moment coefficient compared with experiment (black markers).

$|k|$ (up to 0.04). Hence, the experimental results include some unsteady effects, and the model accurately predicts most of the unsteady effects on the lift and drag.

The final flight D covers the angle of attack range of -1 to 6 deg with the maximum $|k|$ limited to $\approx$0.01. The time history is shown in Fig. 6.17 and is representative of the gentler quasi-steady flights. The flight consists of a fairly steady glide with slightly decreasing speed and subsequently increasing angle of attack.

91
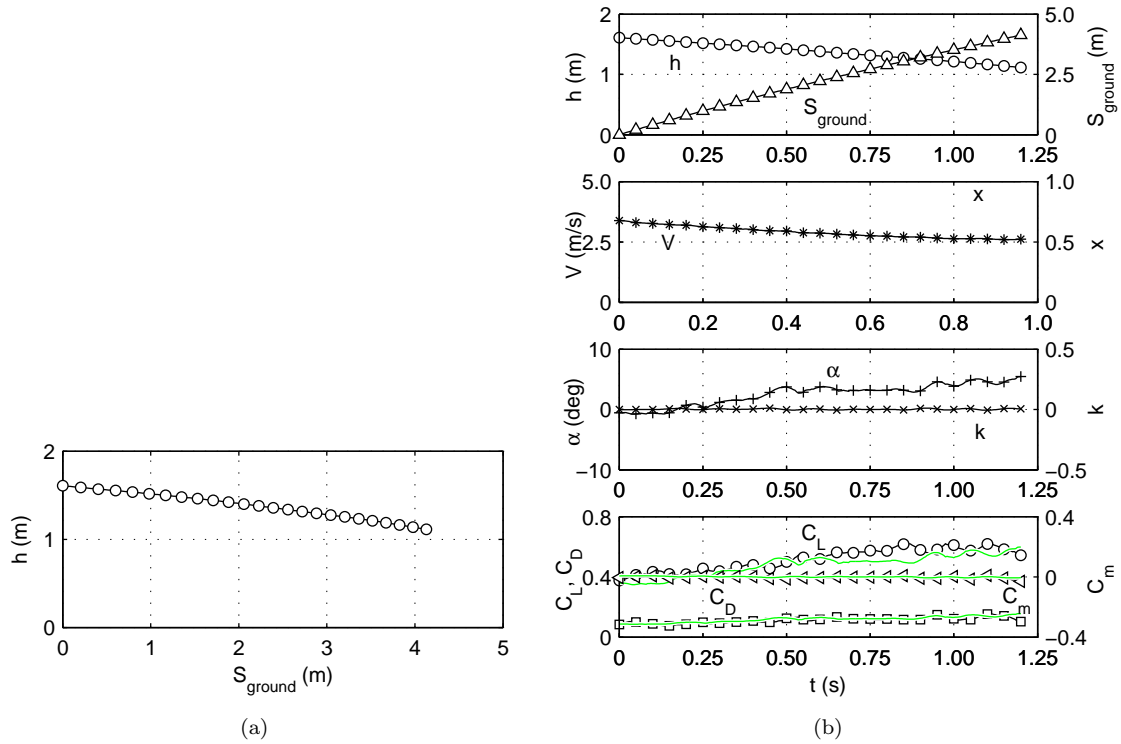
Figure 6.17: The (a) ground track and (b) time history of the modeling results (green lines) for flight D of the Vapor compared with experiment (black markers).
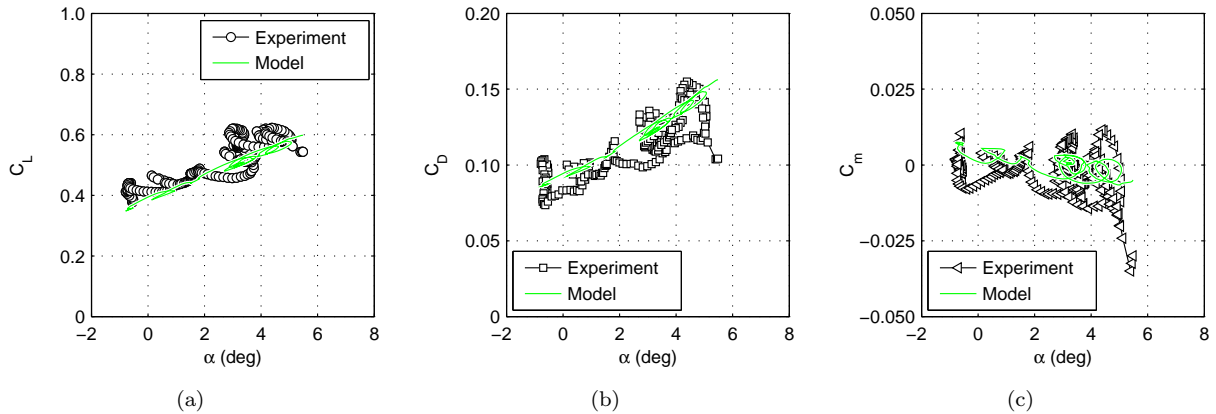
Figure 6.18: The modeling results (green lines) for flight D of the Vapor for the (a) lift, (b) drag, and (c) moment coefficient compared with experiment (black markers).

Figure 6.18 shows the estimates for the aerodynamic coefficients follow the trend lines of the measurements but do not capture the full degree of variations in the experimental data.

Results of the four flights show the applicability of the model to flights ranging from quasi-steady to unsteady. The model for lift, drag, and moment captured the hysteresis loops in the unsteady flights of the Vapor MAV as well as the smaller variations observed in the quasi-steady flights. From the results,

the longitudinal model was shown to be applicable to MAV flights ranging from dynamic agile flights to quasi-steady flights.

6.3   Modeling Results for the Balsa Gliders

The state-space method that was used with the Vapor was also applied to the unsteady flight results of the two balsa gliders from Section 5.2. Both of the gliders had similar geometry and wings with almost the same wing area, but one had a larger aspect ratio than the other (11.7 vs. 6.07) due to different wing chords. The same formulation (Eq. 6.4) for C_L, C_D, and C_m is used with the same lag equation (Eq. 6.1) as was used in the Vapor model. From the test data for each of the balsa gliders, the best values of the time constants and coefficients were determined through concurrently varying the terms. Moreover, the steady-state separation parameter x_o as a function of angle of attack was determined for each MAV, as the x_o curve was unique for each aircraft. This section will outline the model for both of the balsa gliders without going into the same detail as was done with the Vapor.

Figure 6.19 shows the separation parameter for each of the gliders, and the curve follows a similar trend for both gliders. The value of x_o is 1 at low angles of attack and decreases in value as the stall angle is approached. From the experimental results, the glider with an aspect ratio of 6.07 was observed to stall at a higher angle of attack (8 vs. 6.5 deg) than the glider with an aspect ratio of 11.7. Above stall, the separation parameter for both aircraft decreases rapidly to less than 0.2 by an angle of attack of 20 deg before essentially reaching zero close to an angle of attack of 60 deg. The steady-state separation parameter decreases faster at higher angles of attack than with the Vapor (see Fig. 6.5). The difference is ascribed to the variation in aspect ratio. At angles of attack past stall, the lift behavior of low aspect ratio wing such as the Vapor wing with $\mathcal{R} = 2.56$ will be different because of vortex lift.

The coefficients in Eq. 6.4 were found for each MAV individually. From the low angle-of-attack results in Section 4.1.3, the linear lift curve and drag polar terms in Eq. 6.4 were determined based on the values listed Table 4.1. For the unsteady terms, a set of quasi-steady and unsteady flights for each aircraft was used to find the coefficients and time constants—14 flights for the lower aspect ratio glider and 12 for the higher aspect ratio glider. Once the flights were selected, the coefficients were found starting with the time constants (τ_1 and τ_2) and C_{L_k}. The three terms were concurrently varied for each glider, and the values that resulted in the closest match between predicted and experimental C_L were selected.

For the balsa glider with an aspect ratio of 6.07 the values were $\tau_1 = 5.11\,\bar{c}/V$, $\tau_2 = 0.634\,\bar{c}/V$ and $C_{L_k} = 0.511$. The remaining terms were found using a linear least squares regression, and the formulations
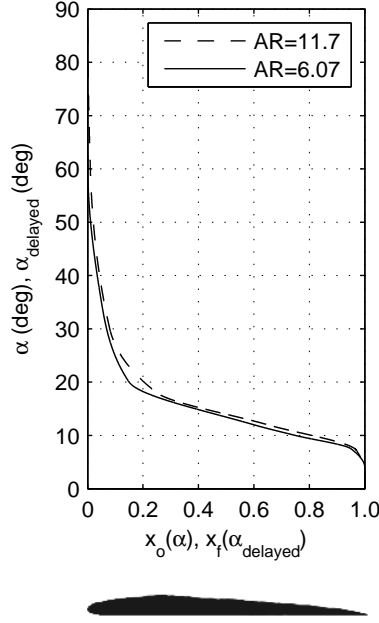
Figure 6.19: The curve showing the change in the separation parameter with the angle of attack for the two balsa gliders together with a representative thin airfoil.

for the aerodynamic coefficients for the lower aspect ratio glider are

$$C_L(\alpha, x, k) = 4.65 \left[(1 + \sqrt{x})/2\right]^2 \cos\alpha \cdot \sin\alpha + 0.103\, x^2 + 0.511\, k \tag{6.8a}$$

$$C_D(\alpha, x, C_L) = 0.048 + 0.178\, C_L^2 + 1.46\, \sin^2\alpha - 2.38\, x \cos\alpha \cdot (1 - \cos\alpha) + 8.03\, x \sin\alpha \cdot (1 - \cos\alpha) \tag{6.8b}$$

$$C_m(\alpha, x, C_L, C_D) = 0.222 - 0.266\, \alpha - 0.016\, \sqrt{(C_L^2 + C_D^2)} - 0.019\, [(1 + \sqrt{x})/2]^2 - 2.55\, k \tag{6.8c}$$

For the balsa glider with an aspect ratio of 11.7 the best match between experimental C_L was with $\tau_1 = 3.33\, \bar{c}/V$, $\tau_2 = 0.375\, \bar{c}/V$ and $C_{L_k} = 2.48$. After finding the remaining terms via a linear least squares regression the aerodynamic coefficients are

$$C_L(\alpha, x, k) = 5.13 \left[(1 + \sqrt{x})/2\right]^2 \cos\alpha \cdot \sin\alpha + 0.153\, x^2 + 2.48\, k \tag{6.9a}$$

$$C_D(\alpha, x, C_L) = 0.046 + 0.159\, C_L^2 + 1.55\, \sin^2\alpha - 7.96\, x \cos\alpha \cdot (1 - \cos\alpha) + 22.63\, x \sin\alpha \cdot (1 - \cos\alpha) \tag{6.9b}$$

$$C_m(\alpha, x, C_L, C_D) = 0.313 - 0.238\, \alpha - 0.160\, \sqrt{(C_L^2 + C_D^2)} - 0.215\, [(1 + \sqrt{x})/2]^2 - 3.67\, k \tag{6.9c}$$

94
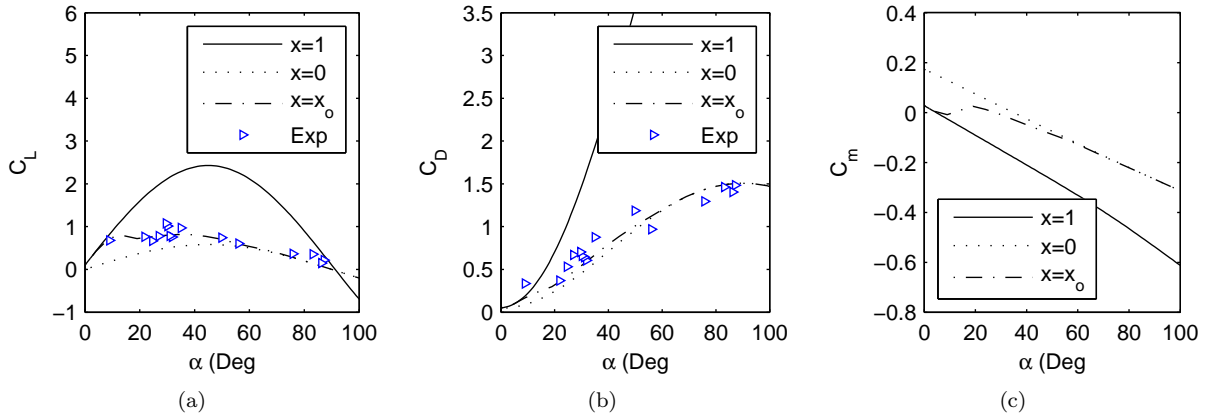
Figure 6.20: Quasi-steady high angle-of-attack experimental results for the 6.07 aspect ratio balsa glider for (a) lift, (b) drag, and (c) moment coefficient along with the curves for the models shown with different values of the separation parameter: $x = 1$ (fully "attached"), $x = 0$ (fully "separated"), and $x = x_o$ (steady-state).
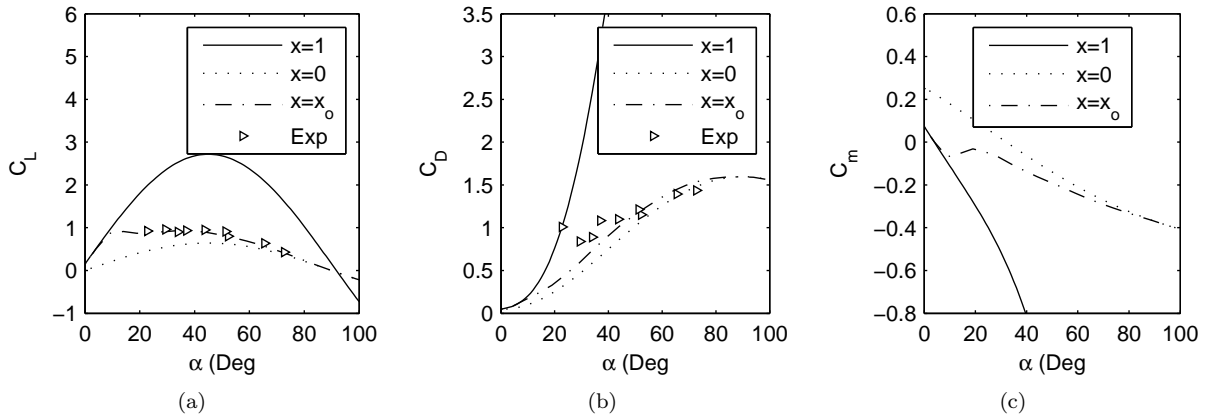
Figure 6.21: Quasi-steady high angle-of-attack experimental results for the 11.7 aspect ratio balsa glider for (a) lift, (b) drag, and (c) moment coefficient along with the curves for the models shown with different values of the separation parameter: $x = 1$ (fully "attached"), $x = 0$ (fully "separated"), and $x = x_o$ (steady-state).

Results for C_L, C_D, and C_m for three values of the separation parameter are shown in Fig. 6.20 and 6.21 for an angle of attack range of 0 to 100 deg. Just as with the Vapor, the separation parameter values are fully "attached," fully "separated," and steady state x_o. As with the Vapor, the results show the sensitivity of the aerodynamic coefficients to the separation parameter. Additionally, the lift and drag results in Fig. 6.20(a–b) and 6.21(a–b) include the experimental deep-stall results from Section 4.1.4 which are for quasi-steady high angle-of-attack flight. The steady-state results of the model can be compared with quasi-steady experimental results in the post-stall regime to further validate and tune the model. After comparing modeling results to the experimental data, the initial x_o curve was modified to better match experimental results. Thus, the experimental and modeling results closely match for the lift and drag shown for the two gliders in Fig. 6.20(a–b) and Fig. 6.21(a–b).

Table 6.2: Characteristics of the Representative Flights for the Balsa Gliders

Flight	α range lower, upper (deg)	k range lower, upper	$A\!R$ of balsa glider
E	1, 96	-0.04, 0.07	6.07
F	4, 54	-0.02, 0.02	6.07
G	6, 8	-0.001, 0.002	6.07
H	4, 95	-0.03, 0.06	11.7
I	3, 54	-0.02, 0.03	11.7
J	3, 4	$\approx\!0$, $\approx\!0$	11.7

The influence of the two trigonometric terms (b_3 and b_4) in the drag formulation [Eq. 6.4(b)] observed for the Vapor MAV continued with the two balsa gliders. For all three aircraft, including the two terms in the drag model increased C_D during the portion of flight with increasing angle of attack and, hence, better matched the pronounced hysteresis loops observed in the experimental C_D. Overall, the trigonometric terms have slightly larger influence on C_D for the two balsa gliders than with the Vapor MAV.

In the next two sections, the model will be applied to three flights for both of the balsa gliders. The results cover unsteady and quasi-steady flights and the details of the flights are listed in Table 6.2. With each balsa glider, the first two flights have varying degrees of unsteadiness and include flight at high angles of attack, while the final flight for both gliders covers low angle-of-attack flight in the quasi-steady regime.

6.3.1 Results for Flights of the Balsa Glider with an Aspect Ratio of 6.07

The comparison between the modeling results and the experimental results for the balsa glider with an aspect ratio of 6.07 begins with flight E which corresponds to the flight labeled as the 'aggressive stall' in Fig. 5.11. Figure 6.22(a) shows the trajectory of flight E which begins with a increase in altitude, then a stall with the angle of attack peaking at almost 100 deg followed by a steep stall recovery dive. As before, Fig. 6.22(b) shows the time history of the experimental results with the black markers plotted at 20 Hz and the predictions plotted as green lines. The flight is similar to flight B for the Vapor (see Fig. 6.13), and it is noted that the separation parameter decreases from 1 all the way to 0 during the recovery dive where the angle of attack is almost 100 deg. The results for the model track the time history of the experimental data. In Fig. 6.23, the model predicts the hysteresis loops in the aerodynamic coefficients. With C_L, the model overpredicts the lift toward the end of the recovery, but the model captures the limited difference between C_L with positive and negative k at angles of attack above 80 deg while showing the hysteresis effects at lower angles of attack.

The flight labeled as the 'gentler stall' in Fig. 5.11 is flight F, and the results of the prediction are presented in Fig. 6.24. Again, the flight begins with a slight climb followed by a stall and dive. The dive is shallower than in Flight E and the separation parameter is above 0 throughout the flight. Again, the model follows the time history for the aerodynamic coefficients. In Fig. 6.25, the dynamic stall hysteresis loops are shown, and, throughout the flight, the model switches between overpredicting and underpredicting C_L. For C_D and C_m, the model captures the hysteresis loops with more accuracy in C_D then C_m. Flight F and E both have dynamic stall with E being aggressive and F being gentler. Results for the flights show the model can predict a variety of unsteady high angle-of-attack flights with differing stall characteristics.

The final flight labeled G covers the low angle-of-attack regime staying just below stall. The trajectory of the glide shown in Fig. 6.26(a) was a steady descent at near-constant speed. Figure 6.26 shows the time history of the model closely matching the experiment. In Fig. 6.27, variations in the experimental coefficients are observed, and the model follows the mean trend while missing most of the instantaneous variations. Flight G was included to show the model accurately predicts longitudinal flight in the low angle-of-attack regime.
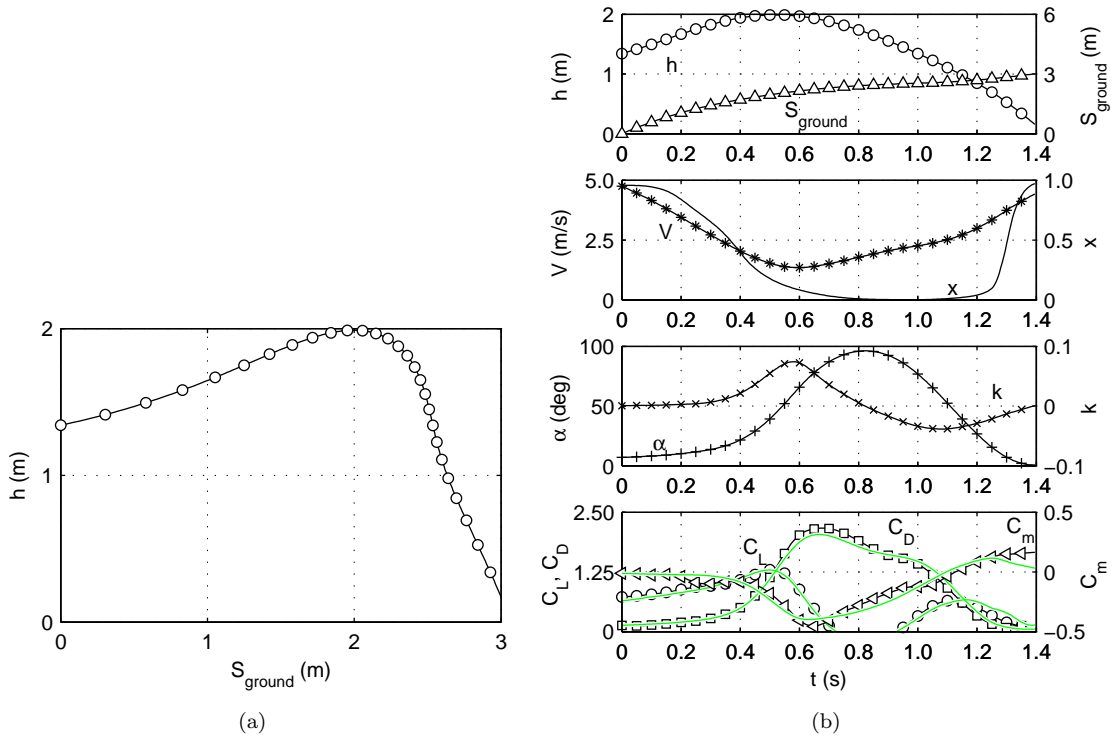
Figure 6.22: The (a) ground track and (b) time history of the modeling results (green lines) for flight E of the balsa glider with an aspect ratio of 6.07 [corresponds to the 'aggressive' flight seen in Fig. 5.10(b)] compared with experiment (black markers).
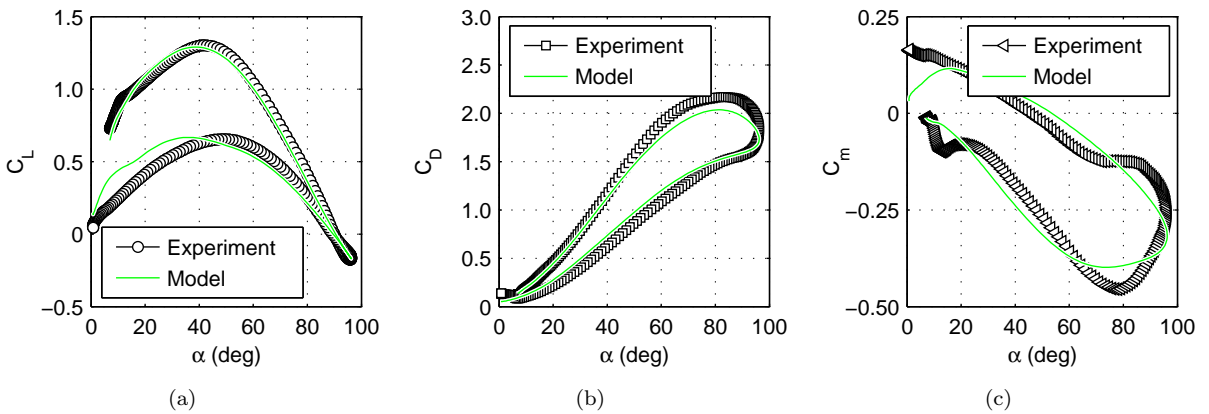
Figure 6.23: The modeling results (green lines) for flight E of the balsa glider with an aspect ratio of 6.07 [corresponds to the 'aggressive' flight seen in Fig. 5.10(b)] for the (a) lift, (b) drag, and (c) moment coefficient compared with experiment (black markers).
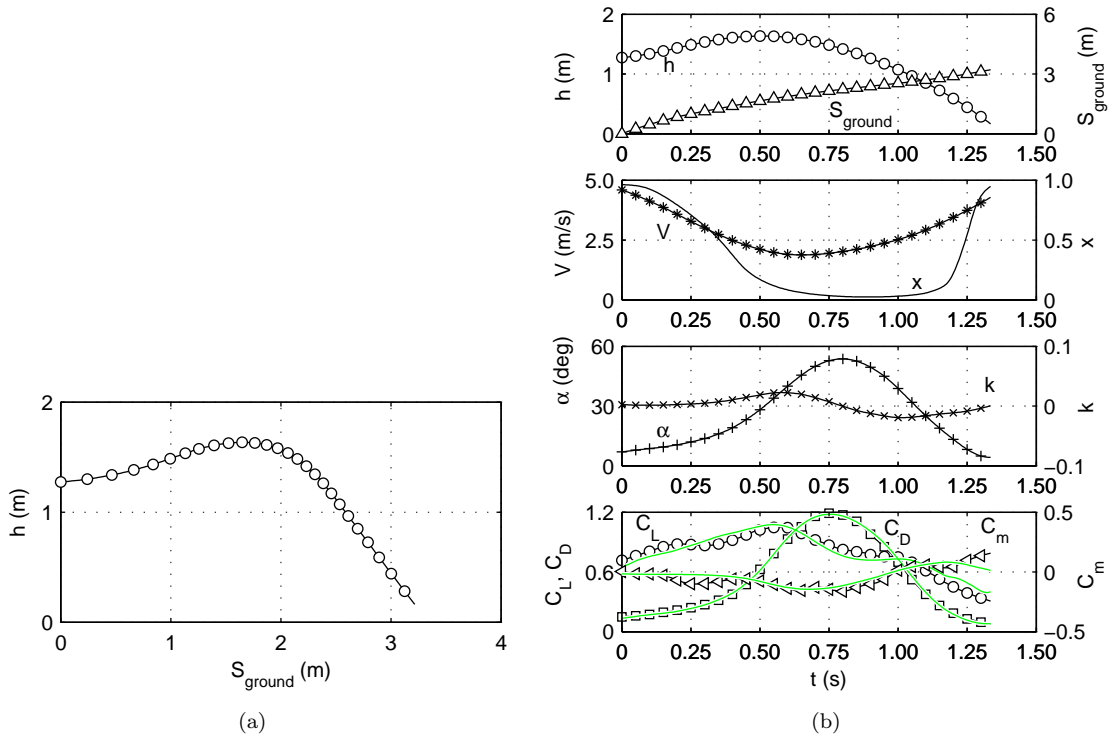
Figure 6.24: The (a) ground track and (b) time history of the modeling results (green lines) for flight F of the balsa glider with an aspect ratio of 6.07 [corresponds to the 'gentler' flight seen in Fig. 5.10(a)] compared with experiment (black markers).
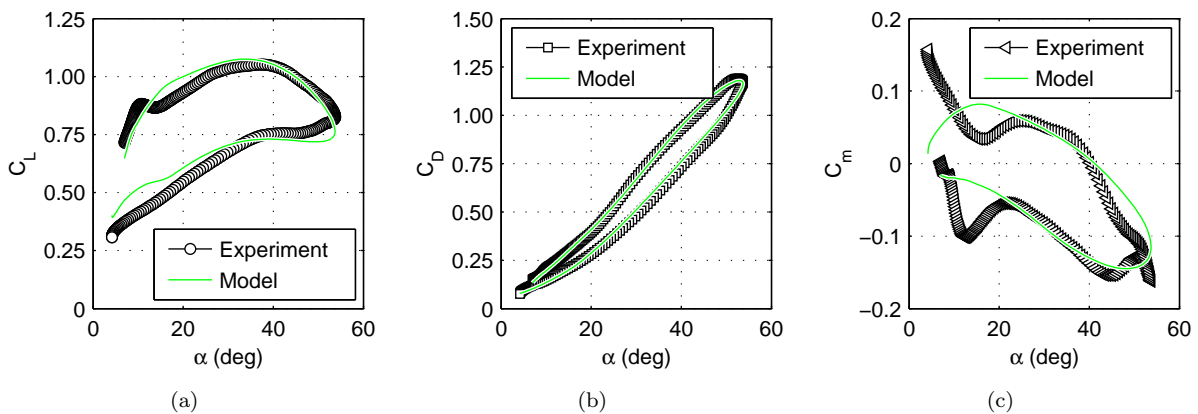
Figure 6.25: The modeling results (green lines) for flight F of the balsa glider with an aspect ratio of 6.07 [corresponds to the 'gentler' flight seen in Fig. 5.10(b)] for the (a) lift, (b) drag, and (c) moment coefficient compared with experiment (black markers).

99
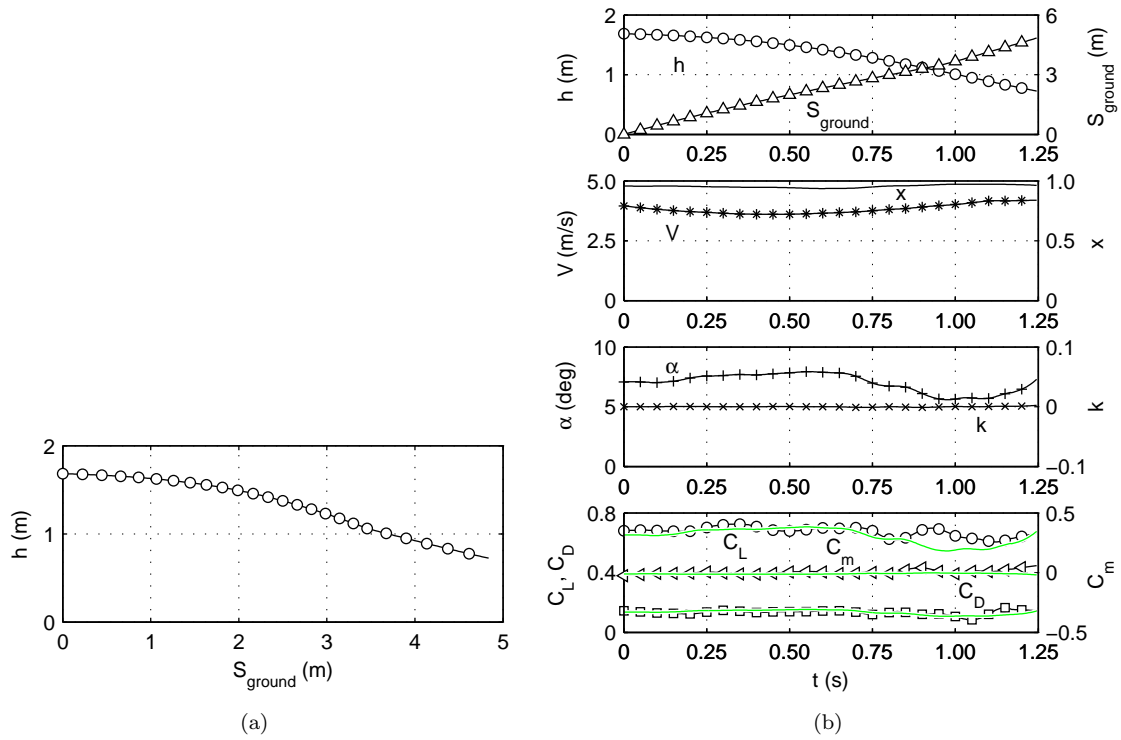
Figure 6.26: The (a) ground track and (b) time history of the modeling results (green lines) for flight G of the balsa glider with an aspect ratio of 6.07 compared with experiment (black markers).
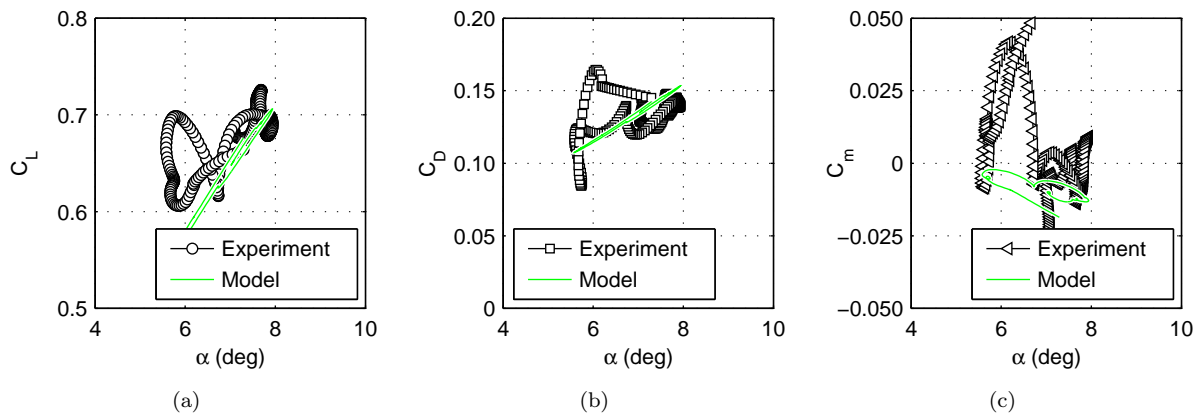
Figure 6.27: The modeling results (green lines) for flight G of the balsa glider with an aspect ratio of 6.07 for the (a) lift, (b) drag, and (c) moment coefficient compared with experiment (black markers).

6.3.2 Results for Flights of the Balsa Glider with an Aspect Ratio of 11.7

For the balsa glider with an aspect ratio of 11.7, the three flights are shown, and they covered a similar flight regime to the three flights with the lower aspect ratio glider. Flight H, which is shown in Fig. 6.28, has an aggressive stall similar to flight E, and the results for the model are similar—x reaches 0 and large dynamic stall hysteresis loops exist. For flight E in Fig. 6.29, the dynamic stall hysteresis loops are captured by the model and the results appear similar to the results for flight E of the lower aspect ratio model glider (shown in Fig. 6.22). Flight I has a shallower stall recovery dive (similar to flight F), and the separation parameter only reaches 0 for a moment as illustrated in Fig 6.30. In Fig. 6.30(b), the predictions for the coefficients have a slight lag and C_L varies around the trend line. Figure 6.31 shows the model capturing the experimental hysteresis loops, but the prediction for C_L varies around the experimental results. The final result in Fig. 6.32 is for flight J which is a steady glide at near constant angle of attack well below the stall angle. Again, the model predicts the averaged aerodynamic coefficients, but does not include the higher-order variations seen in Fig. 6.33.

6.4 Discussion of Modeling Results

Modeling unsteady high angle-of-attack flight is highly applicable to MAVs because they operate over a large flight envelope that includes rapid changes in angle of attack and high angle-of-attack rates. Accurate modeling of unsteady flight cannot be achieved using only the linear flight regime assumptions, but must account for the lag in the unsteady aerodynamic coefficients which depend on the time history of the angle of attack and the angle-of-attack rate. In order to model the lag, the state-space representation for the coefficients was expanded to include a separation parameter that accounted for nonlinear time-dependent effects. The value of the separation parameter was controlled by a first-order differential equation that accounted for the lag. By including the separation parameter and additional terms in the equations for lift, drag, and moment, the model was found to be applicable to a full range of flight conditions.

Within the model for each MAV, the coefficient and constant terms were determined based on experimental results from quasi-steady and unsteady flights. While the modeling approach was completed using experimental results, parts of the model can be determined without experimental results or from limited experimental results. The initial guess for the steady-state separation curve for each MAV was fairly accurate based on the stall angle of attack. The balsa gliders have larger aspect ratio wings than compared with the Vapor, and x_o was steeper after stall and quickly approached zero. In contrast, x_o decreased gradually after stall for the low aspect ratio wing of the Vapor. A number of coefficients in the model were
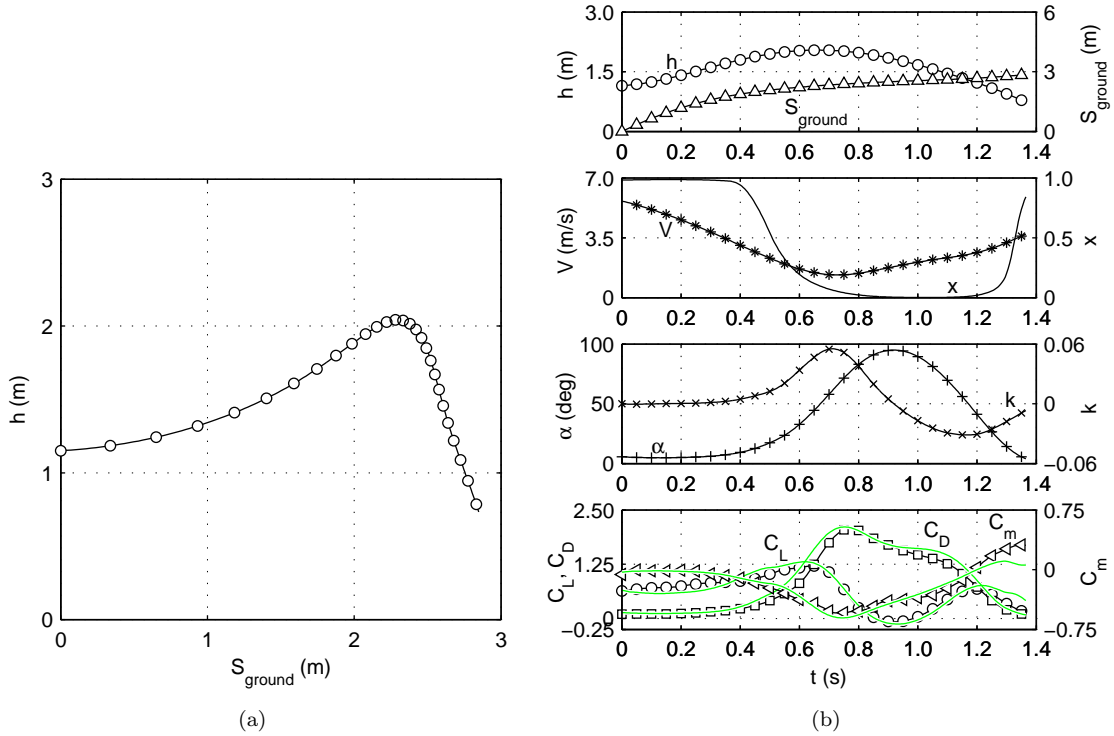
Figure 6.28: The (a) ground track and (b) time history of the modeling results (green lines) for flight H of the balsa glider with an aspect ratio of 11.7 compared with experiment (black markers).
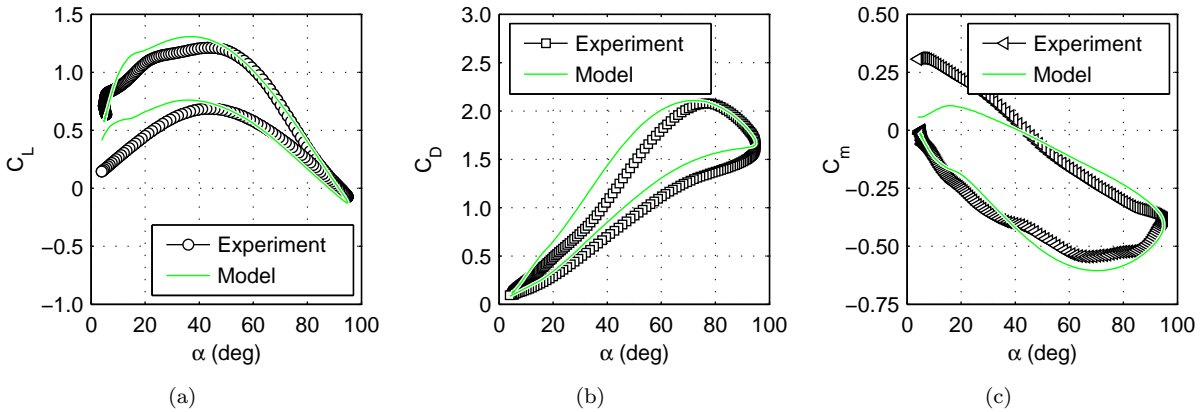
Figure 6.29: The (a) ground track and (b) time history of the modeling results (green lines) for flight H of the balsa glider with an aspect ratio of 11.7 compared with experiment (black markers).

standard low angle-of-attack coefficients (linear lift curve, drag polar, and linear moment curve) which can be easily found. Using these coefficients, a limited number of terms can be found to build a limited model without experimental data, but it would have significant shortcomings. The results in this dissertation do not show enough trends to select the additional terms. Selecting initial values for additional terms would involve looking at the results of the unsteady model and comparing the results from the limited model

102
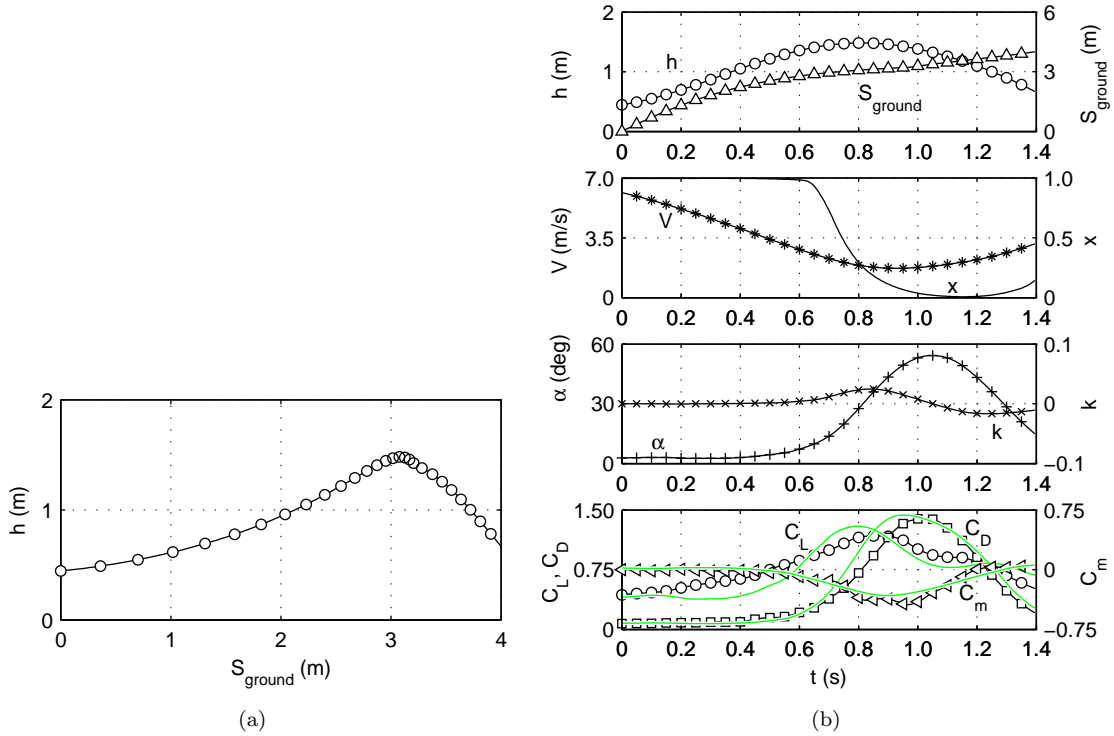
Figure 6.30: The (a) ground track and (b) time history of the modeling results (green lines) for flight I of the balsa glider with an aspect ratio of 11.7 compared with experiment (black markers).
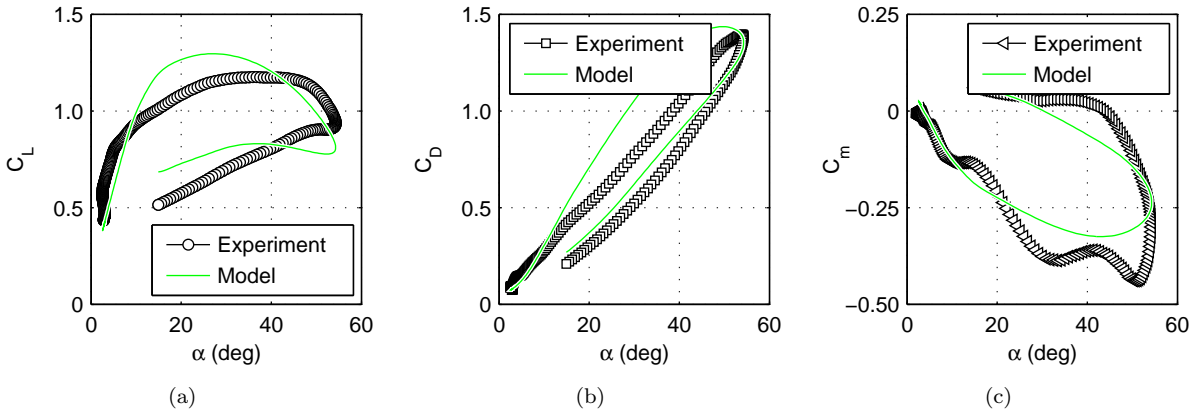
Figure 6.31: The modeling results (green lines) for flight I of the balsa glider with an aspect ratio of 11.7 for the (a) lift, (b) drag, and (c) moment coefficient compared with experiment (black markers).

with expected results. Expected results could involve Computational Fluid Dynamics (CFD) data, any partial experimental results, or simple intuition. In general, data for the unsteady high angle-of-attack aerodynamic characteristics are needed because terms in the model are specific to each aircraft. The steady-state separation parameter varies with each aircraft, as do the coefficients depending on x. However,
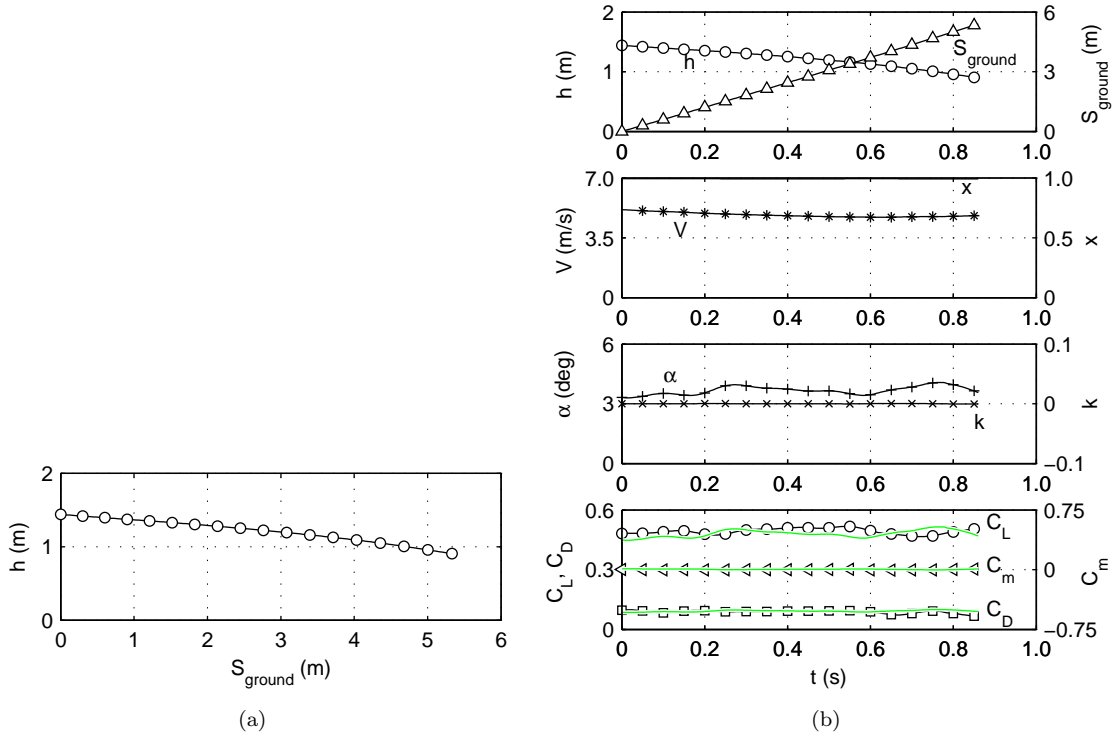
Figure 6.32: The (a) ground track and (b) time history of the modeling results (green lines) for flight J of the balsa glider with an aspect ratio of 11.7 compared with experiment (black markers).
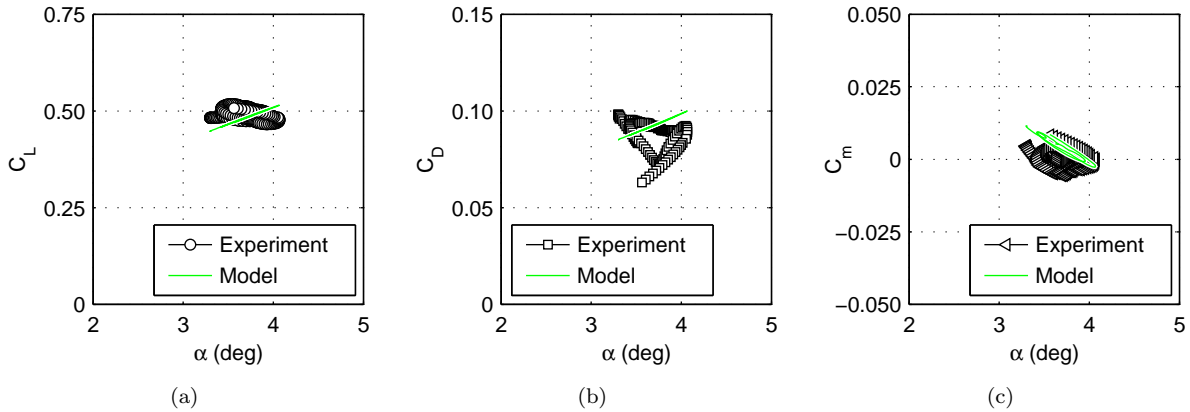
Figure 6.33: The modeling results (green lines) for flight J of the balsa glider with an aspect ratio of 11.7 for the (a) lift, (b) drag, and (c) moment coefficient compared with experiment (black markers).

the functional form of the model was applicable to three different aircraft so, given experimental data, it should be possible to apply the method to more MAVs.

Modeling results from ten representative flights show the applicability of the model to unsteady high angle-of-attack flight with varying degrees of unsteadiness. Results for each MAV showed an aggressive stall with the maximum angle of attack close to or above 90 deg as well as a stall with a lower maximum

104

angle of attack. The final flight for each MAV showed the model was also applicable to quasi-steady low angle-of-attack flight. In the unsteady flights, the model captured a range of hysteresis loops in the coefficients, but sometimes the predictions included lag, overpredictions, or underpredictions. In the quasi-steady cases, the model captured the general average of the experimental coefficients and lacked the higher order variations which is expected with a reduced-order modeling method. The new modeling approach is a reduced-order method most applicable to work with simulator or control law design and validation, and the results in unsteady flight at high angles of attack confirmed the model captured the effects of dynamic stall as would occur in rapid maneuvers such as perching, deep stall descent, and agile maneuvering in confined spaces. Results show that the model is applicable not only to MAVs during rapid maneuvers but is also applicable during nominal glide low angle-of-attack flight.

Chapter 7

Summary, Conclusions, and Recommendations

7.1   Summary

The work presented in this dissertation explored the aerodynamic characteristics of MAVs in flight. Results from flight tests were recorded using off-board motion tracking which generated a time history of each flight trajectory (Earth-referenced position and attitude). From the trajectories, the body-fixed forces and moments were calculated, and the results showed that off-board measurements could be used to determine the aerodynamic characteristics of MAVs during flight. An uncertainty analysis was completed and showed the off-board motion tracking system was accurate with a standard deviation on the order of 0.1 mm (0.004 in) and 0.05 deg for stationary MAVs. During simple motion the noise increased slightly, and the acceleration of a heavy falling sphere was accurately determined from the captured trajectory. Repeatability flights which used a launcher showed a small glider had a similar trajectory and the same characteristics across multiple flights. The results from ten repeatability flights followed the same trend as a larger set of over 50 hand-launched flights. While the hand-launched flights had greater variations, the data followed a trend line and most of the data points were clustered close to the trend line.

After outlining and verifying the method used to gather and process MAV flight trajectories, experimental results were recorded and presented for low Reynolds number flight. Lift and drag results for small angles of attack were presented for four low Reynolds number gliders. First, quasi-steady flights with the Vapor showed the lift and drag data throughout 14 flights. The lift curve was linear with angle of attack and the drag curve was well described by the parabolic drag polar. By using the pitching moment, the lift curve of just the wing was found and the slope was less than that of an ideal finite wing because of the low Reynolds number effects. The quasi-steady nature of the Vapor flights resulted in variations along the linear lift curve as was expected. After the Vapor, the SU-26xp was tested at different trim conditions across numerous flights. Instead of analyzing complete time histories, the trim points of the flights were used to find the quasi-steady lift and drag curve. The trim point analysis was also completed for the two balsa gliders. From the trim points, the lift curves and drag polars were found at angles of attack below as well as above stall,

and the method was applied to three aircraft (SU-26xp and the two balsa gliders). From the results, the linear lift curve slopes and parabolic drag polars for each MAV were found. Just above the stall angle of attack, the trim analysis for the three aircraft captured the lift decrease and drag increase expected after stall. The two balsa gliders were tested at trim conditions at high angles of attack (up to 105 deg), and the resulting lift and drag curves showed the aerodynamic characteristics of the two gliders in quasi-steady deep stall.

Some of the static stability terms for the model glider, the SU-26xp, and the balsa gliders were determined from the time history of the moment coefficients. The neutral point, which is a function of the longitudinal stability, varied with angle of attack for the SU-26xp, but for the two balsa gliders the neutral point stayed essentially constant until stall. The varying neutral point for the SU-26xp indicates that some of the linear assumptions in the calculations (Eq. 4.19) do not always hold at low Reynolds numbers. The relatively constant neutral point for the two balsa gliders show the thin, stiff, balsa wings follow the linear lift curve assumptions (up to stall) that are in the neutral point calculations. For lateral stability, the weather vane, and roll due to sideslip were shown for the SU-26xp, the model glider, and the two balsa gliders. All of the aircraft were statically stable and some of the lateral stability terms changed at different trim angles of attack. In the case of the weather vane stability, the two balsa gliders had increased stability at higher angles of attack, while the roll stability for the SU-26xp and model glider increased with angle of attack. Finally, the dynamic stability was explored for the two balsa gliders. Because the short flights limited the time history, only half periods of the phugoid mode were observed. For both balsa gliders, the experimental phugoid mode was shorter than the estimates from the linearized equations of motion. The experimental results presented used the moment coefficient data from flight trajectories to explore the stability characteristics of MAVs at low Reynolds numbers.

Testing was completed for unsteady high angle-of-attack flights for the Vapor and two balsa gliders. During the unsteady flights, the aircraft would enter a stall while the angle of attack was rapidly increasing, which delayed stall and generated large lift coefficients. The nondimensionalized angle-of-attack rate, or reduced frequency, during the Vapor flights peaked at 0.4 indicating highly unsteady flow. The unsteadiness in the flights caused the lift, drag, and moment curves to have hysteresis loops with differences between the portion of the flights with increasing and decreasing angle of attack. From the numerous unsteady flights for the three aircraft, additional details and trends can be observed within the data. The largest values of the reduced frequency ($k = 0.4$) were observed for the Vapor which also had the largest values of C_L and C_D. The two balsa gliders had smaller values of reduced frequency (on the order of 0.1), lower values of peak angle of attack and had smaller values for both C_L and C_D. Both balsa gliders exhibited aggressive

stalls where the angle of attack exceeded 100 deg as well as gentler unsteady stalls with lower values of reduced frequency, peak angle of attack, and smaller increases in C_L and C_D. The test results showed highly unsteady MAV flight data and show the effect of the unsteadiness on the aerodynamic characteristics during rapid maneuvers over a large flight envelope.

An unsteady model was developed and refined based on existing unsteady modeling approaches, and the model was found to be applicable to the captured unsteady flight data for the Vapor and two balsa gliders. The influence of the rapidly changing angle of attack on the aerodynamic coefficients was modeled using an additional variable called the separation parameter, and it depended on a first-order lag equation that was a function of the angle of attack and the angle-of-attack rate. Expanding on work in literature, a variety of formulations for the lift, drag, and moment coefficient based on the separation parameter were explored before developing the presented modeling method that had a formulation applicable to all three aircraft. First-order lag in the separation parameter was included in the model as well as additional coefficient terms to account for the high angle of attack and instantaneous angle-of-attack rate. For each aircraft, the different parameters in the model were determined based on a limited number of flights over a wide range of flight conditions. The results of the model were shown for a number of flights of each aircraft, and the modeling results for the lift, drag, and moment coefficient had good agreement with the experimental data. Results from the flights showed the model was applicable to a wide variety of flight conditions including unsteady high angle-of-attack flights, flights with less unsteadiness, and lower angles of attack, and quasi-steady low angle-of-attack flight. The developed models are applicable to MAVs flying over a large flight envelope ranging from low angle-of-attack nominal gliding flight to unsteady flight at angles of attack exceeding 90 deg.

7.2   Conclusions

Motion tracking of MAV flights was used to gather experimental data over a large range of angles of attack (0–100 deg). The flight test results demonstrated the wide range and depth of aerodynamic data that can be determined from MAV flight trajectories. Based on the data, a modeling methodology applicable to the large flight envelopes of MAVs was developed, and the model was able to track the aerodynamic characteristics during unsteady and quasi-steady MAV flight.

- This research outlined the methodology to gather experimental MAV flight test data using modern motion-tracking techniques. Prior to this dissertation, the feasibility of using motion tracking to

gather aerodynamic data had been shown, but large data sets had not been gathered or studied from an aerodynamic point of view.

- Flight test results at low angles of attack (below stall) were gathered and analyzed. The results showed that the flights included a small degree of unsteadiness which was considered quasi-steady. In order to decrease the effect of the quasi-steady nature of the flights, a novel method that analyzed trim points across multiple flights was developed and applied to the MAVs. With the trim point analysis, the data from the flights at different angles of attack closely followed a trend line and did not exhibit the variation caused by the quasi-steady nature of the flights.

- Results from the quasi-steady flights were obtained for lift and drag in the low angle-of-attack regime where the lift coefficient was linear and the drag coefficient was well described by the classical polar. Additionally, quasi-steady results were obtained at high angles of attack (approximately 30–90 deg) in deep stall descent. The methodology to gather these new data was developed, and the results showed the aerodynamic characteristics of MAVs in deep stall descent.

- Numerous unsteady high angle-of-attack flights showed the effect of changing angle of attack during dynamic maneuvers—specifically a large increase in lift and drag relative to steady-state values. Additionally, during the unsteady flights, the lift, drag, and moment had hysteresis loops due to dynamic stall. The flights covered a range of unsteadiness and a range of peak angle of attack (30-110 deg) so the varying effect of unsteadiness in the aerodynamic coefficients was illustrated.

- From the large set of unsteady flight tests, a modeling formulation applicable to three MAVs was developed based on a time lagged separation parameter. Terms within the model were determined based on experimental results for each of the MAVs. The model was applied to experimental flights that covered a wide range of conditions from quasi-steady low angle-of-attack to unsteady high angle-of-attack. Results from the model were compared with experimental results for the three airplanes, and the comparison showed that the model can accurately track the hysteresis loops in a variety of unsteady flights. The model was also capable of tracking the experimental results in the low angle-of-attack nominal gliding flight regime. Overall, the work showed how to apply the new model to a MAV and that the new model was capable of estimating the longitudinal characteristics of MAVs in agile flight.

- While the modeling approach for the MAVs was developed using unsteady high angle-of-attack data, certain terms within the model can be estimated without experimental results. These include the

109

linear lift curves, the parabolic drag polar, and the linear moment curve. Additionally, the steady-state separation parameter can be estimated based on the general stall characteristics of the wing and the steady-state high angle-of-attack lift curve. The complete model can only be estimated with unsteady experimental data (or perhaps CFD). However, the formulation of the model was applicable to three different MAVs, and thus it should be applicable to additional MAVs.

7.3   Recommendations

In the course of this research, the framework for studying MAV flight dynamics with motion tracking was developed and shown to be applicable to a wide variety of flight conditions. During the testing, ideas for a number of future studies that could be completed with motion tracking became clear. Additionally, further refinements for the modeling approach also exist. The recommendations for future research are:

- In this work, motion tracking was used to gather data in the Reynolds number range of approximately 8,000 to 30,000, but future studies should explore even lower Reynolds numbers using even smaller gliders.

- Beyond gliding flights, the exploration of powered flight would further the understanding of MAV aerodynamics. In powered flight, the propeller wake effects the aerodynamics during steady level flight, and the additional force from the propeller further expands the flight envelope into unsteady and high angle-of-attack maneuvers. A previous study investigated MAVs in powered steady-level flight [95], but it did not use the trim methodology to understand the varying flight conditions. Further refinement in the processing and presentation of results for powered flight is needed to more completely show the performance of powered MAV flight. MAV performance would be more fully understood with experimental data and modeling results for powered flight.

- An additional step is to move beyond uncontrolled glides. Flight testing while controlling the airplane would allow additional flight conditions to be explored. Obviously, control surface effectiveness and control derivatives could be determined. Additionally, gathering data during controlled flight at high angles of attack would allow complex unstable 3-D flight such as hovering to be analyzed. These data would result in further model refinement and a better understanding of the complex dynamics of controlled high angle-of-attack flight.

- Within the constraints of the current testing facility, the dynamic stability was difficult to observe because of the short test length. Further testing in a larger facility (or with a slower aircraft) would

allow more data to be gather and the dynamic stability modes of MAVs to be better understood. Further dynamic stability modes (such as the short period and dutch roll) could be observed by varying the control surfaces in flight. Another dynamic mode, aircraft spin, could be analyzed in a more vertical capture volume.

- The current modeling approach treats the whole aircraft as one unit and is limited to lift, drag, and pitching moment, while the yawing moment, rolling moment, and the side force are not modeled. The current method calculates the forces and pitching moment for the whole aircraft and is unable to model differences between the left and right wing which is key to determining the roll and yaw moments. By modeling the stall delay of individual components (left wing, right wing, horizontal tail, vertical tail) and then using a build-up approach the determine the overall forces and moments, all of the forces and moments can be determined. The complexity of this approach may require unsteady testing of individual subcomponents in order to determine the numerous parameters before assembling the results for the whole aircraft.

- The development of the unsteady model was based on experimental data, as was done with most of the work in the literature. Incorporating unsteady CFD results into the model development, by basing the coefficients and time constants on CFD results, would allow the modeling approach to be applied independent of experimental results. Subsequent validation of a model with CFD-tuned coefficients against experimental data would allow unsteady models to be applied earlier in the design process.

- In the literature various techniques for fixed-wing perching have been demonstrated, but in general the models for tuning the controller and running the path planning algorithms have not included the unsteady aerodynamics. By using a model for unsteady flight, as was outlined in this dissertation, the aerodynamic model will be more accurate, particularly, during the unsteady high angle-of-attack terminal portion of a perching maneuver.
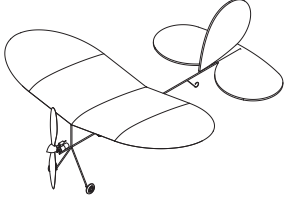
Appendix A

Test Data for the Vapor

Appendix A lists the data for selected flights of the Vapor MAV. The data is downsampled from the recording rate of 200 Hz to 40 Hz. Flights A, B, C, and D (as listed in Table 6.1) are included as well as the ten regression flights. The tables include some of the specific test conditions and a time history of the important parameters.

The trajectory and determined quantities tabulated for flight A of the Vapor which is shown in Figs. 6.10 and 6.11.

Test Conditions				
aircraft	Vapor	flight	A	
test number	2437			
m (g)	14.44	I_{xx} (g·cm^2)	369.9	
I_{yy} (g·cm^2)	1129.1	I_{zz} (g·cm^2)	1242.2	
I_{xz} (g·cm^2)	87.6	δ_e (deg)	1.8	

time	x	y	z	ϕ	θ	ψ	V	α	$\dot{\alpha}$	C_L	C_D	C_m
(s)	(m)	(m)	(m)	(deg)	(deg)	(deg)	(m/s)	(deg)	(deg/s)			
0.000	-1.1367	-0.6602	1.6744	-5.000	-4.692	20.277	-0.07	15.40	4.065	0.370	0.087	-0.016
0.025	-1.0420	-0.6287	1.6676	-5.672	-3.152	20.705	0.11	-7.85	4.024	0.382	0.083	-0.010
0.050	-0.9486	-0.5967	1.6634	-6.316	-1.754	21.227	-0.10	-12.19	3.952	0.398	0.090	-0.003
0.075	-0.8567	-0.5646	1.6615	-6.967	-0.525	21.813	-0.94	-2.53	3.862	0.423	0.098	0.007
0.100	-0.7672	-0.5331	1.6627	-6.546	1.038	21.853	-0.25	8.94	3.791	0.412	0.091	0.001
0.125	-0.6794	-0.5021	1.6655	-6.480	2.474	21.947	0.05	11.87	3.717	0.433	0.089	0.005
0.150	-0.5937	-0.4712	1.6706	-6.279	4.071	22.018	0.09	7.51	3.633	0.447	0.091	0.002
0.175	-0.5100	-0.4412	1.6775	-6.081	5.665	21.948	0.36	15.93	3.553	0.460	0.092	0.000
0.200	-0.4287	-0.4114	1.6863	-5.839	7.306	21.979	0.90	23.41	3.467	0.463	0.095	-0.004

continued on next page

time	x	y	z	ϕ	θ	ψ	V	α	$\dot{\alpha}$	C_L	C_D	C_m
(s)	(m)	(m)	(m)	(deg)	(deg)	(deg)	(m/s)	(deg)	(deg/s)			
0.225	-0.3498	-0.3820	1.6964	-5.690	8.847	22.135	1.58	22.96	3.366	0.481	0.102	-0.004
0.250	-0.2732	-0.3535	1.7076	-5.525	10.332	22.209	2.07	19.85	3.275	0.500	0.107	-0.004
0.275	-0.1991	-0.3254	1.7197	-5.416	11.714	22.336	2.46	16.89	3.181	0.528	0.118	-0.001
0.300	-0.1278	-0.2981	1.7328	-5.100	13.134	22.308	3.05	20.54	3.070	0.552	0.129	-0.003
0.325	-0.0592	-0.2718	1.7466	-4.801	14.491	22.240	3.44	25.01	2.949	0.583	0.130	-0.005
0.350	0.0064	-0.2461	1.7608	-4.486	15.812	22.169	4.28	28.62	2.838	0.605	0.125	-0.010
0.375	0.0695	-0.2208	1.7752	-4.202	16.986	22.173	4.89	29.83	2.750	0.623	0.113	-0.011
0.400	0.1302	-0.1961	1.7896	-3.856	18.070	22.157	5.74	27.83	2.654	0.648	0.136	-0.009
0.425	0.1883	-0.1717	1.8037	-3.565	19.032	22.212	6.41	33.12	2.539	0.696	0.166	-0.001
0.450	0.2436	-0.1480	1.8174	-2.436	20.076	21.328	7.27	44.17	2.416	0.734	0.175	-0.019
0.475	0.2964	-0.1253	1.8305	-1.201	21.078	20.174	8.62	58.20	2.307	0.746	0.171	-0.042
0.500	0.3471	-0.1039	1.8423	-0.875	21.767	19.907	10.21	61.92	2.217	0.775	0.170	-0.044
0.525	0.3959	-0.0832	1.8528	-1.383	22.126	20.670	11.72	48.11	2.128	0.832	0.207	-0.044
0.550	0.4427	-0.0632	1.8620	-2.150	22.290	21.699	12.80	34.55	2.029	0.923	0.249	-0.030
0.575	0.4873	-0.0439	1.8700	-2.941	22.370	22.773	13.46	40.53	1.927	1.008	0.284	-0.002
0.600	0.5296	-0.0245	1.8769	-2.690	22.516	22.766	14.67	64.26	1.830	1.056	0.312	-0.026
0.625	0.5699	-0.0059	1.8823	-2.480	22.550	22.782	16.71	80.87	1.747	1.103	0.367	-0.037
0.650	0.6084	0.0120	1.8858	-2.679	22.379	23.226	18.93	83.89	1.665	1.185	0.439	-0.027
0.675	0.6448	0.0300	1.8877	-1.849	22.192	22.666	20.71	87.04	1.577	1.270	0.493	-0.055
0.700	0.6796	0.0480	1.8876	-0.843	21.793	22.092	23.13	98.58	1.513	1.337	0.585	-0.087
0.725	0.7127	0.0650	1.8857	-0.586	21.161	22.205	25.78	108.50	1.452	1.394	0.714	-0.084
0.750	0.7443	0.0814	1.8817	-0.728	20.277	22.741	28.55	103.60	1.395	1.461	0.880	-0.103
0.775	0.7743	0.0974	1.8758	-1.000	19.173	23.460	31.06	102.52	1.330	1.563	1.089	-0.086
0.800	0.8029	0.1119	1.8679	-2.180	17.840	24.861	33.29	109.89	1.266	1.688	1.281	-0.028
0.825	0.8298	0.1257	1.8584	-2.120	16.617	24.582	36.52	118.75	1.243	1.587	1.269	-0.134
0.850	0.8555	0.1389	1.8467	-2.757	15.044	25.038	39.45	115.93	1.211	1.583	1.322	-0.173
0.875	0.8802	0.1518	1.8328	-3.736	13.143	25.880	42.11	90.05	1.230	1.465	1.205	-0.191
0.900	0.9041	0.1660	1.8165	-4.518	10.834	26.958	44.04	57.72	1.274	1.342	1.330	-0.156
0.925	0.9270	0.1802	1.7982	-5.098	8.211	27.961	44.93	32.87	1.278	1.310	1.493	-0.126
0.950	0.9492	0.1938	1.7781	-5.855	5.329	28.884	45.47	13.40	1.275	1.278	1.606	-0.100
0.975	0.9709	0.2065	1.7562	-6.671	2.210	29.536	45.82	-9.95	1.281	1.228	1.591	-0.087
1.000	0.9921	0.2181	1.7328	-7.500	-1.053	29.779	45.05	-39.58	1.332	1.154	1.290	-0.120
1.025	1.0135	0.2297	1.7072	-8.834	-4.643	30.243	43.60	-67.49	1.408	1.030	1.179	-0.120
1.050	1.0350	0.2418	1.6795	-8.948	-8.658	30.606	41.70	-92.14	1.448	0.984	1.062	-0.087
1.075	1.0569	0.2536	1.6497	-9.560	-12.882	31.106	39.10	-122.95	1.534	0.902	0.865	-0.055
1.100	1.0795	0.2653	1.6176	-10.676	-17.272	31.826	35.62	-150.91	1.630	0.838	0.736	-0.020

continued on next page

time	x	y	z	ϕ	θ	ψ	V	α	$\dot{\alpha}$	C_L	C_D	C_m
(s)	(m)	(m)	(m)	(deg)	(deg)	(deg)	(m/s)	(deg)	(deg/s)			
1.125	1.1031	0.2770	1.5831	-12.134	-21.746	32.708	31.54	-162.20	1.730	0.763	0.614	0.011
1.150	1.1278	0.2887	1.5464	-13.869	-26.060	33.759	27.51	-154.86	1.840	0.641	0.485	0.012
1.175	1.1537	0.3007	1.5067	-15.984	-30.305	35.101	23.77	-143.30	1.943	0.547	0.416	0.022
1.200	1.1805	0.3133	1.4642	-16.527	-34.487	36.252	20.42	-144.16	2.097	0.474	0.290	0.028
1.225	1.2086	0.3261	1.4182	-18.027	-38.482	37.769	16.74	-155.66	2.243	0.443	0.247	0.040
1.250	1.2383	0.3393	1.3690	-19.645	-42.231	39.440	12.71	-157.36	2.387	0.419	0.217	0.061
1.275	1.2698	0.3530	1.3168	-20.979	-45.539	41.120	8.84	-126.74	2.528	0.379	0.189	0.081
1.300	1.3030	0.3668	1.2618	-21.715	-48.061	42.407	6.24	-77.57	2.670	0.307	0.150	0.073
1.325	1.3374	0.3814	1.2034	-22.271	-49.854	43.458	5.00	-45.74	2.824	0.272	0.129	0.053
1.350	1.3728	0.3968	1.1415	-22.822	-51.108	44.319	4.12	-48.07	2.982	0.303	0.132	0.041
1.375	1.4102	0.4133	1.0767	-22.901	-51.857	44.896	2.61	-60.97	3.124	0.337	0.138	0.028
1.400	1.4503	0.4311	1.0099	-21.518	-52.330	45.435	0.94	-48.97	3.242	0.356	0.133	0.026
1.425	1.4936	0.4500	0.9414	-18.722	-52.584	45.781	0.03	-19.06	3.364	0.355	0.118	0.031
1.450	1.5403	0.4699	0.8718	-14.861	-52.347	45.457	0.09	-5.47	3.503	0.322	0.083	0.027
1.475	1.5893	0.4918	0.7997	-13.049	-51.776	44.497	-0.01	-10.91	3.673	0.326	0.081	0.030
1.500	1.6413	0.5156	0.7264	-12.720	-50.604	42.696	-0.76	-19.53	3.808	0.330	0.094	0.021
1.525	1.6966	0.5412	0.6528	-12.863	-49.034	40.502	-1.12	-13.35	3.899	0.324	0.107	0.003
1.550	1.7556	0.5681	0.5797	-12.181	-47.380	38.437	-1.29	5.48	3.968	0.298	0.092	-0.015

The trajectory and determined quantities tabulated for flight B of the Vapor which is shown in Figs. 5.4, 6.12, and 6.13.

Test Conditions											

aircraft	Vapor	flight	B
test number	2453		
m (g)	14.44	I_{xx} (g·cm^2)	369.9
I_{yy} (g·cm^2)	1129.1	I_{zz} (g·cm^2)	1242.2
I_{xz} (g·cm^2)	87.6	δ_e (deg)	11.8
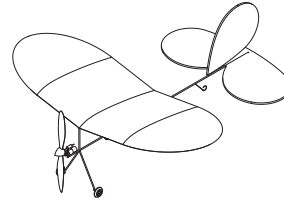
time	x	y	z	ϕ	θ	ψ	V	α	$\dot{\alpha}$	C_L	C_D	C_m
(s)	(m)	(m)	(m)	(deg)	(deg)	(deg)	(m/s)	(deg)	(deg/s)			
0.000	-1.7026	-0.4697	1.8471	-7.989	-27.871	12.935	11.57	-136.66	3.084	0.848	0.149	0.223
0.025	-1.6423	-0.4626	1.7997	-10.328	-26.153	11.842	8.67	-57.46	3.152	0.799	0.159	0.145
0.050	-1.5785	-0.4530	1.7568	-12.193	-22.378	11.331	8.19	-0.85	3.195	0.782	0.180	0.080
0.075	-1.5119	-0.4421	1.7188	-13.539	-17.349	11.307	9.00	33.15	3.207	0.792	0.206	0.022
0.100	-1.4430	-0.4307	1.6858	-14.405	-12.000	11.762	9.43	40.64	3.187	0.817	0.225	-0.017
0.125	-1.3723	-0.4195	1.6589	-14.154	-6.984	12.224	10.68	17.30	3.130	0.805	0.251	-0.047
0.150	-1.3009	-0.4089	1.6366	-13.912	-2.962	12.959	11.08	-8.23	3.056	0.854	0.282	-0.028
0.175	-1.2298	-0.4001	1.6197	-13.022	0.372	13.176	9.89	-19.34	2.983	0.893	0.253	0.006
0.200	-1.1596	-0.3907	1.6086	-10.942	3.867	12.481	9.93	8.91	2.891	0.891	0.234	-0.000
0.225	-1.0907	-0.3815	1.6017	-9.292	7.362	11.993	10.48	46.18	2.813	0.887	0.238	-0.011
0.250	-1.0238	-0.3736	1.5984	-7.732	10.838	11.077	11.98	49.21	2.716	0.894	0.243	-0.035
0.275	-0.9589	-0.3660	1.5980	-6.498	13.988	10.243	13.26	34.65	2.622	0.909	0.244	-0.046
0.300	-0.8961	-0.3581	1.5998	-6.187	16.587	10.235	13.55	15.30	2.527	0.968	0.260	-0.031
0.325	-0.8360	-0.3503	1.6040	-6.011	18.967	10.323	13.97	13.86	2.428	1.011	0.290	-0.015
0.350	-0.7789	-0.3420	1.6103	-5.604	21.295	10.318	14.29	17.89	2.301	1.067	0.334	-0.013
0.375	-0.7251	-0.3346	1.6178	-5.142	23.491	9.911	15.38	30.13	2.156	1.147	0.391	-0.014
0.400	-0.6750	-0.3276	1.6261	-4.526	25.699	9.283	15.81	53.14	2.025	1.209	0.381	-0.035
0.425	-0.6283	-0.3206	1.6349	-3.879	27.792	8.587	17.73	79.17	1.897	1.218	0.391	-0.074
0.450	-0.5842	-0.3136	1.6428	-3.439	29.442	8.231	19.91	102.36	1.781	1.263	0.446	-0.087
0.475	-0.5427	-0.3067	1.6497	-3.164	30.707	8.077	22.50	101.76	1.667	1.336	0.554	-0.081
0.500	-0.5040	-0.3002	1.6551	-3.003	31.692	7.935	25.40	111.21	1.548	1.424	0.704	-0.074
0.525	-0.4678	-0.2944	1.6586	-3.021	32.364	7.779	27.78	137.79	1.421	1.624	0.894	-0.053
0.550	-0.4347	-0.2884	1.6605	-3.119	33.058	7.910	32.14	175.47	1.301	1.668	1.112	-0.114

time	x	y	z	ϕ	θ	ψ	V	α	$\dot{\alpha}$	C_L	C_D	C_m
(s)	(m)	(m)	(m)	(deg)	(deg)	(deg)	(m/s)	(deg)	(deg/s)			
0.575	-0.4039	-0.2831	1.6599	-3.369	33.404	7.925	37.09	210.67	1.209	1.779	1.388	-0.115
0.600	-0.3757	-0.2780	1.6569	-3.730	33.579	8.124	42.51	237.67	1.118	1.844	1.745	-0.141
0.625	-0.3498	-0.2734	1.6514	-4.201	33.515	8.383	48.67	271.53	1.036	1.855	2.104	-0.186
0.650	-0.3261	-0.2690	1.6431	-4.726	33.220	8.737	55.99	295.90	0.993	1.637	2.301	-0.268
0.675	-0.3043	-0.2648	1.6320	-5.324	32.579	9.078	63.56	291.15	0.987	1.303	2.342	-0.329
0.700	-0.2839	-0.2608	1.6176	-6.058	31.485	9.548	70.47	263.00	1.007	0.975	2.404	-0.315
0.725	-0.2650	-0.2570	1.6001	-6.867	29.908	9.962	76.46	226.31	1.033	0.656	2.546	-0.263
0.750	-0.2477	-0.2535	1.5798	-7.326	27.956	9.801	81.71	181.63	1.065	0.377	2.552	-0.244
0.775	-0.2321	-0.2506	1.5568	-7.344	25.592	8.985	85.66	126.95	1.105	0.223	2.398	-0.286
0.800	-0.2179	-0.2482	1.5311	-7.971	22.771	8.724	87.98	69.84	1.165	0.108	2.297	-0.266
0.825	-0.2052	-0.2465	1.5031	-9.090	19.526	8.932	89.00	21.80	1.221	0.043	2.248	-0.258
0.850	-0.1937	-0.2455	1.4734	-10.317	15.813	9.215	89.01	-22.22	1.262	0.022	2.171	-0.259
0.875	-0.1833	-0.2452	1.4419	-11.756	11.596	9.817	87.91	-78.34	1.302	0.008	2.038	-0.235
0.900	-0.1737	-0.2453	1.4086	-12.599	6.683	9.885	85.30	-143.67	1.362	0.085	1.848	-0.234
0.925	-0.1645	-0.2456	1.3736	-12.769	1.086	9.519	80.78	-197.82	1.437	0.185	1.655	-0.198
0.950	-0.1553	-0.2459	1.3369	-13.103	-5.037	9.712	75.18	-234.85	1.490	0.208	1.498	-0.151
0.975	-0.1461	-0.2472	1.2982	-13.275	-11.684	9.994	69.15	-265.68	1.561	0.284	1.306	-0.092
1.000	-0.1367	-0.2493	1.2575	-13.356	-18.620	10.392	62.10	-305.08	1.655	0.398	1.105	-0.034
1.025	-0.1264	-0.2517	1.2147	-13.437	-25.601	11.100	53.99	-340.44	1.756	0.485	0.918	0.014
1.050	-0.1148	-0.2541	1.1696	-13.477	-32.499	12.172	45.26	-338.82	1.853	0.535	0.758	0.063
1.075	-0.1016	-0.2562	1.1221	-13.512	-38.999	13.728	36.87	-304.79	1.961	0.498	0.573	0.090
1.100	-0.0869	-0.2580	1.0719	-13.852	-44.957	15.730	30.12	-269.95	2.111	0.409	0.403	0.107
1.125	-0.0709	-0.2603	1.0181	-14.709	-50.383	17.908	23.92	-244.35	2.272	0.417	0.322	0.147
1.150	-0.0528	-0.2624	0.9612	-15.854	-54.614	20.163	17.79	-205.31	2.428	0.363	0.252	0.148
1.175	-0.0331	-0.2640	0.9009	-17.099	-57.609	22.514	13.40	-126.08	2.587	0.300	0.214	0.136
1.200	-0.0121	-0.2653	0.8372	-17.806	-59.256	24.478	11.26	-49.22	2.744	0.257	0.195	0.106
1.225	0.0100	-0.2665	0.7701	-17.816	-59.788	25.730	10.99	-35.18	2.899	0.280	0.194	0.070
1.250	0.0338	-0.2679	0.6997	-17.212	-59.880	26.255	9.99	-64.84	3.037	0.394	0.199	0.070
1.275	0.0613	-0.2691	0.6275	-15.782	-59.136	25.869	7.35	-82.10	3.164	0.472	0.177	0.067
1.300	0.0939	-0.2693	0.5539	-14.006	-57.524	24.854	5.63	-51.08	3.303	0.492	0.162	0.063
1.325	0.1317	-0.2686	0.4796	-12.399	-55.031	23.223	4.98	-7.78	3.431	0.504	0.161	0.056
1.350	0.1750	-0.2671	0.4054	-11.390	-51.530	20.972	5.30	7.85	3.538	0.521	0.169	0.035
1.375	0.2236	-0.2648	0.3320	-11.310	-47.464	18.366	5.26	-2.01	3.624	0.578	0.166	0.015
1.400	0.2786	-0.2618	0.2610	-11.942	-43.180	15.835	4.81	-34.81	3.703	0.633	0.147	-0.006

The trajectory and determined quantities tabulated for flight C of the Vapor which is shown in Figs. 6.15 and 6.16.

Test Conditions											

aircraft	Vapor	flight	C								
test number	2419										
m (g)	14.44	I_{xx} (g·cm^2)	369.9								
I_{yy} (g·cm^2)	1129.1	I_{zz} (g·cm^2)	1242.2								
I_{xz} (g·cm^2)	87.6	δ_e (deg)	-2.5								
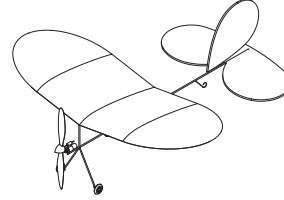
time	x	y	z	ϕ	θ	ψ	V	α	$\dot{\alpha}$	C_L	C_D	C_m
(s)	(m)	(m)	(m)	(deg)	(deg)	(deg)	(m/s)	(deg)	(deg/s)			
0.000	-1.1719	-0.9630	1.6095	-12.422	-5.150	25.583	-0.55	1.54	3.386	0.376	0.084	-0.005
0.025	-1.0912	-0.9407	1.5997	-12.051	-5.259	24.987	-0.57	-3.87	3.355	0.393	0.100	-0.000
0.050	-1.0112	-0.9191	1.5900	-11.685	-5.386	24.272	-0.73	-1.53	3.305	0.413	0.100	0.001
0.075	-0.9320	-0.8981	1.5808	-11.085	-5.460	23.402	-0.71	-0.15	3.280	0.419	0.089	-0.000
0.100	-0.8531	-0.8781	1.5714	-11.124	-5.605	22.625	-0.60	-0.61	3.265	0.434	0.088	0.008
0.125	-0.7748	-0.8578	1.5626	-9.172	-5.674	21.140	-0.70	4.19	3.238	0.439	0.078	0.000
0.150	-0.6968	-0.8374	1.5543	-7.291	-5.607	19.776	-0.54	15.90	3.223	0.420	0.076	-0.008
0.175	-0.6192	-0.8176	1.5457	-6.227	-5.532	18.749	0.12	25.08	3.203	0.411	0.083	-0.006
0.200	-0.5422	-0.7985	1.5368	-5.948	-5.504	18.008	0.69	12.55	3.192	0.417	0.087	-0.003
0.225	-0.4655	-0.7801	1.5278	-6.470	-5.470	17.632	0.95	-3.22	3.162	0.433	0.102	-0.001
0.250	-0.3895	-0.7626	1.5186	-7.796	-5.462	17.540	0.39	-2.05	3.128	0.455	0.099	0.004
0.275	-0.3141	-0.7449	1.5098	-7.248	-5.403	16.862	0.64	10.06	3.110	0.440	0.089	-0.001
0.300	-0.2392	-0.7274	1.5007	-7.334	-5.314	16.526	1.18	17.03	3.092	0.439	0.093	-0.002
0.325	-0.1647	-0.7102	1.4914	-7.475	-5.267	16.279	1.46	9.28	3.074	0.450	0.098	-0.000
0.350	-0.0907	-0.6932	1.4818	-7.503	-5.241	16.082	1.55	2.99	3.050	0.467	0.101	0.003
0.375	-0.0173	-0.6759	1.4723	-7.823	-5.125	16.229	1.64	3.72	3.032	0.476	0.105	0.004
0.400	0.0554	-0.6584	1.4631	-7.178	-4.925	16.152	1.77	11.00	3.005	0.479	0.108	0.001
0.425	0.1276	-0.6408	1.4538	-5.428	-4.739	15.771	2.11	21.83	2.977	0.469	0.101	-0.008
0.450	0.1994	-0.6238	1.4441	-4.623	-4.592	15.725	2.82	27.68	2.965	0.458	0.098	-0.010
0.475	0.2708	-0.6075	1.4338	-4.723	-4.581	15.936	3.52	14.32	2.955	0.469	0.108	-0.008
0.500	0.3419	-0.5919	1.4230	-6.343	-4.615	16.655	3.73	-6.97	2.949	0.500	0.125	-0.013
0.525	0.4124	-0.5762	1.4122	-7.270	-4.701	17.101	3.17	-11.81	2.913	0.527	0.131	0.007
0.550	0.4825	-0.5603	1.4017	-5.987	-4.776	16.614	2.88	2.05	2.880	0.529	0.116	-0.005

time	x	y	z	ϕ	θ	ψ	V	α	$\dot{\alpha}$	C_L	C_D	C_m
(s)	(m)	(m)	(m)	(deg)	(deg)	(deg)	(m/s)	(deg)	(deg/s)			
0.575	0.5521	-0.5446	1.3912	-4.761	-4.793	16.152	3.37	15.66	2.873	0.517	0.110	-0.000
0.600	0.6214	-0.5295	1.3805	-4.862	-4.764	16.204	3.75	7.21	2.866	0.519	0.118	-0.004
0.625	0.6902	-0.5149	1.3696	-5.913	-4.762	16.537	3.70	-7.93	2.848	0.544	0.125	-0.006
0.650	0.7587	-0.5007	1.3588	-7.796	-4.747	17.163	3.27	-11.50	2.821	0.563	0.134	0.002
0.675	0.8267	-0.4863	1.3482	-7.820	-4.769	17.026	3.14	-4.80	2.805	0.559	0.125	-0.000
0.700	0.8943	-0.4718	1.3378	-7.555	-4.805	16.802	3.16	2.36	2.790	0.560	0.123	-0.002
0.725	0.9615	-0.4572	1.3273	-7.408	-4.861	16.691	3.20	1.57	2.773	0.566	0.121	-0.001
0.750	1.0283	-0.4425	1.3170	-7.230	-4.900	16.653	3.19	-0.65	2.756	0.575	0.121	-0.001
0.775	1.0948	-0.4280	1.3066	-7.004	-4.958	16.575	3.14	1.48	2.747	0.570	0.115	-0.002
0.800	1.1611	-0.4133	1.2962	-6.837	-5.060	16.602	3.20	2.93	2.739	0.573	0.121	0.002
0.825	1.2269	-0.3988	1.2856	-6.885	-5.149	16.632	3.41	-2.13	2.720	0.600	0.125	0.008
0.850	1.2924	-0.3839	1.2752	-6.365	-5.143	16.467	3.20	-7.98	2.708	0.617	0.117	0.009
0.875	1.3577	-0.3688	1.2652	-5.352	-5.032	16.132	2.91	0.11	2.704	0.612	0.112	0.003
0.900	1.4227	-0.3539	1.2554	-4.721	-4.814	15.907	3.09	20.46	2.697	0.579	0.117	-0.009
0.925	1.4874	-0.3392	1.2454	-4.669	-4.714	15.902	3.91	25.32	2.682	0.559	0.131	-0.014
0.950	1.5517	-0.3246	1.2348	-5.295	-4.779	16.231	4.60	7.88	2.660	0.582	0.149	-0.009
0.975	1.6156	-0.3109	1.2237	-6.537	-4.928	16.523	4.17	-8.48	2.643	0.620	0.136	0.005
1.000	1.6792	-0.2972	1.2128	-7.010	-5.007	16.457	3.85	-1.28	2.634	0.611	0.123	0.002
1.025	1.7427	-0.2834	1.2017	-6.935	-5.073	16.223	4.18	16.32	2.634	0.585	0.116	-0.006
1.050	1.8060	-0.2697	1.1902	-7.349	-5.140	16.207	4.87	14.73	2.633	0.575	0.116	-0.015
1.075	1.8694	-0.2556	1.1779	-7.774	-5.445	16.559	5.06	-4.96	2.640	0.589	0.137	-0.005
1.100	1.9325	-0.2415	1.1653	-8.105	-5.774	17.036	4.58	-13.96	2.628	0.619	0.153	0.010
1.125	1.9954	-0.2280	1.1529	-8.226	-5.924	17.203	4.16	-2.71	2.608	0.609	0.149	0.004
1.150	2.0580	-0.2148	1.1403	-8.317	-6.050	17.256	4.54	15.37	2.599	0.584	0.142	-0.007
1.175	2.1202	-0.2014	1.1271	-8.276	-6.193	17.386	5.02	19.99	2.597	0.568	0.125	-0.020
1.200	2.1825	-0.1879	1.1133	-8.129	-6.489	17.589	5.49	10.45	2.613	0.544	0.104	-0.030

The trajectory and determined quantities tabulated for flight D of the Vapor which is shown in Figs. 6.17 and 6.18.

Test Conditions					
aircraft	Vapor	flight	D		
test number	2420				
m (g)	14.44	I_{xx} (g·cm^2)	369.9		
I_{yy} (g·cm^2)	1129.1	I_{zz} (g·cm^2)	1242.2		
I_{xz} (g·cm^2)	87.6	δ_e (deg)	-2.4		
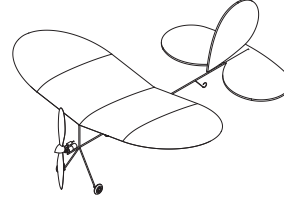
time	x	y	z	ϕ	θ	ψ	V	α	$\dot{\alpha}$	C_L	C_D	C_m
(s)	(m)	(m)	(m)	(deg)	(deg)	(deg)	(m/s)	(deg)	(deg/s)			
0.000	-0.6585	-0.7180	1.8843	-6.834	10.039	19.571	1.06	17.07	2.982	0.461	0.080	0.002
0.025	-0.5882	-0.6994	1.8949	-6.591	10.269	19.130	1.51	22.74	2.897	0.495	0.098	0.003
0.050	-0.5199	-0.6815	1.9052	-6.105	10.624	18.574	2.06	40.82	2.812	0.488	0.101	-0.010
0.075	-0.4533	-0.6645	1.9142	-5.935	10.831	18.223	3.36	45.39	2.748	0.486	0.099	-0.017
0.100	-0.3879	-0.6480	1.9217	-6.169	10.830	18.238	4.53	30.14	2.678	0.539	0.127	-0.011
0.125	-0.3244	-0.6319	1.9284	-6.490	10.756	18.314	4.78	4.35	2.597	0.596	0.144	-0.004
0.150	-0.2624	-0.6167	1.9341	-6.908	10.525	18.389	4.84	0.78	2.519	0.664	0.158	0.014
0.175	-0.2026	-0.6021	1.9397	-6.840	10.549	18.081	4.78	16.81	2.434	0.688	0.139	0.007
0.200	-0.1443	-0.5877	1.9448	-6.648	10.616	17.837	5.76	34.41	2.380	0.685	0.130	-0.003
0.225	-0.0873	-0.5736	1.9489	-6.389	10.696	17.650	6.65	46.22	2.330	0.679	0.131	-0.016
0.250	-0.0314	-0.5600	1.9517	-6.343	10.562	17.661	7.81	36.49	2.279	0.716	0.159	-0.012
0.275	0.0232	-0.5467	1.9536	-6.373	10.415	17.785	8.79	32.31	2.220	0.750	0.192	-0.009
0.300	0.0767	-0.5341	1.9542	-6.644	10.127	17.975	8.81	28.40	2.153	0.823	0.211	-0.002
0.325	0.1286	-0.5221	1.9542	-6.466	9.903	17.765	10.11	30.02	2.109	0.809	0.214	-0.021
0.350	0.1796	-0.5102	1.9526	-6.580	9.428	17.824	10.64	30.80	2.052	0.901	0.267	0.000
0.375	0.2291	-0.4992	1.9507	-5.950	9.092	17.112	11.52	28.88	1.995	0.907	0.263	-0.023
0.400	0.2778	-0.4889	1.9471	-5.633	8.459	16.491	12.26	32.87	1.957	0.968	0.267	-0.009
0.425	0.3256	-0.4788	1.9427	-5.423	7.839	15.934	13.22	25.31	1.933	1.015	0.301	0.004
0.450	0.3722	-0.4691	1.9378	-4.770	7.334	15.100	13.74	15.38	1.895	1.039	0.310	-0.003
0.475	0.4180	-0.4593	1.9319	-4.077	6.774	14.402	14.03	25.16	1.855	1.067	0.322	-0.012
0.500	0.4630	-0.4496	1.9251	-3.307	6.188	13.716	14.67	47.08	1.820	1.061	0.316	-0.035
0.525	0.5071	-0.4405	1.9175	-2.827	5.634	13.058	16.59	57.02	1.823	0.961	0.279	-0.063
0.550	0.5509	-0.4302	1.9080	-1.220	4.686	12.183	17.68	47.23	1.824	0.939	0.257	-0.074

time	x	y	z	ϕ	θ	ψ	V	α	$\dot{\alpha}$	C_L	C_D	C_m
(s)	(m)	(m)	(m)	(deg)	(deg)	(deg)	(m/s)	(deg)	(deg/s)			
0.575	0.5948	-0.4191	1.8965	-1.206	3.337	12.581	18.45	23.37	1.837	0.965	0.323	-0.047
0.600	0.6382	-0.4082	1.8836	-1.972	1.827	13.468	18.91	-5.26	1.850	0.987	0.409	-0.043
0.625	0.6812	-0.3975	1.8696	-3.353	0.165	14.694	18.45	-31.17	1.832	1.072	0.499	-0.020
0.650	0.7238	-0.3875	1.8549	-4.976	-1.461	15.887	17.19	-29.54	1.800	1.130	0.557	0.027
0.675	0.7656	-0.3791	1.8397	-6.242	-2.900	16.175	16.73	-11.68	1.771	1.136	0.508	0.016
0.700	0.8070	-0.3704	1.8237	-5.652	-4.295	15.302	16.96	-8.48	1.790	1.093	0.382	-0.016
0.725	0.8487	-0.3615	1.8065	-5.886	-5.820	15.111	16.44	-26.52	1.827	1.087	0.347	-0.016
0.750	0.8910	-0.3523	1.7886	-6.116	-7.338	15.076	15.38	-36.60	1.867	1.020	0.322	-0.029
0.775	0.9336	-0.3422	1.7696	-6.302	-9.017	15.434	14.51	-25.52	1.904	0.951	0.331	-0.027
0.800	0.9768	-0.3316	1.7495	-6.404	-10.834	16.020	14.08	-23.20	1.922	0.882	0.363	-0.019
0.825	1.0201	-0.3212	1.7279	-6.519	-12.844	16.503	13.67	-37.90	1.957	0.890	0.343	0.018
0.850	1.0639	-0.3110	1.7053	-6.423	-14.649	16.840	12.32	-41.54	2.004	0.846	0.293	0.030
0.875	1.1084	-0.3007	1.6816	-6.208	-16.243	17.177	11.14	-21.04	2.050	0.765	0.257	0.014
0.900	1.1536	-0.2905	1.6563	-6.009	-17.705	17.421	11.25	-0.10	2.114	0.666	0.229	-0.022
0.925	1.1994	-0.2795	1.6290	-5.816	-19.367	17.937	11.37	-14.85	2.183	0.648	0.219	-0.022
0.950	1.2463	-0.2682	1.6000	-5.599	-21.124	18.487	10.58	-45.27	2.256	0.609	0.198	-0.020
0.975	1.2942	-0.2563	1.5689	-5.568	-23.168	19.233	8.81	-55.94	2.328	0.607	0.179	0.002
1.000	1.3435	-0.2443	1.5365	-5.570	-25.115	19.932	7.65	-49.66	2.411	0.556	0.158	0.006
1.025	1.3940	-0.2320	1.5024	-5.698	-26.999	20.600	6.62	-48.75	2.499	0.512	0.143	0.010
1.050	1.4459	-0.2194	1.4663	-5.949	-28.817	21.237	5.35	-52.79	2.590	0.489	0.129	0.018
1.075	1.4991	-0.2059	1.4285	-6.193	-30.517	21.947	3.78	-48.81	2.681	0.471	0.117	0.026
1.100	1.5538	-0.1920	1.3891	-6.369	-31.893	22.552	2.91	-39.47	2.779	0.438	0.108	0.025
1.125	1.6101	-0.1774	1.3480	-6.572	-33.021	23.156	2.02	-34.03	2.877	0.420	0.102	0.024
1.150	1.6680	-0.1623	1.3054	-6.767	-33.868	23.737	1.20	-28.48	2.972	0.403	0.095	0.022
1.175	1.7276	-0.1464	1.2614	-6.940	-34.396	24.295	0.55	-13.46	3.069	0.370	0.090	0.011
1.200	1.7889	-0.1300	1.2160	-7.110	-34.772	24.805	0.43	-2.00	3.166	0.326	0.087	-0.003
1.225	1.8516	-0.1126	1.1684	-7.439	-35.331	25.532	0.47	-9.64	3.262	0.321	0.094	0.002
1.250	1.9158	-0.0946	1.1193	-7.808	-35.865	26.267	0.07	-29.90	3.351	0.338	0.097	0.011
1.275	1.9818	-0.0760	1.0694	-7.947	-36.146	26.888	-1.03	-29.35	3.430	0.334	0.087	0.011
1.300	2.0498	-0.0570	1.0187	-8.041	-36.207	27.230	-1.76	-7.39	3.518	0.294	0.077	-0.003
1.325	2.1194	-0.0374	0.9666	-8.280	-36.345	27.641	-1.33	1.50	3.607	0.266	0.070	-0.013
1.350	2.1907	-0.0170	0.9132	-8.523	-36.663	28.178	-1.25	-13.77	3.705	0.254	0.056	-0.015

The trajectory and determined quantities tabulated for the ten regression flights of the Vapor which are identified in Figs. 6.4. The tables include the specific test conditions and a time history of the important parameters for each of the ten flights.

Test Conditions					
aircraft	Vapor	flight	regression 1		
test number	2418				
m (g)	14.44	I_{xx} (g·cm^2)	369.9		
I_{yy} (g·cm^2)	1129.1	I_{zz} (g·cm^2)	1242.2		
I_{xz} (g·cm^2)	87.6	δ_e (deg)	-3.3		

time	x	y	z	ϕ	θ	ψ	V	α	$\dot{\alpha}$	C_L	C_D	C_m
(s)	(m)	(m)	(m)	(deg)	(deg)	(deg)	(m/s)	(deg)	(deg/s)			
0.000	-1.3969	-0.5720	1.5111	-4.508	-10.463	16.198	2.04	11.59	2.970	0.459	0.105	-0.011
0.025	-1.3257	-0.5580	1.4943	-3.932	-10.634	15.864	2.23	5.51	2.975	0.460	0.104	-0.008
0.050	-1.2545	-0.5438	1.4772	-3.588	-10.889	15.729	2.29	0.39	2.981	0.459	0.103	-0.006
0.075	-1.1832	-0.5294	1.4597	-3.335	-11.208	15.705	2.25	-3.77	2.988	0.459	0.101	-0.004
0.100	-1.1118	-0.5147	1.4418	-3.002	-11.572	15.678	2.21	-7.64	2.996	0.462	0.098	0.001
0.125	-1.0403	-0.4996	1.4237	-2.357	-11.909	15.592	1.85	-2.97	3.008	0.455	0.092	0.001
0.150	-0.9687	-0.4840	1.4053	-2.083	-12.187	15.665	1.93	3.18	3.025	0.433	0.094	-0.002
0.175	-0.8969	-0.4683	1.3863	-2.779	-12.491	16.014	2.13	4.26	3.041	0.427	0.107	-0.006
0.200	-0.8251	-0.4529	1.3667	-4.408	-12.846	16.544	2.06	-6.42	3.040	0.436	0.114	-0.002
0.225	-0.7533	-0.4371	1.3467	-4.929	-13.258	16.773	1.88	-13.69	3.044	0.443	0.106	0.002
0.250	-0.6814	-0.4212	1.3262	-5.735	-13.626	17.075	1.30	-13.05	3.057	0.451	0.096	0.004
0.275	-0.6091	-0.4046	1.3059	-5.278	-13.924	17.124	1.19	-6.18	3.083	0.432	0.088	0.001
0.300	-0.5365	-0.3875	1.2851	-5.145	-14.214	17.347	1.08	2.59	3.106	0.411	0.092	0.000
0.325	-0.4636	-0.3702	1.2638	-5.024	-14.492	17.594	1.28	6.13	3.113	0.401	0.099	-0.000
0.350	-0.3906	-0.3527	1.2418	-4.946	-14.775	17.828	1.45	5.82	3.129	0.395	0.097	-0.001
0.375	-0.3174	-0.3350	1.2193	-4.963	-15.071	18.038	1.54	0.73	3.147	0.391	0.092	-0.004
0.400	-0.2439	-0.3169	1.1959	-5.106	-15.426	18.311	1.45	-2.96	3.175	0.388	0.092	-0.004
0.425	-0.1700	-0.2987	1.1720	-5.226	-15.872	18.506	1.39	-4.53	3.196	0.385	0.091	0.001
0.450	-0.0958	-0.2799	1.1476	-5.348	-16.301	18.841	1.30	-3.73	3.217	0.382	0.095	0.006
0.475	-0.0213	-0.2605	1.1226	-5.550	-16.587	19.237	1.15	-3.58	3.242	0.382	0.103	0.006
0.500	0.0533	-0.2411	1.0971	-5.768	-16.797	19.428	1.10	-5.34	3.253	0.391	0.108	0.002
0.525	0.1282	-0.2219	1.0715	-5.877	-17.011	19.391	0.94	-9.43	3.263	0.398	0.103	0.001
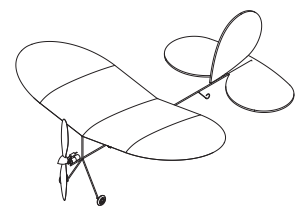
time	x	y	z	ϕ	θ	ψ	V	α	$\dot{\alpha}$	C_L	C_D	C_m
(s)	(m)	(m)	(m)	(deg)	(deg)	(deg)	(m/s)	(deg)	(deg/s)			
0.550	0.2037	-0.2026	1.0458	-5.914	-17.222	19.229	0.63	-12.58	3.277	0.400	0.099	0.002
0.575	0.2795	-0.1835	1.0200	-5.912	-17.440	18.981	0.27	-11.06	3.307	0.397	0.086	0.004
0.600	0.3558	-0.1635	0.9942	-5.957	-17.568	19.096	0.06	-9.24	3.334	0.395	0.087	0.004
0.625	0.4327	-0.1430	0.9686	-6.000	-17.559	19.414	-0.09	-8.58	3.349	0.389	0.093	-0.000
0.650	0.5099	-0.1223	0.9430	-5.995	-17.570	19.776	-0.38	-6.56	3.366	0.381	0.091	-0.002
0.675	0.5876	-0.1014	0.9175	-5.890	-17.638	20.149	-0.50	-2.14	3.384	0.366	0.089	-0.003
0.700	0.6657	-0.0802	0.8917	-5.779	-17.764	20.524	-0.45	0.49	3.402	0.351	0.090	-0.003
0.725	0.7440	-0.0586	0.8656	-5.690	-17.950	20.905	-0.43	-0.42	3.419	0.342	0.090	-0.003
0.750	0.8226	-0.0367	0.8390	-5.599	-18.197	21.288	-0.52	-0.30	3.436	0.336	0.089	-0.001
0.775	0.9015	-0.0147	0.8120	-5.539	-18.443	21.621	-0.51	2.09	3.455	0.325	0.087	-0.001
0.800	0.9807	0.0076	0.7843	-5.659	-18.708	21.940	-0.40	2.19	3.477	0.320	0.088	-0.001
0.825	1.0601	0.0301	0.7559	-6.009	-19.001	22.282	-0.37	-3.16	3.499	0.322	0.091	0.000
0.850	1.1398	0.0528	0.7271	-6.423	-19.275	22.608	-0.53	-9.61	3.516	0.328	0.093	0.002
0.875	1.2198	0.0758	0.6979	-6.687	-19.526	22.909	-0.85	-9.24	3.532	0.331	0.092	0.003
0.900	1.3001	0.0992	0.6687	-6.671	-19.695	23.117	-1.08	-3.99	3.549	0.320	0.089	-0.000
0.925	1.3807	0.1231	0.6390	-6.295	-19.949	23.342	-0.99	0.15	3.570	0.317	0.086	0.003
0.950	1.4617	0.1472	0.6089	-6.103	-20.113	23.542	-0.98	1.54	3.594	0.314	0.083	0.005
0.975	1.5431	0.1713	0.5786	-6.157	-20.144	23.693	-0.99	1.79	3.619	0.305	0.082	0.002
1.000	1.6249	0.1955	0.5477	-6.463	-20.216	23.818	-0.89	4.13	3.643	0.301	0.084	-0.000
1.025	1.7071	0.2200	0.5164	-6.961	-20.244	23.999	-0.81	2.70	3.664	0.299	0.086	-0.003
1.050	1.7897	0.2447	0.4851	-6.826	-20.247	24.075	-0.66	1.64	3.682	0.281	0.080	-0.010
1.075	1.8728	0.2699	0.4527	-6.859	-20.547	24.425	-0.75	0.42	3.707	0.275	0.083	-0.009

aircraft	Vapor	flight	regression 2
test number	2421		
m (g)	14.44	I_{xx} (g·cm^2)	369.9
I_{yy} (g·cm^2)	1129.1	I_{zz} (g·cm^2)	1242.2
I_{xz} (g·cm^2)	87.6	δ_e (deg)	-2.6
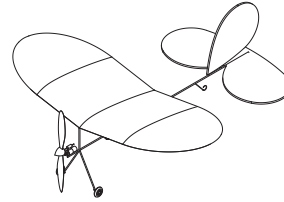
| time | x | y | z | ϕ | θ | ψ | V | α | $\dot{\alpha}$ | C_L | C_D | C_m |
(s)	(m)	(m)	(m)	(deg)	(deg)	(deg)	(m/s)	(deg)	(deg/s)			
0.000	-1.0155	-0.7806	1.5944	-3.985	-2.532	25.122	-2.51	-44.35	4.092	0.291	0.096	-0.005
0.025	-0.9200	-0.7482	1.5938	-6.414	-2.845	26.151	-3.65	-30.76	3.982	0.315	0.097	0.014
0.050	-0.8267	-0.7162	1.5946	-5.968	-2.745	25.454	-4.19	2.81	3.902	0.305	0.079	0.003
0.075	-0.7350	-0.6845	1.5955	-4.163	-2.556	23.892	-3.58	29.80	3.857	0.277	0.058	-0.006
0.100	-0.6444	-0.6527	1.5958	-3.646	-2.448	23.118	-2.55	33.90	3.816	0.272	0.062	-0.009
0.125	-0.5550	-0.6211	1.5951	-3.732	-2.549	22.806	-2.02	6.72	3.768	0.287	0.074	-0.006
0.150	-0.4669	-0.5897	1.5941	-4.155	-2.734	22.856	-1.92	-12.61	3.711	0.309	0.086	-0.001
0.175	-0.3803	-0.5591	1.5926	-4.719	-3.017	23.012	-2.89	-8.89	3.637	0.337	0.088	0.007
0.200	-0.2952	-0.5292	1.5917	-4.368	-2.981	22.590	-2.44	6.96	3.571	0.315	0.080	-0.006
0.225	-0.2117	-0.4988	1.5902	-3.855	-3.099	22.404	-2.06	18.37	3.527	0.318	0.075	-0.005
0.250	-0.1293	-0.4681	1.5879	-2.986	-3.315	22.285	-1.81	13.77	3.489	0.320	0.070	-0.002
0.275	-0.0481	-0.4372	1.5850	-2.750	-3.556	22.699	-1.47	14.00	3.456	0.323	0.075	0.002
0.300	0.0322	-0.4069	1.5811	-3.142	-3.767	23.389	-1.06	11.73	3.411	0.340	0.087	0.002
0.325	0.1114	-0.3776	1.5768	-3.966	-3.871	24.133	-0.74	5.02	3.367	0.358	0.089	0.002
0.350	0.1898	-0.3491	1.5718	-4.881	-3.907	24.707	-0.80	3.24	3.328	0.378	0.088	0.004
0.375	0.2671	-0.3201	1.5668	-4.797	-3.853	25.002	-0.64	9.42	3.290	0.380	0.088	-0.002
0.400	0.3433	-0.2908	1.5613	-4.531	-3.881	25.311	-0.31	15.22	3.255	0.389	0.102	-0.002
0.425	0.4186	-0.2622	1.5556	-4.110	-3.924	25.364	0.16	13.55	3.202	0.396	0.108	-0.003
0.450	0.4929	-0.2345	1.5494	-3.760	-4.034	25.114	0.33	9.52	3.154	0.409	0.092	-0.004
0.475	0.5662	-0.2062	1.5426	-3.540	-4.231	25.089	0.54	5.09	3.137	0.422	0.081	-0.003
0.500	0.6388	-0.1774	1.5356	-3.439	-4.445	25.267	0.62	-2.25	3.129	0.437	0.079	-0.001
0.525	0.7106	-0.1477	1.5285	-3.290	-4.656	25.648	0.46	-7.90	3.111	0.447	0.089	0.004
0.550	0.7815	-0.1176	1.5214	-3.100	-4.838	26.161	0.17	-2.73	3.067	0.465	0.106	0.011
0.575	0.8517	-0.0881	1.5143	-2.865	-4.871	26.402	0.25	7.66	3.034	0.471	0.107	0.011
0.600	0.9210	-0.0590	1.5072	-2.662	-4.729	26.489	0.68	14.05	3.009	0.477	0.105	0.008
0.625	0.9894	-0.0300	1.5001	-2.514	-4.447	26.484	0.97	15.38	2.978	0.485	0.102	-0.000

continued on next page

time	x	y	z	ϕ	θ	ψ	V	α	$\dot{\alpha}$	C_L	C_D	C_m
(s)	(m)	(m)	(m)	(deg)	(deg)	(deg)	(m/s)	(deg)	(deg/s)			
0.650	1.0571	-0.0006	1.4928	-2.395	-4.201	26.548	1.30	14.30	2.954	0.488	0.102	-0.008
0.675	1.1240	0.0292	1.4853	-2.261	-4.124	26.753	1.75	11.76	2.934	0.497	0.113	-0.006
0.700	1.1901	0.0589	1.4777	-2.113	-4.090	26.869	1.97	6.09	2.903	0.507	0.111	-0.001
0.725	1.2554	0.0888	1.4700	-2.047	-4.086	27.050	2.01	3.97	2.872	0.524	0.114	0.002
0.750	1.3199	0.1190	1.4621	-2.444	-4.085	27.498	2.08	4.51	2.854	0.540	0.123	0.005
0.775	1.3836	0.1490	1.4543	-2.687	-3.974	27.722	2.32	2.97	2.830	0.557	0.141	0.006
0.800	1.4463	0.1798	1.4469	-0.184	-3.761	26.697	2.32	4.14	2.774	0.574	0.129	-0.019
0.825	1.5081	0.2112	1.4393	3.256	-3.634	25.428	2.40	13.83	2.738	0.569	0.090	-0.034
0.850	1.5696	0.2421	1.4314	4.695	-3.652	25.136	2.97	26.15	2.757	0.519	0.067	-0.010
0.875	1.6307	0.2732	1.4228	4.690	-3.844	25.657	3.74	22.26	2.779	0.499	0.074	-0.025
0.900	1.6916	0.3042	1.4131	1.906	-4.302	27.583	4.19	5.18	2.777	0.527	0.119	-0.031
0.925	1.7521	0.3351	1.4027	-2.233	-4.827	30.050	3.91	-11.84	2.750	0.569	0.168	0.005
0.950	1.8115	0.3664	1.3923	-2.181	-5.140	30.460	3.56	-18.19	2.701	0.610	0.152	0.019
0.975	1.8704	0.3982	1.3822	-0.425	-5.252	30.002	3.16	-9.12	2.676	0.630	0.100	0.010
1.000	1.9293	0.4302	1.3724	0.662	-5.211	29.671	3.06	8.27	2.697	0.587	0.088	0.006

Test Conditions							
aircraft	Vapor	flight	regression 3				
test number	2422						
m (g)	14.44	I_{xx} (g·cm^2)	369.9				
I_{yy} (g·cm^2)	1129.1	I_{zz} (g·cm^2)	1242.2				
I_{xz} (g·cm^2)	87.6	δ_e (deg)	2.2				
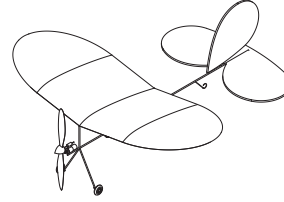
time	x	y	z	ϕ	θ	ψ	V	α	$\dot{\alpha}$	C_L	C_D	C_m
(s)	(m)	(m)	(m)	(deg)	(deg)	(deg)	(m/s)	(deg)	(deg/s)			
0.000	-0.8756	-0.8001	1.8525	-4.834	29.667	23.610	8.95	-50.13	2.292	0.928	0.339	0.061
0.025	-0.8279	-0.7819	1.8722	-5.379	30.270	23.965	8.84	18.98	2.118	0.961	0.304	0.040
0.050	-0.7836	-0.7653	1.8906	-5.347	31.039	23.420	9.85	70.15	1.965	0.967	0.263	-0.001
0.075	-0.7422	-0.7500	1.9071	-5.060	31.779	22.471	11.91	103.39	1.832	0.937	0.214	-0.054
0.100	-0.7027	-0.7356	1.9212	-4.951	32.210	21.792	15.26	116.95	1.738	0.950	0.225	-0.062
0.125	-0.6647	-0.7219	1.9323	-5.105	32.421	21.623	17.81	116.37	1.620	1.124	0.352	-0.070
0.150	-0.6291	-0.7089	1.9413	-5.184	32.397	21.344	20.77	116.45	1.511	1.217	0.443	-0.079
0.175	-0.5952	-0.6967	1.9474	-5.357	32.103	21.213	23.92	139.70	1.403	1.368	0.607	-0.068
0.200	-0.5632	-0.6853	1.9509	-5.486	31.626	20.917	27.45	172.88	1.304	1.461	0.777	-0.071
0.225	-0.5331	-0.6750	1.9515	-5.566	31.021	20.417	32.53	203.20	1.233	1.494	0.981	-0.078
0.250	-0.5047	-0.6653	1.9490	-5.822	30.253	20.175	37.78	215.68	1.160	1.587	1.291	-0.091
0.275	-0.4780	-0.6563	1.9435	-6.142	29.355	20.002	43.14	217.59	1.099	1.697	1.642	-0.114
0.300	-0.4533	-0.6478	1.9355	-6.398	28.291	19.724	48.65	229.70	1.059	1.599	1.876	-0.169
0.325	-0.4302	-0.6399	1.9246	-6.701	26.936	19.454	54.45	235.54	1.038	1.454	2.101	-0.203
0.350	-0.4085	-0.6327	1.9108	-6.989	25.270	19.083	60.39	218.43	1.042	1.217	2.242	-0.216
0.375	-0.3883	-0.6261	1.8942	-7.228	23.282	18.600	65.40	175.86	1.062	1.018	2.285	-0.224
0.400	-0.3693	-0.6200	1.8748	-7.425	20.906	18.105	69.10	128.33	1.087	0.868	2.363	-0.206
0.425	-0.3516	-0.6144	1.8530	-7.461	18.205	17.468	71.63	86.96	1.114	0.743	2.366	-0.215
0.450	-0.3352	-0.6092	1.8290	-7.312	15.166	16.800	73.52	43.81	1.159	0.609	2.219	-0.226
0.475	-0.3197	-0.6044	1.8029	-7.037	11.707	16.162	73.90	-6.57	1.207	0.557	2.048	-0.224
0.500	-0.3049	-0.5997	1.7745	-6.730	7.806	15.663	73.08	-54.57	1.269	0.523	1.916	-0.196
0.525	-0.2907	-0.5952	1.7443	-6.258	3.525	15.267	71.12	-95.57	1.325	0.508	1.741	-0.185
0.550	-0.2769	-0.5907	1.7120	-5.781	-1.199	15.102	68.40	-134.64	1.386	0.518	1.578	-0.156
0.575	-0.2630	-0.5863	1.6778	-5.261	-6.277	15.133	64.41	-175.18	1.457	0.538	1.359	-0.133
0.600	-0.2490	-0.5820	1.6415	-4.846	-11.747	15.470	59.63	-213.09	1.545	0.570	1.134	-0.090
0.625	-0.2343	-0.5775	1.6029	-4.595	-17.479	16.115	53.91	-240.11	1.651	0.581	0.919	-0.053

time	x	y	z	ϕ	θ	ψ	V	α	$\dot{\alpha}$	C_L	C_D	C_m
(s)	(m)	(m)	(m)	(deg)	(deg)	(deg)	(m/s)	(deg)	(deg/s)			
0.650	-0.2186	-0.5727	1.5618	-4.637	-23.395	17.147	47.64	-256.49	1.754	0.561	0.767	-0.021
0.675	-0.2017	-0.5677	1.5183	-4.827	-29.353	18.392	41.16	-261.55	1.871	0.514	0.591	-0.005
0.700	-0.1836	-0.5624	1.4718	-5.441	-35.387	19.978	34.64	-258.59	2.006	0.462	0.460	0.021
0.725	-0.1640	-0.5566	1.4221	-6.432	-41.328	21.895	28.31	-249.27	2.157	0.395	0.360	0.058
0.750	-0.1432	-0.5506	1.3690	-7.774	-46.945	24.038	22.32	-229.31	2.311	0.357	0.292	0.098
0.775	-0.1210	-0.5444	1.3126	-9.347	-51.809	26.163	16.91	-193.08	2.464	0.324	0.237	0.119
0.800	-0.0975	-0.5380	1.2527	-11.052	-55.617	28.219	12.55	-150.25	2.622	0.296	0.191	0.116
0.825	-0.0728	-0.5315	1.1895	-12.756	-58.193	29.884	9.44	-117.52	2.789	0.298	0.156	0.087
0.850	-0.0463	-0.5243	1.1228	-14.297	-59.819	31.315	6.74	-101.83	2.954	0.313	0.133	0.058
0.875	-0.0172	-0.5162	1.0529	-15.522	-60.804	32.541	4.29	-90.33	3.119	0.309	0.114	0.039
0.900	0.0148	-0.5072	0.9800	-16.468	-61.382	33.476	2.13	-71.77	3.285	0.303	0.106	0.034
0.925	0.0500	-0.4974	0.9042	-17.211	-61.553	33.928	0.63	-53.51	3.444	0.298	0.106	0.033
0.950	0.0885	-0.4867	0.8261	-17.763	-61.232	33.854	-0.49	-41.53	3.588	0.298	0.105	0.030
0.975	0.1304	-0.4753	0.7460	-18.130	-60.343	33.199	-1.45	-33.88	3.726	0.305	0.101	0.017
1.000	0.1762	-0.4630	0.6643	-18.280	-59.173	32.348	-2.24	-27.12	3.863	0.304	0.094	0.007
1.025	0.2263	-0.4497	0.5815	-18.317	-57.884	31.565	-2.81	-24.55	3.994	0.297	0.088	0.002
1.050	0.2807	-0.4353	0.4977	-18.316	-56.582	30.998	-3.39	-23.26	4.120	0.290	0.085	0.001
1.075	0.3394	-0.4198	0.4133	-18.231	-55.251	30.558	-4.07	-18.75	4.241	0.281	0.080	0.002
1.100	0.4025	-0.4031	0.3286	-17.908	-53.839	30.146	-4.36	-12.31	4.354	0.263	0.080	-0.002
1.125	0.4696	-0.3852	0.2436	-17.399	-52.481	29.730	-4.51	-3.86	4.458	0.248	0.082	-0.005
1.150	0.5403	-0.3661	0.1587	-16.712	-51.272	29.272	-4.62	6.62	4.551	0.235	0.084	-0.008

	Test Conditions				

aircraft	Vapor	flight	regression 4	
test number	2425			
m (g)	14.44	I_{xx} (g·cm^2)	369.9	
I_{yy} (g·cm^2)	1129.1	I_{zz} (g·cm^2)	1242.2	
I_{xz} (g·cm^2)	87.6	δ_e (deg)	2.1	
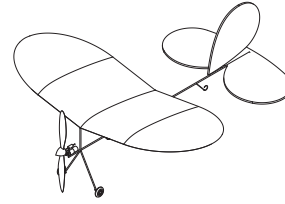
time	x	y	z	ϕ	θ	ψ	V	α	$\dot{\alpha}$	C_L	C_D	C_m
(s)	(m)	(m)	(m)	(deg)	(deg)	(deg)	(m/s)	(deg)	(deg/s)			
0.000	-1.5515	-1.0325	1.6202	-13.369	-4.710	25.844	-0.14	-34.21	3.770	0.527	0.147	0.009
0.025	-1.4652	-1.0002	1.6129	-12.313	-2.797	25.983	-0.68	-14.05	3.683	0.523	0.132	0.004
0.050	-1.3803	-0.9697	1.6093	-11.305	-0.937	25.561	-0.84	1.96	3.601	0.516	0.121	-0.000
0.075	-1.2969	-0.9405	1.6088	-10.400	0.862	24.807	-0.68	13.82	3.522	0.505	0.114	-0.004
0.100	-1.2153	-0.9125	1.6108	-9.662	2.562	23.896	-0.18	21.74	3.438	0.500	0.102	-0.006
0.125	-1.1356	-0.8846	1.6147	-9.153	4.212	23.341	0.41	24.38	3.363	0.503	0.108	-0.007
0.150	-1.0577	-0.8583	1.6200	-8.713	5.708	22.548	0.97	21.55	3.285	0.510	0.097	-0.006
0.175	-0.9814	-0.8328	1.6267	-8.426	7.116	21.825	1.58	20.75	3.216	0.518	0.099	-0.005
0.200	-0.9070	-0.8083	1.6345	-8.319	8.443	21.123	1.98	24.43	3.131	0.534	0.102	-0.003
0.225	-0.8348	-0.7842	1.6432	-8.386	9.774	20.575	2.70	27.28	3.053	0.548	0.097	-0.003
0.250	-0.7644	-0.7607	1.6527	-8.472	11.091	20.175	3.44	24.99	2.979	0.572	0.105	-0.002
0.275	-0.6962	-0.7375	1.6629	-8.504	12.432	20.060	3.98	19.63	2.887	0.605	0.122	-0.004
0.300	-0.6301	-0.7156	1.6736	-8.374	13.707	19.757	4.43	23.63	2.796	0.624	0.128	-0.007
0.325	-0.5662	-0.6948	1.6848	-8.256	14.915	19.477	5.12	36.45	2.694	0.635	0.139	-0.010
0.350	-0.5043	-0.6752	1.6958	-8.193	16.007	19.163	6.28	48.64	2.598	0.643	0.150	-0.011
0.375	-0.4448	-0.6565	1.7062	-8.296	17.021	18.970	7.57	52.00	2.508	0.662	0.158	-0.011
0.400	-0.3872	-0.6388	1.7160	-8.548	17.978	18.909	8.86	49.93	2.411	0.701	0.176	-0.016
0.425	-0.3316	-0.6220	1.7248	-8.927	18.793	18.958	9.99	47.52	2.318	0.752	0.194	-0.016
0.450	-0.2780	-0.6062	1.7329	-9.362	19.513	19.102	11.22	44.66	2.227	0.807	0.215	-0.014
0.475	-0.2264	-0.5914	1.7400	-9.789	20.153	19.290	12.32	43.67	2.138	0.868	0.248	-0.011
0.500	-0.1767	-0.5774	1.7463	-10.105	20.715	19.410	13.38	47.12	2.043	0.933	0.287	-0.009
0.525	-0.1291	-0.5645	1.7516	-10.319	21.231	19.412	14.67	54.66	1.948	1.000	0.330	-0.014
0.550	-0.0834	-0.5526	1.7557	-10.466	21.656	19.301	16.24	68.18	1.857	1.062	0.374	-0.021
0.575	-0.0397	-0.5416	1.7587	-10.548	21.961	19.071	17.92	74.13	1.769	1.125	0.431	-0.028
0.600	0.0022	-0.5315	1.7600	-10.752	22.092	18.971	20.04	67.78	1.692	1.229	0.518	-0.019
0.625	0.0422	-0.5224	1.7601	-10.667	22.170	18.547	21.53	72.29	1.597	1.380	0.621	-0.016
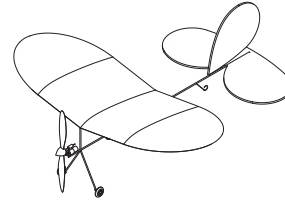
time	x	y	z	ϕ	θ	ψ	V	α	$\dot{\alpha}$	C_L	C_D	C_m
(s)	(m)	(m)	(m)	(deg)	(deg)	(deg)	(m/s)	(deg)	(deg/s)			
0.650	0.0802	-0.5140	1.7592	-10.160	22.233	17.688	23.25	95.69	1.511	1.388	0.652	-0.081
0.675	0.1166	-0.5067	1.7563	-10.076	21.995	17.197	26.42	133.05	1.450	1.415	0.752	-0.101
0.700	0.1516	-0.4999	1.7515	-9.656	21.461	16.378	29.93	138.88	1.402	1.417	0.867	-0.125
0.725	0.1851	-0.4940	1.7447	-9.535	20.618	15.771	33.47	113.33	1.361	1.432	1.022	-0.126
0.750	0.2173	-0.4888	1.7355	-9.844	19.389	15.573	35.59	88.66	1.303	1.654	1.305	-0.066
0.775	0.2480	-0.4845	1.7246	-10.057	17.934	15.211	37.52	68.01	1.256	1.849	1.565	0.002
0.800	0.2767	-0.4811	1.7131	-9.714	16.645	14.251	39.42	79.27	1.203	1.874	1.677	-0.022
0.825	0.3041	-0.4779	1.7000	-8.431	15.182	12.706	41.20	113.07	1.159	1.863	1.721	-0.205
0.850	0.3302	-0.4740	1.6855	-4.710	13.518	9.687	44.70	139.88	1.164	1.463	1.414	-0.522
0.875	0.3560	-0.4703	1.6679	-2.699	11.283	8.215	48.63	117.87	1.242	1.132	1.206	-0.313
0.900	0.3815	-0.4668	1.6474	-2.168	8.468	8.109	50.65	46.09	1.315	0.986	1.319	-0.222
0.925	0.4066	-0.4640	1.6241	-3.053	5.070	9.189	50.52	-13.98	1.313	1.093	1.675	-0.120
0.950	0.4306	-0.4617	1.5996	-3.995	1.635	10.365	49.75	-41.10	1.321	1.086	1.666	-0.076
0.975	0.4539	-0.4596	1.5735	-3.481	-2.031	10.532	48.65	-63.17	1.341	1.094	1.579	-0.111
1.000	0.4769	-0.4573	1.5462	-1.281	-5.879	9.704	46.94	-95.51	1.404	1.039	1.223	-0.113
1.025	0.5004	-0.4545	1.5167	0.240	-10.049	9.634	43.88	-126.66	1.475	0.978	1.027	-0.084
1.050	0.5244	-0.4506	1.4851	1.576	-14.457	10.045	40.47	-136.55	1.566	0.842	0.847	-0.058
1.075	0.5489	-0.4462	1.4512	2.655	-19.124	10.840	36.97	-139.69	1.667	0.727	0.687	-0.034
1.100	0.5742	-0.4411	1.4145	3.285	-23.999	11.998	33.61	-155.92	1.770	0.643	0.602	-0.009
1.125	0.6004	-0.4361	1.3752	3.507	-28.939	13.143	29.34	-179.34	1.877	0.617	0.490	0.013
1.150	0.6276	-0.4309	1.3332	3.334	-33.840	14.216	24.54	-191.66	2.009	0.579	0.359	0.031
1.175	0.6563	-0.4247	1.2883	2.761	-38.550	15.354	19.78	-182.93	2.151	0.506	0.281	0.042
1.200	0.6865	-0.4174	1.2404	1.893	-43.012	16.500	15.60	-161.35	2.297	0.417	0.225	0.059
1.225	0.7181	-0.4096	1.1891	0.805	-47.095	17.538	11.80	-130.70	2.453	0.346	0.184	0.083
1.250	0.7509	-0.4016	1.1344	-0.639	-50.446	18.468	8.92	-97.14	2.605	0.305	0.161	0.095
1.275	0.7848	-0.3935	1.0763	-2.316	-52.791	19.311	7.02	-69.79	2.762	0.292	0.139	0.087
1.300	0.8200	-0.3852	1.0149	-4.235	-54.116	20.002	5.48	-54.90	2.917	0.304	0.125	0.063
1.325	0.8573	-0.3768	0.9505	-6.158	-54.653	20.518	4.18	-44.54	3.071	0.307	0.111	0.037
1.350	0.8970	-0.3681	0.8832	-8.201	-54.773	20.938	3.11	-36.56	3.229	0.303	0.100	0.022
1.375	0.9395	-0.3587	0.8132	-10.468	-54.664	21.405	2.38	-34.40	3.381	0.306	0.104	0.020
1.400	0.9849	-0.3487	0.7410	-12.682	-54.258	21.920	1.47	-35.01	3.522	0.317	0.106	0.022
1.425	1.0336	-0.3381	0.6671	-14.635	-53.416	22.369	0.55	-34.58	3.651	0.330	0.106	0.020
1.450	1.0858	-0.3268	0.5918	-16.579	-52.205	22.680	-0.14	-29.42	3.776	0.357	0.112	0.017
1.475	1.1425	-0.3149	0.5167	-17.156	-50.485	22.876	-0.95	-25.64	3.880	0.352	0.105	0.005
1.500	1.2035	-0.3024	0.4416	-17.450	-48.751	23.060	-1.50	-23.96	3.980	0.349	0.100	-0.002
1.525	1.2687	-0.2889	0.3671	-17.246	-47.114	23.313	-2.17	-24.16	4.073	0.343	0.092	-0.002

time	x	y	z	ϕ	θ	ψ	V	α	$\dot{\alpha}$	C_L	C_D	C_m
(s)	(m)	(m)	(m)	(deg)	(deg)	(deg)	(m/s)	(deg)	(deg/s)			
1.550	1.3384	-0.2747	0.2933	-16.536	-45.682	23.642	-2.69	-22.32	4.166	0.340	0.085	0.007
1.575	1.4123	-0.2596	0.2206	-15.686	-44.178	23.789	-3.25	-15.01	4.258	0.338	0.075	0.018
1.600	1.4902	-0.2434	0.1493	-14.919	-42.298	23.567	-3.46	-3.61	4.350	0.335	0.065	0.029

	Test Conditions										
aircraft	Vapor	flight	regression 5								
test number	2432										
m (g)	14.44	I_{xx} (g·cm^2)	369.9								
I_{yy} (g·cm^2)	1129.1	I_{zz} (g·cm^2)	1242.2								
I_{xz} (g·cm^2)	87.6	δ_e (deg)	1.5								

time	x	y	z	ϕ	θ	ψ	V	α	$\dot{\alpha}$	C_L	C_D	C_m
(s)	(m)	(m)	(m)	(deg)	(deg)	(deg)	(m/s)	(deg)	(deg/s)			
0.000	-0.8236	-0.6631	1.7716	-7.566	4.163	19.701	8.39	0.46	2.590	0.696	0.181	-0.012
0.025	-0.7639	-0.6408	1.7672	-8.377	4.582	20.314	8.37	3.74	2.544	0.705	0.171	-0.008
0.050	-0.7051	-0.6189	1.7630	-9.061	4.996	21.036	8.56	7.66	2.504	0.713	0.178	-0.008
0.075	-0.6475	-0.5975	1.7591	-9.590	5.377	21.732	8.83	8.96	2.458	0.721	0.178	-0.011
0.100	-0.5905	-0.5768	1.7550	-9.988	5.642	22.348	9.01	9.18	2.413	0.738	0.186	-0.011
0.125	-0.5344	-0.5568	1.7508	-10.262	5.832	22.932	9.24	11.89	2.371	0.745	0.196	-0.013
0.150	-0.4791	-0.5375	1.7463	-10.375	5.913	23.443	9.60	13.90	2.333	0.746	0.204	-0.016
0.175	-0.4248	-0.5185	1.7414	-10.478	5.866	24.010	10.02	13.47	2.287	0.770	0.228	-0.016
0.200	-0.3714	-0.5003	1.7361	-10.406	5.711	24.416	10.25	11.41	2.239	0.787	0.233	-0.021
0.225	-0.3188	-0.4827	1.7301	-10.288	5.348	24.692	10.52	7.52	2.205	0.800	0.228	-0.019
0.250	-0.2669	-0.4657	1.7234	-10.151	4.801	24.886	10.74	7.75	2.177	0.825	0.240	-0.006
0.275	-0.2156	-0.4492	1.7163	-9.712	4.220	24.839	10.81	11.48	2.145	0.827	0.248	-0.002
0.300	-0.1651	-0.4331	1.7084	-9.250	3.611	24.710	11.30	18.98	2.115	0.833	0.265	-0.000
0.325	-0.1153	-0.4174	1.6996	-8.790	2.996	24.499	11.81	22.85	2.087	0.860	0.272	-0.002
0.350	-0.0662	-0.4019	1.6902	-8.152	2.413	24.129	12.35	15.49	2.069	0.864	0.268	-0.010
0.375	-0.0176	-0.3868	1.6799	-7.564	1.746	23.743	12.72	13.27	2.057	0.881	0.275	-0.011
0.400	0.0305	-0.3717	1.6689	-6.920	1.017	23.273	12.81	16.50	2.040	0.884	0.275	-0.015
0.425	0.0783	-0.3568	1.6571	-6.282	0.236	22.730	13.56	18.46	2.035	0.855	0.274	-0.022
0.450	0.1258	-0.3423	1.6442	-5.914	-0.685	22.135	13.95	13.34	2.031	0.862	0.268	-0.018
0.475	0.1731	-0.3272	1.6303	-5.743	-1.699	21.760	14.08	1.73	2.045	0.853	0.288	-0.010
0.500	0.2201	-0.3121	1.6155	-5.711	-2.764	21.422	14.15	-0.24	2.047	0.849	0.315	-0.003
0.525	0.2668	-0.2973	1.5998	-5.749	-3.836	20.986	14.00	2.21	2.034	0.861	0.322	0.002
0.550	0.3133	-0.2831	1.5833	-5.794	-4.863	20.406	14.17	2.73	2.037	0.844	0.292	-0.005
0.575	0.3600	-0.2690	1.5656	-6.059	-5.937	19.893	14.20	-4.03	2.062	0.841	0.268	-0.010
0.600	0.4069	-0.2547	1.5469	-6.289	-7.066	19.439	14.04	-18.10	2.106	0.821	0.248	-0.013
0.625	0.4542	-0.2398	1.5274	-6.675	-8.252	19.328	13.34	-28.22	2.123	0.824	0.280	-0.006

continued on next page

130

time	x	y	z	ϕ	θ	ψ	V	α	$\dot{\alpha}$	C_L	C_D	C_m
(s)	(m)	(m)	(m)	(deg)	(deg)	(deg)	(m/s)	(deg)	(deg/s)			
0.650	0.5019	-0.2253	1.5072	-7.072	-9.494	19.080	12.54	-26.78	2.138	0.806	0.279	-0.002
0.675	0.5500	-0.2112	1.4862	-7.481	-10.765	18.749	11.96	-19.88	2.161	0.772	0.255	-0.000
0.700	0.5985	-0.1973	1.4643	-7.929	-12.071	18.364	11.67	-18.31	2.200	0.735	0.217	0.003
0.725	0.6477	-0.1827	1.4413	-8.485	-13.318	18.226	11.09	-23.22	2.253	0.704	0.213	0.007
0.750	0.6975	-0.1679	1.4172	-9.036	-14.515	18.224	10.34	-27.84	2.294	0.691	0.214	0.011
0.775	0.7481	-0.1535	1.3922	-9.582	-15.608	18.112	9.71	-28.66	2.334	0.677	0.208	0.005
0.800	0.7996	-0.1395	1.3663	-10.053	-16.678	18.007	8.96	-30.58	2.375	0.648	0.189	-0.002
0.825	0.8521	-0.1257	1.3394	-10.509	-17.794	17.971	8.20	-28.52	2.430	0.615	0.167	0.004
0.850	0.9056	-0.1117	1.3115	-10.918	-18.902	18.082	7.40	-21.35	2.494	0.582	0.150	0.018
0.875	0.9602	-0.0975	1.2824	-11.408	-19.787	18.322	7.15	-17.30	2.555	0.555	0.154	0.020
0.900	1.0158	-0.0831	1.2522	-11.900	-20.486	18.566	6.73	-21.95	2.613	0.560	0.157	0.018
0.925	1.0725	-0.0688	1.2212	-12.145	-20.992	18.754	6.02	-30.46	2.667	0.568	0.153	0.014
0.950	1.1306	-0.0544	1.1897	-12.087	-21.386	18.872	5.19	-29.96	2.722	0.565	0.144	0.012
0.975	1.1900	-0.0400	1.1580	-11.710	-21.687	18.905	4.53	-21.95	2.777	0.543	0.134	0.011
1.000	1.2509	-0.0256	1.1260	-11.315	-21.896	18.897	4.11	-13.86	2.834	0.526	0.128	0.014
1.025	1.3131	-0.0112	1.0937	-11.031	-21.944	18.843	3.80	-11.25	2.888	0.517	0.124	0.014
1.050	1.3767	0.0034	1.0611	-10.847	-21.809	18.836	3.51	-12.67	2.942	0.514	0.125	0.012
1.075	1.4415	0.0181	1.0286	-10.556	-21.540	18.834	3.20	-11.31	2.989	0.515	0.121	0.011
1.100	1.5078	0.0332	0.9965	-10.105	-21.109	18.889	2.89	-8.33	3.036	0.504	0.122	0.008
1.125	1.5753	0.0486	0.9646	-9.481	-20.629	18.885	2.83	-4.29	3.074	0.503	0.123	0.010
1.150	1.6440	0.0641	0.9333	-8.662	-20.023	18.647	2.71	-0.06	3.108	0.501	0.118	0.008
1.175	1.7139	0.0799	0.9028	-7.743	-19.328	18.180	2.78	4.13	3.141	0.485	0.109	0.002
1.200	1.7848	0.0962	0.8727	-6.961	-18.591	17.649	2.94	7.37	3.176	0.474	0.098	-0.004
1.225	1.8569	0.1132	0.8431	-6.390	-17.961	17.184	3.05	2.52	3.227	0.461	0.093	-0.003
1.250	1.9302	0.1314	0.8141	-6.201	-17.331	17.041	3.15	-2.59	3.262	0.454	0.117	0.002

	Test Conditions										
aircraft		Vapor	flight		regression 6						
test number		2434									
m (g)		14.44	I_{xx} (g·cm^2)		369.9						
I_{yy} (g·cm^2)		1129.1	I_{zz} (g·cm^2)		1242.2						
I_{xz} (g·cm^2)		87.6	δ_e (deg)		4.8						
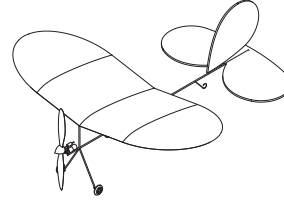
time	x	y	z	ϕ	θ	ψ	V	α	$\dot{\alpha}$	C_L	C_D	C_m
(s)	(m)	(m)	(m)	(deg)	(deg)	(deg)	(m/s)	(deg)	(deg/s)			
0.000	-1.6050	-0.4535	1.8871	-10.573	15.712	-12.710	12.72	62.84	1.921	0.988	0.192	0.006
0.025	-1.5629	-0.4760	1.8865	-10.912	15.658	-13.841	14.07	63.40	1.879	1.033	0.255	-0.003
0.050	-1.5222	-0.4986	1.8847	-10.168	15.378	-16.256	15.76	65.00	1.834	1.085	0.327	-0.029
0.075	-1.4831	-0.5216	1.8817	-8.926	14.944	-19.478	17.54	67.64	1.785	1.141	0.406	-0.047
0.100	-1.4459	-0.5452	1.8776	-7.993	14.479	-22.983	19.21	74.00	1.733	1.138	0.452	-0.071
0.125	-1.4103	-0.5690	1.8720	-8.121	13.889	-25.763	20.86	75.23	1.677	1.184	0.513	-0.056
0.150	-1.3758	-0.5924	1.8652	-8.906	13.193	-27.690	23.01	53.33	1.643	1.214	0.579	-0.064
0.175	-1.3422	-0.6151	1.8570	-10.500	12.301	-28.382	24.00	28.51	1.603	1.328	0.659	-0.031
0.200	-1.3098	-0.6374	1.8476	-12.222	11.318	-28.863	23.84	14.14	1.566	1.448	0.709	-0.000
0.225	-1.2786	-0.6593	1.8373	-12.303	10.160	-30.609	24.76	16.71	1.526	1.499	0.827	0.004
0.250	-1.2494	-0.6815	1.8263	-12.514	8.994	-32.525	25.18	33.14	1.487	1.561	0.862	-0.013
0.275	-1.2219	-0.7038	1.8144	-12.242	7.790	-34.884	25.86	42.13	1.459	1.477	0.822	-0.091
0.300	-1.1949	-0.7260	1.8010	-12.567	6.301	-36.637	27.62	46.08	1.455	1.448	0.840	-0.078
0.325	-1.1688	-0.7481	1.7862	-12.169	4.560	-38.695	28.32	35.21	1.462	1.394	0.842	-0.086
0.350	-1.1434	-0.7702	1.7702	-11.756	2.649	-40.538	28.95	17.65	1.470	1.290	0.839	-0.090
0.375	-1.1184	-0.7923	1.7521	-11.840	0.460	-41.934	29.33	15.37	1.479	1.277	0.880	-0.045
0.400	-1.0943	-0.8147	1.7325	-11.960	-1.819	-43.333	29.45	-0.34	1.497	1.285	0.840	-0.020
0.425	-1.0708	-0.8373	1.7118	-11.314	-4.039	-44.917	29.54	-19.88	1.540	1.152	0.763	-0.041
0.450	-1.0472	-0.8602	1.6890	-11.437	-6.431	-45.771	28.56	-29.36	1.579	1.166	0.757	-0.021
0.475	-1.0239	-0.8834	1.6649	-10.500	-8.813	-47.019	27.77	-25.47	1.622	1.044	0.713	-0.032
0.500	-1.0011	-0.9072	1.6394	-9.590	-11.228	-48.181	27.58	-20.02	1.670	0.927	0.646	-0.038
0.525	-0.9782	-0.9316	1.6115	-9.232	-13.838	-49.047	26.89	-41.69	1.736	0.863	0.593	-0.031
0.550	-0.9555	-0.9566	1.5816	-9.143	-16.631	-49.874	25.52	-75.13	1.803	0.911	0.515	-0.008
0.575	-0.9322	-0.9824	1.5504	-7.620	-19.360	-50.822	23.06	-92.18	1.888	0.794	0.442	-0.011
0.600	-0.9081	-1.0091	1.5171	-6.932	-22.137	-51.413	20.78	-80.15	1.974	0.736	0.403	0.003
0.625	-0.8832	-1.0370	1.4820	-6.582	-24.833	-51.987	19.02	-67.91	2.053	0.649	0.397	0.002

time	x	y	z	ϕ	θ	ψ	V	α	$\dot{\alpha}$	C_L	C_D	C_m
(s)	(m)	(m)	(m)	(deg)	(deg)	(deg)	(m/s)	(deg)	(deg/s)			
0.650	-0.8586	-1.0663	1.4452	-6.907	-27.539	-52.541	17.54	-86.31	2.130	0.619	0.334	0.014
0.675	-0.8337	-1.0972	1.4062	-7.746	-30.273	-53.043	14.90	-101.46	2.220	0.615	0.290	0.044
0.700	-0.8086	-1.1298	1.3654	-8.646	-32.774	-53.608	11.81	-83.70	2.335	0.566	0.224	0.065
0.725	-0.7829	-1.1638	1.3227	-8.217	-34.707	-54.338	10.86	-40.37	2.451	0.459	0.192	0.068
0.750	-0.7562	-1.1988	1.2775	-8.606	-35.989	-54.770	10.34	-18.33	2.560	0.450	0.193	0.060
0.775	-0.7290	-1.2356	1.2303	-9.258	-36.655	-55.120	9.75	-31.46	2.662	0.472	0.190	0.041
0.800	-0.7014	-1.2743	1.1814	-10.325	-36.927	-55.394	8.73	-44.68	2.771	0.504	0.166	0.027
0.825	-0.6727	-1.3156	1.1314	-11.510	-36.973	-55.689	7.36	-50.63	2.875	0.511	0.147	0.021
0.850	-0.6430	-1.3598	1.0806	-12.638	-36.867	-55.900	6.36	-47.12	2.981	0.507	0.143	0.022
0.875	-0.6124	-1.4070	1.0296	-13.868	-36.442	-56.008	5.11	-39.55	3.080	0.491	0.130	0.020
0.900	-0.5808	-1.4567	0.9781	-14.852	-35.744	-55.913	4.27	-30.80	3.176	0.484	0.124	0.020
0.925	-0.5480	-1.5096	0.9270	-15.656	-34.614	-55.669	3.64	-18.13	3.264	0.467	0.126	0.013
0.950	-0.5144	-1.5650	0.8762	-16.279	-33.297	-55.396	3.21	-15.22	3.345	0.464	0.127	0.008
0.975	-0.4797	-1.6229	0.8263	-16.714	-31.757	-55.015	3.00	-17.44	3.405	0.468	0.126	0.000
1.000	-0.4446	-1.6838	0.7774	-17.200	-30.269	-54.619	2.25	-24.81	3.461	0.475	0.120	-0.000
1.025	-0.4089	-1.7477	0.7301	-17.927	-28.767	-54.208	1.76	-27.66	3.522	0.461	0.113	-0.001
1.050	-0.3730	-1.8142	0.6840	-18.525	-27.403	-53.775	0.86	-26.41	3.580	0.473	0.111	0.010
1.075	-0.3363	-1.8838	0.6403	-19.415	-25.612	-53.382	0.46	-27.35	3.628	0.470	0.132	0.005
1.100	-0.2986	-1.9551	0.5990	-20.239	-23.814	-52.958	-0.39	-29.44	3.638	0.495	0.156	0.008
1.125	-0.2601	-2.0279	0.5614	-21.100	-21.752	-52.634	-1.16	-35.55	3.619	0.528	0.181	0.005
1.150	-0.2213	-2.1016	0.5281	-21.936	-19.682	-52.601	-2.17	-44.89	3.574	0.573	0.204	0.002

	Test Conditions										

aircraft	Vapor	flight	regression 7
test number	2443		
m (g)	14.44	I_{xx} (g·cm^2)	369.9
I_{yy} (g·cm^2)	1129.1	I_{zz} (g·cm^2)	1242.2
I_{xz} (g·cm^2)	87.6	δ_e (deg)	1.6
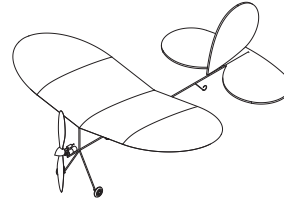
time	x	y	z	ϕ	θ	ψ	V	α	$\dot{\alpha}$	C_L	C_D	C_m
(s)	(m)	(m)	(m)	(deg)	(deg)	(deg)	(m/s)	(deg)	(deg/s)			
0.000	-0.4568	-0.7520	1.5039	-13.829	-1.816	8.994	5.44	-24.47	2.713	0.609	0.145	0.002
0.025	-0.3902	-0.7470	1.4943	-14.056	-1.717	8.286	5.10	0.63	2.692	0.650	0.140	0.013
0.050	-0.3240	-0.7426	1.4854	-14.165	-1.372	7.663	4.96	-2.93	2.662	0.655	0.148	0.007
0.075	-0.2586	-0.7391	1.4768	-14.246	-1.006	6.885	5.07	3.95	2.641	0.681	0.137	0.010
0.100	-0.1935	-0.7359	1.4690	-14.158	-0.484	6.226	5.16	8.06	2.623	0.689	0.141	0.013
0.125	-0.1289	-0.7330	1.4617	-13.148	0.045	5.153	5.36	19.03	2.596	0.692	0.144	0.012
0.150	-0.0651	-0.7310	1.4550	-12.606	0.896	4.339	6.06	36.44	2.570	0.671	0.154	-0.006
0.175	-0.0021	-0.7297	1.4483	-12.637	1.735	3.884	7.17	39.88	2.535	0.664	0.165	-0.023
0.200	0.0602	-0.7297	1.4413	-13.191	2.354	3.631	8.16	25.23	2.502	0.680	0.175	-0.026
0.225	0.1218	-0.7306	1.4339	-13.659	2.682	3.227	8.36	7.19	2.476	0.710	0.173	-0.019
0.250	0.1828	-0.7322	1.4266	-14.319	2.878	2.944	8.42	0.07	2.445	0.730	0.184	-0.017
0.275	0.2431	-0.7347	1.4190	-14.234	2.731	2.081	8.38	-1.75	2.414	0.753	0.187	-0.011
0.300	0.3026	-0.7379	1.4115	-14.346	2.576	1.367	8.41	-7.89	2.381	0.779	0.196	-0.002
0.325	0.3613	-0.7417	1.4042	-14.393	2.398	0.750	8.10	-10.30	2.352	0.801	0.188	0.012
0.350	0.4192	-0.7462	1.3970	-14.359	2.319	0.057	7.82	-0.87	2.328	0.812	0.183	0.014
0.375	0.4764	-0.7512	1.3899	-14.239	2.441	-0.578	8.00	15.77	2.304	0.803	0.190	0.001
0.400	0.5329	-0.7570	1.3828	-14.078	2.603	-1.262	8.67	24.82	2.278	0.786	0.204	-0.016
0.425	0.5886	-0.7637	1.3750	-13.883	2.530	-2.150	9.25	23.26	2.249	0.795	0.205	-0.020
0.450	0.6437	-0.7709	1.3667	-13.722	2.330	-2.901	9.72	14.37	2.229	0.801	0.209	-0.020
0.475	0.6981	-0.7787	1.3578	-13.603	1.992	-3.555	10.03	6.47	2.215	0.819	0.214	-0.013
0.500	0.7520	-0.7872	1.3485	-13.520	1.569	-4.182	10.06	1.88	2.198	0.833	0.221	-0.005
0.525	0.8054	-0.7961	1.3388	-13.452	1.122	-4.750	10.11	3.92	2.179	0.846	0.233	0.005
0.550	0.8581	-0.8057	1.3286	-13.349	0.740	-5.396	10.29	11.34	2.160	0.849	0.242	0.006
0.575	0.9101	-0.8160	1.3179	-13.176	0.377	-6.185	10.68	16.25	2.152	0.845	0.235	0.001
0.600	0.9616	-0.8267	1.3067	-12.892	0.039	-6.895	11.10	16.71	2.142	0.851	0.246	-0.004
0.625	1.0127	-0.8379	1.2948	-12.591	-0.308	-7.567	11.46	12.50	2.134	0.863	0.248	-0.008

continued on next page

time	x	y	z	ϕ	θ	ψ	V	α	$\dot{\alpha}$	C_L	C_D	C_m
(s)	(m)	(m)	(m)	(deg)	(deg)	(deg)	(m/s)	(deg)	(deg/s)			
0.650	1.0634	-0.8495	1.2823	-12.248	-0.720	-8.168	11.72	7.09	2.129	0.876	0.254	-0.006
0.675	1.1139	-0.8615	1.2694	-11.888	-1.180	-8.787	11.82	1.91	2.125	0.891	0.260	-0.001
0.700	1.1640	-0.8739	1.2562	-11.525	-1.633	-9.431	11.87	-1.43	2.121	0.903	0.266	0.002
0.725	1.2138	-0.8867	1.2426	-11.164	-2.066	-10.089	11.77	-0.75	2.116	0.907	0.267	0.002
0.750	1.2633	-0.8999	1.2288	-10.860	-2.476	-10.742	11.76	1.76	2.113	0.905	0.266	0.002
0.775	1.3126	-0.9135	1.2146	-10.643	-2.849	-11.339	11.89	3.24	2.115	0.900	0.265	0.001
0.800	1.3617	-0.9275	1.2001	-10.460	-3.225	-11.923	11.96	2.31	2.117	0.900	0.266	0.003
0.825	1.4106	-0.9418	1.1853	-10.238	-3.560	-12.519	11.99	3.75	2.120	0.890	0.266	0.000
0.850	1.4595	-0.9565	1.1701	-10.023	-3.901	-13.111	12.08	6.94	2.123	0.882	0.267	-0.001
0.875	1.5082	-0.9713	1.1544	-9.833	-4.222	-13.669	12.33	4.49	2.129	0.873	0.268	-0.004

	Test Conditions						
aircraft	Vapor	flight	regression 8				
test number	2438						
m (g)	14.44	I_{xx} (g·cm^2)	369.9				
I_{yy} (g·cm^2)	1129.1	I_{zz} (g·cm^2)	1242.2				
I_{xz} (g·cm^2)	87.6	δ_e (deg)	1.1				
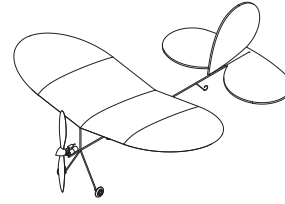
time	x	y	z	ϕ	θ	ψ	V	α	$\dot{\alpha}$	C_L	C_D	C_m
(s)	(m)	(m)	(m)	(deg)	(deg)	(deg)	(m/s)	(deg)	(deg/s)			
0.000	-1.2186	-0.5490	1.4443	-14.289	-27.897	16.065	-1.06	1.83	3.748	0.401	0.072	-0.011
0.025	-1.1362	-0.5402	1.4001	-13.175	-26.653	15.224	-1.07	-6.05	3.808	0.397	0.072	-0.006
0.050	-1.0514	-0.5304	1.3577	-12.529	-25.479	14.559	-1.29	-9.96	3.858	0.395	0.073	-0.001
0.075	-0.9645	-0.5197	1.3173	-12.169	-24.289	14.038	-1.59	-9.91	3.900	0.394	0.074	0.004
0.100	-0.8754	-0.5082	1.2793	-11.811	-22.881	13.709	-1.73	-4.00	3.931	0.379	0.089	0.002
0.125	-0.7853	-0.4972	1.2433	-11.543	-21.481	13.245	-1.79	5.78	3.944	0.375	0.092	0.000
0.150	-0.6941	-0.4865	1.2094	-11.113	-20.091	12.680	-1.45	9.76	3.939	0.371	0.098	-0.002
0.175	-0.6022	-0.4762	1.1775	-10.819	-18.770	12.051	-1.24	3.82	3.930	0.383	0.094	0.000
0.200	-0.5096	-0.4659	1.1479	-10.615	-17.413	11.462	-1.29	-4.66	3.931	0.394	0.087	0.002
0.225	-0.4163	-0.4557	1.1207	-10.557	-16.024	11.034	-1.61	-4.89	3.945	0.404	0.079	0.005
0.250	-0.3223	-0.4454	1.0964	-10.530	-14.450	10.774	-1.64	-2.84	3.933	0.411	0.083	0.003
0.275	-0.2280	-0.4354	1.0749	-10.534	-12.820	10.531	-1.56	-4.09	3.911	0.423	0.086	0.004
0.300	-0.1336	-0.4250	1.0566	-10.500	-11.077	10.534	-1.81	-3.03	3.888	0.430	0.084	0.004
0.325	-0.0395	-0.4144	1.0416	-10.332	-9.189	10.591	-1.85	8.68	3.860	0.421	0.083	0.000
0.350	0.0541	-0.4040	1.0294	-10.123	-7.303	10.690	-1.36	23.72	3.816	0.410	0.088	-0.004
0.375	0.1470	-0.3939	1.0195	-9.895	-5.495	10.738	-0.64	27.01	3.767	0.401	0.094	-0.008
0.400	0.2390	-0.3847	1.0111	-9.653	-3.952	10.566	0.05	20.94	3.716	0.407	0.095	-0.006
0.425	0.3299	-0.3759	1.0044	-9.242	-2.572	10.233	0.36	14.31	3.661	0.424	0.097	-0.003
0.450	0.4195	-0.3667	0.9996	-8.286	-1.241	9.753	0.71	11.01	3.602	0.439	0.099	-0.003
0.475	0.5077	-0.3577	0.9967	-7.607	0.118	9.331	1.03	12.55	3.541	0.447	0.099	-0.004
0.500	0.5944	-0.3491	0.9955	-7.405	1.407	9.126	1.26	12.76	3.479	0.455	0.098	-0.005
0.525	0.6796	-0.3407	0.9958	-7.667	2.640	9.134	1.68	11.01	3.414	0.465	0.102	-0.004
0.550	0.7631	-0.3328	0.9974	-8.404	3.799	9.357	1.86	6.18	3.345	0.488	0.107	0.001
0.575	0.8448	-0.3251	1.0004	-8.528	5.028	9.259	1.94	2.52	3.271	0.510	0.108	0.001
0.600	0.9245	-0.3175	1.0047	-8.611	6.219	9.247	2.00	5.37	3.192	0.541	0.111	0.004
0.625	1.0022	-0.3104	1.0105	-8.633	7.553	9.193	2.24	12.05	3.114	0.558	0.112	0.002

continued on next page

time	x	y	z	ϕ	θ	ψ	V	α	$\dot\alpha$	C_L	C_D	C_m
(s)	(m)	(m)	(m)	(deg)	(deg)	(deg)	(m/s)	(deg)	(deg/s)			
0.650	1.0778	-0.3036	1.0177	-8.616	8.943	9.122	2.59	16.85	3.032	0.577	0.115	-0.001
0.675	1.1512	-0.2971	1.0258	-8.200	10.277	8.775	3.13	19.52	2.947	0.595	0.119	-0.007
0.700	1.2225	-0.2912	1.0347	-8.063	11.512	8.637	3.53	22.64	2.861	0.617	0.127	-0.006
0.725	1.2915	-0.2857	1.0442	-7.742	12.699	8.412	4.19	27.31	2.769	0.636	0.142	-0.005
0.750	1.3580	-0.2801	1.0540	-5.904	13.739	6.875	4.94	34.00	2.671	0.660	0.139	-0.021
0.775	1.4225	-0.2750	1.0638	-5.075	14.678	6.308	5.79	35.21	2.580	0.686	0.146	-0.018
0.800	1.4846	-0.2704	1.0734	-4.701	15.567	6.084	6.77	29.36	2.496	0.719	0.153	-0.018
0.825	1.5446	-0.2665	1.0829	-5.303	16.381	6.653	7.34	19.57	2.408	0.767	0.172	-0.025
0.850	1.6023	-0.2632	1.0920	-6.687	17.098	7.884	7.62	18.50	2.307	0.826	0.193	-0.005
0.875	1.6579	-0.2600	1.1007	-7.152	17.678	8.244	8.09	26.57	2.209	0.891	0.210	-0.002
0.900	1.7110	-0.2570	1.1091	-6.253	18.288	7.300	9.25	37.86	2.123	0.912	0.206	-0.013
0.925	1.7622	-0.2539	1.1167	-5.891	18.773	7.094	10.18	54.33	2.038	0.942	0.224	-0.009
0.950	1.8113	-0.2515	1.1233	-5.843	19.238	6.867	11.60	67.50	1.952	0.979	0.249	-0.015
0.975	1.8586	-0.2493	1.1286	-5.902	19.639	6.863	13.72	67.54	1.872	1.045	0.291	-0.019
1.000	1.9041	-0.2472	1.1327	-5.963	19.984	6.945	15.25	64.60	1.799	1.115	0.373	-0.026
1.025	1.9476	-0.2451	1.1356	-5.856	20.219	6.922	16.45	70.70	1.704	1.199	0.459	-0.041
1.050	1.9892	-0.2435	1.1367	-5.743	20.205	6.770	18.88	89.98	1.615	1.330	0.587	-0.031
1.075	2.0283	-0.2426	1.1367	-5.450	20.161	6.144	21.09	88.18	1.518	1.428	0.651	-0.054
1.100	2.0657	-0.2419	1.1349	-5.341	19.902	5.567	23.52	83.55	1.456	1.529	0.673	-0.067
1.125	2.1014	-0.2408	1.1318	-5.126	19.498	5.183	25.00	101.80	1.405	1.575	0.683	-0.091
1.150	2.1361	-0.2393	1.1268	-4.858	18.808	4.923	28.35	120.42	1.368	1.523	0.804	-0.119
1.175	2.1693	-0.2372	1.1200	-4.437	17.892	4.848	31.94	125.86	1.348	1.462	0.915	-0.131
1.200	2.2017	-0.2350	1.1106	-4.237	16.341	5.074	33.93	94.53	1.281	1.752	1.267	0.027

	Test Conditions										

aircraft	Vapor	flight	regression 9
test number	2423		
m (g)	14.44	I_{xx} (g·cm^2)	369.9
I_{yy} (g·cm^2)	1129.1	I_{zz} (g·cm^2)	1242.2
I_{xz} (g·cm^2)	87.6	δ_e (deg)	1.1

time	x	y	z	ϕ	θ	ψ	V	α	$\dot{\alpha}$	C_L	C_D	C_m
(s)	(m)	(m)	(m)	(deg)	(deg)	(deg)	(m/s)	(deg)	(deg/s)			
0.000	-1.3744	-0.9041	1.7565	-7.812	-7.580	23.037	10.98	-0.08	2.321	0.827	0.285	-0.020
0.025	-1.3228	-0.8860	1.7377	-7.677	-7.402	23.009	10.99	-5.60	2.312	0.823	0.276	-0.014
0.050	-1.2711	-0.8682	1.7191	-7.502	-7.331	22.874	10.72	-10.49	2.314	0.827	0.238	-0.008
0.075	-1.2190	-0.8500	1.7008	-7.285	-7.301	22.818	10.37	-8.26	2.329	0.806	0.216	-0.006
0.100	-1.1666	-0.8314	1.6826	-7.097	-7.302	22.842	10.34	-3.17	2.353	0.776	0.220	-0.003
0.125	-1.1140	-0.8125	1.6644	-6.913	-7.320	22.882	10.33	-1.08	2.350	0.773	0.237	-0.002
0.150	-1.0614	-0.7937	1.6464	-6.571	-7.328	22.748	10.18	-1.46	2.346	0.764	0.218	-0.009
0.175	-1.0084	-0.7751	1.6281	-6.353	-7.428	22.546	10.16	-0.98	2.358	0.751	0.200	-0.013
0.200	-0.9551	-0.7567	1.6096	-6.244	-7.654	22.302	10.15	-5.85	2.387	0.738	0.171	-0.012
0.225	-0.9012	-0.7376	1.5909	-6.280	-7.952	22.300	9.98	-14.79	2.416	0.724	0.176	-0.006
0.250	-0.8468	-0.7182	1.5721	-6.459	-8.293	22.456	9.43	-17.88	2.430	0.718	0.195	-0.000
0.275	-0.7923	-0.6985	1.5532	-6.548	-8.642	22.578	8.98	-13.05	2.437	0.707	0.195	0.003
0.300	-0.7376	-0.6785	1.5342	-6.516	-8.949	22.635	8.85	-6.25	2.450	0.689	0.200	0.002
0.325	-0.6827	-0.6586	1.5151	-6.568	-9.254	22.509	8.68	-6.12	2.455	0.683	0.192	0.002
0.350	-0.6277	-0.6388	1.4957	-6.705	-9.561	22.310	8.47	-8.59	2.469	0.690	0.167	0.003
0.375	-0.5721	-0.6186	1.4761	-6.903	-9.815	22.189	8.20	-11.02	2.496	0.673	0.158	-0.002
0.400	-0.5161	-0.5983	1.4564	-7.194	-10.093	22.181	8.00	-12.56	2.524	0.656	0.157	-0.002
0.425	-0.4595	-0.5777	1.4364	-7.584	-10.390	22.331	7.63	-10.89	2.550	0.647	0.165	0.002
0.450	-0.4024	-0.5572	1.4162	-7.947	-10.665	22.536	7.35	-10.84	2.557	0.644	0.182	0.006
0.475	-0.3452	-0.5368	1.3960	-8.220	-10.886	22.675	7.16	-11.30	2.564	0.650	0.172	0.007
0.500	-0.2875	-0.5166	1.3756	-8.376	-11.018	22.751	6.76	-15.04	2.585	0.648	0.154	0.003
0.525	-0.2292	-0.4962	1.3553	-8.442	-11.123	22.861	6.43	-13.70	2.608	0.642	0.150	-0.001
0.550	-0.1704	-0.4756	1.3352	-8.263	-11.225	22.930	6.02	-7.87	2.630	0.614	0.138	-0.007
0.575	-0.1110	-0.4547	1.3148	-8.286	-11.434	23.086	6.00	-7.89	2.652	0.599	0.142	-0.006
0.600	-0.0512	-0.4336	1.2942	-8.433	-11.705	23.266	5.79	-13.31	2.673	0.601	0.149	0.000
0.625	0.0090	-0.4124	1.2737	-8.527	-11.971	23.346	5.26	-21.43	2.690	0.597	0.142	0.004

time	x	y	z	ϕ	θ	ψ	V	α	$\dot{\alpha}$	C_L	C_D	C_m
(s)	(m)	(m)	(m)	(deg)	(deg)	(deg)	(m/s)	(deg)	(deg/s)			
0.650	0.0697	-0.3910	1.2532	-8.574	-12.213	23.358	4.75	-15.63	2.704	0.592	0.136	0.006
0.675	0.1308	-0.3693	1.2326	-8.571	-12.435	23.340	4.21	-5.50	2.721	0.591	0.133	0.010
0.700	0.1924	-0.3475	1.2123	-8.231	-12.480	23.115	4.54	-3.16	2.747	0.561	0.127	0.004
0.725	0.2545	-0.3258	1.1916	-8.204	-12.549	22.893	4.36	-5.25	2.768	0.566	0.128	0.004
0.750	0.3172	-0.3042	1.1709	-8.186	-12.580	22.636	4.08	-6.81	2.784	0.562	0.124	0.002
0.775	0.3804	-0.2827	1.1503	-8.168	-12.556	22.331	4.08	-1.31	2.805	0.541	0.119	-0.002
0.800	0.4440	-0.2609	1.1295	-8.318	-12.604	22.186	4.05	0.22	2.828	0.538	0.118	0.004
0.825	0.5082	-0.2390	1.1087	-8.551	-12.588	22.084	4.04	-3.93	2.848	0.541	0.123	0.009
0.850	0.5727	-0.2171	1.0879	-8.753	-12.437	21.949	3.87	-6.77	2.863	0.547	0.124	0.007
0.875	0.6378	-0.1952	1.0675	-8.824	-12.202	21.705	3.69	-2.28	2.876	0.539	0.121	0.001
0.900	0.7033	-0.1732	1.0473	-8.869	-11.989	21.438	3.71	6.86	2.891	0.517	0.120	-0.001
0.925	0.7691	-0.1514	1.0271	-9.049	-11.790	21.169	4.08	11.72	2.903	0.499	0.120	-0.002
0.950	0.8354	-0.1297	1.0066	-9.431	-11.646	20.990	4.36	8.71	2.917	0.499	0.122	0.003
0.975	0.9019	-0.1083	0.9859	-9.912	-11.457	20.840	4.45	3.29	2.928	0.506	0.121	0.006
1.000	0.9689	-0.0871	0.9652	-10.517	-11.185	20.766	4.47	2.24	2.943	0.516	0.124	0.009
1.025	1.0362	-0.0663	0.9448	-11.177	-10.796	20.732	4.54	1.25	2.952	0.530	0.129	0.011
1.050	1.1038	-0.0458	0.9247	-11.914	-10.262	20.750	4.59	-4.35	2.955	0.555	0.137	0.014
1.075	1.1717	-0.0257	0.9053	-12.605	-9.525	20.762	4.38	-10.42	2.954	0.585	0.142	0.012
1.100	1.2399	-0.0058	0.8873	-12.986	-8.651	20.672	4.02	-11.08	2.945	0.603	0.141	0.007
1.125	1.3082	0.0137	0.8706	-13.059	-7.703	20.416	3.81	-5.89	2.934	0.608	0.135	0.000
1.150	1.3768	0.0327	0.8552	-13.000	-6.802	20.083	3.75	-2.22	2.922	0.608	0.133	-0.002
1.175	1.4455	0.0512	0.8411	-12.881	-5.962	19.655	3.75	-2.43	2.910	0.607	0.131	-0.004
1.200	1.5142	0.0691	0.8282	-12.714	-5.180	19.152	3.64	0.21	2.893	0.602	0.128	-0.005
1.225	1.5828	0.0864	0.8162	-12.492	-4.460	18.629	3.67	7.88	2.873	0.587	0.124	-0.008
1.250	1.6513	0.1031	0.8049	-12.288	-3.844	18.121	4.04	16.22	2.857	0.574	0.122	-0.008
1.275	1.7196	0.1192	0.7940	-12.093	-3.328	17.634	4.49	13.64	2.843	0.563	0.121	-0.009
1.300	1.7876	0.1349	0.7832	-11.991	-2.964	17.274	4.77	3.37	2.826	0.586	0.124	0.002
1.325	1.8554	0.1502	0.7729	-11.829	-2.548	16.884	4.65	0.59	2.809	0.601	0.124	0.010

	Test Conditions							

aircraft	Vapor	flight	regression 10
test number	2428		
m (g)	14.44	I_{xx} (g·cm^2)	369.9
I_{yy} (g·cm^2)	1129.1	I_{zz} (g·cm^2)	1242.2
I_{xz} (g·cm^2)	87.6	δ_e (deg)	1.3
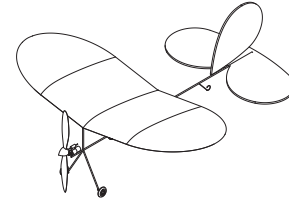
time	x	y	z	ϕ	θ	ψ	V	α	$\dot{\alpha}$	C_L	C_D	C_m
(s)	(m)	(m)	(m)	(deg)	(deg)	(deg)	(m/s)	(deg)	(deg/s)			
0.000	-1.8911	-0.7321	1.8230	-10.933	-33.249	26.472	6.59	-15.55	2.526	0.629	0.193	0.025
0.025	-1.8448	-0.7177	1.7816	-11.423	-32.502	26.636	6.04	-23.95	2.612	0.643	0.180	0.013
0.050	-1.7959	-0.7026	1.7399	-11.731	-31.639	26.766	5.36	-23.78	2.699	0.624	0.167	0.002
0.075	-1.7443	-0.6867	1.6981	-11.861	-30.776	26.853	4.91	-16.34	2.784	0.587	0.165	-0.005
0.100	-1.6905	-0.6702	1.6562	-11.861	-30.024	26.833	4.55	-11.50	2.863	0.557	0.167	-0.005
0.125	-1.6345	-0.6529	1.6144	-11.737	-29.374	26.745	4.32	-16.47	2.914	0.547	0.173	-0.000
0.150	-1.5766	-0.6358	1.5728	-11.439	-28.776	26.342	3.81	-23.62	2.974	0.555	0.146	0.004
0.175	-1.5164	-0.6177	1.5317	-10.960	-28.095	25.940	3.03	-24.27	3.045	0.539	0.126	0.004
0.200	-1.4541	-0.5984	1.4913	-10.440	-27.344	25.568	2.54	-15.38	3.119	0.514	0.114	0.004
0.225	-1.3897	-0.5781	1.4515	-9.984	-26.525	25.203	2.34	-6.76	3.182	0.493	0.114	0.002
0.250	-1.3233	-0.5573	1.4123	-9.626	-25.715	24.788	2.23	-7.91	3.230	0.482	0.117	0.003
0.275	-1.2552	-0.5361	1.3739	-9.417	-24.867	24.319	1.95	-11.09	3.282	0.480	0.111	0.004
0.300	-1.1853	-0.5147	1.3362	-9.284	-23.998	23.846	1.58	-11.35	3.332	0.481	0.102	0.007
0.325	-1.1135	-0.4925	1.3000	-9.151	-22.946	23.472	1.38	-10.35	3.376	0.469	0.105	0.004
0.350	-1.0403	-0.4697	1.2648	-9.377	-21.830	23.302	1.19	-7.28	3.411	0.480	0.115	0.004
0.375	-0.9656	-0.4460	1.2317	-7.688	-20.616	22.845	0.95	-0.09	3.425	0.464	0.104	-0.004
0.400	-0.8898	-0.4219	1.2000	-6.480	-19.476	22.497	1.11	8.75	3.451	0.442	0.098	-0.007
0.425	-0.8129	-0.3975	1.1694	-5.921	-18.464	22.249	1.45	10.99	3.480	0.426	0.097	-0.005
0.450	-0.7351	-0.3728	1.1398	-6.181	-17.567	22.075	1.61	-0.59	3.506	0.425	0.104	0.001
0.475	-0.6568	-0.3480	1.1116	-7.352	-16.600	21.951	1.54	-9.03	3.504	0.439	0.109	0.003
0.500	-0.5779	-0.3227	1.0846	-8.763	-15.592	21.924	0.95	-9.57	3.497	0.462	0.110	0.005
0.525	-0.4986	-0.2971	1.0598	-8.479	-14.458	21.639	1.04	-5.17	3.507	0.456	0.101	0.003
0.550	-0.4188	-0.2711	1.0368	-8.729	-13.256	21.616	0.94	-0.57	3.505	0.458	0.104	0.001
0.575	-0.3387	-0.2452	1.0156	-8.883	-12.019	21.693	0.88	0.81	3.491	0.461	0.106	0.001
0.600	-0.2585	-0.2191	0.9963	-8.963	-10.779	21.840	0.98	1.20	3.470	0.468	0.111	0.002
0.625	-0.1784	-0.1935	0.9788	-8.968	-9.557	21.773	1.08	-0.51	3.453	0.482	0.105	0.004

time	x	y	z	ϕ	θ	ψ	V	α	$\dot{\alpha}$	C_L	C_D	C_m
(s)	(m)	(m)	(m)	(deg)	(deg)	(deg)	(m/s)	(deg)	(deg/s)			
0.650	-0.0985	-0.1670	0.9636	-8.810	-8.154	21.849	0.87	1.80	3.431	0.480	0.108	0.002
0.675	-0.0192	-0.1408	0.9502	-8.547	-6.797	21.766	1.10	11.33	3.396	0.483	0.104	0.000
0.700	0.0596	-0.1144	0.9387	-8.313	-5.390	21.768	1.51	20.06	3.362	0.481	0.104	-0.003
0.725	0.1378	-0.0880	0.9288	-8.133	-4.013	21.816	2.09	16.35	3.330	0.480	0.105	-0.006
0.750	0.2153	-0.0620	0.9202	-8.089	-2.765	21.905	2.43	13.01	3.294	0.491	0.108	-0.004
0.775	0.2921	-0.0369	0.9127	-8.092	-1.636	21.835	2.50	10.44	3.255	0.505	0.107	-0.001
0.800	0.3681	-0.0116	0.9069	-8.057	-0.415	21.877	3.11	11.80	3.199	0.508	0.123	-0.005
0.825	0.4429	0.0129	0.9021	-7.986	0.657	21.751	3.20	13.70	3.153	0.520	0.125	-0.006
0.850	0.5166	0.0368	0.8984	-7.850	1.622	21.423	3.57	12.83	3.090	0.530	0.129	-0.005
0.875	0.5891	0.0600	0.8955	-7.696	2.481	21.064	3.94	12.02	3.030	0.552	0.128	-0.001
0.900	0.6603	0.0825	0.8935	-7.426	3.322	20.539	4.19	6.98	2.974	0.577	0.113	0.004
0.925	0.7302	0.1053	0.8926	-7.162	4.289	20.318	4.35	10.10	2.937	0.587	0.106	0.005
0.950	0.7987	0.1284	0.8928	-6.849	5.403	20.305	4.58	23.32	2.891	0.585	0.114	-0.003
0.975	0.8659	0.1514	0.8938	-6.498	6.516	20.427	5.47	34.29	2.825	0.576	0.135	-0.014
1.000	0.9316	0.1739	0.8947	-6.279	7.367	20.570	6.51	37.23	2.757	0.591	0.161	-0.011
1.025	0.9959	0.1951	0.8958	-5.759	8.164	20.205	7.26	34.44	2.681	0.595	0.162	-0.021
1.050	1.0588	0.2153	0.8963	-5.565	8.648	19.821	8.09	30.18	2.620	0.620	0.155	-0.021
1.075	1.1204	0.2351	0.8963	-5.658	8.917	19.752	8.77	17.49	2.563	0.675	0.164	-0.010
1.100	1.1805	0.2547	0.8965	-5.804	9.169	19.827	9.00	-6.66	2.509	0.731	0.177	-0.002
1.125	1.2391	0.2742	0.8970	-5.904	9.415	19.960	8.59	-15.38	2.447	0.787	0.182	0.006
1.150	1.2961	0.2936	0.8978	-5.833	9.673	20.112	7.96	-0.15	2.372	0.839	0.190	0.010
1.175	1.3514	0.3127	0.8995	-5.021	10.159	19.720	8.61	24.15	2.312	0.803	0.191	-0.015
1.200	1.4053	0.3313	0.9008	-4.278	10.441	19.341	9.41	34.53	2.254	0.796	0.187	-0.022
1.225	1.4579	0.3496	0.9012	-4.222	10.502	19.448	10.25	32.77	2.201	0.826	0.217	-0.002
1.250	1.5088	0.3684	0.9013	-2.464	10.676	18.385	10.96	39.07	2.133	0.837	0.216	-0.031
1.275	1.5586	0.3866	0.9005	-1.112	10.741	17.442	12.15	53.06	2.085	0.813	0.201	-0.064
1.300	1.6074	0.4046	0.8981	-0.580	10.365	17.176	13.58	54.10	2.056	0.812	0.212	-0.057
1.325	1.6554	0.4224	0.8944	-0.834	9.657	17.544	14.97	27.20	2.029	0.855	0.259	-0.044
1.350	1.7023	0.4399	0.8895	-1.758	8.724	18.478	15.19	2.64	1.991	0.921	0.299	-0.012
1.375	1.7483	0.4572	0.8835	-3.159	7.768	19.800	14.77	8.40	1.936	0.992	0.354	0.035
1.400	1.7928	0.4747	0.8770	-2.894	7.172	20.002	15.46	38.60	1.898	0.969	0.344	0.000
1.425	1.8363	0.4918	0.8693	-2.932	6.604	20.379	16.90	47.22	1.876	0.944	0.367	-0.032
1.450	1.8791	0.5087	0.8601	-3.179	5.745	20.956	18.15	30.20	1.849	1.002	0.394	-0.027
1.475	1.9211	0.5258	0.8498	-3.471	4.779	21.603	18.19	15.78	1.832	1.025	0.449	-0.018
1.500	1.9621	0.5426	0.8386	-3.694	3.758	22.192	18.72	17.99	1.802	1.043	0.488	-0.014
1.525	2.0022	0.5593	0.8262	-3.820	2.678	22.736	19.30	23.73	1.771	1.077	0.501	-0.017

time	x	y	z	ϕ	θ	ψ	V	α	$\dot{\alpha}$	C_L	C_D	C_m
(s)	(m)	(m)	(m)	(deg)	(deg)	(deg)	(m/s)	(deg)	(deg/s)			
1.550	2.0415	0.5759	0.8128	-3.800	1.547	23.239	19.84	9.99	1.761	1.079	0.472	-0.028
1.575	2.0804	0.5926	0.7984	-3.763	0.318	23.782	19.99	0.47	1.768	1.066	0.441	-0.037
1.600	2.1190	0.6093	0.7826	-3.739	-1.126	24.407	19.58	1.58	1.788	1.041	0.397	-0.028
1.625	2.1578	0.6266	0.7659	-3.745	-2.654	25.149	20.06	7.71	1.800	0.943	0.422	-0.030

Appendix B

Test Data for the Balsa Glider with an Aspect Ratio 6.07

Appendix B lists the data for selected flights of the balsa glider with an aspect ratio 6.07. The data is downsampled from the recording rate of 200 Hz to 40 Hz. Flights E, F and G (as listed in Table 6.2) are included as well as the 14 regression flights. The tables include some of the specific test conditions and a time history of the important parameters.

The trajectory and determined quantities tabulated for flight E of the balsa glider with an aspect ratio of 6.07 which is labeled as the 'aggressive' flight in Fig. 5.10 and was shown in Figs. 6.22 and 6.23.

Test Conditions				
aircraft	balsa glider	flight	E	
aspect ratio	6.07	test number	6053	
m (g)	5.91	I_{xx} (g·cm^2)	126.21	
I_{yy} (g·cm^2)	280.69	I_{zz} (g·cm^2)	401.99	
I_{xz} (g·cm^2)	7.42	I_{xy} (g·cm^2)	0.27	
I_{yz} (g·cm^2)	-0.10	δ_e (deg)	0	
CG (%c)	76.5			

time	x	y	z	ϕ	θ	ψ	V	α	$\dot{\alpha}$	C_L	C_D	C_m
(s)	(m)	(m)	(m)	(deg)	(deg)	(deg)	(m/s)	(deg)	(deg/s)			
0.000	-0.3865	-0.0322	1.3422	3.917	22.582	35.592	6.98	7.11	4.752	0.727	0.130	-0.010
0.025	-0.2924	0.0284	1.3764	3.814	25.083	35.801	7.20	10.06	4.607	0.738	0.125	-0.013
0.050	-0.2026	0.0871	1.4136	3.752	27.498	35.991	7.47	12.29	4.461	0.750	0.124	-0.015
0.075	-0.1174	0.1438	1.4532	3.726	29.816	36.166	7.79	13.80	4.309	0.764	0.127	-0.018
0.100	-0.0365	0.1982	1.4948	3.731	32.054	36.342	8.17	14.07	4.152	0.782	0.138	-0.025
0.125	0.0397	0.2503	1.5376	3.767	34.118	36.483	8.51	15.78	3.983	0.801	0.152	-0.024
0.150	0.1115	0.3001	1.5811	3.816	36.048	36.632	8.94	19.44	3.808	0.822	0.165	-0.020

continued on next page

143

time	x	y	z	ϕ	θ	ψ	V	α	$\dot{\alpha}$	C_L	C_D	C_m
(s)	(m)	(m)	(m)	(deg)	(deg)	(deg)	(m/s)	(deg)	(deg/s)			
0.175	0.1789	0.3474	1.6246	3.886	37.905	36.790	9.50	23.81	3.630	0.849	0.179	-0.024
0.200	0.2420	0.3922	1.6677	4.015	39.678	36.948	10.14	26.66	3.449	0.881	0.193	-0.039
0.225	0.3010	0.4347	1.7098	4.250	41.321	37.069	10.84	29.02	3.265	0.912	0.208	-0.065
0.250	0.3560	0.4749	1.7505	4.611	42.716	37.134	11.60	32.73	3.081	0.932	0.224	-0.087
0.275	0.4073	0.5131	1.7893	5.064	43.816	37.143	12.49	39.11	2.899	0.945	0.247	-0.098
0.300	0.4552	0.5495	1.8257	5.551	44.626	37.133	13.58	48.87	2.717	0.957	0.277	-0.097
0.325	0.5000	0.5840	1.8591	6.023	45.194	37.140	14.96	61.89	2.538	0.976	0.316	-0.090
0.350	0.5420	0.6170	1.8892	6.467	45.568	37.210	16.70	78.28	2.364	1.003	0.363	-0.082
0.375	0.5814	0.6485	1.9157	6.870	45.793	37.356	18.90	98.06	2.197	1.039	0.421	-0.080
0.400	0.6186	0.6787	1.9384	7.232	45.891	37.580	21.63	121.25	2.039	1.083	0.500	-0.082
0.425	0.6536	0.7076	1.9570	7.524	45.876	37.855	24.98	147.61	1.892	1.136	0.608	-0.090
0.450	0.6867	0.7354	1.9714	7.730	45.750	38.218	29.02	176.04	1.756	1.194	0.748	-0.106
0.475	0.7180	0.7620	1.9815	7.834	45.510	38.693	33.78	204.83	1.635	1.253	0.926	-0.136
0.500	0.7476	0.7875	1.9873	7.822	45.139	39.340	39.25	231.86	1.532	1.296	1.137	-0.181
0.525	0.7756	0.8118	1.9888	7.662	44.612	40.179	45.34	255.05	1.450	1.292	1.383	-0.229
0.550	0.8021	0.8351	1.9859	7.341	43.919	41.233	51.94	271.91	1.391	1.221	1.635	-0.284
0.575	0.8270	0.8573	1.9787	6.843	43.052	42.485	58.84	278.02	1.356	1.074	1.864	-0.344
0.600	0.8506	0.8783	1.9673	6.176	41.999	43.922	65.76	269.51	1.347	0.882	2.022	-0.404
0.625	0.8727	0.8982	1.9515	5.329	40.742	45.514	72.25	246.42	1.362	0.676	2.112	-0.443
0.650	0.8935	0.9170	1.9317	4.309	39.274	47.217	78.02	214.40	1.398	0.485	2.149	-0.455
0.675	0.9130	0.9345	1.9079	3.135	37.585	48.977	82.92	180.67	1.449	0.296	2.167	-0.438
0.700	0.9311	0.9509	1.8804	1.829	35.686	50.762	87.03	148.79	1.507	0.127	2.157	-0.406
0.725	0.9479	0.9658	1.8493	0.386	33.582	52.524	90.37	119.05	1.571	-0.017	2.120	-0.369
0.750	0.9634	0.9794	1.8150	-1.201	31.285	54.229	92.98	89.38	1.639	-0.114	2.059	-0.334
0.775	0.9776	0.9914	1.7777	-2.924	28.800	55.858	94.85	59.12	1.708	-0.165	1.986	-0.306
0.800	0.9906	1.0020	1.7376	-4.713	26.122	57.394	95.92	27.47	1.777	-0.176	1.903	-0.280
0.825	1.0025	1.0112	1.6950	-6.448	23.236	58.789	96.23	-4.62	1.846	-0.161	1.816	-0.255
0.850	1.0134	1.0192	1.6500	-8.039	20.101	59.948	95.69	-35.79	1.916	-0.137	1.731	-0.225
0.875	1.0237	1.0261	1.6029	-9.413	16.690	60.817	94.43	-66.08	1.984	-0.110	1.654	-0.201
0.900	1.0334	1.0318	1.5537	-10.547	12.961	61.364	92.41	-95.66	2.050	-0.069	1.600	-0.178
0.925	1.0427	1.0366	1.5028	-11.369	8.911	61.636	89.64	-126.51	2.111	-0.006	1.563	-0.156
0.950	1.0518	1.0406	1.4502	-11.843	4.560	61.707	86.11	-157.28	2.165	0.089	1.536	-0.134
0.975	1.0608	1.0442	1.3963	-11.870	-0.015	61.716	81.78	-186.12	2.212	0.207	1.493	-0.125
1.000	1.0696	1.0477	1.3411	-11.468	-4.785	61.737	76.82	-210.95	2.258	0.330	1.420	-0.124
1.025	1.0787	1.0515	1.2848	-10.659	-9.720	61.844	71.27	-230.90	2.310	0.443	1.315	-0.123
1.050	1.0883	1.0561	1.2272	-9.559	-14.842	62.050	65.30	-247.44	2.371	0.537	1.194	-0.107

time	x	y	z	ϕ	θ	ψ	V	α	$\dot{\alpha}$	C_L	C_D	C_m
(s)	(m)	(m)	(m)	(deg)	(deg)	(deg)	(m/s)	(deg)	(deg/s)			
1.075	1.0987	1.0615	1.1682	-8.211	-20.127	62.395	58.97	-259.17	2.439	0.608	1.062	-0.075
1.100	1.1099	1.0682	1.1077	-6.709	-25.526	62.896	52.36	-265.25	2.516	0.650	0.917	-0.035
1.125	1.1222	1.0766	1.0454	-5.079	-30.964	63.614	45.74	-264.78	2.608	0.650	0.760	-0.003
1.150	1.1353	1.0868	0.9811	-3.445	-36.413	64.551	39.17	-259.55	2.719	0.620	0.603	0.027
1.175	1.1492	1.0991	0.9142	-1.870	-41.828	65.732	32.81	-251.57	2.847	0.568	0.459	0.055
1.200	1.1641	1.1135	0.8445	-0.453	-47.163	67.107	26.65	-239.87	2.993	0.503	0.334	0.085
1.225	1.1797	1.1302	0.7713	0.748	-52.323	68.638	20.84	-222.95	3.159	0.427	0.233	0.108
1.250	1.1960	1.1491	0.6943	1.661	-57.199	70.199	15.54	-198.52	3.341	0.342	0.159	0.125
1.275	1.2128	1.1702	0.6130	2.226	-61.665	71.672	10.93	-168.42	3.535	0.261	0.111	0.140
1.300	1.2299	1.1931	0.5271	2.452	-65.570	72.944	7.15	-135.91	3.736	0.193	0.083	0.151
1.325	1.2475	1.2176	0.4357	2.421	-68.755	73.954	4.18	-102.11	3.936	0.148	0.120	0.151
1.350	1.2653	1.2431	0.3401	2.252	-71.200	74.692	2.06	-65.42	4.116	0.106	0.127	0.156
1.375	1.2833	1.2694	0.2401	2.007	-72.772	75.090	0.90	-26.14	4.289	0.070	0.133	0.161

The trajectory and determined quantities tabulated for flight F of the balsa glider with an aspect ratio of 6.07 which is labeled as the 'gentler' flight in Fig. 5.10 and shown in Fig. 6.24 and 6.25.

Test Conditions				
aircraft	balsa glider	flight	F	
aspect ratio	6.07	test number	6056	
m (g)	5.91	I_{xx} (g·cm^2)	126.21	
I_{yy} (g·cm^2)	280.69	I_{zz} (g·cm^2)	401.99	
I_{xz} (g·cm^2)	7.42	I_{xy} (g·cm^2)	0.27	
I_{yz} (g·cm^2)	-0.10	δ_e (deg)	0	
CG (%c)	76.5			

time	x	y	z	ϕ	θ	ψ	V	α	$\dot{\alpha}$	C_L	C_D	C_m
(s)	(m)	(m)	(m)	(deg)	(deg)	(deg)	(m/s)	(deg)	(deg/s)			
0.000	0.4466	-0.0982	1.2753	-15.340	15.188	17.785	6.96	26.25	4.596	0.716	0.149	0.003
0.025	0.5592	-0.0866	1.2864	-14.502	17.328	16.994	7.38	24.09	4.488	0.739	0.155	-0.005
0.050	0.6688	-0.0774	1.3008	-13.681	19.407	16.028	7.84	16.68	4.374	0.762	0.161	-0.014
0.075	0.7752	-0.0704	1.3181	-12.898	21.357	14.904	8.24	15.65	4.254	0.785	0.165	-0.018
0.100	0.8782	-0.0653	1.3379	-12.220	23.197	13.696	8.63	15.51	4.130	0.807	0.172	-0.016
0.125	0.9775	-0.0622	1.3600	-11.668	24.965	12.460	9.02	16.25	4.000	0.831	0.182	-0.018
0.150	1.0731	-0.0610	1.3838	-11.176	26.685	11.176	9.46	18.16	3.862	0.854	0.195	-0.028
0.175	1.1646	-0.0615	1.4089	-10.663	28.286	9.800	9.94	21.26	3.719	0.872	0.206	-0.046
0.200	1.2522	-0.0636	1.4349	-10.074	29.694	8.311	10.52	24.84	3.573	0.881	0.217	-0.068
0.225	1.3358	-0.0672	1.4611	-9.416	30.825	6.740	11.19	28.10	3.427	0.880	0.227	-0.088
0.250	1.4156	-0.0717	1.4869	-8.708	31.638	5.152	11.93	30.96	3.281	0.875	0.240	-0.099
0.275	1.4918	-0.0772	1.5119	-7.984	32.127	3.581	12.74	34.65	3.137	0.869	0.254	-0.101
0.300	1.5647	-0.0833	1.5353	-7.244	32.329	2.050	13.66	39.85	2.996	0.866	0.272	-0.097
0.325	1.6344	-0.0899	1.5569	-6.468	32.297	0.558	14.74	46.08	2.860	0.870	0.292	-0.089
0.350	1.7013	-0.0969	1.5763	-5.604	32.083	-0.875	15.99	53.14	2.730	0.882	0.315	-0.080
0.375	1.7655	-0.1040	1.5932	-4.652	31.733	-2.253	17.41	61.66	2.606	0.900	0.342	-0.070
0.400	1.8272	-0.1113	1.6074	-3.639	31.296	-3.545	19.07	71.76	2.490	0.920	0.374	-0.060
0.425	1.8867	-0.1188	1.6188	-2.662	30.808	-4.744	21.00	82.12	2.384	0.944	0.416	-0.054
0.450	1.9440	-0.1263	1.6273	-1.756	30.276	-5.824	23.18	91.37	2.286	0.972	0.473	-0.056
0.475	1.9993	-0.1337	1.6327	-0.901	29.690	-6.783	25.57	99.88	2.196	1.002	0.544	-0.064
0.500	2.0526	-0.1410	1.6350	0.013	29.035	-7.633	28.15	108.39	2.114	1.023	0.625	-0.075

time	x	y	z	ϕ	θ	ψ	V	α	$\dot{\alpha}$	C_L	C_D	C_m
(s)	(m)	(m)	(m)	(deg)	(deg)	(deg)	(m/s)	(deg)	(deg/s)			
0.525	2.1041	-0.1480	1.6341	1.030	28.298	-8.415	30.96	116.12	2.042	1.038	0.707	-0.088
0.550	2.1538	-0.1547	1.6300	2.110	27.475	-9.120	33.95	120.75	1.982	1.046	0.785	-0.104
0.575	2.2018	-0.1611	1.6226	3.122	26.541	-9.700	36.99	120.85	1.936	1.052	0.861	-0.119
0.600	2.2481	-0.1673	1.6121	3.978	25.470	-10.098	39.96	117.40	1.903	1.045	0.929	-0.137
0.625	2.2930	-0.1733	1.5984	4.647	24.223	-10.297	42.81	111.17	1.884	1.024	0.992	-0.152
0.650	2.3365	-0.1790	1.5815	5.183	22.774	-10.318	45.50	101.93	1.878	0.987	1.055	-0.153
0.675	2.3786	-0.1843	1.5615	5.601	21.120	-10.183	47.90	89.19	1.882	0.955	1.109	-0.141
0.700	2.4194	-0.1892	1.5385	5.876	19.285	-9.906	49.93	73.74	1.895	0.923	1.159	-0.129
0.725	2.4590	-0.1938	1.5127	5.960	17.285	-9.484	51.56	56.87	1.914	0.898	1.185	-0.129
0.750	2.4975	-0.1982	1.4841	5.796	15.124	-8.904	52.76	38.69	1.943	0.868	1.190	-0.145
0.775	2.5350	-0.2022	1.4529	5.385	12.774	-8.175	53.49	18.83	1.980	0.845	1.183	-0.156
0.800	2.5716	-0.2059	1.4192	4.747	10.231	-7.320	53.70	-2.33	2.021	0.824	1.171	-0.162
0.825	2.6074	-0.2092	1.3832	3.945	7.479	-6.377	53.38	-23.56	2.066	0.815	1.151	-0.150
0.850	2.6426	-0.2122	1.3449	2.970	4.549	-5.407	52.53	-43.25	2.113	0.804	1.110	-0.131
0.875	2.6774	-0.2151	1.3046	1.821	1.473	-4.491	51.22	-60.58	2.167	0.794	1.048	-0.112
0.900	2.7120	-0.2178	1.2622	0.474	-1.717	-3.665	49.50	-76.14	2.229	0.775	0.979	-0.101
0.925	2.7465	-0.2203	1.2178	-1.006	-5.036	-2.955	47.42	-91.77	2.296	0.761	0.914	-0.087
0.950	2.7813	-0.2226	1.1713	-2.541	-8.486	-2.384	44.94	-108.11	2.365	0.754	0.852	-0.062
0.975	2.8164	-0.2247	1.1229	-4.018	-12.058	-1.974	42.03	-123.42	2.437	0.755	0.783	-0.022
1.000	2.8521	-0.2268	1.0726	-5.396	-15.682	-1.725	38.79	-134.12	2.515	0.750	0.700	0.014
1.025	2.8887	-0.2290	1.0204	-6.660	-19.292	-1.622	35.34	-138.91	2.603	0.732	0.610	0.037
1.050	2.9264	-0.2316	0.9662	-7.796	-22.839	-1.664	31.88	-138.98	2.700	0.697	0.523	0.045
1.075	2.9654	-0.2344	0.9098	-8.751	-26.316	-1.839	28.43	-136.01	2.805	0.656	0.446	0.053
1.100	3.0060	-0.2374	0.8511	-9.474	-29.690	-2.113	25.09	-131.11	2.919	0.614	0.376	0.059
1.125	3.0481	-0.2406	0.7900	-9.928	-32.909	-2.433	21.89	-124.68	3.041	0.573	0.314	0.055
1.150	3.0921	-0.2441	0.7262	-10.098	-35.949	-2.736	18.86	-118.32	3.171	0.530	0.263	0.042
1.175	3.1379	-0.2479	0.6598	-10.009	-38.855	-3.010	15.98	-112.83	3.306	0.487	0.222	0.034
1.200	3.1857	-0.2520	0.5905	-9.688	-41.672	-3.269	13.23	-107.87	3.446	0.449	0.187	0.044
1.225	3.2356	-0.2562	0.5182	-9.210	-44.351	-3.545	10.62	-100.46	3.592	0.418	0.155	0.069
1.250	3.2876	-0.2607	0.4430	-8.636	-46.747	-3.853	8.23	-87.53	3.744	0.390	0.129	0.096
1.275	3.3420	-0.2654	0.3646	-8.016	-48.685	-4.208	6.28	-67.93	3.899	0.362	0.114	0.118
1.300	3.3986	-0.2704	0.2831	-7.403	-50.035	-4.630	4.90	-41.83	4.056	0.338	0.097	0.136
1.325	3.4577	-0.2758	0.1984	-6.857	-50.644	-5.132	4.24	-9.33	4.217	0.316	0.081	0.152

The trajectory and determined quantities tabulated for flight G of the balsa glider with an aspect ratio of 6.07 which is shown in Fig. 6.26 and 6.27.

Test Conditions						
aircraft	balsa glider	flight	G			
aspect ratio	6.07	test number	6012			
m (g)	6.75	I_{xx} (g·cm^2)	126.40			
I_{yy} (g·cm^2)	315.61	I_{zz} (g·cm^2)	436.72			
I_{xz} (g·cm^2)	10.00	I_{xy} (g·cm^2)	0.27			
I_{yz} (g·cm^2)	-0.10	δ_e (deg)	0			
CG (%c)	52.9					

time	x	y	z	ϕ	θ	ψ	V	α	$\dot{\alpha}$	C_L	C_D	C_m
(s)	(m)	(m)	(m)	(deg)	(deg)	(deg)	(m/s)	(deg)	(deg/s)			
0.000	0.3793	-0.4095	1.6858	-12.643	6.382	17.629	7.07	1.87	3.956	0.681	0.145	-0.025
0.025	0.4761	-0.3920	1.6815	-12.340	6.203	16.716	7.09	-0.14	3.915	0.683	0.141	-0.021
0.050	0.5721	-0.3758	1.6771	-12.094	5.939	15.808	7.07	-1.09	3.878	0.684	0.137	-0.017
0.075	0.6674	-0.3607	1.6724	-11.901	5.609	14.906	7.05	-0.99	3.844	0.684	0.134	-0.012
0.100	0.7620	-0.3468	1.6674	-11.742	5.222	14.004	7.02	0.34	3.812	0.681	0.130	-0.006
0.125	0.8559	-0.3339	1.6619	-11.667	4.836	13.119	7.07	2.12	3.785	0.679	0.128	-0.004
0.150	0.9493	-0.3220	1.6558	-11.631	4.445	12.230	7.13	4.00	3.758	0.677	0.127	-0.006
0.175	1.0421	-0.3111	1.6491	-11.610	4.031	11.356	7.25	5.28	3.734	0.676	0.125	-0.007
0.200	1.1344	-0.3011	1.6416	-11.594	3.588	10.516	7.40	5.30	3.716	0.678	0.124	-0.004
0.225	1.2263	-0.2919	1.6333	-11.605	3.131	9.718	7.52	3.42	3.699	0.688	0.128	0.002
0.250	1.3178	-0.2836	1.6242	-11.668	2.694	8.958	7.57	1.44	3.683	0.702	0.135	0.005
0.275	1.4088	-0.2764	1.6145	-11.766	2.288	8.222	7.58	0.91	3.665	0.714	0.144	0.003
0.300	1.4995	-0.2703	1.6042	-11.855	1.901	7.490	7.61	1.45	3.647	0.720	0.147	-0.003
0.325	1.5897	-0.2651	1.5933	-11.897	1.497	6.759	7.66	1.37	3.630	0.724	0.147	-0.008
0.350	1.6794	-0.2608	1.5818	-11.876	1.060	6.045	7.69	0.26	3.617	0.725	0.141	-0.011
0.375	1.7689	-0.2576	1.5696	-11.799	0.582	5.361	7.68	-0.29	3.609	0.721	0.135	-0.013
0.400	1.8581	-0.2553	1.5567	-11.686	0.062	4.718	7.67	0.47	3.606	0.709	0.133	-0.014
0.425	1.9472	-0.2539	1.5429	-11.585	-0.509	4.101	7.70	1.65	3.603	0.695	0.134	-0.011
0.450	2.0361	-0.2534	1.5283	-11.536	-1.124	3.489	7.76	2.02	3.603	0.684	0.137	-0.006
0.475	2.1248	-0.2538	1.5125	-11.538	-1.768	2.865	7.80	1.85	3.604	0.679	0.138	0.000
0.500	2.2134	-0.2548	1.4958	-11.555	-2.414	2.226	7.84	1.93	3.608	0.678	0.138	0.005

time	x	y	z	ϕ	θ	ψ	V	α	$\dot{\alpha}$	C_L	C_D	C_m
(s)	(m)	(m)	(m)	(deg)	(deg)	(deg)	(m/s)	(deg)	(deg/s)			
0.525	2.3019	-0.2565	1.4780	-11.546	-3.032	1.596	7.89	1.72	3.615	0.681	0.138	0.008
0.550	2.3904	-0.2590	1.4593	-11.499	-3.610	1.004	7.93	0.59	3.625	0.687	0.139	0.009
0.575	2.4789	-0.2623	1.4396	-11.418	-4.136	0.470	7.92	-0.84	3.636	0.695	0.141	0.009
0.600	2.5676	-0.2666	1.4191	-11.313	-4.610	-0.017	7.88	-1.27	3.648	0.699	0.143	0.006
0.625	2.6563	-0.2717	1.3979	-11.177	-5.046	-0.494	7.85	-1.00	3.660	0.698	0.145	-0.001
0.650	2.7451	-0.2775	1.3760	-10.975	-5.494	-0.983	7.83	-2.19	3.673	0.697	0.145	-0.008
0.675	2.8341	-0.2841	1.3534	-10.692	-5.975	-1.470	7.75	-5.65	3.688	0.698	0.142	-0.010
0.700	2.9232	-0.2914	1.3302	-10.371	-6.505	-1.945	7.55	-9.84	3.705	0.701	0.136	-0.004
0.725	3.0127	-0.2994	1.3064	-10.095	-7.044	-2.399	7.27	-11.57	3.726	0.697	0.126	0.002
0.750	3.1025	-0.3084	1.2822	-9.935	-7.560	-2.884	6.97	-9.49	3.752	0.680	0.120	0.002
0.775	3.1928	-0.3183	1.2574	-9.876	-8.057	-3.416	6.80	-4.81	3.780	0.650	0.124	-0.005
0.800	3.2835	-0.3290	1.2317	-9.846	-8.594	-3.968	6.73	-1.22	3.805	0.624	0.133	-0.007
0.825	3.3743	-0.3403	1.2051	-9.779	-9.188	-4.484	6.73	-1.90	3.824	0.617	0.140	0.002
0.850	3.4654	-0.3521	1.1776	-9.689	-9.784	-4.948	6.64	-6.20	3.844	0.633	0.134	0.023
0.875	3.5568	-0.3645	1.1493	-9.671	-10.262	-5.399	6.41	-10.61	3.874	0.660	0.125	0.037
0.900	3.6489	-0.3777	1.1206	-9.757	-10.558	-5.883	6.11	-11.71	3.908	0.686	0.121	0.041
0.925	3.7416	-0.3918	1.0918	-9.868	-10.626	-6.375	5.84	-9.47	3.939	0.698	0.122	0.030
0.950	3.8349	-0.4070	1.0633	-9.889	-10.528	-6.832	5.66	-4.98	3.963	0.692	0.124	0.011
0.975	3.9288	-0.4230	1.0349	-9.818	-10.380	-7.239	5.58	0.13	3.986	0.671	0.118	-0.003
1.000	4.0232	-0.4398	1.0066	-9.749	-10.278	-7.636	5.64	2.81	4.012	0.647	0.106	-0.008
1.025	4.1182	-0.4575	0.9780	-9.780	-10.253	-8.061	5.74	1.68	4.044	0.635	0.090	0.000
1.050	4.2140	-0.4761	0.9492	-9.892	-10.251	-8.569	5.73	-0.86	4.086	0.629	0.085	0.012
1.075	4.3106	-0.4956	0.9202	-10.017	-10.190	-9.187	5.68	-0.32	4.129	0.623	0.095	0.014
1.100	4.4079	-0.5160	0.8911	-10.070	-10.073	-9.911	5.71	3.87	4.160	0.611	0.121	0.009
1.125	4.5057	-0.5372	0.8620	-10.075	-9.936	-10.673	5.87	6.78	4.170	0.606	0.152	0.011
1.150	4.6034	-0.5591	0.8330	-10.171	-9.729	-11.262	6.09	7.18	4.165	0.616	0.164	0.022
1.175	4.7008	-0.5819	0.8041	-10.391	-9.364	-11.558	6.22	7.58	4.173	0.631	0.153	0.032
1.200	4.7985	-0.6054	0.7756	-10.643	-8.809	-11.685	6.46	11.78	4.179	0.643	0.151	0.042
1.225	4.8962	-0.6298	0.7475	-10.969	-7.980	-11.519	6.85	18.76	4.185	0.654	0.148	0.052

149

The trajectory and determined quantities tabulated for the 14 regression flights of the balsa glider with an aspect ratio of 6.07. The tables include the specific test conditions and a time history of the important parameters for each of the 14 flights.

Test Conditions			
aircraft	balsa glider	flight	regression 1
aspect ratio	6.07	test number	6054
m (g)	5.91	I_{xx} (g·cm^2)	126.21
I_{yy} (g·cm^2)	280.69	I_{zz} (g·cm^2)	401.99
I_{xz} (g·cm^2)	7.42	I_{xy} (g·cm^2)	0.27
I_{yz} (g·cm^2)	-0.10	δ_e (deg)	0.0
CG (%c)	76.5		

time	x	y	z	ϕ	θ	ψ	V	α	$\dot{\alpha}$	C_L	C_D	C_m
(s)	(m)	(m)	(m)	(deg)	(deg)	(deg)	(m/s)	(deg)	(deg/s)			
0.000	0.4139	-0.0611	1.0511	-4.922	11.243	26.305	5.32	6.60	5.483	0.589	0.105	-0.003
0.025	0.5409	-0.0151	1.0664	-4.593	13.664	26.076	5.51	7.67	5.376	0.598	0.102	-0.003
0.050	0.6647	0.0294	1.0866	-4.375	16.053	25.860	5.70	8.13	5.264	0.609	0.101	-0.004
0.075	0.7853	0.0721	1.1113	-4.248	18.408	25.657	5.90	7.99	5.146	0.622	0.101	-0.005
0.100	0.9023	0.1131	1.1400	-4.181	20.723	25.460	6.10	7.07	5.021	0.638	0.105	-0.006
0.125	1.0155	0.1522	1.1724	-4.189	22.996	25.298	6.26	6.11	4.888	0.657	0.109	-0.006
0.150	1.1245	0.1891	1.2081	-4.229	25.222	25.161	6.40	5.56	4.746	0.677	0.114	-0.008
0.175	1.2293	0.2239	1.2467	-4.271	27.385	25.011	6.54	5.62	4.598	0.697	0.119	-0.009
0.200	1.3297	0.2564	1.2876	-4.326	29.481	24.850	6.69	6.34	4.443	0.718	0.123	-0.010
0.225	1.4255	0.2867	1.3304	-4.390	31.509	24.683	6.87	8.27	4.283	0.737	0.127	-0.012
0.250	1.5167	0.3148	1.3745	-4.444	33.470	24.538	7.11	11.29	4.119	0.757	0.132	-0.013
0.275	1.6034	0.3406	1.4194	-4.464	35.362	24.418	7.44	14.69	3.952	0.777	0.140	-0.016
0.300	1.6856	0.3644	1.4646	-4.448	37.176	24.309	7.85	18.19	3.780	0.801	0.151	-0.020
0.325	1.7634	0.3860	1.5095	-4.394	38.902	24.162	8.36	22.47	3.603	0.825	0.165	-0.027
0.350	1.8369	0.4057	1.5536	-4.287	40.515	23.932	8.98	28.65	3.423	0.847	0.181	-0.038
0.375	1.9062	0.4235	1.5965	-4.079	41.977	23.573	9.79	36.82	3.240	0.864	0.200	-0.053
0.400	1.9715	0.4396	1.6376	-3.731	43.244	23.073	10.83	46.08	3.057	0.881	0.226	-0.070
0.425	2.0331	0.4542	1.6763	-3.231	44.284	22.434	12.11	55.53	2.872	0.902	0.258	-0.082
0.450	2.0911	0.4675	1.7123	-2.600	45.096	21.662	13.62	65.12	2.688	0.935	0.292	-0.088
0.475	2.1459	0.4797	1.7451	-1.856	45.710	20.771	15.38	76.07	2.508	0.979	0.331	-0.091

time	x	y	z	ϕ	θ	ψ	V	α	$\dot{\alpha}$	C_L	C_D	C_m
(s)	(m)	(m)	(m)	(deg)	(deg)	(deg)	(m/s)	(deg)	(deg/s)			
0.500	2.1977	0.4909	1.7746	-1.003	46.153	19.746	17.44	89.79	2.335	1.033	0.382	-0.092
0.525	2.2467	0.5013	1.8005	-0.028	46.470	18.570	19.90	107.96	2.168	1.092	0.456	-0.094
0.550	2.2931	0.5108	1.8227	1.056	46.688	17.230	22.86	130.42	2.006	1.154	0.559	-0.100
0.575	2.3370	0.5196	1.8409	2.252	46.842	15.753	26.46	156.79	1.854	1.218	0.698	-0.111
0.600	2.3786	0.5279	1.8550	3.526	46.947	14.221	30.74	187.01	1.711	1.280	0.878	-0.127
0.625	2.4179	0.5356	1.8648	4.870	47.017	12.741	35.81	220.16	1.583	1.317	1.083	-0.169
0.650	2.4550	0.5431	1.8702	6.246	47.005	11.319	41.74	253.82	1.474	1.324	1.314	-0.210
0.675	2.4901	0.5503	1.8712	7.611	46.909	10.008	48.47	283.95	1.391	1.267	1.523	-0.269
0.700	2.5233	0.5575	1.8676	8.892	46.676	8.806	55.86	307.03	1.341	1.135	1.728	-0.289
0.725	2.5547	0.5646	1.8596	10.030	46.304	7.857	63.70	317.51	1.316	0.930	1.896	-0.322
0.750	2.5844	0.5715	1.8471	10.972	45.735	7.230	71.63	308.56	1.321	0.682	1.972	-0.376
0.775	2.6123	0.5784	1.8301	11.716	44.910	6.936	79.06	278.84	1.354	0.443	1.973	-0.422
0.800	2.6386	0.5851	1.8087	12.240	43.764	6.937	85.49	236.24	1.410	0.235	1.951	-0.417
0.825	2.6631	0.5917	1.7831	12.509	42.277	7.295	90.76	188.95	1.480	0.059	1.916	-0.400
0.850	2.6859	0.5980	1.7534	12.453	40.412	8.046	94.93	141.00	1.556	-0.091	1.888	-0.389
0.875	2.7068	0.6041	1.7199	12.019	38.178	9.245	97.86	95.40	1.637	-0.185	1.841	-0.406
0.900	2.7257	0.6099	1.6829	11.147	35.558	10.788	99.69	56.53	1.719	-0.267	1.814	-0.396
0.925	2.7426	0.6154	1.6427	9.797	32.591	12.604	100.69	25.21	1.796	-0.325	1.796	-0.384
0.950	2.7573	0.6207	1.5997	7.929	29.332	14.625	101.00	-3.79	1.867	-0.346	1.775	-0.387
0.975	2.7698	0.6259	1.5541	5.577	25.813	16.778	100.55	-32.97	1.934	-0.324	1.756	-0.380
1.000	2.7802	0.6309	1.5065	2.795	22.090	18.967	99.35	-60.13	1.994	-0.270	1.740	-0.358
1.025	2.7890	0.6356	1.4571	-0.326	18.181	21.049	97.52	-84.90	2.045	-0.212	1.716	-0.326
1.050	2.7962	0.6400	1.4061	-3.690	14.063	22.898	95.12	-110.55	2.093	-0.143	1.674	-0.292
1.075	2.8023	0.6442	1.3538	-7.200	9.688	24.469	92.02	-138.32	2.142	-0.069	1.624	-0.229
1.100	2.8075	0.6482	1.3002	-10.726	5.016	25.678	88.17	-166.85	2.189	0.009	1.585	-0.127
1.125	2.8123	0.6520	1.2455	-14.050	0.055	26.439	83.65	-195.77	2.229	0.092	1.547	-0.015
1.150	2.8171	0.6552	1.1898	-16.968	-5.124	26.705	78.41	-226.89	2.266	0.203	1.472	0.054
1.175	2.8223	0.6578	1.1330	-19.308	-10.473	26.500	72.36	-257.87	2.311	0.330	1.342	0.068
1.200	2.8284	0.6600	1.0749	-21.001	-15.976	25.923	65.55	-282.28	2.374	0.449	1.178	0.045
1.225	2.8358	0.6622	1.0152	-22.033	-21.618	25.138	58.30	-294.38	2.452	0.533	1.012	0.021
1.250	2.8447	0.6645	0.9535	-22.425	-27.331	24.336	50.91	-292.96	2.542	0.581	0.859	0.011
1.275	2.8554	0.6671	0.8897	-22.217	-32.998	23.693	43.72	-280.77	2.645	0.596	0.714	0.019
1.300	2.8683	0.6700	0.8234	-21.475	-38.469	23.354	36.94	-261.70	2.761	0.584	0.579	0.039
1.325	2.8833	0.6736	0.7545	-20.319	-43.643	23.384	30.68	-239.73	2.893	0.548	0.458	0.063
1.350	2.9006	0.6780	0.6827	-18.899	-48.446	23.788	24.99	-216.51	3.038	0.496	0.357	0.084
1.375	2.9202	0.6833	0.6076	-17.295	-52.842	24.536	19.87	-191.21	3.195	0.433	0.276	0.100

time	x	y	z	ϕ	θ	ψ	V	α	$\dot{\alpha}$	C_L	C_D	C_m
(s)	(m)	(m)	(m)	(deg)	(deg)	(deg)	(m/s)	(deg)	(deg/s)			
1.400	2.9421	0.6898	0.5290	-15.539	-56.783	25.588	15.40	-164.63	3.363	0.366	0.214	0.112
1.425	2.9659	0.6976	0.4464	-13.651	-60.236	26.903	11.64	-138.84	3.549	0.302	0.191	0.119

aircraft	balsa glider	flight	regression 2
aspect ratio	6.07	test number	6065
m (g)	5.91	I_{xx} (g·cm^2)	126.21
I_{yy} (g·cm^2)	280.69	I_{zz} (g·cm^2)	401.99
I_{xz} (g·cm^2)	7.42	I_{xy} (g·cm^2)	0.27
I_{yz} (g·cm^2)	-0.10	δ_e (deg)	0.0
CG (%c)	76.5		

time	x	y	z	ϕ	θ	ψ	V	α	$\dot{\alpha}$	C_L	C_D	C_m
(s)	(m)	(m)	(m)	(deg)	(deg)	(deg)	(m/s)	(deg)	(deg/s)			
0.000	-0.4704	-0.0979	1.2556	1.230	20.917	45.427	8.17	6.09	4.654	0.801	0.188	-0.011
0.025	-0.3822	-0.0304	1.2835	1.408	23.676	45.154	8.34	8.05	4.495	0.819	0.175	-0.014
0.050	-0.2983	0.0343	1.3152	1.383	26.342	44.985	8.55	9.29	4.338	0.835	0.166	-0.018
0.075	-0.2186	0.0961	1.3499	1.181	28.895	44.922	8.79	9.83	4.181	0.852	0.163	-0.023
0.100	-0.1429	0.1548	1.3870	0.837	31.326	44.959	9.06	9.02	4.020	0.873	0.168	-0.031
0.125	-0.0714	0.2103	1.4259	0.353	33.574	45.110	9.26	9.56	3.852	0.891	0.174	-0.035
0.150	-0.0038	0.2624	1.4659	-0.260	35.653	45.398	9.54	12.83	3.681	0.904	0.183	-0.035
0.175	0.0601	0.3111	1.5062	-0.909	37.570	45.750	9.94	19.29	3.506	0.918	0.198	-0.030
0.200	0.1205	0.3565	1.5462	-1.474	39.399	46.120	10.51	28.37	3.326	0.938	0.218	-0.035
0.225	0.1775	0.3987	1.5852	-1.778	41.120	46.358	11.34	38.02	3.143	0.968	0.243	-0.049
0.250	0.2313	0.4379	1.6227	-1.752	42.692	46.390	12.44	45.58	2.959	1.006	0.272	-0.070
0.275	0.2820	0.4742	1.6582	-1.345	44.026	46.081	13.66	52.49	2.775	1.053	0.306	-0.084
0.300	0.3298	0.5077	1.6915	-0.639	45.139	45.475	15.09	65.59	2.591	1.088	0.339	-0.094
0.325	0.3748	0.5388	1.7220	0.313	46.050	44.595	16.94	88.19	2.410	1.106	0.376	-0.094
0.350	0.4173	0.5678	1.7493	1.375	46.834	43.586	19.52	115.22	2.240	1.103	0.422	-0.103
0.375	0.4576	0.5950	1.7730	2.503	47.492	42.499	22.75	140.14	2.079	1.121	0.501	-0.114
0.400	0.4959	0.6207	1.7928	3.656	48.044	41.369	26.54	162.23	1.926	1.170	0.629	-0.138
0.425	0.5322	0.6449	1.8085	4.852	48.469	40.182	30.85	186.10	1.778	1.237	0.806	-0.160
0.450	0.5665	0.6677	1.8200	6.101	48.781	38.958	35.84	214.42	1.642	1.294	1.018	-0.185
0.475	0.5990	0.6893	1.8271	7.418	48.988	37.703	41.59	245.95	1.523	1.319	1.250	-0.215
0.500	0.6297	0.7097	1.8299	8.762	49.091	36.465	48.13	277.22	1.427	1.290	1.504	-0.259
0.525	0.6586	0.7290	1.8282	10.082	49.073	35.311	55.40	303.84	1.358	1.183	1.755	-0.310
0.550	0.6859	0.7473	1.8220	11.307	48.890	34.342	63.24	320.26	1.317	0.987	1.981	-0.347

time	x	y	z	ϕ	θ	ψ	V	α	$\dot{\alpha}$	C_L	C_D	C_m
(s)	(m)	(m)	(m)	(deg)	(deg)	(deg)	(m/s)	(deg)	(deg/s)			
0.575	0.7115	0.7647	1.8112	12.383	48.492	33.702	71.31	320.90	1.305	0.724	2.135	-0.372
0.600	0.7355	0.7811	1.7960	13.244	47.826	33.468	79.17	302.92	1.322	0.436	2.210	-0.377
0.625	0.7579	0.7965	1.7764	13.850	46.857	33.675	86.36	268.58	1.362	0.173	2.218	-0.370
0.650	0.7785	0.8110	1.7525	14.157	45.574	34.326	92.53	224.37	1.420	-0.040	2.175	-0.376
0.675	0.7973	0.8244	1.7245	14.130	43.963	35.399	97.53	177.27	1.490	-0.213	2.104	-0.401
0.700	0.8143	0.8369	1.6926	13.732	41.994	36.889	101.39	132.36	1.568	-0.344	2.021	-0.433
0.725	0.8294	0.8482	1.6570	12.945	39.643	38.791	104.16	91.29	1.651	-0.441	1.940	-0.458
0.750	0.8425	0.8583	1.6181	11.730	36.902	41.103	105.97	53.37	1.733	-0.496	1.877	-0.476
0.775	0.8535	0.8672	1.5761	10.070	33.809	43.769	106.87	18.31	1.812	-0.513	1.832	-0.502
0.800	0.8626	0.8749	1.5314	7.959	30.392	46.657	106.90	-13.74	1.885	-0.505	1.798	-0.521
0.825	0.8698	0.8812	1.4845	5.431	26.682	49.578	106.19	-42.01	1.951	-0.482	1.770	-0.513
0.850	0.8754	0.8862	1.4356	2.524	22.670	52.330	104.81	-68.42	2.011	-0.447	1.750	-0.456
0.875	0.8796	0.8899	1.3850	-0.713	18.387	54.773	102.79	-94.74	2.063	-0.393	1.733	-0.375
0.900	0.8828	0.8924	1.3331	-4.191	13.846	56.827	100.06	-121.79	2.108	-0.317	1.718	-0.269
0.925	0.8851	0.8939	1.2800	-7.799	9.095	58.452	96.67	-150.95	2.148	-0.222	1.693	-0.167
0.950	0.8871	0.8946	1.2261	-11.356	4.129	59.603	92.51	-183.91	2.184	-0.103	1.652	-0.068
0.975	0.8889	0.8948	1.1712	-14.649	-1.043	60.263	87.49	-220.39	2.219	0.031	1.583	0.007
1.000	0.8909	0.8950	1.1154	-17.447	-6.431	60.462	81.51	-255.43	2.259	0.168	1.477	0.051
1.025	0.8935	0.8954	1.0584	-19.616	-12.010	60.267	74.74	-283.67	2.310	0.296	1.340	0.068
1.050	0.8969	0.8963	1.0001	-21.087	-17.732	59.769	67.40	-301.96	2.374	0.413	1.195	0.067
1.075	0.9015	0.8979	0.9400	-21.874	-23.479	59.142	59.74	-308.26	2.449	0.517	1.056	0.052
1.100	0.9075	0.9006	0.8782	-21.984	-29.127	58.589	52.05	-302.09	2.532	0.591	0.925	0.028
1.125	0.9148	0.9047	0.8143	-21.484	-34.582	58.310	44.68	-286.60	2.623	0.624	0.786	0.006
1.150	0.9236	0.9106	0.7483	-20.459	-39.852	58.402	37.79	-267.16	2.729	0.613	0.639	0.005
1.175	0.9338	0.9187	0.6799	-19.086	-44.952	58.872	31.36	-246.62	2.853	0.562	0.492	0.025
1.200	0.9453	0.9290	0.6085	-17.571	-49.878	59.643	25.45	-224.92	2.998	0.491	0.364	0.062
1.225	0.9578	0.9415	0.5337	-15.997	-54.544	60.738	20.12	-203.30	3.163	0.419	0.272	0.109
1.250	0.9712	0.9563	0.4550	-14.436	-58.819	62.157	15.42	-179.89	3.341	0.374	0.222	0.163
1.275	0.9852	0.9736	0.3725	-13.045	-62.452	63.687	11.15	-150.54	3.508	0.341	0.181	0.201
1.300	0.9999	0.9934	0.2862	-11.950	-65.251	65.189	7.82	-114.23	3.689	0.306	0.143	0.227
1.325	1.0150	1.0158	0.1957	-11.260	-67.042	66.581	5.52	-71.69	3.876	0.275	0.110	0.243

	Test Conditions				
aircraft	balsa glider	flight	regression 3		
aspect ratio	6.07	test number	6066		
m (g)	5.91	I_{xx} (g·cm^2)	126.21		
I_{yy} (g·cm^2)	280.69	I_{zz} (g·cm^2)	401.99		
I_{xz} (g·cm^2)	7.42	I_{xy} (g·cm^2)	0.27		
I_{yz} (g·cm^2)	-0.10	δ_e (deg)	0.0		
CG (%c)	76.5				

time	x	y	z	ϕ	θ	ψ	V	α	$\dot{\alpha}$	C_L	C_D	C_m
(s)	(m)	(m)	(m)	(deg)	(deg)	(deg)	(m/s)	(deg)	(deg/s)			
0.000	0.4394	0.1406	1.1030	-7.556	21.915	29.491	6.08	10.36	4.816	0.665	0.110	-0.012
0.025	0.5457	0.1831	1.1352	-7.883	24.088	29.123	6.28	7.03	4.683	0.676	0.113	-0.010
0.050	0.6484	0.2229	1.1700	-8.353	26.202	28.818	6.45	6.20	4.544	0.692	0.117	-0.010
0.075	0.7474	0.2597	1.2070	-8.936	28.259	28.590	6.62	6.98	4.400	0.709	0.121	-0.010
0.100	0.8427	0.2935	1.2456	-9.575	30.275	28.448	6.80	7.63	4.251	0.729	0.128	-0.013
0.125	0.9342	0.3243	1.2854	-10.180	32.220	28.334	7.00	8.18	4.097	0.753	0.135	-0.015
0.150	1.0219	0.3521	1.3260	-10.673	34.079	28.174	7.23	8.96	3.938	0.780	0.144	-0.016
0.175	1.1057	0.3768	1.3668	-11.022	35.849	27.941	7.46	11.49	3.775	0.808	0.154	-0.017
0.200	1.1858	0.3986	1.4076	-11.262	37.548	27.646	7.80	17.01	3.609	0.829	0.164	-0.027
0.225	1.2620	0.4174	1.4477	-11.419	39.134	27.301	8.32	24.56	3.441	0.843	0.178	-0.042
0.250	1.3346	0.4337	1.4867	-11.519	40.542	26.879	9.04	31.70	3.271	0.854	0.195	-0.059
0.275	1.4038	0.4475	1.5240	-11.568	41.709	26.362	9.93	37.89	3.100	0.869	0.214	-0.072
0.300	1.4696	0.4591	1.5591	-11.574	42.611	25.725	10.95	45.10	2.932	0.886	0.234	-0.078
0.325	1.5323	0.4687	1.5916	-11.512	43.262	24.979	12.19	55.90	2.768	0.906	0.260	-0.078
0.350	1.5922	0.4765	1.6213	-11.324	43.698	24.100	13.76	70.79	2.608	0.931	0.298	-0.079
0.375	1.6494	0.4829	1.6478	-10.933	43.944	23.064	15.76	88.36	2.451	0.970	0.354	-0.081
0.400	1.7039	0.4880	1.6709	-10.290	44.028	21.797	18.21	108.09	2.298	1.022	0.425	-0.091
0.425	1.7560	0.4920	1.6905	-9.383	43.968	20.249	21.17	130.37	2.150	1.081	0.505	-0.116
0.450	1.8056	0.4949	1.7064	-8.209	43.772	18.391	24.72	154.18	2.012	1.133	0.593	-0.162
0.475	1.8529	0.4970	1.7186	-6.768	43.432	16.241	28.87	176.22	1.887	1.176	0.692	-0.219
0.500	1.8982	0.4984	1.7268	-5.038	42.946	13.836	33.53	194.21	1.779	1.206	0.823	-0.269
0.525	1.9415	0.4992	1.7310	-3.036	42.341	11.245	38.56	209.18	1.685	1.216	1.007	-0.306
0.550	1.9828	0.4995	1.7313	-0.780	41.668	8.564	43.94	222.39	1.604	1.189	1.227	-0.339

time	x	y	z	ϕ	θ	ψ	V	α	$\dot{\alpha}$	C_L	C_D	C_m
(s)	(m)	(m)	(m)	(deg)	(deg)	(deg)	(m/s)	(deg)	(deg/s)			
0.575	2.0221	0.4995	1.7275	1.654	40.965	5.902	49.63	232.07	1.538	1.123	1.434	-0.376
0.600	2.0594	0.4994	1.7196	4.167	40.219	3.363	55.50	233.94	1.496	1.021	1.579	-0.411
0.625	2.0948	0.4992	1.7076	6.668	39.380	0.990	61.30	226.47	1.482	0.904	1.664	-0.428
0.650	2.1284	0.4991	1.6915	9.092	38.402	-1.191	66.78	212.33	1.491	0.770	1.722	-0.408
0.675	2.1604	0.4990	1.6715	11.376	37.246	-3.153	71.85	194.73	1.519	0.621	1.777	-0.347
0.700	2.1907	0.4992	1.6476	13.469	35.906	-4.816	76.47	174.47	1.559	0.467	1.807	-0.282
0.725	2.2192	0.4996	1.6201	15.265	34.339	-6.051	80.53	149.10	1.610	0.324	1.799	-0.231
0.750	2.2460	0.5006	1.5890	16.682	32.493	-6.762	83.89	116.87	1.669	0.208	1.753	-0.212
0.775	2.2710	0.5020	1.5545	17.665	30.289	-6.875	86.33	77.65	1.736	0.128	1.693	-0.222
0.800	2.2944	0.5041	1.5169	18.172	27.655	-6.365	87.73	32.20	1.808	0.095	1.634	-0.256
0.825	2.3160	0.5065	1.4762	18.080	24.529	-5.249	87.96	-16.19	1.880	0.107	1.601	-0.305
0.850	2.3362	0.5093	1.4329	17.237	20.916	-3.657	86.96	-61.14	1.949	0.149	1.592	-0.363
0.875	2.3550	0.5124	1.3872	15.533	16.867	-1.769	84.92	-95.91	2.010	0.196	1.601	-0.405
0.900	2.3727	0.5157	1.3397	12.968	12.489	0.183	82.18	-119.73	2.062	0.245	1.605	-0.415
0.925	2.3894	0.5195	1.2906	9.575	7.880	2.014	78.96	-138.81	2.107	0.299	1.586	-0.398
0.950	2.4053	0.5238	1.2402	5.484	3.080	3.568	75.26	-160.37	2.150	0.368	1.538	-0.353
0.975	2.4207	0.5288	1.1886	0.852	-1.928	4.777	70.95	-187.15	2.196	0.457	1.470	-0.261
1.000	2.4361	0.5343	1.1358	-4.075	-7.161	5.537	65.90	-217.64	2.244	0.548	1.387	-0.119
1.025	2.4520	0.5400	1.0821	-9.052	-12.603	5.732	60.09	-247.11	2.294	0.628	1.282	0.047
1.050	2.4689	0.5455	1.0272	-13.838	-18.215	5.226	53.61	-268.90	2.350	0.675	1.129	0.185
1.075	2.4870	0.5505	0.9708	-18.250	-24.004	3.991	46.70	-277.80	2.424	0.672	0.929	0.265
1.100	2.5066	0.5549	0.9126	-22.085	-29.961	2.116	39.79	-273.05	2.524	0.622	0.718	0.278
1.125	2.5279	0.5590	0.8519	-25.176	-36.015	-0.158	33.16	-257.18	2.650	0.549	0.534	0.250
1.150	2.5509	0.5627	0.7881	-27.417	-41.997	-2.547	27.01	-231.78	2.795	0.471	0.395	0.214
1.175	2.5757	0.5661	0.7209	-28.824	-47.657	-4.760	21.59	-199.02	2.952	0.388	0.293	0.183
1.200	2.6023	0.5693	0.6500	-29.466	-52.750	-6.578	17.08	-163.63	3.122	0.308	0.219	0.160
1.225	2.6305	0.5723	0.5749	-29.412	-57.116	-7.846	13.43	-131.35	3.302	0.245	0.167	0.152
1.250	2.6602	0.5752	0.4955	-28.766	-60.627	-8.527	10.52	-103.44	3.489	0.202	0.135	0.150
1.275	2.6914	0.5782	0.4116	-27.650	-63.239	-8.669	8.25	-76.10	3.674	0.174	0.121	0.149
1.300	2.7241	0.5813	0.3234	-26.213	-64.974	-8.376	6.69	-46.17	3.862	0.148	0.104	0.155
1.325	2.7581	0.5845	0.2306	-24.567	-65.754	-7.657	5.93	-14.75	4.052	0.128	0.090	0.160

Test Conditions

aircraft	balsa glider	flight	regression 4
aspect ratio	6.07	test number	6058
m (g)	5.91	I_{xx} (g·cm²)	126.21
I_{yy} (g·cm²)	280.69	I_{zz} (g·cm²)	401.99
I_{xz} (g·cm²)	7.42	I_{xy} (g·cm²)	0.27
I_{yz} (g·cm²)	-0.10	δ_e (deg)	0.0
CG (%c)	76.5		

time	x	y	z	ϕ	θ	ψ	V	α	$\dot{\alpha}$	C_L	C_D	C_m
(s)	(m)	(m)	(m)	(deg)	(deg)	(deg)	(m/s)	(deg)	(deg/s)			
0.000	0.2961	0.2623	1.4236	-4.160	22.743	32.389	7.00	16.45	4.415	0.702	0.133	-0.004
0.025	0.3910	0.3063	1.4534	-3.793	24.637	32.091	7.35	14.63	4.277	0.727	0.138	-0.008
0.050	0.4825	0.3480	1.4850	-3.510	26.481	31.777	7.72	15.71	4.137	0.749	0.141	-0.012
0.075	0.5703	0.3874	1.5179	-3.344	28.253	31.484	8.17	17.59	3.996	0.772	0.146	-0.015
0.100	0.6547	0.4248	1.5518	-3.283	29.950	31.230	8.62	17.45	3.853	0.799	0.155	-0.017
0.125	0.7354	0.4599	1.5862	-3.236	31.570	30.984	9.05	17.85	3.702	0.831	0.170	-0.021
0.150	0.8124	0.4929	1.6209	-3.118	33.101	30.711	9.51	21.04	3.546	0.860	0.187	-0.030
0.175	0.8858	0.5238	1.6555	-2.884	34.519	30.373	10.11	27.05	3.384	0.881	0.203	-0.044
0.200	0.9555	0.5525	1.6893	-2.549	35.770	29.962	10.89	34.53	3.222	0.894	0.221	-0.059
0.225	1.0218	0.5794	1.7218	-2.156	36.820	29.482	11.84	42.36	3.059	0.903	0.240	-0.076
0.250	1.0849	0.6045	1.7527	-1.733	37.629	28.925	13.00	50.29	2.899	0.911	0.262	-0.088
0.275	1.1450	0.6281	1.7813	-1.302	38.186	28.327	14.37	58.46	2.742	0.923	0.291	-0.092
0.300	1.2023	0.6503	1.8073	-0.871	38.513	27.738	15.95	67.92	2.590	0.943	0.328	-0.085
0.325	1.2569	0.6712	1.8304	-0.404	38.662	27.187	17.78	81.10	2.441	0.968	0.377	-0.072
0.350	1.3091	0.6909	1.8503	0.142	38.689	26.651	20.00	98.55	2.298	0.993	0.433	-0.067
0.375	1.3590	0.7096	1.8669	0.804	38.631	26.078	22.72	117.67	2.165	1.016	0.496	-0.082
0.400	1.4068	0.7275	1.8799	1.566	38.473	25.393	25.90	135.14	2.043	1.044	0.571	-0.109
0.425	1.4526	0.7446	1.8891	2.403	38.193	24.581	29.47	149.88	1.934	1.071	0.662	-0.144
0.450	1.4964	0.7613	1.8946	3.279	37.755	23.667	33.37	163.05	1.840	1.092	0.765	-0.164
0.475	1.5384	0.7774	1.8961	4.199	37.156	22.759	37.59	174.39	1.762	1.097	0.892	-0.163
0.500	1.5788	0.7929	1.8937	5.147	36.408	21.931	42.07	182.26	1.702	1.094	1.040	-0.145
0.525	1.6175	0.8078	1.8875	6.093	35.537	21.267	46.68	185.97	1.656	1.077	1.218	-0.124
0.550	1.6545	0.8221	1.8774	6.960	34.557	20.814	51.32	185.53	1.624	1.044	1.397	-0.109

time	x	y	z	ϕ	θ	ψ	V	α	$\dot{\alpha}$	C_L	C_D	C_m
(s)	(m)	(m)	(m)	(deg)	(deg)	(deg)	(m/s)	(deg)	(deg/s)			
0.575	1.6899	0.8357	1.8636	7.704	33.480	20.640	55.93	181.56	1.605	0.978	1.549	-0.123
0.600	1.7235	0.8488	1.8462	8.283	32.277	20.698	60.36	172.76	1.602	0.882	1.655	-0.161
0.625	1.7555	0.8613	1.8254	8.649	30.917	20.939	64.53	158.05	1.614	0.764	1.708	-0.219
0.650	1.7857	0.8734	1.8011	8.709	29.336	21.276	68.22	136.63	1.642	0.652	1.725	-0.249
0.675	1.8143	0.8852	1.7734	8.356	27.498	21.761	71.32	109.35	1.682	0.561	1.734	-0.251
0.700	1.8413	0.8965	1.7426	7.544	25.394	22.474	73.67	79.18	1.727	0.504	1.743	-0.240
0.725	1.8667	0.9073	1.7088	6.271	23.062	23.523	75.27	49.56	1.775	0.467	1.746	-0.247
0.750	1.8907	0.9178	1.6724	4.591	20.534	24.882	76.16	23.60	1.824	0.438	1.737	-0.265
0.775	1.9134	0.9278	1.6335	2.529	17.839	26.438	76.44	0.56	1.875	0.412	1.716	-0.289
0.800	1.9348	0.9376	1.5924	0.165	14.954	27.990	76.19	-22.86	1.925	0.398	1.691	-0.287
0.825	1.9550	0.9471	1.5493	-2.388	11.861	29.372	75.32	-49.32	1.973	0.408	1.652	-0.250
0.850	1.9742	0.9564	1.5044	-5.006	8.529	30.435	73.73	-77.56	2.022	0.437	1.596	-0.181
0.875	1.9926	0.9655	1.4577	-7.599	4.976	31.135	71.43	-104.48	2.073	0.474	1.520	-0.115
0.900	2.0107	0.9744	1.4094	-10.091	1.220	31.498	68.51	-128.65	2.128	0.511	1.431	-0.064
0.925	2.0288	0.9829	1.3595	-12.429	-2.708	31.586	65.02	-150.67	2.185	0.548	1.326	-0.035
0.950	2.0470	0.9912	1.3080	-14.508	-6.821	31.442	61.00	-170.99	2.248	0.584	1.212	-0.017
0.975	2.0656	0.9996	1.2548	-16.231	-11.115	31.087	56.50	-188.51	2.320	0.618	1.088	0.000
1.000	2.0849	1.0081	1.1999	-17.495	-15.569	30.558	51.62	-201.13	2.398	0.651	0.965	0.019
1.025	2.1052	1.0166	1.1431	-18.241	-20.098	29.894	46.48	-207.07	2.485	0.672	0.839	0.027
1.050	2.1268	1.0253	1.0842	-18.443	-24.633	29.159	41.31	-205.61	2.581	0.681	0.717	0.028
1.075	2.1501	1.0342	1.0233	-18.132	-29.069	28.440	36.23	-198.69	2.689	0.663	0.602	0.016
1.100	2.1751	1.0437	0.9601	-17.368	-33.386	27.858	31.39	-189.41	2.806	0.629	0.499	0.008
1.125	2.2019	1.0539	0.8945	-16.240	-37.573	27.491	26.78	-180.10	2.933	0.586	0.406	0.009
1.150	2.2307	1.0649	0.8262	-14.799	-41.645	27.410	22.39	-172.00	3.070	0.544	0.327	0.031
1.175	2.2615	1.0769	0.7550	-13.100	-45.523	27.610	18.21	-163.12	3.218	0.508	0.264	0.064
1.200	2.2944	1.0900	0.6808	-11.185	-49.100	28.106	14.25	-151.62	3.372	0.478	0.212	0.097
1.225	2.3295	1.1044	0.6034	-9.116	-52.250	28.842	10.66	-134.78	3.531	0.447	0.171	0.116
1.250	2.3671	1.1201	0.5229	-7.005	-54.920	29.681	7.53	-112.40	3.698	0.412	0.134	0.128
1.275	2.4071	1.1373	0.4390	-5.005	-57.033	30.381	5.07	-86.59	3.871	0.373	0.106	0.133
1.300	2.4494	1.1560	0.3516	-3.260	-58.511	30.774	3.25	-59.11	4.049	0.340	0.081	0.133
1.325	2.4942	1.1763	0.2606	-1.908	-59.289	30.664	2.13	-29.40	4.233	0.310	0.060	0.132

					Test Conditions						

aircraft	balsa glider	flight	regression 5
aspect ratio	6.07	test number	6067
m (g)	5.91	I_{xx} (g·cm^2)	126.21
I_{yy} (g·cm^2)	280.69	I_{zz} (g·cm^2)	401.99
I_{xz} (g·cm^2)	7.42	I_{xy} (g·cm^2)	0.27
I_{yz} (g·cm^2)	-0.10	δ_e (deg)	0.0
CG (%c)	76.5		

time	x	y	z	ϕ	θ	ψ	V	α	$\dot{\alpha}$	C_L	C_D	C_m
(s)	(m)	(m)	(m)	(deg)	(deg)	(deg)	(m/s)	(deg)	(deg/s)			
0.000	0.0869	-0.3563	1.4460	-14.423	25.483	22.523	8.04	14.52	3.901	0.871	0.079	-0.031
0.025	0.1802	-0.3454	1.4686	-13.988	27.110	21.241	8.46	20.01	3.810	0.856	0.093	-0.040
0.050	0.2709	-0.3369	1.4925	-13.534	28.518	19.727	9.03	25.01	3.709	0.845	0.117	-0.050
0.075	0.3588	-0.3307	1.5171	-13.040	29.688	18.006	9.71	29.53	3.597	0.838	0.151	-0.062
0.100	0.4441	-0.3263	1.5420	-12.499	30.634	16.120	10.49	33.38	3.455	0.844	0.227	-0.082
0.125	0.5253	-0.3238	1.5661	-11.843	31.235	14.043	11.38	37.47	3.313	0.844	0.238	-0.093
0.150	0.6032	-0.3228	1.5893	-11.065	31.528	11.813	12.36	41.54	3.174	0.847	0.250	-0.093
0.175	0.6780	-0.3229	1.6110	-10.210	31.596	9.529	13.46	44.94	3.041	0.855	0.265	-0.096
0.200	0.7499	-0.3241	1.6310	-9.298	31.477	7.249	14.62	47.99	2.911	0.869	0.283	-0.099
0.225	0.8189	-0.3261	1.6490	-8.356	31.184	5.034	15.86	51.51	2.787	0.886	0.308	-0.098
0.250	0.8853	-0.3288	1.6648	-7.362	30.742	2.887	17.21	56.71	2.667	0.906	0.341	-0.090
0.275	0.9492	-0.3321	1.6781	-6.296	30.192	0.802	18.71	64.17	2.552	0.926	0.377	-0.080
0.300	1.0108	-0.3356	1.6888	-5.136	29.592	-1.224	20.42	73.69	2.444	0.945	0.414	-0.078
0.325	1.0701	-0.3394	1.6968	-3.875	28.962	-3.185	22.39	83.40	2.346	0.963	0.456	-0.083
0.350	1.1274	-0.3432	1.7018	-2.518	28.298	-5.067	24.59	91.12	2.259	0.982	0.506	-0.090
0.375	1.1828	-0.3470	1.7039	-1.086	27.592	-6.839	26.94	96.53	2.181	1.006	0.569	-0.093
0.400	1.2364	-0.3507	1.7029	0.380	26.845	-8.467	29.40	101.11	2.112	1.026	0.638	-0.092
0.425	1.2883	-0.3543	1.6989	1.842	26.057	-9.936	31.98	105.88	2.054	1.036	0.709	-0.094
0.450	1.3384	-0.3577	1.6918	3.240	25.218	-11.229	34.69	110.10	2.007	1.031	0.778	-0.106
0.475	1.3870	-0.3609	1.6817	4.527	24.285	-12.313	37.47	111.79	1.973	1.017	0.842	-0.114
0.500	1.4341	-0.3638	1.6683	5.589	23.228	-13.150	40.25	109.53	1.951	0.999	0.896	-0.114
0.525	1.4798	-0.3665	1.6519	6.363	22.016	-13.693	42.92	103.02	1.943	0.980	0.943	-0.110
0.550	1.5243	-0.3689	1.6325	6.735	20.641	-13.931	45.38	93.61	1.946	0.954	0.989	-0.117

time	x	y	z	ϕ	θ	ψ	V	α	$\dot{\alpha}$	C_L	C_D	C_m
(s)	(m)	(m)	(m)	(deg)	(deg)	(deg)	(m/s)	(deg)	(deg/s)			
0.575	1.5675	-0.3711	1.6102	6.726	19.087	-13.889	47.57	82.55	1.958	0.918	1.036	-0.130
0.600	1.6096	-0.3729	1.5850	6.325	17.344	-13.638	49.48	69.49	1.976	0.879	1.076	-0.144
0.625	1.6505	-0.3744	1.5570	5.557	15.401	-13.215	51.03	52.94	2.000	0.848	1.104	-0.152
0.650	1.6904	-0.3756	1.5265	4.359	13.264	-12.670	52.12	32.47	2.030	0.835	1.119	-0.153
0.675	1.7293	-0.3766	1.4935	2.731	10.944	-12.036	52.65	10.63	2.065	0.833	1.130	-0.148
0.700	1.7674	-0.3774	1.4582	0.670	8.478	-11.352	52.63	-9.98	2.102	0.829	1.129	-0.146
0.725	1.8048	-0.3783	1.4209	-1.717	5.856	-10.644	52.15	-28.71	2.140	0.819	1.116	-0.135
0.750	1.8416	-0.3793	1.3816	-4.356	3.089	-9.995	51.20	-47.62	2.183	0.811	1.083	-0.111
0.775	1.8780	-0.3805	1.3404	-7.104	0.176	-9.487	49.78	-67.78	2.230	0.810	1.039	-0.070
0.800	1.9141	-0.3819	1.2975	-9.877	-2.856	-9.200	47.83	-87.35	2.281	0.813	0.977	-0.036
0.825	1.9503	-0.3839	1.2527	-12.571	-6.028	-9.184	45.41	-104.31	2.338	0.804	0.898	-0.013
0.850	1.9866	-0.3864	1.2062	-15.092	-9.363	-9.468	42.64	-117.89	2.405	0.780	0.805	0.005
0.875	2.0234	-0.3897	1.1577	-17.365	-12.899	-10.037	39.56	-128.72	2.482	0.746	0.709	0.032
0.900	2.0607	-0.3937	1.1072	-19.319	-16.588	-10.848	36.25	-135.18	2.568	0.707	0.618	0.054
0.925	2.0988	-0.3986	1.0544	-20.884	-20.355	-11.853	32.81	-135.49	2.664	0.661	0.532	0.057
0.950	2.1378	-0.4044	0.9992	-21.991	-24.124	-12.948	29.48	-131.12	2.768	0.607	0.452	0.043
0.975	2.1778	-0.4111	0.9415	-22.600	-27.869	-14.052	26.29	-126.17	2.882	0.556	0.380	0.030
1.000	2.2189	-0.4187	0.8810	-22.722	-31.561	-15.081	23.20	-123.06	3.005	0.517	0.318	0.031
1.025	2.2614	-0.4271	0.8177	-22.402	-35.130	-15.997	20.14	-119.57	3.136	0.487	0.265	0.045
1.050	2.3052	-0.4365	0.7513	-21.698	-38.459	-16.758	17.21	-113.51	3.275	0.462	0.221	0.058
1.075	2.3507	-0.4469	0.6820	-20.683	-41.469	-17.372	14.48	-105.00	3.419	0.439	0.186	0.068
1.100	2.3980	-0.4585	0.6095	-19.430	-44.116	-17.859	11.99	-95.25	3.568	0.423	0.159	0.081
1.125	2.4473	-0.4711	0.5340	-18.037	-46.351	-18.299	9.74	-83.60	3.720	0.412	0.137	0.097
1.150	2.4988	-0.4849	0.4555	-16.590	-48.074	-18.748	7.83	-68.44	3.875	0.406	0.119	0.110
1.175	2.5527	-0.5001	0.3740	-15.153	-49.203	-19.268	6.35	-49.00	4.031	0.398	0.105	0.117
1.200	2.6091	-0.5168	0.2898	-13.778	-49.692	-19.876	5.41	-25.50	4.188	0.391	0.091	0.124
1.225	2.6683	-0.5349	0.2028	-12.542	-49.455	-20.635	5.11	2.03	4.348	0.382	0.077	0.129

Test Conditions				
aircraft	balsa glider	flight	regression 6	
aspect ratio	6.07	test number	6061	
m (g)	5.91	I_{xx} (g·cm^2)	126.21	
I_{yy} (g·cm^2)	280.69	I_{zz} (g·cm^2)	401.99	
I_{xz} (g·cm^2)	7.42	I_{xy} (g·cm^2)	0.27	
I_{yz} (g·cm^2)	-0.10	δ_e (deg)	0	
CG (%c)	76.5			

time	x	y	z	ϕ	θ	ψ	V	α	$\dot{\alpha}$	C_L	C_D	C_m
(s)	(m)	(m)	(m)	(deg)	(deg)	(deg)	(m/s)	(deg)	(deg/s)			
0.000	0.2831	0.2276	1.4618	-2.637	26.670	30.397	9.55	16.68	3.924	0.807	0.168	-0.016
0.025	0.3655	0.2680	1.4909	-2.745	28.349	30.321	9.89	16.02	3.767	0.829	0.186	-0.032
0.050	0.4443	0.3062	1.5207	-2.779	29.864	30.242	10.33	19.83	3.618	0.837	0.193	-0.046
0.075	0.5196	0.3423	1.5505	-2.654	31.161	30.097	10.93	26.85	3.471	0.836	0.201	-0.054
0.100	0.5916	0.3766	1.5798	-2.335	32.225	29.845	11.68	32.86	3.323	0.837	0.215	-0.058
0.125	0.6605	0.4092	1.6081	-1.876	33.078	29.485	12.58	38.65	3.175	0.842	0.234	-0.064
0.150	0.7265	0.4402	1.6348	-1.349	33.724	29.051	13.61	44.08	3.028	0.854	0.256	-0.071
0.175	0.7895	0.4697	1.6597	-0.805	34.166	28.569	14.79	49.34	2.884	0.870	0.281	-0.080
0.200	0.8499	0.4979	1.6824	-0.226	34.394	28.069	16.09	55.27	2.743	0.889	0.311	-0.085
0.225	0.9078	0.5248	1.7026	0.445	34.411	27.542	17.56	62.99	2.608	0.908	0.347	-0.084
0.250	0.9632	0.5507	1.7200	1.240	34.257	26.971	19.25	73.46	2.478	0.924	0.390	-0.083
0.275	1.0164	0.5755	1.7345	2.185	33.954	26.344	21.23	85.84	2.355	0.938	0.436	-0.080
0.300	1.0674	0.5994	1.7458	3.249	33.535	25.681	23.55	98.73	2.243	0.951	0.486	-0.079
0.325	1.1165	0.6226	1.7537	4.399	33.012	25.034	26.17	110.87	2.144	0.965	0.546	-0.076
0.350	1.1637	0.6451	1.7582	5.552	32.405	24.453	29.08	121.86	2.057	0.977	0.614	-0.078
0.375	1.2091	0.6670	1.7591	6.648	31.698	23.970	32.25	131.23	1.983	0.987	0.696	-0.079
0.400	1.2529	0.6883	1.7564	7.627	30.890	23.629	35.62	138.18	1.922	0.991	0.785	-0.083
0.425	1.2951	0.7092	1.7502	8.453	29.966	23.458	39.13	141.84	1.877	0.988	0.883	-0.085
0.450	1.3356	0.7296	1.7403	9.070	28.917	23.504	42.69	141.68	1.845	0.976	0.983	-0.093
0.475	1.3746	0.7494	1.7270	9.421	27.725	23.782	46.19	137.59	1.824	0.954	1.082	-0.108
0.500	1.4122	0.7687	1.7102	9.468	26.377	24.286	49.53	129.68	1.817	0.921	1.164	-0.129
0.525	1.4483	0.7875	1.6902	9.180	24.858	24.999	52.63	117.81	1.820	0.878	1.235	-0.150
0.550	1.4829	0.8059	1.6669	8.522	23.160	25.923	55.38	100.78	1.835	0.842	1.282	-0.172

time	x	y	z	ϕ	θ	ψ	V	α	$\dot{\alpha}$	C_L	C_D	C_m
(s)	(m)	(m)	(m)	(deg)	(deg)	(deg)	(m/s)	(deg)	(deg/s)			
0.575	1.5161	0.8239	1.6406	7.454	21.279	27.032	57.67	79.23	1.858	0.819	1.326	-0.188
0.600	1.5479	0.8416	1.6115	5.986	19.232	28.326	59.34	56.34	1.888	0.797	1.361	-0.204
0.625	1.5785	0.8590	1.5797	4.138	17.035	29.708	60.47	36.19	1.920	0.769	1.387	-0.210
0.650	1.6079	0.8760	1.5455	1.961	14.708	31.103	61.13	18.82	1.955	0.730	1.399	-0.211
0.675	1.6363	0.8925	1.5090	-0.520	12.251	32.392	61.41	0.18	1.992	0.697	1.381	-0.202
0.700	1.6638	0.9086	1.4703	-3.232	9.654	33.516	61.15	-22.38	2.035	0.680	1.337	-0.192
0.725	1.6905	0.9243	1.4295	-6.075	6.866	34.435	60.27	-48.81	2.084	0.683	1.277	-0.169
0.750	1.7168	0.9396	1.3867	-8.877	3.856	35.144	58.72	-75.87	2.139	0.691	1.216	-0.122
0.775	1.7428	0.9548	1.3419	-11.502	0.619	35.608	56.49	-100.28	2.195	0.702	1.155	-0.062
0.800	1.7688	0.9697	1.2953	-13.836	-2.808	35.814	53.73	-118.51	2.254	0.707	1.085	-0.002
0.825	1.7949	0.9844	1.2469	-15.841	-6.353	35.761	50.59	-129.98	2.318	0.704	1.000	0.029
0.850	1.8215	0.9991	1.1966	-17.454	-9.956	35.515	47.26	-137.29	2.388	0.697	0.905	0.034
0.875	1.8486	1.0137	1.1445	-18.615	-13.604	35.115	43.77	-143.03	2.467	0.695	0.806	0.024
0.900	1.8765	1.0283	1.0903	-19.232	-17.294	34.598	40.13	-147.97	2.554	0.696	0.708	0.008
0.925	1.9056	1.0428	1.0340	-19.250	-21.017	34.025	36.40	-149.94	2.649	0.693	0.617	-0.002
0.950	1.9361	1.0575	0.9757	-18.666	-24.718	33.496	32.64	-147.92	2.752	0.679	0.534	-0.005
0.975	1.9682	1.0725	0.9152	-17.549	-28.319	33.130	29.00	-142.82	2.860	0.652	0.461	-0.004
1.000	2.0018	1.0882	0.8524	-15.995	-31.797	32.997	25.51	-137.52	2.976	0.621	0.393	-0.004
1.025	2.0372	1.1048	0.7874	-14.081	-35.175	33.114	22.13	-135.33	3.098	0.594	0.333	0.004
1.050	2.0744	1.1224	0.7200	-11.831	-38.476	33.486	18.77	-136.20	3.228	0.576	0.282	0.029
1.075	2.1136	1.1412	0.6501	-9.261	-41.635	34.161	15.37	-133.23	3.362	0.565	0.240	0.072
1.100	2.1549	1.1616	0.5779	-6.462	-44.513	35.156	12.07	-122.38	3.499	0.544	0.201	0.114
1.125	2.1986	1.1836	0.5034	-3.649	-46.965	36.312	9.30	-104.60	3.643	0.513	0.164	0.133
1.150	2.2445	1.2075	0.4264	-1.081	-48.918	37.340	6.94	-83.47	3.793	0.490	0.132	0.146
1.175	2.2929	1.2335	0.3468	1.080	-50.237	38.147	5.15	-58.07	3.948	0.466	0.104	0.151

Test Conditions					
aircraft	balsa glider	flight	regression 7		
aspect ratio	6.07	test number	6051		
m (g)	5.91	I_{xx} (g·cm^2)	126.21		
I_{yy} (g·cm^2)	280.69	I_{zz} (g·cm^2)	401.99		
I_{xz} (g·cm^2)	7.42	I_{xy} (g·cm^2)	0.27		
I_{yz} (g·cm^2)	-0.10	δ_e (deg)	0		
CG (%c)	76.5				

time	x	y	z	ϕ	θ	ψ	V	α	$\dot{\alpha}$	C_L	C_D	C_m
(s)	(m)	(m)	(m)	(deg)	(deg)	(deg)	(m/s)	(deg)	(deg/s)			
0.000	0.2978	-0.5342	1.2651	5.950	18.082	-0.993	16.53	22.13	3.100	0.840	0.308	-0.058
0.025	0.3744	-0.5345	1.2664	7.916	18.224	-2.462	17.12	25.13	3.019	0.834	0.319	-0.052
0.050	0.4490	-0.5341	1.2664	9.625	18.309	-3.745	17.80	28.46	2.944	0.831	0.333	-0.059
0.075	0.5217	-0.5331	1.2650	11.020	18.260	-4.794	18.54	30.41	2.873	0.829	0.352	-0.068
0.100	0.5926	-0.5314	1.2620	12.028	17.989	-5.534	19.33	32.11	2.807	0.829	0.371	-0.069
0.125	0.6618	-0.5290	1.2571	12.619	17.454	-5.903	20.15	35.11	2.746	0.829	0.391	-0.060
0.150	0.7293	-0.5260	1.2503	12.731	16.672	-5.894	21.07	39.53	2.694	0.832	0.410	-0.051
0.175	0.7953	-0.5225	1.2414	12.310	15.699	-5.552	22.13	43.92	2.648	0.839	0.432	-0.051
0.200	0.8599	-0.5185	1.2305	11.315	14.570	-4.929	23.26	46.06	2.608	0.851	0.451	-0.061
0.225	0.9231	-0.5140	1.2176	9.751	13.297	-4.033	24.41	45.08	2.576	0.864	0.470	-0.079
0.250	0.9850	-0.5092	1.2027	7.638	11.894	-2.900	25.49	40.71	2.552	0.874	0.486	-0.097
0.275	1.0459	-0.5041	1.1857	5.047	10.380	-1.594	26.43	33.54	2.534	0.879	0.502	-0.109
0.300	1.1057	-0.4988	1.1668	2.069	8.784	-0.221	27.15	24.64	2.522	0.877	0.515	-0.109
0.325	1.1647	-0.4935	1.1460	-1.168	7.134	1.130	27.65	15.03	2.517	0.865	0.523	-0.100
0.350	1.2229	-0.4883	1.1232	-4.545	5.442	2.389	27.90	5.17	2.518	0.845	0.525	-0.093
0.375	1.2804	-0.4832	1.0984	-7.968	3.680	3.515	27.90	-5.90	2.528	0.818	0.520	-0.080
0.400	1.3373	-0.4784	1.0715	-11.340	1.812	4.456	27.62	-17.82	2.546	0.794	0.510	-0.050
0.425	1.3938	-0.4740	1.0425	-14.558	-0.165	5.167	27.01	-29.23	2.572	0.775	0.494	-0.009
0.450	1.4501	-0.4702	1.0112	-17.477	-2.213	5.628	26.16	-37.89	2.606	0.759	0.473	0.024
0.475	1.5063	-0.4672	0.9777	-19.969	-4.290	5.858	25.13	-42.97	2.649	0.744	0.451	0.034
0.500	1.5626	-0.4650	0.9419	-21.942	-6.382	5.895	24.02	-46.05	2.698	0.728	0.428	0.025
0.525	1.6190	-0.4637	0.9039	-23.338	-8.513	5.769	22.86	-48.51	2.755	0.710	0.404	0.005
0.550	1.6758	-0.4633	0.8637	-24.098	-10.738	5.523	21.61	-50.65	2.817	0.691	0.380	-0.012

time	x	y	z	ϕ	θ	ψ	V	α	$\dot{\alpha}$	C_L	C_D	C_m
(s)	(m)	(m)	(m)	(deg)	(deg)	(deg)	(m/s)	(deg)	(deg/s)			
0.575	1.7330	-0.4637	0.8213	-24.179	-13.054	5.225	20.32	-51.35	2.884	0.670	0.356	-0.023
0.600	1.7908	-0.4649	0.7768	-23.545	-15.440	4.939	19.04	-50.88	2.956	0.651	0.333	-0.025
0.625	1.8493	-0.4669	0.7301	-22.219	-17.832	4.727	17.78	-51.02	3.034	0.638	0.312	-0.019
0.650	1.9087	-0.4695	0.6815	-20.260	-20.186	4.637	16.49	-53.46	3.114	0.640	0.294	-0.002
0.675	1.9692	-0.4725	0.6310	-17.778	-22.419	4.691	15.11	-57.41	3.195	0.652	0.276	0.017
0.700	2.0311	-0.4759	0.5790	-14.889	-24.494	4.883	13.62	-59.79	3.278	0.663	0.252	0.038
0.725	2.0946	-0.4796	0.5256	-11.743	-26.339	5.198	12.12	-58.17	3.366	0.659	0.225	0.046
0.750	2.1599	-0.4836	0.4710	-8.485	-27.990	5.592	10.73	-53.25	3.458	0.639	0.199	0.049
0.775	2.2273	-0.4877	0.4152	-5.277	-29.474	6.011	9.49	-47.67	3.554	0.611	0.178	0.053
0.800	2.2969	-0.4915	0.3581	-2.275	-30.797	6.371	8.38	-41.56	3.652	0.584	0.161	0.067
0.825	2.3686	-0.4948	0.2998	0.368	-31.856	6.577	7.41	-33.83	3.751	0.561	0.144	0.079
0.850	2.4425	-0.4976	0.2402	2.503	-32.528	6.533	6.69	-23.63	3.853	0.538	0.128	0.085
0.875	2.5188	-0.4995	0.1793	3.978	-32.766	6.153	6.25	-11.27	3.958	0.517	0.113	0.091

Test Conditions

aircraft	balsa glider	flight	regression 8
aspect ratio	6.07	test number	5943
m (g)	6.51	I_{xx} (g·cm^2)	126.35
I_{yy} (g·cm^2)	306.55	I_{zz} (g·cm^2)	427.71
I_{xz} (g·cm^2)	9.33	I_{xy} (g·cm^2)	0.27
I_{yz} (g·cm^2)	-0.10	δ_e (deg)	0
CG (%c)	58.8		

time	x	y	z	ϕ	θ	ψ	V	α	$\dot{\alpha}$	C_L	C_D	C_m
(s)	(m)	(m)	(m)	(deg)	(deg)	(deg)	(m/s)	(deg)	(deg/s)			
0.000	0.2427	0.1910	1.4188	4.916	9.945	37.314	6.81	10.25	3.914	0.672	0.112	-0.026
0.025	0.3238	0.2443	1.4246	4.747	10.139	37.677	7.04	8.27	3.859	0.679	0.115	-0.023
0.050	0.4033	0.2973	1.4302	4.523	10.230	38.100	7.24	7.31	3.804	0.686	0.119	-0.019
0.075	0.4814	0.3500	1.4355	4.281	10.238	38.572	7.42	7.38	3.749	0.693	0.125	-0.015
0.100	0.5580	0.4024	1.4404	4.052	10.185	39.085	7.62	8.51	3.694	0.699	0.129	-0.011
0.125	0.6333	0.4545	1.4447	3.893	10.088	39.620	7.85	10.76	3.641	0.706	0.140	-0.006
0.150	0.7072	0.5063	1.4484	3.831	9.976	40.166	8.15	13.81	3.584	0.715	0.153	-0.003
0.175	0.7796	0.5576	1.4514	3.892	9.858	40.723	8.54	16.76	3.527	0.727	0.162	-0.004
0.200	0.8507	0.6085	1.4535	4.083	9.733	41.268	8.98	18.26	3.472	0.743	0.168	-0.007
0.225	0.9205	0.6591	1.4547	4.412	9.578	41.787	9.44	17.63	3.422	0.763	0.174	-0.010
0.250	0.9888	0.7094	1.4550	4.867	9.382	42.277	9.86	15.58	3.373	0.787	0.183	-0.013
0.275	1.0558	0.7595	1.4545	5.419	9.135	42.763	10.22	13.76	3.324	0.810	0.198	-0.015
0.300	1.1214	0.8094	1.4533	6.042	8.836	43.229	10.54	13.11	3.274	0.827	0.211	-0.021
0.325	1.1857	0.8590	1.4511	6.724	8.470	43.682	10.87	13.16	3.224	0.837	0.222	-0.033
0.350	1.2485	0.9083	1.4481	7.443	8.005	44.109	11.20	12.45	3.177	0.838	0.224	-0.051
0.375	1.3100	0.9575	1.4439	8.195	7.364	44.551	11.49	9.90	3.136	0.833	0.222	-0.068
0.400	1.3702	1.0066	1.4385	8.957	6.481	45.035	11.68	4.42	3.102	0.828	0.217	-0.074
0.425	1.4293	1.0557	1.4316	9.735	5.333	45.550	11.71	-3.83	3.075	0.828	0.213	-0.066
0.450	1.4872	1.1050	1.4233	10.550	3.953	46.053	11.51	-11.50	3.056	0.832	0.215	-0.043
0.475	1.5440	1.1547	1.4135	11.440	2.430	46.588	11.13	-14.60	3.041	0.825	0.224	-0.023
0.500	1.5996	1.2048	1.4022	12.385	0.814	47.198	10.78	-12.08	3.026	0.806	0.230	-0.011
0.525	1.6539	1.2554	1.3891	13.295	-0.878	47.935	10.53	-8.39	3.014	0.778	0.225	-0.011
0.550	1.7070	1.3065	1.3741	14.024	-2.662	48.740	10.38	-8.08	3.015	0.753	0.211	-0.011

time	x	y	z	ϕ	θ	ψ	V	α	$\dot{\alpha}$	C_L	C_D	C_m
(s)	(m)	(m)	(m)	(deg)	(deg)	(deg)	(m/s)	(deg)	(deg/s)			
0.575	1.7592	1.3581	1.3570	14.466	-4.521	49.536	10.14	-10.57	3.029	0.738	0.193	-0.000
0.600	1.8106	1.4103	1.3378	14.628	-6.408	50.304	9.82	-13.62	3.050	0.734	0.178	0.021
0.625	1.8614	1.4634	1.3165	14.590	-8.245	51.099	9.46	-15.65	3.080	0.736	0.167	0.044
0.650	1.9116	1.5173	1.2931	14.413	-9.973	51.965	9.06	-16.42	3.117	0.753	0.147	0.066
0.675	1.9613	1.5724	1.2679	14.037	-11.438	52.825	8.65	-14.74	3.168	0.751	0.147	0.063
0.700	2.0106	1.6289	1.2410	13.454	-12.662	53.628	8.32	-9.27	3.216	0.744	0.160	0.048
0.725	2.0595	1.6866	1.2124	12.713	-13.678	54.411	8.15	-4.93	3.260	0.722	0.181	0.021
0.750	2.1078	1.7453	1.1823	11.934	-14.647	55.256	8.11	-4.71	3.296	0.714	0.183	0.011
0.775	2.1556	1.8052	1.1507	11.221	-15.618	56.232	7.89	-7.40	3.346	0.711	0.164	0.019
0.800	2.2031	1.8663	1.1176	10.519	-16.471	57.241	7.71	-7.98	3.399	0.701	0.154	0.018
0.825	2.2503	1.9288	1.0832	9.901	-17.254	58.331	7.54	-7.37	3.456	0.690	0.143	0.018
0.850	2.2973	1.9927	1.0474	9.409	-17.967	59.508	7.36	-5.58	3.517	0.679	0.133	0.019

	Test Conditions		
aircraft	balsa glider	flight	regression 9
aspect ratio	6.07	test number	5954
m (g)	6.51	I_{xx} (g·cm^2)	126.35
I_{yy} (g·cm^2)	306.55	I_{zz} (g·cm^2)	427.71
I_{xz} (g·cm^2)	9.33	I_{xy} (g·cm^2)	0.27
I_{yz} (g·cm^2)	-0.10	δ_e (deg)	0
CG (%c)	58.8		

time	x	y	z	ϕ	θ	ψ	V	α	$\dot{\alpha}$	C_L	C_D	C_m
(s)	(m)	(m)	(m)	(deg)	(deg)	(deg)	(m/s)	(deg)	(deg/s)			
0.000	1.7088	1.0937	1.2714	2.173	-10.631	26.654	7.40	-1.44	3.238	0.732	0.147	0.061
0.025	1.7790	1.1257	1.2457	2.098	-11.456	26.557	7.41	1.88	3.278	0.729	0.148	0.051
0.050	1.8498	1.1582	1.2186	1.853	-12.115	26.465	7.48	4.07	3.320	0.726	0.148	0.042
0.075	1.9211	1.1911	1.1903	1.471	-12.638	26.385	7.60	5.14	3.364	0.723	0.147	0.033
0.100	1.9931	1.2244	1.1606	0.974	-13.040	26.314	7.74	4.89	3.409	0.720	0.144	0.021
0.125	2.0657	1.2583	1.1299	0.418	-13.384	26.287	7.84	3.96	3.458	0.712	0.143	0.016
0.150	2.1390	1.2928	1.0982	-0.183	-13.688	26.282	7.93	3.11	3.507	0.707	0.146	0.020
0.175	2.2132	1.3276	1.0655	-0.817	-13.917	26.299	7.99	2.66	3.554	0.706	0.151	0.022
0.200	2.2882	1.3629	1.0319	-1.443	-14.055	26.371	8.05	1.34	3.599	0.711	0.154	0.021
0.225	2.3640	1.3986	0.9978	-2.033	-14.094	26.505	8.07	-1.22	3.642	0.718	0.154	0.014
0.250	2.4408	1.4347	0.9633	-2.567	-14.077	26.659	7.99	-4.38	3.687	0.724	0.149	0.010
0.275	2.5187	1.4711	0.9285	-3.023	-14.017	26.806	7.85	-6.47	3.731	0.724	0.147	0.007
0.300	2.5975	1.5080	0.8936	-3.416	-13.933	26.927	7.66	-7.25	3.774	0.720	0.144	0.005
0.325	2.6775	1.5453	0.8588	-3.754	-13.819	27.028	7.49	-7.95	3.815	0.711	0.142	0.001
0.350	2.7585	1.5830	0.8240	-4.047	-13.709	27.104	7.28	-9.28	3.854	0.702	0.137	-0.001
0.375	2.8405	1.6210	0.7893	-4.299	-13.617	27.142	7.04	-10.15	3.893	0.689	0.131	0.000
0.400	2.9237	1.6594	0.7548	-4.529	-13.550	27.107	6.79	-7.12	3.934	0.668	0.125	0.009
0.425	3.0078	1.6981	0.7204	-4.733	-13.427	26.995	6.67	0.55	3.973	0.639	0.115	0.013
0.450	3.0930	1.7372	0.6858	-4.926	-13.228	26.810	6.79	8.52	4.015	0.612	0.107	0.008
0.475	3.1790	1.7768	0.6509	-5.120	-12.984	26.616	7.08	9.34	4.061	0.600	0.104	-0.000
0.500	3.2661	1.8169	0.6156	-5.338	-12.768	26.431	7.27	0.88	4.109	0.613	0.113	0.001
0.525	3.3542	1.8574	0.5803	-5.584	-12.565	26.274	7.14	-9.51	4.146	0.638	0.126	0.010
0.550	3.4434	1.8979	0.5455	-5.842	-12.313	26.094	6.77	-13.24	4.170	0.657	0.134	0.019

time	x	y	z	ϕ	θ	ψ	V	α	$\dot{\alpha}$	C_L	C_D	C_m
(s)	(m)	(m)	(m)	(deg)	(deg)	(deg)	(m/s)	(deg)	(deg/s)			
0.575	3.5336	1.9384	0.5115	-6.079	-11.938	25.884	6.47	-8.64	4.190	0.657	0.130	0.016
0.600	3.6249	1.9787	0.4784	-6.274	-11.465	25.635	6.37	-2.04	4.214	0.645	0.120	0.008
0.625	3.7172	2.0189	0.4461	-6.423	-10.952	25.372	6.40	1.14	4.242	0.630	0.111	0.002
0.650	3.8104	2.0592	0.4144	-6.548	-10.464	25.083	6.42	1.52	4.269	0.623	0.107	0.004
0.675	3.9046	2.0996	0.3833	-6.651	-9.961	24.751	6.45	1.78	4.294	0.618	0.104	0.007
0.700	3.9997	2.1400	0.3530	-6.753	-9.424	24.386	6.52	3.47	4.318	0.613	0.101	0.009
0.725	4.0957	2.1805	0.3233	-6.863	-8.842	23.976	6.64	6.02	4.340	0.607	0.098	0.011

Test Conditions

aircraft	balsa glider	flight	regression 10
aspect ratio	6.07	test number	5994
m (g)	6.51	I_{xx} (g·cm^2)	126.35
I_{yy} (g·cm^2)	306.55	I_{zz} (g·cm^2)	427.71
I_{xz} (g·cm^2)	9.33	I_{xy} (g·cm^2)	0.27
I_{yz} (g·cm^2)	-0.10	δ_e (deg)	1.9
CG (%c)	58.8		

time	x	y	z	ϕ	θ	ψ	V	α	$\dot{\alpha}$	C_L	C_D	C_m
(s)	(m)	(m)	(m)	(deg)	(deg)	(deg)	(m/s)	(deg)	(deg/s)			
0.000	0.1495	-0.2467	1.3254	-4.725	-13.363	26.851	5.23	-3.92	4.030	0.515	0.113	0.001
0.025	0.2372	-0.2086	1.2923	-4.772	-13.939	26.668	5.12	-4.84	4.067	0.507	0.107	0.002
0.050	0.3256	-0.1705	1.2581	-4.893	-14.510	26.418	4.99	-5.38	4.107	0.498	0.102	0.003
0.075	0.4148	-0.1324	1.2229	-5.058	-15.069	26.118	4.86	-5.53	4.151	0.488	0.097	0.004
0.100	0.5048	-0.0943	1.1866	-5.247	-15.622	25.786	4.72	-5.19	4.198	0.479	0.091	0.006
0.125	0.5958	-0.0559	1.1492	-5.398	-16.132	25.453	4.59	-4.39	4.247	0.469	0.085	0.004
0.150	0.6876	-0.0174	1.1106	-5.485	-16.618	25.135	4.49	-4.22	4.299	0.459	0.080	0.002
0.175	0.7804	0.0215	1.0710	-5.540	-17.090	24.843	4.39	-5.48	4.355	0.451	0.076	0.000
0.200	0.8743	0.0607	1.0302	-5.586	-17.561	24.615	4.22	-7.66	4.414	0.443	0.074	0.000
0.225	0.9694	0.1001	0.9884	-5.616	-18.027	24.444	4.01	-8.83	4.471	0.433	0.075	-0.000
0.250	1.0656	0.1397	0.9457	-5.642	-18.491	24.319	3.78	-7.86	4.528	0.418	0.077	-0.000
0.275	1.1628	0.1796	0.9019	-5.684	-18.952	24.194	3.62	-5.52	4.583	0.398	0.077	-0.002
0.300	1.2611	0.2196	0.8570	-5.802	-19.433	24.039	3.51	-3.45	4.639	0.379	0.074	-0.002
0.325	1.3604	0.2599	0.8108	-6.039	-19.937	23.829	3.44	-2.84	4.698	0.363	0.070	-0.001
0.350	1.4607	0.3003	0.7631	-6.388	-20.464	23.575	3.36	-3.78	4.761	0.353	0.066	0.001
0.375	1.5623	0.3409	0.7140	-6.792	-20.984	23.303	3.25	-5.69	4.828	0.347	0.063	0.002
0.400	1.6650	0.3816	0.6634	-7.165	-21.484	23.055	3.08	-7.55	4.896	0.343	0.063	0.002
0.425	1.7690	0.4224	0.6116	-7.440	-21.955	22.849	2.87	-8.34	4.962	0.335	0.064	-0.001
0.450	1.8744	0.4635	0.5585	-7.606	-22.418	22.704	2.66	-7.61	5.028	0.320	0.064	-0.006
0.475	1.9809	0.5047	0.5042	-7.689	-22.922	22.607	2.49	-6.07	5.094	0.299	0.063	-0.009
0.500	2.0885	0.5460	0.4483	-7.731	-23.511	22.573	2.36	-5.32	5.161	0.276	0.061	-0.010
0.525	2.1972	0.5876	0.3906	-7.734	-24.197	22.569	2.23	-5.57	5.232	0.256	0.061	-0.005
0.550	2.3069	0.6294	0.3310	-7.698	-24.929	22.583	2.07	-5.52	5.302	0.241	0.062	-0.001

time	x	y	z	ϕ	θ	ψ	V	α	$\dot{\alpha}$	C_L	C_D	C_m
(s)	(m)	(m)	(m)	(deg)	(deg)	(deg)	(m/s)	(deg)	(deg/s)			
0.575	2.4175	0.6714	0.2693	-7.608	-25.665	22.604	1.96	-3.29	5.374	0.225	0.062	0.003
0.600	2.5289	0.7137	0.2054	-7.462	-26.373	22.614	1.93	0.65	5.447	0.210	0.062	0.007
0.625	2.6411	0.7561	0.1391	-7.256	-27.017	22.598	2.02	6.31	5.521	0.196	0.061	0.011

	Test Conditions			
aircraft	balsa glider	flight	regression 11	
aspect ratio	6.07	test number	5988	
m (g)	6.51	I_{xx} (g·cm^2)	126.35	
I_{yy} (g·cm^2)	306.55	I_{zz} (g·cm^2)	427.71	
I_{xz} (g·cm^2)	9.33	I_{xy} (g·cm^2)	0.27	
I_{yz} (g·cm^2)	-0.10	δ_e (deg)	1.9	
CG (%c)	58.8			

time	x	y	z	ϕ	θ	ψ	V	α	$\dot{\alpha}$	C_L	C_D	C_m
(s)	(m)	(m)	(m)	(deg)	(deg)	(deg)	(m/s)	(deg)	(deg/s)			
0.000	0.5352	-0.1410	1.1238	-4.407	-16.886	24.428	2.31	8.59	4.874	0.298	0.096	-0.007
0.025	0.6436	-0.1028	1.0823	-4.314	-17.467	23.910	2.48	5.46	4.905	0.296	0.089	-0.006
0.050	0.7522	-0.0645	1.0391	-4.230	-18.081	23.511	2.58	2.72	4.942	0.293	0.081	-0.005
0.075	0.8612	-0.0258	0.9941	-4.138	-18.722	23.214	2.62	0.38	4.985	0.290	0.074	-0.004
0.100	0.9706	0.0131	0.9475	-4.040	-19.385	22.999	2.60	-1.44	5.042	0.286	0.060	-0.003
0.125	1.0808	0.0525	0.8991	-3.870	-20.062	22.850	2.55	-3.45	5.098	0.282	0.063	-0.002
0.150	1.1918	0.0922	0.8489	-3.627	-20.749	22.750	2.44	-5.88	5.152	0.280	0.063	-0.001
0.175	1.3035	0.1323	0.7970	-3.362	-21.442	22.671	2.26	-7.99	5.210	0.277	0.060	0.000
0.200	1.4160	0.1727	0.7436	-3.146	-22.125	22.597	2.05	-8.21	5.272	0.270	0.057	0.001
0.225	1.5295	0.2135	0.6885	-3.018	-22.796	22.533	1.85	-6.21	5.337	0.257	0.056	0.001
0.250	1.6440	0.2546	0.6317	-2.981	-23.447	22.494	1.74	-3.03	5.404	0.241	0.056	0.000
0.275	1.7592	0.2962	0.5730	-2.989	-24.089	22.519	1.70	-0.54	5.470	0.226	0.057	-0.001
0.300	1.8753	0.3381	0.5123	-3.005	-24.740	22.617	1.71	0.13	5.536	0.213	0.058	-0.003
0.325	1.9919	0.3805	0.4493	-3.012	-25.417	22.779	1.71	-0.40	5.603	0.202	0.057	-0.003
0.350	2.1093	0.4233	0.3841	-3.034	-26.132	22.971	1.68	-0.99	5.674	0.191	0.056	-0.003
0.375	2.2272	0.4665	0.3164	-3.090	-26.876	23.161	1.65	-1.15	5.748	0.180	0.054	-0.002
0.400	2.3459	0.5102	0.2463	-3.177	-27.633	23.333	1.63	-1.00	5.824	0.170	0.053	-0.001
0.425	2.4652	0.5544	0.1736	-3.313	-28.406	23.457	1.61	-0.56	5.903	0.160	0.052	-0.001

Test Conditions											

aircraft	balsa glider		flight		regression 12						
aspect ratio	6.07		test number		6002						
m (g)	6.75		I_{xx} (g·cm^2)		126.40						
I_{yy} (g·cm^2)	315.61		I_{zz} (g·cm^2)		436.72						
I_{xz} (g·cm^2)	10.00		I_{xy} (g·cm^2)		0.27						
I_{yz} (g·cm^2)	-0.10		δ_e (deg)		1.9						
CG (%c)	52.9										

time	x	y	z	ϕ	θ	ψ	V	α	$\dot{\alpha}$	C_L	C_D	C_m
(s)	(m)	(m)	(m)	(deg)	(deg)	(deg)	(m/s)	(deg)	(deg/s)			
0.000	0.0753	-0.0613	1.4087	-8.818	-11.917	23.603	3.98	-6.83	4.473	0.433	0.108	0.005
0.025	0.1746	-0.0198	1.3773	-9.118	-12.555	23.349	3.84	-4.46	4.495	0.419	0.098	0.003
0.050	0.2744	0.0209	1.3446	-9.528	-13.201	22.964	3.75	-2.51	4.523	0.404	0.088	0.001
0.075	0.3749	0.0611	1.3105	-10.012	-13.864	22.485	3.71	-0.99	4.557	0.388	0.078	-0.000
0.100	0.4761	0.1009	1.2750	-10.528	-14.544	21.944	3.70	0.32	4.597	0.371	0.067	-0.003
0.125	0.5782	0.1405	1.2379	-11.067	-15.270	21.393	3.71	0.46	4.648	0.354	0.060	-0.004
0.150	0.6811	0.1799	1.1989	-11.552	-16.041	20.857	3.73	-0.91	4.703	0.342	0.061	-0.003
0.175	0.7848	0.2192	1.1581	-11.982	-16.844	20.347	3.67	-2.95	4.757	0.335	0.066	0.001
0.200	0.8895	0.2582	1.1156	-12.287	-17.650	19.812	3.57	-4.20	4.806	0.329	0.072	0.002
0.225	0.9950	0.2969	1.0713	-12.455	-18.459	19.197	3.46	-4.26	4.855	0.322	0.072	0.001
0.250	1.1013	0.3352	1.0252	-12.463	-19.282	18.498	3.36	-4.36	4.907	0.312	0.069	-0.002
0.275	1.2085	0.3732	0.9774	-12.397	-20.133	17.749	3.25	-4.95	4.966	0.301	0.064	-0.002
0.300	1.3167	0.4109	0.9277	-12.358	-21.014	16.965	3.11	-5.41	5.029	0.290	0.062	-0.001
0.325	1.4260	0.4483	0.8761	-12.392	-21.910	16.131	2.98	-4.85	5.093	0.277	0.061	-0.000
0.350	1.5364	0.4853	0.8224	-12.496	-22.827	15.231	2.87	-3.53	5.159	0.263	0.062	-0.000
0.375	1.6477	0.5219	0.7666	-12.628	-23.764	14.260	2.81	-2.37	5.226	0.247	0.063	-0.001
0.400	1.7601	0.5579	0.7085	-12.807	-24.742	13.231	2.75	-1.89	5.294	0.233	0.063	-0.002
0.425	1.8734	0.5935	0.6480	-13.008	-25.765	12.140	2.70	-1.90	5.364	0.220	0.063	-0.003

	Test Conditions			
aircraft	balsa glider	flight	regression 13	
aspect ratio	6.07	test number	5982	
m (g)	6.51	I_{xx} (g·cm^2)	126.35	
I_{yy} (g·cm^2)	306.55	I_{zz} (g·cm^2)	427.71	
I_{xz} (g·cm^2)	9.33	I_{xy} (g·cm^2)	0.27	
I_{yz} (g·cm^2)	-0.10	δ_e (deg)	1.42	
CG (%c)	58.8			

time	x	y	z	ϕ	θ	ψ	V	α	$\dot{\alpha}$	C_L	C_D	C_m
(s)	(m)	(m)	(m)	(deg)	(deg)	(deg)	(m/s)	(deg)	(deg/s)			
0.000	0.2160	-0.3806	1.2351	-3.903	-6.375	25.764	4.13	9.36	4.621	0.409	0.100	-0.016
0.025	0.3226	-0.3420	1.2129	-3.765	-6.614	25.405	4.32	5.06	4.618	0.414	0.096	-0.012
0.050	0.4291	-0.3036	1.1900	-3.486	-6.929	25.053	4.40	1.83	4.619	0.419	0.092	-0.008
0.075	0.5355	-0.2654	1.1665	-3.112	-7.287	24.714	4.42	-0.36	4.623	0.423	0.088	-0.003
0.100	0.6419	-0.2271	1.1423	-2.707	-7.661	24.383	4.39	-1.22	4.631	0.424	0.083	0.002
0.125	0.7484	-0.1888	1.1174	-2.261	-8.015	24.109	4.36	-2.25	4.641	0.431	0.078	0.006
0.150	0.8551	-0.1502	1.0920	-1.851	-8.309	23.882	4.29	-3.42	4.658	0.437	0.073	0.008
0.175	0.9621	-0.1114	1.0663	-1.595	-8.537	23.651	4.19	-3.37	4.677	0.438	0.071	0.006
0.200	1.0694	-0.0723	1.0402	-1.569	-8.713	23.380	4.11	-1.57	4.695	0.432	0.073	0.002
0.225	1.1770	-0.0330	1.0138	-1.744	-8.878	23.074	4.11	0.45	4.710	0.422	0.075	-0.002
0.250	1.2848	0.0065	0.9869	-2.078	-9.071	22.788	4.14	1.02	4.724	0.414	0.075	-0.003
0.275	1.3929	0.0461	0.9595	-2.471	-9.301	22.556	4.16	-0.04	4.741	0.410	0.073	-0.002
0.300	1.5013	0.0858	0.9315	-2.854	-9.550	22.383	4.13	-1.57	4.761	0.409	0.071	0.001
0.325	1.6100	0.1256	0.9029	-3.173	-9.785	22.243	4.08	-2.43	4.782	0.409	0.070	0.002
0.350	1.7191	0.1655	0.8738	-3.399	-10.000	22.143	4.01	-2.34	4.804	0.407	0.069	0.001
0.375	1.8287	0.2057	0.8442	-3.535	-10.200	22.112	3.96	-1.82	4.827	0.403	0.070	-0.001
0.400	1.9387	0.2460	0.8142	-3.624	-10.404	22.156	3.92	-1.57	4.848	0.397	0.071	-0.003
0.425	2.0491	0.2863	0.7837	-3.685	-10.630	22.256	3.88	-2.27	4.869	0.394	0.073	-0.002
0.450	2.1599	0.3267	0.7527	-3.731	-10.877	22.372	3.81	-4.02	4.889	0.393	0.075	-0.001
0.475	2.2711	0.3672	0.7212	-3.723	-11.134	22.501	3.68	-5.97	4.909	0.394	0.074	0.000
0.500	2.3827	0.4078	0.6893	-3.636	-11.386	22.649	3.52	-6.38	4.929	0.391	0.072	0.001
0.525	2.4948	0.4486	0.6571	-3.484	-11.633	22.821	3.36	-4.15	4.952	0.384	0.069	0.002
0.550	2.6073	0.4896	0.6245	-3.320	-11.851	22.989	3.31	-0.41	4.978	0.372	0.067	0.002

continued on next page

time	x	y	z	ϕ	θ	ψ	V	α	$\dot{\alpha}$	C_L	C_D	C_m
(s)	(m)	(m)	(m)	(deg)	(deg)	(deg)	(m/s)	(deg)	(deg/s)			
0.575	2.7202	0.5308	0.5913	-3.219	-12.052	23.115	3.35	2.33	5.005	0.360	0.067	-0.000
0.600	2.8337	0.5722	0.5574	-3.216	-12.252	23.197	3.43	2.65	5.030	0.351	0.069	-0.003
0.625	2.9475	0.6137	0.5227	-3.271	-12.497	23.259	3.47	1.26	5.054	0.346	0.070	-0.004
0.650	3.0617	0.6553	0.4872	-3.315	-12.770	23.329	3.48	-0.41	5.080	0.343	0.069	-0.002
0.675	3.1765	0.6970	0.4509	-3.292	-13.065	23.423	3.45	-1.58	5.108	0.341	0.068	-0.000
0.700	3.2916	0.7389	0.4139	-3.178	-13.351	23.519	3.40	-2.33	5.136	0.338	0.065	-0.001
0.725	3.4073	0.7809	0.3762	-3.018	-13.652	23.612	3.34	-2.63	5.166	0.332	0.059	-0.002
0.750	3.5236	0.8233	0.3376	-2.876	-13.986	23.721	3.28	-1.93	5.205	0.322	0.054	0.000
0.775	3.6406	0.8659	0.2982	-2.795	-14.323	23.863	3.25	0.38	5.249	0.312	0.055	0.005
0.800	3.7583	0.9091	0.2578	-2.761	-14.606	24.038	3.30	3.59	5.288	0.303	0.061	0.005
0.825	3.8763	0.9528	0.2163	-2.745	-14.828	24.215	3.43	6.10	5.318	0.297	0.067	0.003
0.850	3.9947	0.9971	0.1739	-2.651	-15.016	24.356	3.60	6.99	5.352	0.290	0.069	-0.002
0.875	4.1134	1.0420	0.1303	-2.428	-15.239	24.473	3.76	6.41	5.383	0.284	0.074	-0.005
0.900	4.2322	1.0877	0.0857	-2.017	-15.507	24.532	3.90	4.41	5.411	0.279	0.078	-0.008

aircraft	balsa glider	flight	regression 14
aspect ratio	6.07	test number	6043
m (g)	6.75	I_{xx} (g·cm^2)	126.40
I_{yy} (g·cm^2)	315.61	I_{zz} (g·cm^2)	436.72
I_{xz} (g·cm^2)	10.00	I_{xy} (g·cm^2)	0.27
I_{yz} (g·cm^2)	-0.10	δ_e (deg)	-2.8
CG (%c)	52.9		

time	x	y	z	ϕ	θ	ψ	V	α	$\dot{\alpha}$	C_L	C_D	C_m
(s)	(m)	(m)	(m)	(deg)	(deg)	(deg)	(m/s)	(deg)	(deg/s)			
0.000	0.0679	-0.2313	1.1970	-3.060	-0.561	23.547	9.01	3.14	3.571	0.722	0.204	-0.026
0.025	0.1490	-0.1979	1.1818	-3.357	-1.019	23.457	9.05	0.20	3.554	0.722	0.198	-0.021
0.050	0.2297	-0.1650	1.1657	-3.596	-1.557	23.361	9.03	-1.81	3.542	0.721	0.192	-0.016
0.075	0.3102	-0.1325	1.1489	-3.781	-2.155	23.272	8.97	-2.90	3.535	0.718	0.186	-0.011
0.100	0.3905	-0.1003	1.1313	-3.888	-2.802	23.189	8.89	-2.93	3.531	0.715	0.180	-0.004
0.125	0.4707	-0.0686	1.1128	-4.000	-3.449	23.164	8.82	-2.25	3.532	0.708	0.172	-0.001
0.150	0.5509	-0.0371	1.0934	-4.084	-4.083	23.184	8.78	-1.55	3.538	0.702	0.164	-0.002
0.175	0.6312	-0.0058	1.0730	-4.035	-4.722	23.222	8.74	-1.44	3.548	0.694	0.156	-0.004
0.200	0.7116	0.0255	1.0516	-3.829	-5.385	23.261	8.70	-2.08	3.563	0.688	0.151	-0.001
0.225	0.7922	0.0567	1.0291	-3.506	-6.052	23.324	8.64	-3.15	3.583	0.683	0.149	0.002
0.250	0.8730	0.0879	1.0057	-3.129	-6.715	23.420	8.54	-4.19	3.604	0.683	0.153	0.008
0.275	0.9542	0.1191	0.9813	-2.715	-7.337	23.547	8.43	-4.50	3.622	0.682	0.158	0.012
0.300	1.0355	0.1503	0.9561	-2.308	-7.915	23.677	8.32	-4.05	3.640	0.682	0.157	0.013
0.325	1.1172	0.1817	0.9301	-1.924	-8.442	23.810	8.23	-3.45	3.663	0.679	0.153	0.014
0.350	1.1992	0.2131	0.9033	-1.629	-8.920	23.925	8.15	-3.08	3.688	0.677	0.149	0.016
0.375	1.2817	0.2447	0.8757	-1.410	-9.338	24.018	8.08	-2.31	3.715	0.674	0.147	0.018
0.400	1.3646	0.2765	0.8475	-1.274	-9.683	24.072	8.03	-0.55	3.742	0.671	0.145	0.019
0.425	1.4480	0.3087	0.8186	-1.147	-9.937	24.089	8.04	0.98	3.771	0.669	0.144	0.016
0.450	1.5318	0.3413	0.7892	-1.028	-10.124	24.088	8.08	0.54	3.801	0.669	0.144	0.011
0.475	1.6161	0.3743	0.7592	-0.897	-10.280	24.088	8.08	-2.06	3.831	0.676	0.146	0.010
0.500	1.7009	0.4078	0.7289	-0.799	-10.397	24.091	7.98	-4.34	3.858	0.683	0.146	0.014
0.525	1.7863	0.4418	0.6984	-0.750	-10.456	24.089	7.85	-4.13	3.884	0.687	0.145	0.017
0.550	1.8723	0.4759	0.6678	-0.781	-10.423	24.080	7.77	-2.08	3.911	0.684	0.142	0.014

time	x	y	z	ϕ	θ	ψ	V	α	$\dot{\alpha}$	C_L	C_D	C_m
(s)	(m)	(m)	(m)	(deg)	(deg)	(deg)	(m/s)	(deg)	(deg/s)			
0.575	1.9589	0.5104	0.6373	-0.854	-10.318	24.074	7.76	-0.56	3.938	0.680	0.141	0.006
0.600	2.0462	0.5451	0.6067	-0.924	-10.185	24.085	7.75	-1.11	3.963	0.676	0.139	-0.000
0.625	2.1340	0.5803	0.5762	-0.961	-10.070	24.101	7.70	-3.01	3.988	0.673	0.138	-0.000
0.650	2.2224	0.6158	0.5458	-1.009	-9.978	24.133	7.60	-4.01	4.013	0.671	0.135	0.006
0.675	2.3114	0.6517	0.5156	-1.121	-9.866	24.165	7.49	-3.32	4.038	0.668	0.135	0.015
0.700	2.4011	0.6878	0.4855	-1.313	-9.664	24.189	7.45	-0.65	4.060	0.667	0.138	0.017
0.725	2.4913	0.7243	0.4558	-1.543	-9.377	24.202	7.45	2.47	4.078	0.668	0.139	0.018
0.750	2.5820	0.7610	0.4264	-1.757	-8.969	24.171	7.56	4.39	4.094	0.671	0.139	0.009
0.775	2.6732	0.7979	0.3974	-1.926	-8.516	24.081	7.66	2.90	4.109	0.675	0.138	-0.001
0.800	2.7650	0.8351	0.3690	-2.085	-8.065	23.951	7.72	-1.20	4.126	0.678	0.137	-0.012
0.825	2.8572	0.8723	0.3411	-2.262	-7.745	23.825	7.60	-4.47	4.138	0.678	0.135	-0.004
0.850	2.9499	0.9097	0.3140	-2.485	-7.431	23.719	7.48	-4.74	4.148	0.678	0.134	0.007
0.875	3.0431	0.9473	0.2875	-2.722	-7.094	23.627	7.39	-2.31	4.157	0.677	0.128	0.018
0.900	3.1367	0.9848	0.2618	-2.968	-6.633	23.500	7.39	1.87	4.167	0.675	0.118	0.017
0.925	3.2308	1.0224	0.2368	-3.239	-6.107	23.334	7.47	7.87	4.182	0.665	0.107	0.018
0.950	3.3255	1.0603	0.2123	-3.596	-5.465	23.124	7.76	13.58	4.201	0.661	0.110	0.017
0.975	3.4207	1.0984	0.1884	-4.068	-4.749	22.936	8.14	14.30	4.216	0.668	0.125	0.017
1.000	3.5161	1.1367	0.1652	-4.632	-3.909	22.761	8.48	8.63	4.213	0.695	0.148	0.004
1.025	3.6115	1.1751	0.1432	-5.182	-3.062	22.584	8.57	1.17	4.197	0.724	0.159	-0.008
1.050	3.7070	1.2130	0.1227	-5.627	-2.258	22.362	8.52	-2.87	4.176	0.738	0.157	-0.015
1.075	3.8025	1.2502	0.1037	-5.918	-1.589	22.088	8.44	-1.90	4.161	0.734	0.146	-0.010
1.100	3.8981	1.2869	0.0859	-6.108	-0.980	21.759	8.42	-0.38	4.148	0.729	0.138	-0.006
1.125	3.9937	1.3231	0.0693	-6.295	-0.388	21.418	8.44	-0.69	4.134	0.730	0.136	-0.005
1.150	4.0893	1.3589	0.0538	-6.551	0.173	21.079	8.38	-2.60	4.118	0.740	0.137	-0.002
1.175	4.1848	1.3940	0.0395	-6.842	0.731	20.738	8.30	-3.59	4.099	0.749	0.137	-0.000
1.200	4.2801	1.4285	0.0264	-7.219	1.287	20.408	8.21	-4.08	4.078	0.759	0.137	0.001
1.225	4.3753	1.4624	0.0145	-7.713	1.848	20.095	8.11	-4.07	4.055	0.770	0.137	0.003

Appendix C

Test Data for the Balsa Glider with an Aspect Ratio 11.7

Appendix C lists the data for selected flights of the balsa glider with an aspect ratio 11.7. The data is downsampled from the recording rate of 200 Hz to 40 Hz. Flights H, I and J (as listed in Table 6.2) are included as well as the 11 regression flights. The tables include some of the specific test conditions and a time history of the important parameters.

The trajectory and determined quantities tabulated for flight H of the balsa glider with an aspect ratio of 11.7 which is shown in Figs. 6.28 and 6.29.

Test Conditions			
aircraft	balsa glider	flight	H
aspect ratio	11.7	test number	6364
m (g)	6.25	I_{xx} (g·cm^2)	290.74
I_{yy} (g·cm^2)	275.64	I_{zz} (g·cm^2)	561.35
I_{xz} (g·cm^2)	7.40	I_{xy} (g·cm^2)	0.74
I_{yz} (g·cm^2)	-0.22	δ_e (deg)	0.94
CG (%c)	0.8		
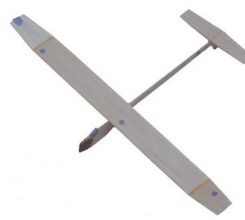
| time | x | y | z | ϕ | θ | ψ | V | α | $\dot{\alpha}$ | C_L | C_D | C_m |
(s)	(m)	(m)	(m)	(deg)	(deg)	(deg)	(m/s)	(deg)	(deg/s)			
0.000	-2.5376	-0.0500	1.1504	-8.419	10.288	17.982	5.58	2.32	5.644	0.635	0.101	-0.062
0.025	-2.4040	-0.0112	1.1644	-9.083	12.920	18.467	5.29	-9.34	5.539	0.654	0.105	-0.008
0.050	-2.2734	0.0246	1.1847	-9.712	15.835	19.056	5.12	-9.89	5.418	0.677	0.108	-0.002
0.075	-2.1463	0.0573	1.2110	-10.244	18.824	19.706	4.95	-5.75	5.288	0.695	0.107	-0.004
0.100	-2.0232	0.0867	1.2427	-10.624	21.834	20.350	4.84	-3.52	5.153	0.705	0.105	-0.012
0.125	-1.9043	0.1128	1.2792	-10.824	24.735	20.911	4.77	-0.56	5.011	0.710	0.104	-0.016
0.150	-1.7900	0.1356	1.3198	-10.869	27.496	21.374	4.80	2.44	4.863	0.714	0.106	-0.015

177

time	x	y	z	ϕ	θ	ψ	V	α	$\dot\alpha$	C_L	C_D	C_m
(s)	(m)	(m)	(m)	(deg)	(deg)	(deg)	(m/s)	(deg)	(deg/s)			
0.175	-1.6803	0.1553	1.3635	-10.818	30.131	21.742	4.90	4.46	4.710	0.725	0.110	-0.010
0.200	-1.5755	0.1719	1.4098	-10.732	32.693	22.029	5.03	5.30	4.549	0.745	0.117	-0.005
0.225	-1.4757	0.1856	1.4580	-10.638	35.232	22.225	5.17	6.54	4.380	0.770	0.125	-0.007
0.250	-1.3812	0.1963	1.5076	-10.532	37.746	22.302	5.36	9.40	4.204	0.794	0.133	-0.017
0.275	-1.2920	0.2041	1.5581	-10.402	40.176	22.255	5.64	13.51	4.022	0.811	0.143	-0.034
0.300	-1.2080	0.2094	1.6088	-10.238	42.443	22.089	6.05	18.15	3.834	0.822	0.154	-0.052
0.325	-1.1290	0.2122	1.6588	-10.031	44.478	21.806	6.56	23.58	3.643	0.830	0.167	-0.065
0.350	-1.0550	0.2128	1.7077	-9.772	46.260	21.385	7.24	30.85	3.450	0.837	0.183	-0.076
0.375	-0.9855	0.2115	1.7546	-9.428	47.784	20.785	8.12	40.72	3.256	0.846	0.203	-0.086
0.400	-0.9202	0.2086	1.7991	-8.962	49.060	19.955	9.28	52.83	3.062	0.861	0.229	-0.103
0.425	-0.8590	0.2043	1.8407	-8.339	50.084	18.863	10.77	66.34	2.869	0.884	0.261	-0.132
0.450	-0.8015	0.1988	1.8790	-7.559	50.833	17.508	12.60	79.92	2.677	0.916	0.300	-0.167
0.475	-0.7473	0.1925	1.9138	-6.628	51.285	15.896	14.79	93.17	2.490	0.963	0.349	-0.200
0.500	-0.6964	0.1855	1.9447	-5.564	51.454	14.027	17.29	107.48	2.307	1.022	0.412	-0.228
0.525	-0.6485	0.1780	1.9718	-4.389	51.383	11.946	20.19	126.51	2.131	1.083	0.489	-0.255
0.550	-0.6034	0.1701	1.9947	-3.131	51.119	9.731	23.62	152.41	1.963	1.127	0.575	-0.293
0.575	-0.5608	0.1620	2.0133	-1.822	50.683	7.493	27.81	182.50	1.809	1.153	0.678	-0.338
0.600	-0.5204	0.1538	2.0274	-0.492	50.075	5.278	32.77	211.53	1.675	1.172	0.812	-0.376
0.625	-0.4820	0.1457	2.0369	0.857	49.302	3.063	38.38	236.06	1.559	1.199	1.004	-0.399
0.650	-0.4454	0.1377	2.0419	2.224	48.395	0.804	44.52	255.86	1.462	1.211	1.249	-0.422
0.675	-0.4106	0.1299	2.0422	3.624	47.389	-1.514	51.10	269.90	1.388	1.179	1.511	-0.468
0.700	-0.3776	0.1224	2.0379	5.062	46.292	-3.821	57.96	275.62	1.342	1.072	1.745	-0.517
0.725	-0.3464	0.1151	2.0291	6.533	45.077	-6.024	64.82	271.29	1.324	0.897	1.928	-0.543
0.750	-0.3167	0.1082	2.0158	8.017	43.719	-8.056	71.44	256.88	1.334	0.670	2.044	-0.540
0.775	-0.2887	0.1018	1.9981	9.490	42.196	-9.914	77.59	233.06	1.366	0.440	2.078	-0.527
0.800	-0.2624	0.0958	1.9762	10.909	40.486	-11.604	83.03	199.92	1.418	0.249	2.027	-0.521
0.825	-0.2378	0.0903	1.9501	12.245	38.549	-13.142	87.55	159.51	1.488	0.118	1.939	-0.499
0.850	-0.2147	0.0854	1.9200	13.450	36.335	-14.467	90.98	116.12	1.569	0.032	1.848	-0.459
0.875	-0.1933	0.0811	1.8862	14.485	33.801	-15.524	93.33	73.28	1.655	-0.026	1.770	-0.414
0.900	-0.1733	0.0774	1.8489	15.305	30.913	-16.263	94.64	31.74	1.741	-0.064	1.697	-0.391
0.925	-0.1549	0.0743	1.8084	15.900	27.629	-16.687	94.92	-9.89	1.828	-0.074	1.627	-0.382
0.950	-0.1378	0.0720	1.7649	16.238	23.917	-16.827	94.16	-51.67	1.913	-0.059	1.565	-0.375
0.975	-0.1221	0.0703	1.7187	16.287	19.753	-16.716	92.34	-92.53	1.994	-0.019	1.514	-0.362
1.000	-0.1074	0.0695	1.6702	16.006	15.142	-16.389	89.54	-131.51	2.070	0.041	1.469	-0.351
1.025	-0.0936	0.0694	1.6194	15.402	10.115	-15.922	85.79	-168.60	2.140	0.123	1.425	-0.339
1.050	-0.0803	0.0701	1.5668	14.500	4.697	-15.372	81.15	-202.86	2.208	0.223	1.381	-0.316

continued on next page

178

time	x	y	z	ϕ	θ	ψ	V	α	$\dot{\alpha}$	C_L	C_D	C_m
(s)	(m)	(m)	(m)	(deg)	(deg)	(deg)	(m/s)	(deg)	(deg/s)			
1.075	-0.0673	0.0714	1.5125	13.302	-1.067	-14.819	75.68	-232.20	2.270	0.331	1.331	-0.277
1.100	-0.0541	0.0731	1.4567	11.755	-7.105	-14.318	69.56	-255.16	2.329	0.439	1.263	-0.235
1.125	-0.0403	0.0752	1.3995	9.830	-13.346	-13.938	62.96	-272.69	2.390	0.540	1.165	-0.185
1.150	-0.0255	0.0776	1.3409	7.562	-19.714	-13.759	55.98	-287.28	2.459	0.623	1.036	-0.130
1.175	-0.0093	0.0800	1.2807	5.097	-26.181	-13.841	48.67	-297.99	2.541	0.675	0.888	-0.058
1.200	0.0088	0.0822	1.2188	2.578	-32.705	-14.217	41.13	-301.17	2.635	0.682	0.728	0.028
1.225	0.0289	0.0840	1.1548	0.125	-39.195	-14.890	33.66	-293.42	2.747	0.639	0.564	0.108
1.250	0.0513	0.0851	1.0883	-2.197	-45.545	-15.820	26.53	-275.16	2.881	0.555	0.412	0.173
1.275	0.0757	0.0855	1.0186	-4.316	-51.631	-16.949	19.98	-248.65	3.037	0.451	0.288	0.220
1.300	0.1022	0.0853	0.9452	-6.171	-57.321	-18.212	14.17	-214.44	3.211	0.345	0.199	0.261
1.325	0.1304	0.0847	0.8676	-7.732	-62.425	-19.532	9.30	-172.51	3.397	0.250	0.142	0.296
1.350	0.1599	0.0837	0.7854	-9.014	-66.704	-20.792	5.56	-124.00	3.593	0.176	0.107	0.312

The trajectory and determined quantities tabulated for flight I of the balsa glider with an aspect ratio of 11.7 which is shown in Figs. 6.30 and 6.31.

Test Conditions			
aircraft	balsa glider	flight	I
aspect ratio	11.7	test number	6345
m (g)	6.25	I_{xx} (g·cm^2)	290.74
I_{yy} (g·cm^2)	275.64	I_{zz} (g·cm^2)	561.35
I_{xz} (g·cm^2)	7.40	I_{xy} (g·cm^2)	0.74
I_{yz} (g·cm^2)	-0.22	δ_e (deg)	0.94
CG (%c)	0.8		

time	x	y	z	ϕ	θ	ψ	V	α	$\dot{\alpha}$	C_L	C_D	C_m
(s)	(m)	(m)	(m)	(deg)	(deg)	(deg)	(m/s)	(deg)	(deg/s)			
0.000	-0.8832	0.3161	0.4461	-11.377	11.340	22.389	2.79	-0.49	6.139	0.434	0.073	-0.000
0.025	-0.7371	0.3534	0.4664	-11.577	13.149	22.280	2.85	2.59	6.035	0.442	0.074	-0.000
0.050	-0.5937	0.3884	0.4905	-11.829	14.983	22.194	2.93	3.70	5.927	0.450	0.075	-0.004
0.075	-0.4532	0.4208	0.5179	-12.107	16.788	22.102	3.02	2.84	5.813	0.457	0.076	-0.009
0.100	-0.3158	0.4507	0.5485	-12.382	18.492	21.966	3.07	1.06	5.696	0.463	0.077	-0.013
0.125	-0.1817	0.4782	0.5818	-12.636	20.049	21.774	3.07	-1.40	5.574	0.471	0.078	-0.012
0.150	-0.0509	0.5031	0.6174	-12.878	21.486	21.551	3.01	-3.85	5.449	0.483	0.080	-0.007
0.175	0.0763	0.5256	0.6551	-13.115	22.859	21.316	2.88	-5.72	5.320	0.500	0.083	0.001
0.200	0.1999	0.5454	0.6948	-13.341	24.266	21.077	2.73	-5.71	5.186	0.521	0.084	0.005
0.225	0.3198	0.5627	0.7362	-13.538	25.730	20.819	2.59	-3.64	5.049	0.541	0.084	0.004
0.250	0.4357	0.5774	0.7792	-13.684	27.239	20.518	2.55	-0.99	4.912	0.557	0.085	-0.005
0.275	0.5477	0.5896	0.8235	-13.773	28.698	20.165	2.56	0.51	4.771	0.570	0.088	-0.011
0.300	0.6557	0.5993	0.8687	-13.811	30.070	19.754	2.58	0.75	4.625	0.584	0.092	-0.016
0.325	0.7596	0.6066	0.9144	-13.833	31.328	19.293	2.59	1.59	4.474	0.597	0.094	-0.017
0.350	0.8595	0.6115	0.9602	-13.873	32.479	18.776	2.65	3.65	4.323	0.607	0.092	-0.018
0.375	0.9555	0.6142	1.0056	-13.969	33.516	18.217	2.78	6.19	4.177	0.618	0.091	-0.013
0.400	1.0478	0.6148	1.0505	-14.134	34.501	17.632	2.97	8.53	4.032	0.633	0.096	-0.008
0.425	1.1365	0.6134	1.0945	-14.363	35.462	17.052	3.21	11.52	3.884	0.654	0.110	-0.004
0.450	1.2214	0.6103	1.1372	-14.621	36.431	16.474	3.53	15.09	3.728	0.681	0.128	-0.011
0.475	1.3026	0.6055	1.1785	-14.892	37.371	15.892	3.96	17.28	3.568	0.714	0.142	-0.024
0.500	1.3801	0.5990	1.2180	-15.158	38.220	15.284	4.42	17.63	3.408	0.751	0.147	-0.035

continued on next page

time	x	y	z	ϕ	θ	ψ	V	α	$\dot{\alpha}$	C_L	C_D	C_m
(s)	(m)	(m)	(m)	(deg)	(deg)	(deg)	(m/s)	(deg)	(deg/s)			
0.525	1.4541	0.5909	1.2556	-15.423	38.937	14.643	4.85	19.29	3.257	0.785	0.150	-0.038
0.550	1.5247	0.5813	1.2911	-15.672	39.538	13.955	5.38	25.89	3.110	0.812	0.161	-0.041
0.575	1.5921	0.5703	1.3242	-15.900	40.039	13.204	6.15	35.89	2.963	0.835	0.184	-0.056
0.600	1.6564	0.5581	1.3547	-16.096	40.408	12.372	7.21	44.95	2.815	0.862	0.212	-0.087
0.625	1.7177	0.5448	1.3824	-16.250	40.573	11.453	8.43	52.15	2.672	0.898	0.240	-0.116
0.650	1.7763	0.5305	1.4069	-16.340	40.481	10.449	9.82	61.78	2.537	0.933	0.272	-0.131
0.675	1.8323	0.5153	1.4282	-16.317	40.131	9.322	11.53	77.93	2.407	0.962	0.322	-0.134
0.700	1.8858	0.4994	1.4461	-16.142	39.543	8.019	13.74	99.84	2.282	0.994	0.384	-0.134
0.725	1.9370	0.4830	1.4604	-15.784	38.760	6.478	16.53	122.65	2.164	1.034	0.450	-0.155
0.750	1.9859	0.4662	1.4710	-15.232	37.806	4.718	19.86	141.77	2.060	1.081	0.519	-0.207
0.775	2.0327	0.4491	1.4780	-14.490	36.669	2.806	23.59	155.87	1.970	1.124	0.604	-0.283
0.800	2.0776	0.4317	1.4813	-13.611	35.312	0.836	27.60	164.38	1.890	1.154	0.708	-0.350
0.825	2.1206	0.4142	1.4810	-12.621	33.700	-1.155	31.77	166.90	1.824	1.170	0.817	-0.384
0.850	2.1619	0.3966	1.4769	-11.544	31.834	-3.166	35.90	162.66	1.774	1.175	0.927	-0.377
0.875	2.2014	0.3791	1.4692	-10.338	29.759	-5.247	39.85	152.45	1.741	1.173	1.037	-0.362
0.900	2.2394	0.3616	1.4580	-8.941	27.532	-7.390	43.48	137.28	1.721	1.169	1.153	-0.369
0.925	2.2759	0.3443	1.4434	-7.272	25.185	-9.588	46.70	118.10	1.712	1.153	1.257	-0.396
0.950	2.3110	0.3273	1.4256	-5.309	22.731	-11.776	49.37	96.64	1.716	1.119	1.328	-0.430
0.975	2.3448	0.3105	1.4047	-3.088	20.153	-13.927	51.49	73.95	1.732	1.065	1.365	-0.436
1.000	2.3774	0.2940	1.3808	-0.741	17.435	-16.005	53.06	49.99	1.759	1.010	1.389	-0.403
1.025	2.4089	0.2779	1.3539	1.651	14.588	-17.985	54.00	24.55	1.795	0.965	1.396	-0.350
1.050	2.4396	0.2622	1.3243	4.008	11.611	-19.835	54.27	-0.87	1.836	0.935	1.384	-0.289
1.075	2.4695	0.2471	1.2921	6.326	8.522	-21.533	53.93	-25.44	1.883	0.917	1.341	-0.246
1.100	2.4989	0.2324	1.2574	8.616	5.294	-23.059	53.01	-50.69	1.938	0.906	1.275	-0.202
1.125	2.5280	0.2183	1.2203	10.857	1.922	-24.409	51.44	-77.15	2.000	0.904	1.198	-0.153
1.150	2.5570	0.2045	1.1809	13.044	-1.611	-25.548	49.17	-101.61	2.067	0.900	1.115	-0.090
1.175	2.5862	0.1913	1.1394	15.159	-5.284	-26.457	46.36	-120.23	2.138	0.879	1.017	-0.035
1.200	2.6158	0.1784	1.0956	17.147	-9.079	-27.141	43.18	-132.96	2.217	0.842	0.908	0.004
1.225	2.6461	0.1659	1.0496	18.938	-12.956	-27.652	39.76	-142.66	2.305	0.803	0.793	0.021
1.250	2.6771	0.1535	1.0012	20.436	-16.898	-28.047	36.09	-150.15	2.402	0.766	0.683	0.029
1.275	2.7091	0.1414	0.9503	21.587	-20.873	-28.373	32.27	-153.94	2.508	0.727	0.579	0.030
1.300	2.7423	0.1292	0.8970	22.388	-24.861	-28.660	28.42	-153.01	2.623	0.680	0.485	0.027
1.325	2.7769	0.1169	0.8409	22.814	-28.841	-28.976	24.65	-148.54	2.747	0.630	0.398	0.039
1.350	2.8130	0.1044	0.7820	22.928	-32.693	-29.411	21.02	-142.46	2.880	0.586	0.322	0.044
1.375	2.8508	0.0915	0.7201	22.720	-36.380	-30.029	17.55	-134.21	3.022	0.545	0.256	0.052

The trajectory and determined quantities tabulated for flight J of the balsa glider with an aspect ratio of 11.7 which is shown in Figs. 6.32 and 6.33.

Test Conditions				
aircraft	balsa glider	flight	regression J	
aspect ratio	11.7	test number	6162	
m (g)	7.92	I_{xx} (g·cm^2)	291.14	
I_{yy} (g·cm^2)	325.10	I_{zz} (g·cm^2)	610.41	
I_{xz} (g·cm^2)	11.85	I_{xy} (g·cm^2)	0.60	
I_{yz} (g·cm^2)	-0.23	δ_e (deg)	0.94	
CG (%c)	33.6			
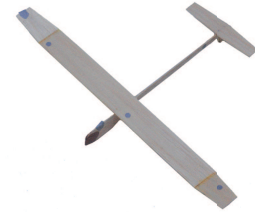
time	x	y	z	ϕ	θ	ψ	V	α	$\dot{\alpha}$	C_L	C_D	C_m
(s)	(m)	(m)	(m)	(deg)	(deg)	(deg)	(m/s)	(deg)	(deg/s)			
0.000	-2.6671	0.0154	1.4876	6.426	-3.144	16.096	3.61	-4.64	5.003	0.527	-0.146	-0.005
0.025	-2.5430	0.0345	1.4750	6.753	-3.125	17.055	3.49	-4.00	5.088	0.504	-0.088	-0.003
0.050	-2.4174	0.0551	1.4627	7.215	-3.130	17.985	3.40	-3.09	5.145	0.487	-0.034	-0.000
0.075	-2.2909	0.0772	1.4506	7.781	-3.149	18.873	3.35	-1.90	5.172	0.478	0.018	0.002
0.100	-2.1637	0.1009	1.4387	8.448	-3.183	19.717	3.31	-0.40	5.138	0.482	0.097	0.004
0.125	-2.0387	0.1258	1.4273	9.092	-3.181	20.465	3.31	1.78	5.104	0.482	0.098	0.004
0.150	-1.9147	0.1522	1.4161	9.760	-3.154	21.138	3.39	3.35	5.073	0.483	0.092	0.001
0.175	-1.7918	0.1801	1.4050	10.427	-3.130	21.748	3.48	2.57	5.049	0.486	0.085	-0.002
0.200	-1.6698	0.2094	1.3940	11.027	-3.136	22.348	3.52	-0.09	5.030	0.491	0.083	-0.001
0.225	-1.5486	0.2401	1.3831	11.555	-3.164	22.951	3.48	-1.95	5.010	0.495	0.087	0.000
0.250	-1.4284	0.2722	1.3723	12.031	-3.201	23.572	3.42	-0.75	4.984	0.494	0.093	0.000
0.275	-1.3093	0.3059	1.3616	12.519	-3.246	24.212	3.44	3.13	4.954	0.486	0.095	-0.002
0.300	-1.1915	0.3411	1.3508	13.016	-3.319	24.881	3.58	6.71	4.926	0.476	0.094	-0.003
0.325	-1.0748	0.3779	1.3395	13.482	-3.433	25.575	3.78	6.92	4.904	0.474	0.090	-0.003
0.350	-0.9591	0.4160	1.3276	13.855	-3.583	26.281	3.92	3.56	4.885	0.481	0.089	-0.002
0.375	-0.8445	0.4555	1.3153	14.149	-3.751	26.972	3.95	-0.63	4.867	0.492	0.089	-0.002
0.400	-0.7308	0.4964	1.3028	14.399	-3.932	27.648	3.89	-2.71	4.849	0.501	0.090	-0.001
0.425	-0.6182	0.5387	1.2900	14.648	-4.127	28.342	3.81	-2.27	4.831	0.503	0.090	0.000
0.450	-0.5067	0.5826	1.2770	14.876	-4.343	29.085	3.78	-1.23	4.815	0.504	0.090	0.001
0.475	-0.3962	0.6280	1.2636	15.091	-4.570	29.886	3.76	-1.20	4.800	0.507	0.091	0.001
0.500	-0.2869	0.6748	1.2498	15.313	-4.807	30.734	3.72	-1.79	4.785	0.511	0.092	0.001

time	x	y	z	ϕ	θ	ψ	V	α	$\dot{\alpha}$	C_L	C_D	C_m
(s)	(m)	(m)	(m)	(deg)	(deg)	(deg)	(m/s)	(deg)	(deg/s)			
0.525	-0.1786	0.7233	1.2358	15.601	-5.055	31.614	3.67	-1.60	4.770	0.512	0.092	-0.001
0.550	-0.0716	0.7733	1.2213	15.976	-5.333	32.528	3.64	-0.46	4.757	0.510	0.092	-0.001
0.575	0.0343	0.8250	1.2064	16.398	-5.648	33.479	3.64	0.00	4.745	0.508	0.092	-0.000
0.600	0.1390	0.8781	1.1910	16.802	-5.997	34.451	3.64	-1.29	4.735	0.511	0.093	0.003
0.625	0.2426	0.9328	1.1750	17.141	-6.337	35.406	3.59	-3.22	4.725	0.516	0.094	0.004
0.650	0.3449	0.9892	1.1587	17.386	-6.645	36.307	3.49	-3.11	4.716	0.516	0.094	0.004
0.675	0.4460	1.0473	1.1419	17.494	-6.921	37.166	3.42	-0.11	4.707	0.507	0.092	0.000
0.700	0.5458	1.1069	1.1244	17.452	-7.203	38.033	3.48	3.39	4.700	0.493	0.087	-0.003
0.725	0.6446	1.1678	1.1063	17.274	-7.520	38.968	3.61	4.72	4.699	0.483	0.080	-0.005
0.750	0.7424	1.2301	1.0873	17.055	-7.885	39.992	3.72	3.81	4.705	0.478	0.074	-0.006
0.775	0.8394	1.2939	1.0673	16.868	-8.293	41.064	3.79	3.25	4.719	0.473	0.074	-0.004
0.800	0.9354	1.3593	1.0463	16.762	-8.702	42.086	3.86	3.87	4.728	0.468	0.081	-0.003
0.825	1.0304	1.4261	1.0244	16.713	-9.108	43.037	3.98	3.77	4.733	0.466	0.090	-0.003
0.850	1.1243	1.4943	1.0014	16.700	-9.526	43.962	4.06	1.41	4.735	0.472	0.092	-0.002
0.875	1.2170	1.5640	0.9774	16.706	-9.988	44.986	4.05	-2.20	4.741	0.483	0.086	0.001
0.900	1.3086	1.6353	0.9527	16.735	-10.480	46.103	3.94	-5.04	4.757	0.491	0.079	0.003
0.925	1.3992	1.7083	0.9272	16.777	-10.999	47.345	3.79	-6.85	4.774	0.499	0.072	0.005
0.950	1.4887	1.7832	0.9011	16.827	-11.554	48.770	3.61	-7.87	4.796	0.506	0.065	0.008

The trajectory and determined quantities tabulated for the 11 regression flights of the balsa glider with an aspect ratio of 11.7. The tables include the specific test conditions and a time history of the important parameters for each of the 11 flights.

Test Conditions				
aircraft	balsa glider	flight	regression 1	
aspect ratio	11.7	test number	6363	
m (g)	6.25	I_{xx} (g·cm^2)	290.74	
I_{yy} (g·cm^2)	275.64	I_{zz} (g·cm^2)	561.35	
I_{xz} (g·cm^2)	7.40	I_{xy} (g·cm^2)	0.74	
I_{yz} (g·cm^2)	-0.22	δ_e (deg)	0.94	
CG (%c)	0.8			

time	x	y	z	ϕ	θ	ψ	V	α	$\dot{\alpha}$	C_L	C_D	C_m
(s)	(m)	(m)	(m)	(deg)	(deg)	(deg)	(m/s)	(deg)	(deg/s)			
0.000	-1.9618	-0.2419	1.0876	-14.707	21.822	13.398	4.32	-2.16	5.427	0.658	0.101	-0.018
0.025	-1.8333	-0.2344	1.1246	-14.808	24.882	13.957	4.26	-1.30	5.284	0.666	0.103	-0.009
0.050	-1.7099	-0.2303	1.1658	-14.766	27.895	14.388	4.28	0.71	5.132	0.680	0.108	-0.008
0.075	-1.5918	-0.2295	1.2106	-14.592	30.816	14.683	4.31	1.79	4.971	0.699	0.113	-0.008
0.100	-1.4794	-0.2318	1.2585	-14.289	33.641	14.815	4.37	2.44	4.802	0.721	0.119	-0.010
0.125	-1.3729	-0.2371	1.3088	-13.876	36.364	14.782	4.44	3.93	4.626	0.744	0.123	-0.011
0.150	-1.2726	-0.2451	1.3610	-13.398	38.994	14.579	4.57	6.81	4.446	0.765	0.129	-0.016
0.175	-1.1784	-0.2556	1.4145	-12.907	41.512	14.219	4.79	10.85	4.260	0.781	0.136	-0.025
0.200	-1.0903	-0.2684	1.4685	-12.440	43.897	13.722	5.12	15.75	4.067	0.792	0.146	-0.037
0.225	-1.0081	-0.2831	1.5223	-12.001	46.098	13.105	5.59	21.73	3.870	0.799	0.158	-0.050
0.250	-0.9317	-0.2994	1.5750	-11.573	48.086	12.369	6.22	29.30	3.670	0.803	0.172	-0.062
0.275	-0.8606	-0.3170	1.6261	-11.128	49.832	11.493	7.06	38.59	3.469	0.808	0.190	-0.073
0.300	-0.7946	-0.3357	1.6750	-10.631	51.334	10.436	8.16	49.34	3.267	0.820	0.213	-0.085
0.325	-0.7331	-0.3551	1.7210	-10.046	52.593	9.156	9.54	61.38	3.066	0.842	0.241	-0.096
0.350	-0.6760	-0.3750	1.7639	-9.354	53.630	7.631	11.24	74.44	2.865	0.876	0.275	-0.113
0.375	-0.6228	-0.3952	1.8033	-8.558	54.459	5.871	13.28	88.56	2.667	0.921	0.320	-0.143
0.400	-0.5733	-0.4156	1.8389	-7.672	55.073	3.903	15.69	104.38	2.472	0.973	0.378	-0.188
0.425	-0.5273	-0.4361	1.8706	-6.692	55.445	1.733	18.53	123.80	2.281	1.027	0.450	-0.237
0.450	-0.4845	-0.4563	1.8981	-5.624	55.569	-0.618	21.90	148.55	2.096	1.077	0.534	-0.285
0.475	-0.4446	-0.4762	1.9212	-4.480	55.464	-3.120	25.97	177.96	1.923	1.119	0.633	-0.334

continued on next page

time	x	y	z	ϕ	θ	ψ	V	α	$\dot{\alpha}$	C_L	C_D	C_m
(s)	(m)	(m)	(m)	(deg)	(deg)	(deg)	(m/s)	(deg)	(deg/s)			
0.500	-0.4071	-0.4957	1.9398	-3.297	55.159	-5.707	30.81	208.45	1.765	1.159	0.754	-0.385
0.525	-0.3719	-0.5148	1.9537	-2.106	54.671	-8.311	36.40	236.68	1.625	1.206	0.922	-0.435
0.550	-0.3386	-0.5333	1.9630	-0.917	54.015	-10.874	42.64	262.97	1.505	1.235	1.152	-0.483
0.575	-0.3073	-0.5512	1.9675	0.279	53.197	-13.342	49.50	288.65	1.405	1.204	1.432	-0.516
0.600	-0.2779	-0.5686	1.9673	1.485	52.234	-15.703	56.98	309.70	1.331	1.071	1.711	-0.543
0.625	-0.2502	-0.5852	1.9623	2.716	51.140	-18.012	64.90	316.60	1.288	0.857	1.919	-0.580
0.650	-0.2241	-0.6011	1.9526	3.979	49.915	-20.326	72.74	303.20	1.281	0.615	2.032	-0.638
0.675	-0.1994	-0.6162	1.9380	5.295	48.541	-22.702	79.98	273.55	1.307	0.389	2.099	-0.678
0.700	-0.1763	-0.6305	1.9189	6.654	46.995	-25.078	86.32	237.54	1.354	0.171	2.131	-0.667
0.725	-0.1547	-0.6439	1.8953	8.022	45.249	-27.346	91.78	200.74	1.416	-0.028	2.115	-0.618
0.750	-0.1348	-0.6563	1.8676	9.347	43.271	-29.358	96.34	161.76	1.489	-0.184	2.029	-0.572
0.775	-0.1166	-0.6676	1.8359	10.589	41.004	-31.040	99.88	118.90	1.574	-0.270	1.906	-0.529
0.800	-0.1000	-0.6778	1.8003	11.724	38.393	-32.374	102.28	74.23	1.667	-0.307	1.796	-0.481
0.825	-0.0849	-0.6868	1.7613	12.773	35.411	-33.456	103.59	31.90	1.759	-0.318	1.717	-0.434
0.850	-0.0713	-0.6946	1.7190	13.706	32.038	-34.310	103.88	-6.59	1.847	-0.320	1.654	-0.389
0.875	-0.0591	-0.7012	1.6738	14.523	28.276	-34.988	103.26	-43.36	1.931	-0.307	1.591	-0.351
0.900	-0.0482	-0.7065	1.6260	15.176	24.108	-35.439	101.73	-80.51	2.014	-0.271	1.529	-0.324
0.925	-0.0383	-0.7106	1.5758	15.656	19.510	-35.654	99.23	-119.63	2.092	-0.210	1.485	-0.297
0.950	-0.0293	-0.7134	1.5235	15.928	14.483	-35.620	95.75	-160.22	2.162	-0.122	1.461	-0.278
0.975	-0.0208	-0.7151	1.4694	15.923	9.045	-35.400	91.24	-200.25	2.223	-0.014	1.442	-0.272
1.000	-0.0126	-0.7160	1.4138	15.519	3.216	-35.037	85.76	-236.46	2.277	0.105	1.412	-0.274
1.025	-0.0044	-0.7164	1.3569	14.665	-2.971	-34.625	79.44	-266.27	2.328	0.225	1.359	-0.268
1.050	0.0043	-0.7164	1.2988	13.363	-9.472	-34.238	72.48	-289.91	2.380	0.347	1.276	-0.231
1.075	0.0138	-0.7162	1.2394	11.746	-16.208	-33.966	65.01	-308.42	2.439	0.466	1.167	-0.163
1.100	0.0245	-0.7161	1.1787	9.911	-23.065	-33.877	57.12	-321.47	2.506	0.574	1.035	-0.081
1.125	0.0369	-0.7164	1.1165	7.918	-29.926	-34.045	48.99	-326.88	2.584	0.647	0.879	-0.004
1.150	0.0512	-0.7177	1.0525	5.803	-36.688	-34.530	40.84	-323.08	2.681	0.666	0.705	0.056
1.175	0.0676	-0.7202	0.9862	3.632	-43.314	-35.346	32.91	-309.71	2.799	0.621	0.530	0.103
1.200	0.0862	-0.7242	0.9171	1.509	-49.776	-36.441	25.43	-287.27	2.942	0.526	0.375	0.152
1.225	0.1067	-0.7296	0.8447	-0.460	-55.991	-37.735	18.61	-256.61	3.107	0.407	0.256	0.207
1.250	0.1288	-0.7362	0.7683	-2.215	-61.802	-39.180	12.67	-217.54	3.290	0.293	0.175	0.262
1.275	0.1524	-0.7438	0.6873	-3.714	-66.964	-40.715	7.76	-172.74	3.484	0.197	0.126	0.304
1.300	0.1769	-0.7521	0.6016	-4.954	-71.197	-42.258	4.09	-124.43	3.686	0.126	0.099	0.313
1.325	0.2022	-0.7607	0.5108	-5.990	-74.374	-43.674	1.59	-73.04	3.885	0.070	0.079	0.314
1.350	0.2281	-0.7695	0.4150	-6.888	-76.384	-44.833	0.43	-18.23	4.093	0.023	0.059	0.317

	Test Conditions				
aircraft	balsa glider	flight	regression 2		
aspect ratio	11.7	test number	6355		
m (g)	6.25	I_{xx} (g·cm^2)	290.74		
I_{yy} (g·cm^2)	275.64	I_{zz} (g·cm^2)	561.35		
I_{xz} (g·cm^2)	7.40	I_{xy} (g·cm^2)	0.74		
I_{yz} (g·cm^2)	-0.22	δ_e (deg)	0.94		
CG (%c)	0.8				
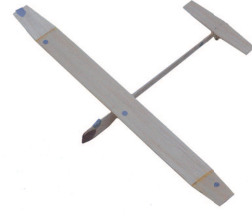
time	x	y	z	ϕ	θ	ψ	V	α	$\dot{\alpha}$	C_L	C_D	C_m
(s)	(m)	(m)	(m)	(deg)	(deg)	(deg)	(m/s)	(deg)	(deg/s)			
0.000	-3.2238	-0.1562	1.1925	-2.679	4.187	31.378	5.84	20.11	5.407	0.650	0.024	-0.136
0.025	-3.1070	-0.0907	1.1915	-3.220	6.748	31.706	5.54	-8.67	5.262	0.685	0.099	-0.051
0.050	-2.9931	-0.0271	1.1969	-3.646	9.122	31.982	5.31	-10.20	5.185	0.687	0.097	-0.008
0.075	-2.8809	0.0348	1.2077	-4.020	11.675	32.261	5.32	0.82	5.097	0.693	0.098	-0.004
0.100	-2.7710	0.0948	1.2238	-4.366	14.235	32.593	5.40	4.44	5.000	0.702	0.100	-0.006
0.125	-2.6635	0.1524	1.2445	-4.669	16.772	32.940	5.50	4.93	4.894	0.713	0.103	-0.011
0.150	-2.5588	0.2076	1.2695	-4.913	19.251	33.244	5.64	4.54	4.781	0.724	0.106	-0.018
0.175	-2.4572	0.2603	1.2984	-5.084	21.606	33.428	5.74	3.22	4.658	0.737	0.110	-0.021
0.200	-2.3590	0.3103	1.3305	-5.208	23.818	33.509	5.79	2.41	4.526	0.751	0.115	-0.019
0.225	-2.2643	0.3575	1.3655	-5.317	25.926	33.532	5.86	3.79	4.388	0.764	0.119	-0.017
0.250	-2.1732	0.4019	1.4027	-5.439	27.965	33.553	5.99	6.94	4.244	0.776	0.123	-0.020
0.275	-2.0858	0.4434	1.4415	-5.566	29.928	33.558	6.22	10.98	4.096	0.784	0.127	-0.029
0.300	-2.0021	0.4820	1.4815	-5.655	31.769	33.512	6.54	15.08	3.943	0.792	0.133	-0.042
0.325	-1.9219	0.5180	1.5218	-5.637	33.429	33.357	6.97	19.01	3.787	0.799	0.141	-0.052
0.350	-1.8453	0.5513	1.5621	-5.471	34.879	33.062	7.49	22.72	3.628	0.809	0.152	-0.060
0.375	-1.7722	0.5822	1.6017	-5.139	36.114	32.610	8.11	26.51	3.467	0.822	0.166	-0.071
0.400	-1.7024	0.6108	1.6401	-4.662	37.135	32.015	8.82	30.95	3.303	0.836	0.183	-0.086
0.425	-1.6359	0.6373	1.6770	-4.074	37.923	31.302	9.66	36.25	3.139	0.848	0.202	-0.106
0.450	-1.5725	0.6620	1.7119	-3.406	38.452	30.505	10.64	42.56	2.975	0.858	0.223	-0.124
0.475	-1.5120	0.6849	1.7443	-2.650	38.711	29.624	11.80	49.80	2.814	0.870	0.247	-0.139
0.500	-1.4542	0.7064	1.7739	-1.783	38.708	28.645	13.15	58.23	2.658	0.883	0.274	-0.154
0.525	-1.3989	0.7267	1.8005	-0.780	38.457	27.574	14.72	68.01	2.507	0.900	0.308	-0.167
0.550	-1.3460	0.7458	1.8237	0.351	37.976	26.453	16.55	79.05	2.364	0.921	0.349	-0.170

continued on next page

186

time	x	y	z	ϕ	θ	ψ	V	α	$\dot{\alpha}$	C_L	C_D	C_m
(s)	(m)	(m)	(m)	(deg)	(deg)	(deg)	(m/s)	(deg)	(deg/s)			
0.575	-1.2952	0.7641	1.8434	1.578	37.308	25.330	18.68	90.83	2.230	0.948	0.398	-0.169
0.600	-1.2464	0.7815	1.8593	2.852	36.481	24.229	21.10	103.08	2.107	0.978	0.455	-0.174
0.625	-1.1995	0.7983	1.8715	4.148	35.513	23.126	23.82	115.34	1.997	1.009	0.520	-0.194
0.650	-1.1544	0.8147	1.8797	5.450	34.395	21.996	26.85	126.44	1.902	1.035	0.596	-0.210
0.675	-1.1109	0.8306	1.8840	6.743	33.126	20.865	30.13	134.79	1.823	1.062	0.683	-0.200
0.700	-1.0689	0.8464	1.8842	8.009	31.727	19.779	33.57	139.20	1.763	1.088	0.782	-0.174
0.725	-1.0284	0.8618	1.8805	9.240	30.228	18.785	37.07	140.41	1.719	1.108	0.889	-0.163
0.750	-0.9894	0.8772	1.8730	10.406	28.633	17.918	40.54	138.40	1.693	1.103	0.987	-0.182
0.775	-0.9518	0.8924	1.8617	11.491	26.915	17.184	43.95	132.07	1.683	1.069	1.069	-0.215
0.800	-0.9155	0.9076	1.8466	12.464	25.016	16.594	47.12	119.90	1.692	1.020	1.138	-0.230
0.825	-0.8804	0.9227	1.8279	13.306	22.911	16.150	49.91	101.37	1.714	0.967	1.202	-0.227
0.850	-0.8466	0.9378	1.8057	13.970	20.587	15.866	52.17	80.11	1.745	0.920	1.252	-0.215
0.875	-0.8140	0.9528	1.7802	14.394	18.040	15.754	53.85	54.81	1.784	0.880	1.269	-0.206
0.900	-0.7822	0.9680	1.7512	14.516	15.241	15.812	54.99	27.83	1.857	0.850	1.439	-0.166
0.925	-0.7518	0.9829	1.7197	14.331	12.278	15.983	55.25	4.45	1.869	0.878	1.654	-0.141
0.950	-0.7233	0.9976	1.6868	13.871	9.229	16.213	55.06	-16.24	1.850	0.899	1.371	-0.203
0.975	-0.6955	1.0125	1.6512	13.122	5.999	16.486	54.50	-39.40	1.921	0.869	0.843	-0.262
1.000	-0.6674	1.0280	1.6120	12.020	2.506	16.821	53.19	-67.41	2.100	0.791	0.585	-0.252
1.025	-0.6388	1.0443	1.5692	10.540	-1.249	17.198	51.09	-92.02	2.280	0.731	0.655	-0.194
1.050	-0.6094	1.0613	1.5230	8.695	-5.230	17.552	48.55	-107.93	2.335	0.731	1.022	-0.116
1.075	-0.5803	1.0785	1.4754	6.574	-9.282	17.790	45.75	-120.39	2.323	0.786	1.160	-0.069
1.100	-0.5517	1.0956	1.4271	4.277	-13.317	17.894	42.59	-133.78	2.371	0.818	0.979	-0.053
1.125	-0.5227	1.1129	1.3773	1.865	-17.406	17.865	39.06	-146.17	2.457	0.816	0.780	-0.017
1.150	-0.4926	1.1306	1.3256	-0.622	-21.521	17.730	35.30	-154.08	2.545	0.801	0.670	0.031
1.175	-0.4613	1.1486	1.2719	-3.136	-25.598	17.473	31.39	-157.21	2.641	0.769	0.564	0.066
1.200	-0.4284	1.1667	1.2161	-5.637	-29.585	17.080	27.47	-156.18	2.749	0.717	0.459	0.076
1.225	-0.3938	1.1853	1.1579	-8.055	-33.505	16.556	23.61	-151.63	2.871	0.646	0.366	0.080
1.250	-0.3573	1.2041	1.0971	-10.318	-37.364	15.918	19.92	-143.97	3.004	0.564	0.291	0.088
1.275	-0.3189	1.2232	1.0334	-12.349	-41.177	15.187	16.45	-132.77	3.145	0.482	0.234	0.117
1.300	-0.2788	1.2426	0.9664	-14.104	-44.834	14.399	13.31	-117.33	3.294	0.414	0.190	0.158
1.325	-0.2369	1.2622	0.8959	-15.568	-48.145	13.632	10.60	-97.87	3.450	0.368	0.156	0.200
1.350	-0.1933	1.2820	0.8218	-16.750	-50.834	13.001	8.44	-75.64	3.612	0.344	0.130	0.218

Test Conditions				
aircraft	balsa glider	flight	regression 3	
aspect ratio	11.7	test number	6099	
m (g)	7.20	I_{xx} (g·cm^2)	290.99	
I_{yy} (g·cm^2)	306.59	I_{zz} (g·cm^2)	592.04	
I_{xz} (g·cm^2)	10.19	I_{xy} (g·cm^2)	0.65	
I_{yz} (g·cm^2)	-0.23	δ_e (deg)	-1.42	
CG (%c)	0.48			
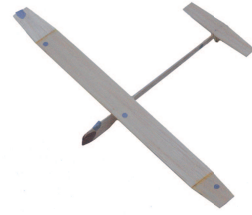
time	x	y	z	ϕ	θ	ψ	V	α	$\dot{\alpha}$	C_L	C_D	C_m
(s)	(m)	(m)	(m)	(deg)	(deg)	(deg)	(m/s)	(deg)	(deg/s)			
0.000	-3.1205	0.0805	0.9817	-1.432	-5.305	10.211	4.02	-4.17	4.994	0.562	0.084	0.004
0.025	-2.9995	0.1040	0.9625	-2.248	-4.551	10.306	3.93	-3.30	4.985	0.565	0.083	0.003
0.050	-2.8784	0.1272	0.9451	-2.793	-3.776	10.411	3.85	-2.92	4.973	0.568	0.082	0.002
0.075	-2.7574	0.1500	0.9296	-3.150	-2.987	10.521	3.77	-3.01	4.958	0.573	0.081	0.001
0.100	-2.6365	0.1725	0.9159	-3.404	-2.191	10.639	3.70	-4.03	4.941	0.580	0.079	0.001
0.125	-2.5157	0.1947	0.9041	-3.639	-1.386	10.743	3.58	-3.73	4.923	0.582	0.079	-0.000
0.150	-2.3953	0.2164	0.8943	-3.959	-0.585	10.842	3.51	-1.64	4.899	0.579	0.083	-0.002
0.175	-2.2753	0.2376	0.8863	-4.395	0.210	10.946	3.51	0.94	4.868	0.576	0.087	-0.003
0.200	-2.1560	0.2582	0.8799	-4.884	0.984	11.047	3.56	2.10	4.833	0.577	0.088	-0.003
0.225	-2.0374	0.2780	0.8749	-5.348	1.744	11.134	3.61	1.94	4.796	0.582	0.086	-0.002
0.250	-1.9195	0.2972	0.8714	-5.757	2.490	11.193	3.65	1.20	4.760	0.590	0.084	-0.000
0.275	-1.8024	0.3156	0.8692	-6.126	3.242	11.239	3.67	0.52	4.724	0.599	0.084	-0.000
0.300	-1.6861	0.3333	0.8684	-6.469	3.996	11.288	3.68	0.48	4.683	0.607	0.087	-0.001
0.325	-1.5708	0.3501	0.8691	-6.779	4.747	11.332	3.69	1.30	4.638	0.614	0.090	-0.003
0.350	-1.4566	0.3661	0.8710	-7.028	5.484	11.355	3.74	2.62	4.589	0.618	0.091	-0.005
0.375	-1.3435	0.3811	0.8741	-7.196	6.189	11.335	3.83	3.97	4.540	0.621	0.092	-0.007
0.400	-1.2316	0.3953	0.8782	-7.281	6.852	11.267	3.94	4.85	4.489	0.625	0.093	-0.009
0.425	-1.1210	0.4086	0.8832	-7.310	7.467	11.160	4.07	4.92	4.436	0.632	0.094	-0.010
0.450	-1.0116	0.4211	0.8889	-7.312	8.025	11.020	4.18	4.03	4.381	0.642	0.096	-0.009
0.475	-0.9036	0.4327	0.8954	-7.305	8.535	10.845	4.27	2.54	4.325	0.655	0.099	-0.008
0.500	-0.7970	0.4435	0.9025	-7.297	9.010	10.636	4.31	1.37	4.267	0.669	0.101	-0.008
0.525	-0.6918	0.4534	0.9103	-7.295	9.451	10.392	4.33	0.94	4.207	0.682	0.103	-0.011
0.550	-0.5881	0.4626	0.9186	-7.302	9.845	10.128	4.36	1.10	4.146	0.691	0.104	-0.014

time	x	y	z	ϕ	θ	ψ	V	α	$\dot{\alpha}$	C_L	C_D	C_m
(s)	(m)	(m)	(m)	(deg)	(deg)	(deg)	(m/s)	(deg)	(deg/s)			
0.575	-0.4859	0.4709	0.9274	-7.301	10.177	9.852	4.40	1.67	4.086	0.699	0.105	-0.014
0.600	-0.3852	0.4784	0.9365	-7.267	10.447	9.551	4.45	2.73	4.024	0.706	0.108	-0.012
0.625	-0.2860	0.4851	0.9457	-7.170	10.676	9.200	4.53	4.34	3.962	0.714	0.112	-0.012
0.650	-0.1884	0.4912	0.9551	-7.003	10.861	8.778	4.66	6.07	3.898	0.719	0.115	-0.019
0.675	-0.0923	0.4965	0.9643	-6.774	10.980	8.290	4.84	7.57	3.835	0.721	0.116	-0.027
0.700	0.0023	0.5013	0.9732	-6.501	10.993	7.764	5.05	9.26	3.774	0.719	0.118	-0.029
0.725	0.0954	0.5053	0.9817	-6.214	10.903	7.220	5.30	11.59	3.714	0.715	0.121	-0.024
0.750	0.1872	0.5088	0.9894	-5.967	10.735	6.677	5.62	14.20	3.656	0.715	0.126	-0.017
0.775	0.2776	0.5118	0.9962	-5.810	10.527	6.133	6.00	15.39	3.599	0.724	0.130	-0.015
0.800	0.3666	0.5143	1.0021	-5.774	10.284	5.594	6.39	14.09	3.545	0.742	0.133	-0.016
0.825	0.4545	0.5165	1.0069	-5.824	10.004	5.064	6.70	10.97	3.494	0.767	0.135	-0.021
0.850	0.5411	0.5181	1.0109	-5.874	9.659	4.534	6.92	7.59	3.446	0.790	0.140	-0.027
0.875	0.6267	0.5193	1.0139	-5.857	9.235	3.996	7.08	4.97	3.400	0.810	0.145	-0.033
0.900	0.7111	0.5199	1.0161	-5.768	8.716	3.457	7.18	3.20	3.355	0.824	0.151	-0.033
0.925	0.7944	0.5201	1.0174	-5.671	8.115	2.933	7.25	2.50	3.312	0.834	0.154	-0.030
0.950	0.8767	0.5197	1.0176	-5.657	7.445	2.447	7.30	2.90	3.273	0.837	0.155	-0.027
0.975	0.9581	0.5188	1.0168	-5.779	6.713	2.007	7.39	3.34	3.239	0.838	0.156	-0.028
1.000	1.0387	0.5174	1.0148	-6.023	5.912	1.591	7.48	2.70	3.209	0.839	0.158	-0.030
1.025	1.1185	0.5154	1.0115	-6.330	5.026	1.182	7.53	1.08	3.182	0.843	0.161	-0.026
1.050	1.1975	0.5129	1.0069	-6.641	4.061	0.771	7.53	0.08	3.159	0.845	0.164	-0.015
1.075	1.2760	0.5100	1.0010	-6.937	3.056	0.366	7.53	0.80	3.141	0.845	0.166	-0.003
1.100	1.3539	0.5065	0.9936	-7.229	2.051	-0.034	7.58	3.10	3.127	0.840	0.168	0.002
1.125	1.4314	0.5025	0.9849	-7.545	1.067	-0.442	7.68	5.71	3.117	0.830	0.169	-0.008
1.150	1.5084	0.4980	0.9746	-7.905	0.065	-0.877	7.85	6.79	3.113	0.815	0.171	-0.028
1.175	1.5851	0.4931	0.9626	-8.286	-1.025	-1.345	8.01	4.36	3.113	0.803	0.174	-0.040
1.200	1.6616	0.4877	0.9490	-8.660	-2.245	-1.845	8.07	-1.63	3.118	0.803	0.178	-0.034
1.225	1.7379	0.4818	0.9336	-9.019	-3.578	-2.366	7.93	-8.26	3.126	0.809	0.181	-0.012
1.250	1.8141	0.4752	0.9167	-9.386	-4.950	-2.909	7.65	-12.04	3.139	0.813	0.179	0.008
1.275	1.8902	0.4680	0.8982	-9.796	-6.299	-3.486	7.33	-12.14	3.156	0.805	0.171	0.014
1.300	1.9664	0.4600	0.8783	-10.251	-7.621	-4.089	7.06	-10.85	3.180	0.787	0.157	0.011
1.325	2.0429	0.4512	0.8567	-10.708	-8.936	-4.716	6.81	-10.19	3.212	0.763	0.140	0.009
1.350	2.1196	0.4417	0.8334	-11.092	-10.264	-5.344	6.56	-9.34	3.252	0.738	0.124	0.017
1.375	2.1969	0.4315	0.8084	-11.393	-11.557	-5.973	6.32	-8.24	3.298	0.709	0.105	0.026
1.400	2.2749	0.4205	0.7814	-11.608	-12.803	-6.582	6.16	-6.73	3.357	0.685	0.106	0.040
1.425	2.3536	0.4087	0.7526	-11.724	-13.954	-7.218	6.00	-4.32	3.410	0.672	0.116	0.053
1.450	2.4329	0.3961	0.7220	-11.693	-14.970	-7.902	5.93	-0.17	3.466	0.653	0.118	0.064

time	x	y	z	ϕ	θ	ψ	V	α	$\dot{\alpha}$	C_L	C_D	C_m
(s)	(m)	(m)	(m)	(deg)	(deg)	(deg)	(m/s)	(deg)	(deg/s)			
1.475	2.5130	0.3827	0.6897	-11.504	-15.816	-8.654	6.00	5.43	3.524	0.635	0.118	0.074

aircraft	balsa glider	flight	regression 4
aspect ratio	11.7	test number	6348
m (g)	6.25	I_{xx} (g·cm^2)	290.74
I_{yy} (g·cm^2)	275.64	I_{zz} (g·cm^2)	561.35
I_{xz} (g·cm^2)	7.40	I_{xy} (g·cm^2)	0.74
I_{yz} (g·cm^2)	-0.22	δ_e (deg)	0.94
CG (%c)	0.8		
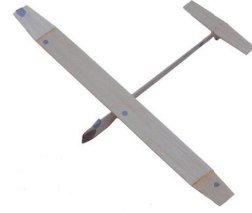
time	x	y	z	ϕ	θ	ψ	V	α	$\dot{\alpha}$	C_L	C_D	C_m
(s)	(m)	(m)	(m)	(deg)	(deg)	(deg)	(m/s)	(deg)	(deg/s)			
0.000	-1.8520	0.2585	1.0083	-8.432	9.267	25.424	3.80	2.82	5.024	0.572	0.082	-0.009
0.025	-1.7367	0.3043	1.0204	-8.681	10.829	25.714	3.87	3.37	4.951	0.574	0.082	-0.008
0.050	-1.6230	0.3483	1.0351	-8.926	12.336	25.945	3.97	3.82	4.871	0.579	0.086	-0.007
0.075	-1.5112	0.3904	1.0521	-9.207	13.806	26.142	4.06	3.41	4.782	0.589	0.091	-0.008
0.100	-1.4015	0.4305	1.0713	-9.499	15.225	26.314	4.14	2.87	4.687	0.602	0.095	-0.009
0.125	-1.2940	0.4684	1.0923	-9.739	16.589	26.424	4.20	2.90	4.589	0.615	0.095	-0.008
0.150	-1.1887	0.5043	1.1150	-9.927	17.888	26.448	4.28	3.60	4.490	0.628	0.095	-0.007
0.175	-1.0858	0.5381	1.1391	-10.114	19.136	26.388	4.38	4.02	4.388	0.645	0.098	-0.004
0.200	-0.9853	0.5698	1.1645	-10.365	20.359	26.286	4.49	3.60	4.283	0.667	0.103	-0.002
0.225	-0.8873	0.5994	1.1909	-10.674	21.578	26.164	4.57	2.84	4.174	0.694	0.109	-0.000
0.250	-0.7918	0.6267	1.2183	-10.974	22.804	26.013	4.63	2.79	4.060	0.724	0.116	-0.002
0.275	-0.6992	0.6517	1.2464	-11.202	24.022	25.800	4.71	4.17	3.942	0.752	0.122	-0.010
0.300	-0.6093	0.6743	1.2751	-11.355	25.192	25.509	4.84	6.21	3.820	0.776	0.128	-0.020
0.325	-0.5222	0.6947	1.3040	-11.491	26.273	25.147	5.03	7.92	3.696	0.796	0.133	-0.031
0.350	-0.4380	0.7128	1.3329	-11.647	27.224	24.725	5.24	9.56	3.571	0.813	0.139	-0.040
0.375	-0.3566	0.7288	1.3615	-11.809	28.028	24.238	5.51	12.32	3.446	0.828	0.147	-0.048
0.400	-0.2780	0.7428	1.3894	-11.940	28.672	23.674	5.86	16.74	3.320	0.839	0.155	-0.059
0.425	-0.2020	0.7550	1.4162	-12.022	29.129	23.027	6.35	21.84	3.195	0.848	0.165	-0.069
0.450	-0.1287	0.7655	1.4416	-12.081	29.386	22.300	6.96	26.50	3.073	0.859	0.176	-0.077
0.475	-0.0577	0.7744	1.4653	-12.140	29.437	21.500	7.68	30.82	2.953	0.873	0.191	-0.081
0.500	0.0109	0.7819	1.4871	-12.201	29.295	20.638	8.50	36.02	2.836	0.890	0.208	-0.084
0.525	0.0773	0.7880	1.5066	-12.246	28.978	19.723	9.47	42.40	2.724	0.906	0.229	-0.094
0.550	0.1417	0.7930	1.5237	-12.258	28.476	18.760	10.63	49.24	2.618	0.924	0.259	-0.108

time	x	y	z	ϕ	θ	ψ	V	α	$\dot{\alpha}$	C_L	C_D	C_m
(s)	(m)	(m)	(m)	(deg)	(deg)	(deg)	(m/s)	(deg)	(deg/s)			
0.575	0.2041	0.7970	1.5383	-12.234	27.776	17.736	11.94	55.59	2.516	0.942	0.297	-0.123
0.600	0.2646	0.7998	1.5500	-12.155	26.860	16.647	13.42	62.35	2.419	0.963	0.337	-0.127
0.625	0.3233	0.8016	1.5588	-11.996	25.737	15.483	15.05	70.61	2.330	0.979	0.371	-0.122
0.650	0.3803	0.8025	1.5645	-11.726	24.449	14.252	16.93	79.23	2.254	0.995	0.407	-0.114
0.675	0.4358	0.8025	1.5672	-11.331	23.031	12.950	19.01	85.72	2.190	1.013	0.451	-0.115
0.700	0.4898	0.8021	1.5667	-10.789	21.503	11.582	21.21	88.39	2.136	1.040	0.510	-0.131
0.725	0.5425	0.8013	1.5631	-10.063	19.864	10.143	23.41	88.27	2.090	1.061	0.572	-0.163
0.750	0.5939	0.8000	1.5564	-9.165	18.089	8.652	25.58	85.73	2.055	1.073	0.629	-0.192
0.775	0.6440	0.7984	1.5467	-8.108	16.165	7.110	27.67	79.42	2.031	1.075	0.675	-0.210
0.800	0.6930	0.7965	1.5340	-6.919	14.084	5.530	29.53	68.04	2.020	1.083	0.714	-0.211
0.825	0.7410	0.7944	1.5184	-5.594	11.868	3.928	31.06	53.20	2.019	1.087	0.746	-0.211
0.850	0.7881	0.7921	1.5000	-4.134	9.527	2.356	32.17	37.92	2.029	1.086	0.769	-0.199
0.875	0.8344	0.7898	1.4789	-2.538	7.082	0.869	32.94	23.75	2.047	1.066	0.779	-0.177
0.900	0.8800	0.7874	1.4551	-0.856	4.540	-0.504	33.36	10.05	2.075	1.038	0.774	-0.144
0.925	0.9252	0.7851	1.4288	0.853	1.921	-1.771	33.45	-3.83	2.112	1.008	0.753	-0.105
0.950	0.9700	0.7827	1.3999	2.510	-0.750	-2.944	33.17	-18.23	2.158	0.984	0.719	-0.065
0.975	1.0147	0.7803	1.3685	4.086	-3.439	-4.021	32.55	-32.71	2.214	0.963	0.676	-0.032
1.000	1.0594	0.7780	1.3347	5.557	-6.117	-4.982	31.57	-44.78	2.277	0.933	0.628	-0.021
1.025	1.1044	0.7760	1.2985	6.928	-8.787	-5.792	30.31	-52.25	2.349	0.874	0.588	-0.038
1.050	1.1499	0.7742	1.2599	8.164	-11.503	-6.502	28.95	-55.91	2.425	0.802	0.555	-0.060
1.075	1.1957	0.7725	1.2189	9.189	-14.322	-7.192	27.51	-61.61	2.504	0.736	0.525	-0.065
1.100	1.2419	0.7708	1.1753	9.923	-17.266	-7.926	25.90	-72.04	2.585	0.701	0.483	-0.039
1.125	1.2887	0.7692	1.1291	10.347	-20.287	-8.692	23.93	-83.44	2.675	0.684	0.427	-0.002
1.150	1.3363	0.7677	1.0805	10.493	-23.309	-9.439	21.71	-90.35	2.776	0.662	0.366	0.019
1.175	1.3851	0.7663	1.0293	10.393	-26.292	-10.130	19.43	-90.97	2.885	0.624	0.315	0.024
1.200	1.4352	0.7649	0.9755	10.037	-29.231	-10.818	17.19	-88.71	3.001	0.579	0.274	0.032
1.225	1.4867	0.7633	0.9190	9.413	-32.111	-11.579	15.03	-85.42	3.120	0.541	0.244	0.055

Test Conditions				
aircraft	balsa glider	flight	regression 5	
aspect ratio	11.7	test number	6366	
m (g)	6.25	I_{xx} (g·cm^2)	290.74	
I_{yy} (g·cm^2)	275.64	I_{zz} (g·cm^2)	561.35	
I_{xz} (g·cm^2)	7.40	I_{xy} (g·cm^2)	0.74	
I_{yz} (g·cm^2)	-0.22	δ_e (deg)	0.94	
CG (%c)	0.8			
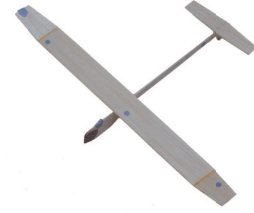
time	x	y	z	ϕ	θ	ψ	V	α	$\dot{\alpha}$	C_L	C_D	C_m
(s)	(m)	(m)	(m)	(deg)	(deg)	(deg)	(m/s)	(deg)	(deg/s)			
0.000	-1.4980	0.2832	0.4064	-10.174	7.043	24.299	3.90	11.01	5.842	0.482	0.084	-0.011
0.025	-1.3587	0.3230	0.4126	-10.573	9.142	24.264	4.13	8.36	5.759	0.491	0.085	-0.007
0.050	-1.2213	0.3607	0.4228	-10.830	11.165	24.134	4.32	6.80	5.669	0.503	0.088	-0.004
0.075	-1.0861	0.3963	0.4370	-10.980	13.144	23.937	4.49	6.32	5.572	0.516	0.091	-0.001
0.100	-0.9533	0.4296	0.4549	-11.076	15.082	23.694	4.64	7.37	5.468	0.532	0.095	0.006
0.125	-0.8234	0.4607	0.4764	-11.095	17.102	23.448	4.84	8.48	5.356	0.553	0.099	0.006
0.150	-0.6965	0.4894	0.5014	-11.124	19.205	23.230	5.06	7.48	5.237	0.575	0.102	-0.002
0.175	-0.5730	0.5156	0.5296	-11.214	21.297	23.027	5.21	3.08	5.112	0.600	0.106	-0.011
0.200	-0.4531	0.5393	0.5609	-11.336	23.284	22.800	5.22	-2.65	4.981	0.627	0.109	-0.012
0.225	-0.3370	0.5604	0.5952	-11.410	25.166	22.507	5.08	-6.03	4.844	0.655	0.110	-0.007
0.250	-0.2251	0.5789	0.6321	-11.374	26.999	22.118	4.91	-5.35	4.703	0.679	0.111	-0.006
0.275	-0.1173	0.5948	0.6714	-11.245	28.805	21.638	4.82	-2.50	4.558	0.696	0.111	-0.014
0.300	-0.0139	0.6081	0.7126	-11.074	30.532	21.079	4.81	-0.50	4.409	0.710	0.113	-0.025
0.325	0.0852	0.6189	0.7551	-10.918	32.121	20.470	4.82	0.63	4.257	0.719	0.116	-0.033
0.350	0.1799	0.6274	0.7984	-10.797	33.548	19.830	4.84	3.44	4.101	0.724	0.118	-0.038
0.375	0.2704	0.6337	0.8420	-10.701	34.811	19.160	4.98	8.90	3.943	0.721	0.121	-0.047
0.400	0.3567	0.6381	0.8851	-10.612	35.879	18.452	5.28	14.53	3.786	0.717	0.127	-0.058
0.425	0.4393	0.6407	0.9272	-10.522	36.716	17.700	5.71	17.47	3.628	0.724	0.136	-0.060
0.450	0.5181	0.6419	0.9678	-10.399	37.324	16.893	6.16	17.75	3.469	0.749	0.150	-0.047
0.475	0.5934	0.6416	1.0068	-10.242	37.791	16.053	6.60	18.29	3.310	0.789	0.166	-0.036
0.500	0.6652	0.6400	1.0438	-10.039	38.190	15.196	7.09	22.20	3.151	0.832	0.184	-0.040
0.525	0.7335	0.6371	1.0787	-9.783	38.520	14.317	7.74	31.13	2.991	0.865	0.202	-0.061
0.550	0.7986	0.6330	1.1113	-9.446	38.722	13.372	8.66	44.41	2.834	0.885	0.220	-0.091

time	x	y	z	ϕ	θ	ψ	V	α	$\dot{\alpha}$	C_L	C_D	C_m
(s)	(m)	(m)	(m)	(deg)	(deg)	(deg)	(m/s)	(deg)	(deg/s)			
0.575	0.8606	0.6279	1.1411	-8.993	38.732	12.305	9.96	59.02	2.683	0.897	0.241	-0.125
0.600	0.9198	0.6222	1.1680	-8.388	38.514	11.087	11.62	71.91	2.538	0.916	0.269	-0.163
0.625	0.9765	0.6159	1.1917	-7.632	38.040	9.740	13.56	82.24	2.400	0.946	0.305	-0.200
0.650	1.0308	0.6094	1.2120	-6.706	37.296	8.264	15.73	92.11	2.270	0.984	0.355	-0.229
0.675	1.0830	0.6025	1.2287	-5.634	36.292	6.684	18.15	103.11	2.147	1.022	0.419	-0.242
0.700	1.1331	0.5954	1.2419	-4.412	35.072	5.018	20.88	114.47	2.035	1.063	0.499	-0.245
0.725	1.1813	0.5883	1.2513	-3.065	33.697	3.321	23.89	125.29	1.933	1.104	0.595	-0.257
0.750	1.2276	0.5811	1.2569	-1.631	32.188	1.647	27.13	138.29	1.845	1.134	0.697	-0.284

Test Conditions

aircraft	balsa glider	flight	regression 6
aspect ratio	11.7	test number	6127
m (g)	7.20	I_{xx} (g·cm^2)	290.99
I_{yy} (g·cm^2)	306.59	I_{zz} (g·cm^2)	592.04
I_{xz} (g·cm^2)	10.19	I_{xy} (g·cm^2)	0.65
I_{yz} (g·cm^2)	-0.23	δ_e (deg)	0.94
CG (%c)	0.76		
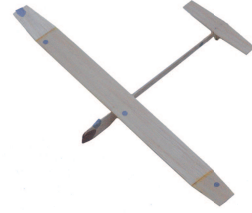
time	x	y	z	ϕ	θ	ψ	V	α	$\dot{\alpha}$	C_L	C_D	C_m
(s)	(m)	(m)	(m)	(deg)	(deg)	(deg)	(m/s)	(deg)	(deg/s)			
0.000	-2.2008	0.3228	1.4404	-5.053	17.185	7.964	4.28	5.20	4.118	0.774	0.121	-0.020
0.025	-2.1016	0.3255	1.4627	-5.224	18.098	7.900	4.44	7.51	4.018	0.783	0.124	-0.019
0.050	-2.0050	0.3275	1.4854	-5.353	18.936	7.819	4.65	9.71	3.917	0.795	0.126	-0.020
0.075	-1.9112	0.3287	1.5084	-5.433	19.707	7.707	4.92	11.85	3.816	0.809	0.129	-0.022
0.100	-1.8199	0.3293	1.5315	-5.485	20.393	7.551	5.24	13.50	3.714	0.828	0.133	-0.022
0.125	-1.7312	0.3293	1.5543	-5.532	21.005	7.345	5.60	14.62	3.611	0.853	0.140	-0.020
0.150	-1.6451	0.3287	1.5768	-5.588	21.554	7.095	5.97	15.46	3.508	0.883	0.150	-0.019
0.175	-1.5615	0.3275	1.5988	-5.655	22.056	6.813	6.37	16.41	3.404	0.916	0.160	-0.025
0.200	-1.4805	0.3257	1.6202	-5.737	22.492	6.522	6.79	17.65	3.299	0.949	0.173	-0.033
0.225	-1.4021	0.3233	1.6407	-5.840	22.850	6.228	7.26	19.49	3.194	0.978	0.188	-0.044
0.250	-1.3261	0.3204	1.6603	-5.971	23.098	5.948	7.78	22.45	3.089	1.002	0.205	-0.056
0.275	-1.2525	0.3169	1.6788	-6.130	23.224	5.670	8.38	26.40	2.984	1.020	0.225	-0.070
0.300	-1.1813	0.3131	1.6957	-6.309	23.201	5.375	9.10	30.97	2.881	1.035	0.244	-0.084
0.325	-1.1123	0.3087	1.7110	-6.492	23.011	5.042	9.94	35.71	2.781	1.045	0.260	-0.100
0.350	-1.0455	0.3040	1.7243	-6.659	22.635	4.671	10.89	41.03	2.688	1.047	0.278	-0.119
0.375	-0.9805	0.2988	1.7355	-6.802	22.051	4.273	11.98	46.74	2.602	1.042	0.300	-0.139
0.400	-0.9173	0.2932	1.7442	-6.892	21.231	3.864	13.22	51.12	2.523	1.038	0.330	-0.148
0.425	-0.8557	0.2873	1.7502	-6.896	20.173	3.422	14.56	53.96	2.451	1.040	0.364	-0.141
0.450	-0.7957	0.2811	1.7536	-6.761	18.907	2.919	15.92	57.55	2.387	1.040	0.405	-0.128
0.475	-0.7371	0.2745	1.7540	-6.469	17.478	2.336	17.40	63.78	2.333	1.027	0.451	-0.126
0.500	-0.6798	0.2678	1.7515	-6.026	15.909	1.695	19.07	68.96	2.285	1.013	0.494	-0.142
0.525	-0.6239	0.2610	1.7458	-5.468	14.177	1.030	20.84	66.56	2.249	1.015	0.529	-0.153
0.550	-0.5690	0.2543	1.7370	-4.805	12.274	0.339	22.42	56.37	2.227	1.041	0.553	-0.147

195

time	x	y	z	ϕ	θ	ψ	V	α	$\dot{\alpha}$	C_L	C_D	C_m
(s)	(m)	(m)	(m)	(deg)	(deg)	(deg)	(m/s)	(deg)	(deg/s)			
0.575	-0.5152	0.2474	1.7253	-4.022	10.217	-0.385	23.63	44.83	2.218	1.063	0.579	-0.132
0.600	-0.4622	0.2405	1.7106	-3.081	8.041	-1.126	24.61	37.30	2.217	1.061	0.605	-0.126
0.625	-0.4100	0.2337	1.6932	-1.966	5.769	-1.843	25.47	30.68	2.224	1.037	0.621	-0.136
0.650	-0.3585	0.2270	1.6729	-0.760	3.382	-2.505	26.16	19.14	2.242	1.017	0.616	-0.146
0.675	-0.3074	0.2204	1.6498	0.455	0.836	-3.100	26.44	2.27	2.273	1.006	0.603	-0.131
0.700	-0.2567	0.2138	1.6240	1.621	-1.858	-3.657	26.26	-14.61	2.314	0.993	0.587	-0.098
0.725	-0.2061	0.2074	1.5955	2.751	-4.656	-4.164	25.70	-26.54	2.361	0.960	0.570	-0.065
0.750	-0.1555	0.2009	1.5645	3.832	-7.515	-4.626	24.92	-35.03	2.416	0.917	0.542	-0.050
0.775	-0.1049	0.1946	1.5309	4.842	-10.429	-5.022	23.97	-44.09	2.479	0.872	0.504	-0.049
0.800	-0.0539	0.1884	1.4946	5.731	-13.415	-5.364	22.74	-55.54	2.552	0.834	0.460	-0.044
0.825	-0.0025	0.1824	1.4557	6.501	-16.472	-5.629	21.21	-66.27	2.634	0.789	0.417	-0.039
0.850	0.0495	0.1766	1.4141	7.152	-19.609	-5.816	19.42	-73.29	2.721	0.735	0.374	-0.035
0.875	0.1023	0.1710	1.3697	7.692	-22.834	-5.908	17.54	-78.15	2.817	0.673	0.330	-0.028
0.900	0.1560	0.1657	1.3225	8.069	-26.130	-5.962	15.55	-83.63	2.921	0.618	0.285	-0.015
0.925	0.2106	0.1604	1.2723	8.243	-29.498	-6.021	13.39	-89.62	3.034	0.575	0.245	0.022
0.950	0.2663	0.1552	1.2190	8.244	-32.845	-6.123	11.09	-92.20	3.155	0.543	0.210	0.073
0.975	0.3233	0.1500	1.1626	8.109	-36.037	-6.262	8.81	-87.83	3.282	0.514	0.179	0.129
1.000	0.3818	0.1449	1.1030	7.848	-38.882	-6.451	6.74	-75.38	3.415	0.486	0.151	0.171
1.025	0.4419	0.1399	1.0402	7.434	-41.212	-6.722	5.06	-56.66	3.554	0.459	0.128	0.186
1.050	0.5038	0.1348	0.9742	6.848	-42.924	-7.099	3.92	-35.71	3.699	0.434	0.111	0.170
1.075	0.5676	0.1295	0.9049	6.124	-44.055	-7.559	3.28	-17.29	3.847	0.415	0.100	0.140

Test Conditions

aircraft	balsa glider	flight	regression 7
aspect ratio	11.7	test number	6143
m (g)	7.20	I_{xx} (g·cm^2)	290.99
I_{yy} (g·cm^2)	306.59	I_{zz} (g·cm^2)	592.04
I_{xz} (g·cm^2)	10.19	I_{xy} (g·cm^2)	0.65
I_{yz} (g·cm^2)	-0.23	δ_e (deg)	0.94
CG (%c)	0.76		

time	x	y	z	ϕ	θ	ψ	V	α	$\dot{\alpha}$	C_L	C_D	C_m
(s)	(m)	(m)	(m)	(deg)	(deg)	(deg)	(m/s)	(deg)	(deg/s)			
0.000	-3.2493	0.4224	0.9138	-2.482	3.597	15.544	1.92	53.29	6.455	0.674	0.119	-0.093
0.025	-3.0936	0.4580	0.9228	-2.238	7.806	15.928	2.77	22.66	6.341	0.665	0.100	-0.079
0.050	-2.9413	0.4924	0.9406	-1.987	11.270	16.205	3.08	1.67	6.230	0.654	0.087	-0.063
0.075	-2.7927	0.5257	0.9661	-1.766	14.159	16.417	3.04	-9.67	6.119	0.642	0.079	-0.047
0.100	-2.6481	0.5578	0.9985	-1.634	16.419	16.582	2.60	-10.24	6.001	0.632	0.079	-0.009
0.125	-2.5081	0.5885	1.0368	-1.559	18.939	16.815	2.50	-4.16	5.874	0.620	0.078	-0.019
0.150	-2.3727	0.6180	1.0803	-1.679	21.288	17.108	2.52	2.78	5.737	0.599	0.079	-0.027
0.175	-2.2423	0.6461	1.1277	-1.994	23.396	17.466	2.63	6.19	5.592	0.576	0.081	-0.028
0.200	-2.1166	0.6728	1.1779	-2.438	25.277	17.860	2.82	10.19	5.443	0.556	0.083	-0.023
0.225	-1.9954	0.6982	1.2298	-2.890	26.991	18.238	3.12	14.14	5.293	0.549	0.087	-0.014
0.250	-1.8787	0.7221	1.2829	-3.205	28.622	18.535	3.52	15.79	5.138	0.562	0.094	-0.003
0.275	-1.7665	0.7447	1.3367	-3.269	30.244	18.692	3.91	14.07	4.978	0.597	0.102	0.006
0.300	-1.6589	0.7658	1.3912	-3.101	31.918	18.709	4.21	10.45	4.812	0.647	0.110	0.009
0.325	-1.5563	0.7853	1.4464	-2.808	33.654	18.616	4.42	7.38	4.640	0.700	0.117	0.007
0.350	-1.4588	0.8033	1.5023	-2.521	35.435	18.460	4.58	5.84	4.463	0.750	0.121	0.001
0.375	-1.3666	0.8197	1.5588	-2.310	37.226	18.280	4.72	5.42	4.283	0.793	0.125	-0.007
0.400	-1.2797	0.8345	1.6154	-2.200	38.991	18.113	4.86	5.75	4.099	0.831	0.129	-0.016
0.425	-1.1981	0.8478	1.6719	-2.190	40.691	17.983	5.02	7.02	3.912	0.863	0.134	-0.027
0.450	-1.1215	0.8596	1.7276	-2.271	42.288	17.891	5.22	9.43	3.723	0.890	0.140	-0.038
0.475	-1.0497	0.8699	1.7821	-2.402	43.754	17.809	5.50	12.81	3.532	0.918	0.149	-0.046
0.500	-0.9826	0.8789	1.8350	-2.543	45.077	17.693	5.87	16.89	3.339	0.950	0.160	-0.050
0.525	-0.9198	0.8866	1.8857	-2.664	46.266	17.515	6.35	21.95	3.145	0.988	0.173	-0.055
0.550	-0.8611	0.8931	1.9339	-2.764	47.335	17.264	6.98	28.55	2.952	1.031	0.190	-0.065

time	x	y	z	ϕ	θ	ψ	V	α	$\dot{\alpha}$	C_L	C_D	C_m
(s)	(m)	(m)	(m)	(deg)	(deg)	(deg)	(m/s)	(deg)	(deg/s)			
0.575	-0.8063	0.8986	1.9792	-2.856	48.281	16.958	7.80	37.52	2.759	1.074	0.214	-0.087
0.600	-0.7549	0.9031	2.0214	-2.954	49.077	16.613	8.88	49.49	2.566	1.113	0.246	-0.122
0.625	-0.7069	0.9068	2.0600	-3.056	49.682	16.236	10.30	64.61	2.376	1.150	0.290	-0.162
0.650	-0.6617	0.9096	2.0948	-3.152	50.062	15.820	12.15	83.23	2.189	1.190	0.344	-0.199
0.675	-0.6191	0.9119	2.1253	-3.227	50.209	15.355	14.51	106.65	2.009	1.237	0.414	-0.228
0.700	-0.5788	0.9135	2.1515	-3.263	50.137	14.825	17.52	136.64	1.837	1.292	0.505	-0.256
0.725	-0.5406	0.9146	2.1731	-3.245	49.864	14.218	21.36	172.92	1.679	1.358	0.629	-0.293
0.750	-0.5042	0.9154	2.1899	-3.157	49.399	13.522	26.20	213.34	1.536	1.439	0.810	-0.333
0.775	-0.4694	0.9158	2.2019	-2.988	48.757	12.733	32.05	256.29	1.412	1.522	1.070	-0.373
0.800	-0.4362	0.9160	2.2091	-2.727	47.955	11.836	38.94	298.57	1.310	1.563	1.419	-0.431
0.825	-0.4046	0.9160	2.2114	-2.361	46.998	10.825	46.86	331.05	1.233	1.525	1.805	-0.521
0.850	-0.3745	0.9157	2.2089	-1.878	45.879	9.680	55.41	341.89	1.189	1.392	2.156	-0.627
0.875	-0.3459	0.9153	2.2015	-1.281	44.580	8.419	63.87	328.02	1.179	1.171	2.448	-0.678
0.900	-0.3187	0.9148	2.1896	-0.594	43.096	7.081	71.66	297.33	1.198	0.874	2.659	-0.668
0.925	-0.2932	0.9142	2.1731	0.152	41.438	5.742	78.59	257.74	1.239	0.541	2.745	-0.655
0.950	-0.2692	0.9134	2.1523	0.946	39.596	4.442	84.51	211.35	1.300	0.257	2.704	-0.655
0.975	-0.2469	0.9126	2.1274	1.798	37.543	3.197	89.18	160.36	1.377	0.077	2.592	-0.660
1.000	-0.2263	0.9117	2.0985	2.730	35.236	1.976	92.52	112.01	1.462	-0.045	2.483	-0.637
1.025	-0.2074	0.9106	2.0660	3.738	32.649	0.802	94.76	72.07	1.549	-0.147	2.384	-0.595
1.050	-0.1901	0.9095	2.0301	4.806	29.767	-0.312	96.12	36.41	1.635	-0.224	2.280	-0.553
1.075	-0.1746	0.9085	1.9912	5.912	26.562	-1.276	96.65	0.06	1.721	-0.248	2.175	-0.503
1.100	-0.1608	0.9077	1.9493	7.035	23.011	-2.071	96.13	-36.79	1.804	-0.223	2.088	-0.453
1.125	-0.1485	0.9074	1.9049	8.164	19.114	-2.707	94.80	-69.55	1.883	-0.212	2.022	-0.411
1.150	-0.1375	0.9075	1.8581	9.283	14.848	-3.159	92.71	-98.97	1.956	-0.199	1.975	-0.375
1.175	-0.1278	0.9082	1.8094	10.376	10.199	-3.408	89.89	-125.05	2.021	-0.184	1.944	-0.344

Test Conditions

aircraft	balsa glider	flight	regression 8
aspect ratio	11.7	test number	6159
m (g)	7.92	I_{xx} (g·cm^2)	291.14
I_{yy} (g·cm^2)	325.10	I_{zz} (g·cm^2)	610.41
I_{xz} (g·cm^2)	11.85	I_{xy} (g·cm^2)	0.60
I_{yz} (g·cm^2)	-0.23	δ_e (deg)	-0.94
CG (%c)	0.34		

time	x	y	z	ϕ	θ	ψ	V	α	$\dot{\alpha}$	C_L	C_D	C_m
(s)	(m)	(m)	(m)	(deg)	(deg)	(deg)	(m/s)	(deg)	(deg/s)			
0.000	-3.2459	0.2117	1.3621	3.694	-9.335	16.841	2.47	1.52	5.536	0.410	0.060	0.003
0.025	-3.1130	0.2397	1.3348	3.840	-9.153	17.436	2.52	1.93	5.546	0.411	0.063	0.002
0.050	-2.9800	0.2686	1.3079	4.018	-8.962	18.068	2.56	1.95	5.553	0.413	0.065	0.002
0.075	-2.8470	0.2984	1.2814	4.228	-8.766	18.717	2.61	1.59	5.558	0.415	0.068	0.001
0.100	-2.7140	0.3291	1.2554	4.471	-8.572	19.368	2.64	0.71	5.561	0.418	0.069	0.000
0.125	-2.5811	0.3609	1.2299	4.746	-8.378	19.990	2.65	-0.00	5.562	0.420	0.073	-0.001
0.150	-2.4484	0.3938	1.2049	5.060	-8.192	20.568	2.64	-0.37	5.558	0.421	0.078	-0.001
0.175	-2.3160	0.4277	1.1806	5.407	-8.021	21.102	2.63	-0.57	5.548	0.422	0.079	-0.001
0.200	-2.1841	0.4627	1.1568	5.746	-7.864	21.605	2.61	-1.01	5.539	0.423	0.077	-0.000
0.225	-2.0525	0.4988	1.1335	6.053	-7.715	22.098	2.58	-1.32	5.533	0.424	0.072	0.001
0.250	-1.9213	0.5360	1.1108	6.345	-7.565	22.581	2.55	-1.02	5.531	0.424	0.070	0.002
0.275	-1.7903	0.5744	1.0885	6.654	-7.401	23.063	2.53	-0.34	5.528	0.425	0.071	0.002
0.300	-1.6598	0.6140	1.0668	7.000	-7.229	23.557	2.53	0.33	5.521	0.425	0.074	0.002
0.325	-1.5298	0.6549	1.0456	7.368	-7.050	24.062	2.55	0.68	5.511	0.426	0.077	0.001
0.350	-1.4005	0.6969	1.0249	7.713	-6.872	24.577	2.57	0.86	5.498	0.427	0.078	-0.000
0.375	-1.2717	0.7401	1.0046	8.014	-6.700	25.086	2.59	1.06	5.485	0.426	0.078	-0.001
0.400	-1.1437	0.7845	0.9848	8.263	-6.542	25.580	2.61	0.96	5.473	0.426	0.077	-0.002
0.425	-1.0164	0.8302	0.9653	8.468	-6.395	26.054	2.64	0.40	5.462	0.426	0.075	-0.002
0.450	-0.8897	0.8771	0.9462	8.636	-6.265	26.507	2.64	-0.45	5.451	0.427	0.075	-0.001
0.475	-0.7638	0.9251	0.9274	8.770	-6.144	26.956	2.62	-0.65	5.439	0.428	0.076	-0.001
0.500	-0.6385	0.9743	0.9089	8.907	-6.032	27.416	2.60	0.20	5.426	0.427	0.077	-0.000
0.525	-0.5141	1.0247	0.8908	9.060	-5.923	27.895	2.63	1.51	5.412	0.425	0.078	-0.000
0.550	-0.3905	1.0762	0.8728	9.255	-5.823	28.393	2.68	2.24	5.398	0.425	0.078	-0.000

time	x	y	z	ϕ	θ	ψ	V	α	$\dot{\alpha}$	C_L	C_D	C_m
(s)	(m)	(m)	(m)	(deg)	(deg)	(deg)	(m/s)	(deg)	(deg/s)			
0.575	-0.2677	1.1288	0.8550	9.467	-5.735	28.903	2.74	1.94	5.384	0.426	0.079	-0.000
0.600	-0.1457	1.1825	0.8373	9.681	-5.657	29.419	2.77	1.09	5.370	0.431	0.081	0.001
0.625	-0.0248	1.2375	0.8198	9.861	-5.572	29.951	2.79	0.24	5.352	0.436	0.083	0.001
0.650	0.0953	1.2934	0.8025	9.998	-5.483	30.476	2.79	-0.40	5.334	0.440	0.084	-0.001
0.675	0.2144	1.3502	0.7856	10.104	-5.402	30.982	2.77	-0.89	5.315	0.442	0.081	-0.002
0.700	0.3326	1.4081	0.7689	10.217	-5.335	31.476	2.75	-0.68	5.300	0.442	0.073	-0.001
0.725	0.4500	1.4672	0.7524	10.349	-5.281	32.038	2.74	1.41	5.293	0.435	0.070	-0.001
0.750	0.5664	1.5278	0.7358	10.474	-5.264	32.730	2.80	4.46	5.286	0.425	0.073	-0.003
0.775	0.6817	1.5897	0.7191	10.540	-5.283	33.521	2.96	5.64	5.275	0.420	0.082	-0.006
0.800	0.7959	1.6527	0.7021	10.516	-5.361	34.331	3.09	2.46	5.252	0.425	0.086	-0.006
0.825	0.9090	1.7167	0.6848	10.444	-5.485	35.101	3.09	-3.03	5.233	0.441	0.081	-0.001
0.850	1.0210	1.7819	0.6675	10.377	-5.605	35.806	2.93	-6.72	5.226	0.455	0.073	0.005
0.875	1.1321	1.8483	0.6503	10.408	-5.670	36.478	2.75	-6.71	5.223	0.463	0.071	0.007
0.900	1.2424	1.9159	0.6335	10.520	-5.672	37.110	2.61	-3.97	5.217	0.462	0.077	0.004
0.925	1.3518	1.9845	0.6171	10.661	-5.646	37.715	2.55	-1.03	5.197	0.457	0.085	-0.001
0.950	1.4601	2.0539	0.6008	10.726	-5.644	38.315	2.57	1.12	5.182	0.449	0.085	-0.004
0.975	1.5674	2.1243	0.5845	10.763	-5.666	38.968	2.60	2.01	5.166	0.443	0.088	-0.007
1.000	1.6736	2.1955	0.5681	10.711	-5.747	39.707	2.65	1.85	5.148	0.436	0.093	-0.011
1.025	1.7786	2.2676	0.5514	10.534	-5.912	40.571	2.69	0.64	5.128	0.429	0.098	-0.015

	Test Conditions		
aircraft	balsa glider	flight	regression 9
aspect ratio	11.7	test number	6165
m (g)	7.92	I_{xx} (g·cm^2)	291.14
I_{yy} (g·cm^2)	325.10	I_{zz} (g·cm^2)	610.41
I_{xz} (g·cm^2)	11.85	I_{xy} (g·cm^2)	0.60
I_{yz} (g·cm^2)	-0.23	δ_e (deg)	-0.94
CG (%c)	0.34		
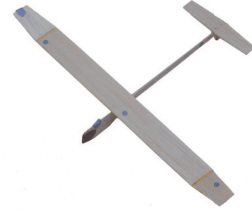
time	x	y	z	ϕ	θ	ψ	V	α	$\dot{\alpha}$	C_L	C_D	C_m
(s)	(m)	(m)	(m)	(deg)	(deg)	(deg)	(m/s)	(deg)	(deg/s)			
0.000	-3.2114	0.2927	1.0965	0.517	-10.545	8.479	2.32	2.45	5.659	0.410	0.053	-0.001
0.025	-3.0768	0.3244	1.0654	-0.301	-10.266	7.728	2.38	2.02	5.677	0.408	0.057	-0.001
0.050	-2.9417	0.3560	1.0348	-1.118	-10.016	7.092	2.42	1.53	5.690	0.407	0.061	-0.001
0.075	-2.8059	0.3872	1.0050	-1.943	-9.789	6.543	2.45	0.98	5.700	0.406	0.064	-0.000
0.100	-2.6698	0.4178	0.9758	-2.784	-9.570	6.053	2.48	0.24	5.708	0.406	0.067	-0.000
0.125	-2.5332	0.4478	0.9474	-3.655	-9.374	5.591	2.47	0.05	5.710	0.407	0.072	0.001
0.150	-2.3963	0.4771	0.9197	-4.577	-9.177	5.130	2.47	0.61	5.706	0.408	0.074	0.003
0.175	-2.2591	0.5054	0.8927	-5.524	-8.972	4.653	2.50	1.25	5.701	0.409	0.073	0.002
0.200	-2.1218	0.5328	0.8665	-6.452	-8.762	4.185	2.54	0.90	5.699	0.410	0.071	0.001
0.225	-1.9841	0.5591	0.8410	-7.325	-8.564	3.755	2.55	0.08	5.698	0.411	0.071	0.001
0.250	-1.8462	0.5844	0.8161	-8.157	-8.366	3.383	2.54	-0.16	5.694	0.412	0.073	0.004
0.275	-1.7081	0.6084	0.7920	-8.998	-8.141	3.063	2.54	0.57	5.684	0.415	0.075	0.006
0.300	-1.5698	0.6309	0.7686	-9.878	-7.869	2.768	2.57	1.49	5.674	0.418	0.074	0.005
0.325	-1.4315	0.6519	0.7460	-10.770	-7.557	2.480	2.61	1.85	5.666	0.421	0.072	0.003
0.350	-1.2930	0.6714	0.7240	-11.618	-7.224	2.183	2.66	1.44	5.658	0.420	0.071	-0.002
0.375	-1.1544	0.6893	0.7028	-12.395	-6.915	1.888	2.68	0.53	5.649	0.418	0.071	-0.006
0.400	-1.0158	0.7057	0.6823	-13.113	-6.663	1.589	2.68	-0.68	5.637	0.413	0.072	-0.008
0.425	-0.8772	0.7204	0.6622	-13.801	-6.501	1.286	2.65	-2.11	5.624	0.410	0.072	-0.006
0.450	-0.7387	0.7335	0.6425	-14.467	-6.404	0.973	2.58	-3.38	5.612	0.409	0.073	-0.000
0.475	-0.6004	0.7449	0.6232	-15.111	-6.328	0.654	2.48	-3.89	5.600	0.413	0.073	0.008
0.500	-0.4622	0.7544	0.6041	-15.740	-6.201	0.310	2.40	-2.58	5.586	0.418	0.074	0.013
0.525	-0.3242	0.7621	0.5855	-16.346	-5.974	-0.053	2.36	0.63	5.572	0.422	0.075	0.013
0.550	-0.1864	0.7677	0.5673	-16.904	-5.645	-0.442	2.43	4.75	5.556	0.423	0.076	0.010

time	x	y	z	ϕ	θ	ψ	V	α	$\dot{\alpha}$	C_L	C_D	C_m
(s)	(m)	(m)	(m)	(deg)	(deg)	(deg)	(m/s)	(deg)	(deg/s)			
0.575	-0.0489	0.7715	0.5494	-17.346	-5.243	-0.848	2.58	7.30	5.539	0.425	0.078	0.005
0.600	0.0882	0.7735	0.5320	-17.672	-4.808	-1.289	2.79	6.34	5.520	0.429	0.079	-0.003
0.625	0.2250	0.7737	0.5151	-17.910	-4.430	-1.777	2.91	2.85	5.501	0.434	0.080	-0.008
0.650	0.3613	0.7722	0.4986	-18.132	-4.151	-2.331	2.92	-0.43	5.481	0.435	0.079	-0.008
0.675	0.4971	0.7687	0.4825	-18.358	-3.977	-2.936	2.89	-0.62	5.462	0.433	0.078	-0.003
0.700	0.6324	0.7634	0.4668	-18.590	-3.838	-3.569	2.89	1.97	5.443	0.429	0.077	0.003
0.725	0.7671	0.7561	0.4512	-18.795	-3.665	-4.206	2.98	4.60	5.424	0.428	0.078	0.003
0.750	0.9013	0.7470	0.4357	-18.978	-3.461	-4.850	3.12	4.46	5.405	0.434	0.079	-0.000
0.775	1.0349	0.7361	0.4204	-19.135	-3.267	-5.513	3.20	0.68	5.386	0.444	0.079	-0.004
0.800	1.1679	0.7233	0.4053	-19.271	-3.132	-6.215	3.16	-4.02	5.367	0.456	0.078	-0.003
0.825	1.3002	0.7086	0.3907	-19.379	-3.063	-6.987	3.00	-6.28	5.349	0.465	0.079	0.002
0.850	1.4319	0.6919	0.3766	-19.494	-3.006	-7.849	2.85	-5.05	5.329	0.466	0.080	0.005
0.875	1.5629	0.6734	0.3630	-19.645	-2.940	-8.802	2.77	-1.05	5.306	0.462	0.081	0.006
0.900	1.6930	0.6529	0.3498	-19.844	-2.868	-9.821	2.80	4.20	5.282	0.452	0.080	0.006
0.925	1.8222	0.6305	0.3367	-20.098	-2.776	-10.854	2.98	9.89	5.261	0.441	0.079	0.007
0.950	1.9507	0.6064	0.3235	-20.436	-2.639	-11.850	3.29	14.65	5.244	0.436	0.083	0.009
0.975	2.0782	0.5805	0.3100	-20.843	-2.417	-12.805	3.69	15.51	5.221	0.441	0.089	0.004
1.000	2.2046	0.5527	0.2962	-21.248	-2.151	-13.752	4.06	12.11	5.192	0.454	0.089	-0.008
1.025	2.3299	0.5230	0.2822	-21.522	-2.003	-14.775	4.26	5.47	5.173	0.468	0.084	-0.016
1.050	2.4543	0.4913	0.2683	-21.803	-1.974	-15.851	4.31	-2.55	5.154	0.482	0.080	-0.026
1.075	2.5777	0.4575	0.2545	-22.028	-2.161	-17.030	4.13	-12.32	5.138	0.496	0.076	-0.036
1.100	2.7001	0.4216	0.2409	-22.182	-2.640	-18.341	3.67	-23.84	5.125	0.509	0.070	-0.047

	Test Conditions			
aircraft	balsa glider	flight	regression 10	
aspect ratio	11.7	test number	6168	
m (g)	7.92	I_{xx} (g·cm^2)	291.14	
I_{yy} (g·cm^2)	325.10	I_{zz} (g·cm^2)	610.41	
I_{xz} (g·cm^2)	11.85	I_{xy} (g·cm^2)	0.60	
I_{yz} (g·cm^2)	-0.23	δ_e (deg)	-1.89	
CG (%c)	0.34			

time	x	y	z	ϕ	θ	ψ	V	α	$\dot{\alpha}$	C_L	C_D	C_m
(s)	(m)	(m)	(m)	(deg)	(deg)	(deg)	(m/s)	(deg)	(deg/s)			
0.000	-2.4840	0.2929	1.6781	-8.433	-0.994	0.515	4.09	-3.44	4.689	0.548	0.114	0.003
0.025	-2.3680	0.3041	1.6692	-9.370	-1.106	0.591	4.00	-3.23	4.658	0.546	0.108	0.002
0.050	-2.2527	0.3139	1.6603	-10.110	-1.210	0.648	3.93	-2.54	4.630	0.544	0.102	0.001
0.075	-2.1379	0.3225	1.6511	-10.685	-1.315	0.678	3.89	-1.35	4.606	0.540	0.096	-0.001
0.100	-2.0237	0.3300	1.6416	-11.151	-1.441	0.688	3.86	0.57	4.585	0.536	0.093	0.000
0.125	-1.9098	0.3363	1.6317	-11.468	-1.562	0.630	3.90	2.46	4.567	0.529	0.086	-0.004
0.150	-1.7964	0.3415	1.6213	-11.724	-1.717	0.529	3.99	2.87	4.557	0.525	0.082	-0.006
0.175	-1.6832	0.3457	1.6103	-12.015	-1.919	0.403	4.05	1.07	4.548	0.527	0.085	-0.003
0.200	-1.5703	0.3489	1.5986	-12.353	-2.150	0.264	4.04	-1.06	4.536	0.533	0.092	0.003
0.225	-1.4578	0.3508	1.5864	-12.713	-2.371	0.084	3.99	-1.42	4.520	0.540	0.097	0.005
0.250	-1.3457	0.3515	1.5737	-13.044	-2.573	-0.147	3.97	0.10	4.506	0.540	0.097	0.004
0.275	-1.2339	0.3509	1.5605	-13.344	-2.771	-0.442	4.00	2.13	4.495	0.537	0.095	0.001
0.300	-1.1225	0.3492	1.5466	-13.633	-2.987	-0.793	4.08	3.34	4.487	0.533	0.095	0.001
0.325	-1.0114	0.3463	1.5321	-13.944	-3.221	-1.199	4.17	3.66	4.480	0.531	0.096	0.001
0.350	-0.9006	0.3424	1.5168	-14.268	-3.465	-1.657	4.25	3.74	4.473	0.530	0.098	0.001
0.375	-0.7901	0.3374	1.5009	-14.601	-3.722	-2.163	4.35	3.94	4.467	0.530	0.099	-0.001
0.400	-0.6799	0.3313	1.4842	-14.929	-3.998	-2.712	4.45	3.56	4.463	0.530	0.100	-0.004
0.425	-0.5700	0.3241	1.4668	-15.236	-4.316	-3.308	4.52	1.84	4.460	0.532	0.101	-0.005
0.450	-0.4603	0.3157	1.4486	-15.501	-4.687	-3.956	4.54	-1.22	4.459	0.540	0.101	-0.004
0.475	-0.3508	0.3061	1.4297	-15.698	-5.112	-4.657	4.46	-5.02	4.460	0.551	0.100	0.001
0.500	-0.2415	0.2953	1.4102	-15.808	-5.553	-5.406	4.30	-7.94	4.462	0.564	0.099	0.006
0.525	-0.1324	0.2830	1.3903	-15.813	-5.971	-6.199	4.07	-8.78	4.467	0.572	0.098	0.008
0.550	-0.0233	0.2694	1.3701	-15.731	-6.346	-7.036	3.86	-7.31	4.471	0.571	0.097	0.003

continued on next page

time	x	y	z	ϕ	θ	ψ	V	α	$\dot{\alpha}$	C_L	C_D	C_m
(s)	(m)	(m)	(m)	(deg)	(deg)	(deg)	(m/s)	(deg)	(deg/s)			
0.575	0.0856	0.2545	1.3496	-15.617	-6.710	-7.917	3.70	-5.19	4.476	0.564	0.095	-0.004
0.600	0.1945	0.2383	1.3288	-15.501	-7.105	-8.831	3.61	-4.28	4.482	0.551	0.092	-0.010
0.625	0.3032	0.2208	1.3075	-15.396	-7.578	-9.776	3.50	-4.37	4.492	0.540	0.090	-0.007
0.650	0.4119	0.2020	1.2855	-15.297	-8.105	-10.758	3.38	-4.03	4.503	0.530	0.087	-0.000
0.675	0.5205	0.1818	1.2627	-15.213	-8.650	-11.789	3.29	-2.51	4.516	0.523	0.086	0.008
0.700	0.6290	0.1603	1.2392	-15.179	-9.158	-12.866	3.26	-0.55	4.532	0.520	0.085	0.013
0.725	0.7375	0.1373	1.2149	-15.221	-9.610	-13.983	3.26	0.65	4.549	0.520	0.083	0.013
0.750	0.8460	0.1129	1.1898	-15.339	-10.003	-15.133	3.29	0.86	4.569	0.521	0.083	0.008
0.775	0.9545	0.0870	1.1641	-15.533	-10.375	-16.297	3.30	0.53	4.589	0.519	0.084	0.002
0.800	1.0630	0.0595	1.1378	-15.778	-10.759	-17.463	3.31	0.06	4.608	0.514	0.086	0.000
0.825	1.1714	0.0305	1.1107	-16.062	-11.172	-18.617	3.31	-0.02	4.626	0.508	0.087	0.002
0.850	1.2798	0.0000	1.0830	-16.361	-11.601	-19.763	3.31	0.49	4.646	0.503	0.087	0.009
0.875	1.3881	-0.0320	1.0546	-16.661	-11.998	-20.906	3.34	1.75	4.668	0.499	0.086	0.012
0.900	1.4963	-0.0657	1.0255	-16.955	-12.340	-22.050	3.40	3.17	4.691	0.497	0.085	0.012
0.925	1.6044	-0.1010	0.9957	-17.239	-12.630	-23.186	3.49	3.51	4.714	0.496	0.083	0.009
0.950	1.7124	-0.1381	0.9652	-17.505	-12.897	-24.297	3.58	2.31	4.739	0.499	0.078	0.008
0.975	1.8204	-0.1770	0.9340	-17.739	-13.130	-25.343	3.62	1.35	4.769	0.503	0.072	0.013
1.000	1.9283	-0.2179	0.9023	-17.986	-13.292	-26.403	3.63	2.38	4.804	0.504	0.070	0.014
1.025	2.0363	-0.2609	0.8702	-18.268	-13.366	-27.504	3.69	3.80	4.840	0.498	0.078	0.003
1.050	2.1441	-0.3058	0.8376	-18.543	-13.464	-28.658	3.84	3.05	4.861	0.495	0.086	-0.007
1.075	2.2518	-0.3525	0.8048	-18.792	-13.658	-29.880	3.86	-0.54	4.884	0.493	0.092	-0.015
1.100	2.3592	-0.4010	0.7717	-19.014	-13.986	-31.200	3.78	-6.53	4.903	0.491	0.098	-0.023

Test Conditions

aircraft	balsa glider	flight	regression 11
aspect ratio	11.7	test number	6128
m (g)	7.20	I_{xx} (g·cm^2)	290.99
I_{yy} (g·cm^2)	306.59	I_{zz} (g·cm^2)	592.04
I_{xz} (g·cm^2)	10.19	I_{xy} (g·cm^2)	0.65
I_{yz} (g·cm^2)	-0.23	δ_e (deg)	0.94
CG (%c)	0.76		

time	x	y	z	ϕ	θ	ψ	V	α	$\dot{\alpha}$	C_L	C_D	C_m
(s)	(m)	(m)	(m)	(deg)	(deg)	(deg)	(m/s)	(deg)	(deg/s)			
0.000	-2.2165	0.5643	1.0741	-6.976	5.792	13.475	3.76	3.31	4.929	0.633	0.103	0.000
0.025	-2.0961	0.5862	1.0788	-7.193	7.093	13.377	3.86	4.36	4.864	0.644	0.102	-0.001
0.050	-1.9773	0.6070	1.0858	-7.330	8.387	13.244	3.98	4.49	4.798	0.658	0.101	-0.002
0.075	-1.8602	0.6266	1.0951	-7.430	9.672	13.088	4.09	3.41	4.728	0.674	0.102	-0.004
0.100	-1.7450	0.6449	1.1066	-7.528	10.938	12.921	4.15	2.09	4.653	0.691	0.106	-0.007
0.125	-1.6317	0.6620	1.1202	-7.644	12.166	12.748	4.18	1.25	4.571	0.707	0.109	-0.010
0.150	-1.5207	0.6777	1.1357	-7.802	13.341	12.566	4.21	0.92	4.486	0.721	0.111	-0.011
0.175	-1.4119	0.6921	1.1529	-8.005	14.458	12.371	4.24	0.74	4.397	0.736	0.113	-0.009
0.200	-1.3055	0.7052	1.1717	-8.258	15.534	12.164	4.26	0.92	4.306	0.751	0.114	-0.009
0.225	-1.2016	0.7168	1.1918	-8.532	16.576	11.950	4.29	2.02	4.213	0.764	0.117	-0.013
0.250	-1.1002	0.7272	1.2130	-8.786	17.562	11.709	4.36	4.03	4.116	0.775	0.120	-0.018
0.275	-1.0013	0.7362	1.2350	-8.980	18.460	11.436	4.49	6.38	4.016	0.785	0.124	-0.019
0.300	-0.9051	0.7440	1.2574	-9.120	19.272	11.123	4.68	8.75	3.915	0.798	0.129	-0.016
0.325	-0.8114	0.7506	1.2802	-9.222	20.019	10.769	4.93	11.26	3.813	0.815	0.135	-0.013
0.350	-0.7203	0.7560	1.3029	-9.312	20.726	10.377	5.24	13.71	3.710	0.837	0.142	-0.015
0.375	-0.6317	0.7601	1.3254	-9.405	21.387	9.951	5.61	15.08	3.605	0.864	0.151	-0.021
0.400	-0.5458	0.7632	1.3475	-9.516	21.979	9.502	5.99	14.52	3.499	0.899	0.159	-0.026
0.425	-0.4624	0.7650	1.3692	-9.667	22.489	9.044	6.34	13.05	3.394	0.937	0.167	-0.028
0.450	-0.3815	0.7658	1.3902	-9.888	22.917	8.586	6.64	12.55	3.290	0.977	0.179	-0.026
0.475	-0.3032	0.7653	1.4106	-10.172	23.281	8.123	6.97	14.25	3.184	1.013	0.197	-0.028
0.500	-0.2274	0.7638	1.4300	-10.501	23.581	7.644	7.37	17.65	3.076	1.047	0.215	-0.036
0.525	-0.1541	0.7612	1.4484	-10.843	23.809	7.142	7.87	22.20	2.969	1.072	0.233	-0.057
0.550	-0.0833	0.7578	1.4655	-11.205	23.915	6.617	8.48	27.71	2.865	1.086	0.249	-0.086

time	x	y	z	ϕ	θ	ψ	V	α	$\dot{\alpha}$	C_L	C_D	C_m
(s)	(m)	(m)	(m)	(deg)	(deg)	(deg)	(m/s)	(deg)	(deg/s)			
0.575	-0.0148	0.7533	1.4810	-11.602	23.846	6.067	9.25	33.52	2.765	1.086	0.267	-0.118
0.600	0.0515	0.7480	1.4945	-12.031	23.531	5.485	10.16	38.18	2.670	1.084	0.289	-0.137
0.625	0.1159	0.7418	1.5059	-12.441	22.949	4.850	11.17	41.60	2.580	1.086	0.315	-0.139
0.650	0.1783	0.7348	1.5148	-12.780	22.116	4.147	12.24	45.91	2.499	1.086	0.343	-0.132
0.675	0.2391	0.7271	1.5211	-13.064	21.070	3.375	13.45	52.88	2.425	1.080	0.376	-0.128
0.700	0.2982	0.7187	1.5246	-13.328	19.844	2.553	14.85	59.83	2.360	1.065	0.414	-0.140
0.725	0.3558	0.7098	1.5252	-13.613	18.423	1.681	16.44	61.93	2.304	1.062	0.454	-0.161
0.750	0.4120	0.7006	1.5227	-13.874	16.771	0.761	17.96	58.09	2.259	1.071	0.490	-0.179
0.775	0.4669	0.6909	1.5172	-14.040	14.856	-0.230	19.30	51.36	2.225	1.091	0.514	-0.173
0.800	0.5207	0.6808	1.5087	-14.009	12.714	-1.286	20.50	45.63	2.205	1.100	0.533	-0.156
0.825	0.5734	0.6703	1.4972	-13.730	10.381	-2.403	21.57	40.25	2.199	1.100	0.551	-0.138
0.850	0.6253	0.6592	1.4828	-13.171	7.917	-3.553	22.52	33.51	2.203	1.096	0.575	-0.134
0.875	0.6765	0.6478	1.4654	-12.346	5.336	-4.724	23.24	24.06	2.214	1.099	0.599	-0.126
0.900	0.7270	0.6359	1.4454	-11.252	2.678	-5.888	23.72	12.73	2.234	1.097	0.609	-0.120
0.925	0.7769	0.6236	1.4226	-9.943	-0.046	-7.026	23.87	1.47	2.263	1.090	0.602	-0.112
0.950	0.8264	0.6109	1.3973	-8.447	-2.805	-8.099	23.76	-9.17	2.302	1.066	0.581	-0.111
0.975	0.8758	0.5979	1.3695	-6.810	-5.607	-9.091	23.41	-20.03	2.349	1.036	0.556	-0.112
1.000	0.9252	0.5846	1.3393	-5.053	-8.463	-9.993	22.77	-33.10	2.406	1.002	0.531	-0.113
1.025	0.9748	0.5712	1.3066	-3.189	-11.408	-10.796	21.77	-47.55	2.468	0.968	0.506	-0.105
1.050	1.0247	0.5576	1.2715	-1.227	-14.450	-11.496	20.40	-59.82	2.535	0.924	0.472	-0.078
1.075	1.0751	0.5438	1.2341	0.761	-17.556	-12.092	18.78	-67.23	2.609	0.859	0.427	-0.050
1.100	1.1261	0.5299	1.1942	2.690	-20.708	-12.600	17.05	-70.79	2.692	0.781	0.372	-0.029
1.125	1.1779	0.5158	1.1517	4.482	-23.896	-13.035	15.26	-74.12	2.786	0.703	0.313	-0.016
1.150	1.2305	0.5017	1.1064	6.105	-27.135	-13.409	13.37	-78.71	2.891	0.638	0.259	0.014
1.175	1.2842	0.4876	1.0579	7.527	-30.390	-13.747	11.35	-81.68	3.007	0.587	0.213	0.067
1.200	1.3390	0.4734	1.0063	8.692	-33.539	-14.098	9.30	-79.68	3.132	0.549	0.179	0.128

References

[1] D. J. Pines and F. Bohorquez. Challenges Facing Future Micro-Air-Vehicle Development. *Journal of Aircraft*, 43(2):290–305, March–April 2006.

[2] U.S. Army USA CoE Staff. FY2010–2035 US Army Unmanned Aerial Systems Roadmap. *U.S. Army UAS Center of Excellence (ATZQ-CDI-C)*, Fort Rucker, AL, 2010.

[3] B. H. Carmichael. Low Reynolds Number Airfoil Survey. NASA CR 165803, 1981.

[4] T. J. Mueller, editor. *Fixed and Flapping Wing Aerodynamics for Micro Air Vehicle Applications*, volume 195 of *Progress in Astronautics and Aeronautics*. AIAA, Reston, VA, 2001.

[5] G. E. Torres and T. J. Mueller. Aerodynamic Characteristics of Low Aspect Ratio Wings at Low Reynolds Numbers. In Thomas J. Mueller, editor, *Fixed and Flapping Wing Aerodynamics for Micro Air Vehicle Applications*, volume 195, pages 115–141. Progress in Astronautics and Aeronautics, AIAA, Reston, VA, 2001.

[6] A. Pelletier and T. J. Mueller. Low Reynolds Number Aerodynamics of Low-Aspect-Ratio, Thin/Flat/Cambered-Plate Wings. *Journal of Aircraft*, 37(5):825–832, September–October 2000.

[7] G. E. Torres and T. J. Mueller. Low-Aspect-Ratio Wing Aerodynamics at Low Reynolds Numbers. *AIAA Journal*, 42(5):865–873, May–June May 2004.

[8] M. S. Selig, J. J. Guglielmo, A. P. Broeren, and P. Giguère. *Summary of Low-Speed Airfoil Data*, volume 1. SoarTech Publications, Virginia Beach, VA, 1995.

[9] M. S. Selig, C. A. Lyon, P. Giguère, C. P. Ninham, and J. J. Guglielmo. *Summary of Low-Speed Airfoil Data*, volume 2. SoarTech Publications, Virginia Beach, VA, 1996.

[10] C. A. Lyon, A. P. Broeren, P. Giguère, A. Gopalarathnam, and M. S. Selig. *Summary of Low-Speed Airfoil Data*, volume 3. SoarTech Publications, Virginia Beach, VA, 1998.

[11] M. S. Selig and B.D. McGranahan. Wind Tunnel Aerodynamic Tests of Six Airfoils for Use on Small Wind Turbines. National Renewable Energy Laboratory, NREL/SR-500-34515, Golden, CO, 2004.

[12] E. V. Laitone. Aerodynamic Lift at Reynolds Numbers below 7 x 10^4. *AIAA Journal*, 34(9):1941–1942, September–October 1996.

[13] G. R. Spedding and J. McArthur. Span Efficiencies of Wings at Low Reynolds Numbers. *Journal of Aircraft*, 47(1):120–128, January–February 2010.

[14] R. Cory and R. Tedrake. Experiments in Fixed-Wing UAV Perching. AIAA Paper 2008-7256, 2008.

[15] A. A. Paranjape, J. Kim, N. Gandhi, and S.-J. Chung. Experimental Demonstration of Perching by an Articulated Wing MAV. AIAA Paper 2011-6403, 2011.

[16] A. Paranjape, S.-J. Chung, and J. Kim. Novel Dihedral-Based Control of Flapping-Wing Aircraft with Application to Perching. *IEEE Transactions on Robotics*, 29(5):1071–1084, October 2013.

[17] A. Frank, J. S. McGrew, M. Valentiz, D. Levinex, and J. P. How. Hover, Transition, and Level Flight Control Design for a Single-Propeller Indoor Airplane. AIAA Paper 2007-6318, 2007.

[18] E. N. Johnson, M. A. Turbe, A. D. Wu, S. K. Kannan, and J. C. Neidhoefer. Flight Test Results of Autonomous Fixed-Wing UAV Transitions to and from Stationary Hover. AIAA Paper 2006-6775, 2006.

[19] D. Kubo, K. Muraoka, N. Okada, and S. Suzuki. High Angle of Attack Flight of a Wing-in-Propeller-Slipstream Mini Unmanned Aircraft. AIAA Paper 2010-3467, 2010.

[20] A. G. Sim. Flight Characteristics of a Manned, Low-speed, Controlled Deep Stall Vehicle. AIAA Paper 84-2074, 1984.

[21] F. M. Sobolic and J. P. How. Nonlinear Agile Control Test Bed for a Fixed-Wing Aircraft in a Constrained Environment. AIAA Paper 2009-1927, 2009.

[22] W. Hoburg and R. Tedrake. System Identification of Post Stall Aerodynamics for UAV Perching. AIAA Paper 2009-1930, 2009.

[23] M. Rhinehart and B. Mettler. Extracting Aerodynamic Coefficients using Direct Trajectory Sampling. AIAA Paper 2008-6899, 2008.

[24] B. F. Mettler. Extracting Micro Air Vehicles Aerodynamic Forces and Coefficients in Free Flight Using Visual Motion Tracking Techniques. *Experiments in Fluids*, 49(3):557–569, February 2010.

[25] C. M. Meckstroth and G. W. Reich. Aerodynamic Modeling of Small UAV for Perching Experiments. AIAA Paper 2013-3191, 2013.

[26] M. Tobak and L. B. Schiff. On the Formulation of the Aerodynamic Characteristics in Aircraft Dynamics. NASA TR R-456, 1976.

[27] M. Tobak. On the Use of the Indicial-Function Concept in the Analysis of Unsteady Motions of Wings and Wing-Tail Combinations. NACA Rept. 1188, 1954.

[28] J. G. Leishman and K. Q. Nguyenj. State-Space Representation of Unsteady Airfoil Behavior. *AIAA Journal*, 28(5):836–844, May–April 1990.

[29] M. Goman and A. Khrabrov. State-Space Representation of Aerodynamic Characteristics of an Aircraft at High Angles of Attack. *Journal of Aircraft*, 31(5):1109–1115, September–October 1994.

[30] M. Goman and A. Khrabrov. State-Space Representation of Aerodynamic Characteristics of an Aircraft at High Angles of Attack. AIAA Paper 92-4651, 1992.

[31] J. Singh and R. V. Jategaonkar. Identification of Lateral-Directional Behavior in Stall from Flight Data. *Journal of Aircraft*, 33(3):627–630, May–June 1996.

[32] G. W. Reich, F. E. Eastep, A. A., and R. Albertani. Transient Poststall Aerodynamic Modeling for Extreme Maneuvers in Micro Air Vehicles. *Journal of Aircraft*, 48(2):403–411, March–April 2011.

[33] Y. Fan and F. H. Lutze. Identification of an Unsteady Aerodynamic Model at High Angles of Attack. AIAA Paper 96-3407, 1996.

[34] M. Sinha, R. A. Kuttieri, A. K. Ghosh, and A. Misra. High Angle of Attack Parameter Estimation of Cascaded Fins Using Neural Network. *Journal of Aircraft*, 50(1):272–291, January–February 2013.

[35] A. Misra, A. K. Ghosh, and K. Ghosh. Cascade Fins–An Alternate Tail Stabilization Unit. AIAA Paper 2008-6884, August 2008.

[36] J. H. McMasters and M. L. Henderson. Low Speed Single Element Airfoil Synthesis. *Technical Soaring*, 6(2):1–21, 1980.

[37] S. J. S. Regisford and J. T. VanderMey. Perching a Minimally-Actuated Micro Air Vehicle. AIAA Paper 2013-0359, 2013.

[38] T. Theodorsen. General Theory of Aerodynamic Instability and the Mechanism of Flutter. NACA Report 496, 1935.

[39] H. Wagner. Über die Entstehung des dynamischen Auftriebes von Tragflügeln. *Zeitschrift für angewandte Mathematik und Mechanik*, 5:17–35, 1925.

[40] J. G. Leishman. *Principles of Helicopter Aerodynamics*. Cambridge Aerospace Series. Cambridge University Press, New York, NY, 2005.

[41] G. Z. McGowan, K. Granlund, M. V. Ol, A. Gopalarathnam, and J. R. Edwards. Investigations of Lift-Based Pitch-Plunge Equivalence for Airfoils at Low Reynolds Numbers. *AIAA Journal*, 49(7): 1511–1524, July 2011.

[42] M. S. Selig. Modeling Full-Envelope Aerodynamics of Small UAVs in Realtime. AIAA Paper 2010–7635, August 2010.

[43] L. E. Ericsson. Challenges in High-Alpha Vehicle Dynamics. *Progress in Aerospace Science*, 31:291–334, 1995.

[44] A. P. Brown, M. E. Beyers, and M. Bastian. Dynamic Stall Flight Data, Effects of Pitch Rate, Surface Roughness and Ground Effect. AIAA Paper 2008-0201, 2008.

[45] M. E. Beyers and A. P. Brown. Pitch-Rate Induced Abrupt Wing Stalling of Straight Wing Aircraft. AIAA Paper 2006-6001, 2006.

[46] L. E. Ericsson and J. P. Reding. Fluid Mechanics of Dynamic Stall Part II. Prediction of Full Scale Characteristics. *Journal of Fluids and Structures*, 2:113–143, March 1988.

[47] W. J. McCroskey. The Phenomenon of Dynamic Stall. NASA TM 81264, 1981.

[48] M. V. Ol, L. Bernal, C.-K. Kang, and W. Shyy. Shallow and Deep Dynamic Stall for Flapping Low Reynolds Number Airfoils. *Experiments in Fluids*, 46(5):883–901, 2009.

[49] Y. S. Baik, L. P. Bernal, K. Granlund, and M. V. Ol. Unsteady Force Generation and Vortex Dynamics of Pitching and Plunging Airfoils. *Journal of Fluid Mechanics*, 709:37–68, 2012.

[50] K. O. Granlund, M. V. Ol, and L. P. Bernal. Unsteady Pitching Flat Plates. *Journal of Fluid Mechanics*, 733, 2013.

[51] V. Klein and E. A. Morelli. *Aircraft System Identification: Theory and Practice*. AIAA Education Series. AIAA, Reston, VA, 2006.

[52] R. V. Jategaonkar. *Flight Vehicle System Identification: A Time Domain Methodology*, volume 216 of *Progress in Astronautics and Aeronautics*. AIAA, Reston, VA, 2006.

[53] Vicon MX System. *System Reference: Revision 1.7*. Vicon Motion Systems, Oxford, UK, 2007.

[54] E. R. Ulrich, J. S. Humbert, and D. J. Pines. Pitch and Heave Control of Robotic Samara Micro Air Vehicles. *Journal of Aircraft*, 47(4):1290–1299, July–August 2010.

[55] J. P. How. Multi-vehicle flight experiments: recent results and future directions. In *Proceedings of the Symposium on Platform Innovations and System Integration for Unmanned Air, Land and Sea Vehicles*, volume RTO-MP-AVT-146, Florence, Italy, NATO 2007.

[56] D. A. Paley and D. S. Warshawsky. Reduced-Order Dynamic Modeling and Stabilizing Control of a Micro-Helicopter. AIAA Paper 2009-1350, 2009.

[57] G. Ducard and R. D'Andrea. Autonomous Quadrotor Flight Using a Vision System and Accommodating Frames Misalignment. IEEE International Symposium on Industrial Embedded Systems, IEEE, doi:10.1109/SIES.2009.5196224, July 2009.

[58] A. B. Bauer. The Laminar Airfoil Problem. *Eighth National Free Flight Society Symposium*, pages 40–45, National Free Flight Society, Lake Charles, CA, 1975.

[59] W. F. Phillips. *Mechanics of Flight.* John Wiley and Sons, New Jersey, 2$^{\text{nd}}$ edition, 2009.

[60] B. W. McCormick. *Aerodynamics Aeronautics and Flight Mechanics.* John Wiley & Sons, New York, NY, 2$^{\text{nd}}$ edition, 1995.

[61] M. Puopolo, R. Reynolds, and J. D. Jacob. Comparison of Three Aerodynamic Models Used in Simulation of a High Angle of Attack UAV Perching Maneuver. AIAA Paper 2013-0242, 2013.

[62] B. H. Wick. Study of the Subsonic Forces and Moments on an Inclined Plate of Infinite Span. NACA TN 3221, 1954.

[63] C. Ostowari and D. Naik. Post Stall Studies of Untwisted Varying Aspect Ratio Blades with NACA 4415 Airfoil Section – Part 1. *Wind Engineering*, 8(3):176–194, 1984.

[64] C. Lindenburg. Stall coefficients. Energy Research Center of the Netherlands, Petten, ECN-RX-01-004, January 2001. Presented at IEA Symposium on the Aerodynamics of Wind Turbines, National Renewable Energy Laboratory, Golden, CO, December, 2000.

[65] D. Fischenberg. Identification of an Unsteady Aerodynamic Stall Model from Flight Test Data. AIAA Paper 95-3438, 1995.

[66] J. Pattinson, M. H. Lowenberg, and M. G. Goman. Investigation of Poststall Pitch Oscillations of an Aircraft Wind-Tunnel Model. *Journal of Aircraft*, 50(2):551–566, March–April 2013.

[67] D. I. Greenwell. A Review of Unsteady Aerodynamic Modelling for Flight Dynamics of Manoeuvrable Aircraft. AIAA Paper 2004-5276, August 2004.

[68] A. A. Paranjape, S.-J. Chung, and M. S. Selig. Flight Mechanics of a Tailless Articulated Wing Aircraft. *Bioinspiration & Biomimetics*, 6:(20 pp), 2011.

[69] C. Jouannet and P. Krus. Unsteady Aerodynamic Modelling: A Simple State-Space Approach. AIAA Paper 2005-855, 2005.

[70] C. Jouannet and P. Krus. Modelling of High Angle of Attack Aerodynamic State-space Approach. AIAA Paper 2006-3845, 2006.

[71] C. Jouannet and P. Krus. Modelling of High Angle of Attack Aerodynamic. AIAA Paper 2007-4295, 2007.

[72] A. Savitzky and M. J.E. Golay. Smoothing and Differentiation of Data by Simplified Least Squares Procedures. *Analytical Chemistry*, 36(8):1627–1639, 1964.

[73] R.W. Schafer. On the Frequency-Domain Properties of Savitzky-Golay Filters. Digital Signal Processing Workshop and IEEE Signal Processing Education Workshop (DSP/SPE), IEEE, doi:10.1109/DSP-SPE.2011.5739186, January 2011.

[74] MATLAB. *Curve Fitting Toolbox™ 2 Users Guide.* The Mathworks Inc., Natick, MA, March 2010.

[75] B. L. Stevens and F. L. Lewis. *Aircraft Control and Simulation.* Wiley-Interscience, New York, NY, 2$^{\text{nd}}$ edition, 2006.

[76] E-Flite. Vapor RTF. `http://www.e-fliterc.com/Products/Default.aspx?ProdID=pkz3300`, Accessed November 2013.

[77] D. V. Uhlig, A. Sareen, P. V. Sukumar, A. H. Rao, and M. S. Selig. Determining Aerodynamic Characteristics of a Micro Air Vehicle Using Motion Tracking. AIAA Paper 2010–8416, 2010.

[78] E-Flite. Sukhoi SU-26xp. `http://www.e-fliterc.com/Products/Default.aspx?ProdID=PKZU1080`, Accessed April 2011.

[79] D. V. Uhlig and M. S. Selig. Stability Characteristics of Micro Air Vehicles from Experimental Measurements. AIAA Paper 2011-3659, 2011.

[80] F. Zaic, editor. *1938 Model Aeronautics Year Book*. Model Aeronautics Publications, New York, NY, 1938.

[81] F. Zaic, editor. *1959–61 Model Aeronautics Year Book*. Model Aeronautics Publications, New York, NY, 1961.

[82] US Digital. H6 Ball Bearing Optical Shaft Encoder. `http://www.usdigital.com/assets/general/120_h6_datasheet_0.pdf`, Accessed April 2012.

[83] S. F. Hoerner. *Fluid-Dynamic Drag*. Published by the Author, Bakersfield, CA, 2nd edition, 1965.

[84] C. Morelli and et al. The International Gravity Standardization Net 1971. International Association of Geodesy, Special Publication 4, Report AF61(052)656 , 1971.

[85] R. E. Moose. The National Geodetic Survey Gravity Network. U.S. Dept. of Commerce, NOAA Technical Report NOS 121 NGS 39, 1986.

[86] National Geodetic Survey. Surface gravity prediction. `http://www.ngs.noaa.gov/cgi-bin/grav_pdx.prl`, Accessed October 2011.

[87] N. C. Barford. *Experimental Measurements: Precision, Error and Truth*. John Wiley & Sons, New York, NY, 2nd edition, 1985.

[88] J. Roskam. *Airplane Flight Dynamics and Automatic Flight Controls*. Part I, DARcorporation, Lawrence, KS, 1995.

[89] D. Ganslen. Sanding Glider Wings. In F. Zaic, editor, *1938 Model Aeronautics Year Book*. Model Aeronautics Publications, New York, NY, 1938.

[90] O. I. Iloputaife. Design of Deep Stall Protection for the C-17A. *Journal of Guidance, Control, and Dynamics*, 20(4):760–767, July–August 1997.

[91] W. A.J. Anemaat, B. Kaushik, and K. Po. A Method to Predict Deep Stall. AIAA Paper 2011-3005, 2011.

[92] C. W. McCutchen. Comment on Low-Aspect-Ratio Wing Aerodynamics at Low Reynolds Numbers. *AIAA Journal*, 44(4):924, April–May 2006.

[93] S. Karnesh and S. Pradeep. Phugoid Approximation Revisited. *Journal of Aircraft*, 36(2):465–467, March–April 1999.

[94] M. H. Dickinson and K. G. Götz. Unsteady Aerodynamic Performance of Model Wings at Low Reynolds Number. *Journal of Experimental Biology*, 174:45–64, 1993.

[95] A. H. Rao, D. V. Uhlig, and M. S. Selig. Glide and Powered Flight Characteristics of Micro Air Vehicles from Experimental Measurements. AIAA Paper 2012-2768, 2012.